

**DESIGN, SYNTHESIS AND CHARACTERIZATION OF
NOVEL HETEROCYCLIC LIGANDS
FOR BIOMEDICAL IMAGING**

THESIS

Submitted to Delhi Technological University
for the Award of the Degree of

DOCTOR OF PHILOSOPHY

in

BIOTECHNOLOGY

by

POOJA SRIVASTAVA

Under the Supervision of

Supervisor

Prof. Pravir Kumar
Professor & Dean (Alumni affairs),
Department of Biotechnology,
Delhi Technological University, Delhi

Co Supervisor

Dr. Anjani Kumar Tiwari
Associate Professor,
Department of Chemistry,
BBAU, Central University, Lucknow



**Department of Biotechnology, Delhi Technological University
(Formerly Delhi College of Engineering) Delhi-110042, INDIA**

October 2019

©Delhi Technological University-2019
All rights reserved

Dedicated to My Beloved Father

“Late Dr. G. Lal”

DECLARATION

I, Pooja Srivastava, certify that the work embodied in this Ph.D. thesis is my own *bona fide* work carried out under the supervision of Dr. Pravir Kumar (Professor & Dean, Department of Biotechnology, Delhi Technological University) and Dr. Anjani Kumar Tiwari (Associate Professor, Baba Bhimrao Ambedker Univeristy, Lucknow) for a period of July 2014 to July 2019 at INMAS and DTU. The matter embodied in this thesis has not been submitted for the award of any other degree/diploma.

I declare that I have devotedly acknowledged, given credit and referred to the research workers wherever their works have been cited in the text and the body of thesis. I further certify that I have not wilfully lifted up some other's work, para, text, data, results etc. reported in the journal, books, reports, dissertations, thesis, etc., or available at websites and included them in Ph.D. thesis and cited as my own work.

Pooja Srivastava
(Reg. No: 2K14/PhD/BT/02)

Date

Place



DELHI TECHNOLOGICAL UNIVERSITY

CERTIFICATE

This is to certify that the Ph.D. thesis entitled “**Design, synthesis and characterization of novel heterocyclic ligands for biomedical imaging**” submitted to the Delhi Technological University, Delhi for the award of Doctor of Philosophy is based on the original research work carried out under our supervision. It is further certified that the work embodied in this thesis has neither partially nor fully submitted to any other university or institution for the award of any degree or diploma.

This is to certify that the above statement made by the candidate is correct to the best of our knowledge.

Prof. Pravir Kumar

(Supervisor)
Professor & Dean (Alumni affairs),
Department of Biotechnology,
Delhi Technological University,
Delhi

Dr. Anjani Kumar Tiwari

(Co Supervisor)
Associate Professor,
Department of Chemistry,
BBAU, Central University,
Lucknow

Prof. Jai Gopal Sharma

(Head)
Department of Biotechnology
Delhi Technological University
Delhi

ACKNOWLEDGEMENT

God's best blessings have made it possible for me to present this work to the world.

I take this opportunity to express my deep sense of gratitude to my supervisor, Prof Pravir Kumar, Professor and Dean, Department of Biotechnology, Delhi Technological University (DTU) for giving me an opportunity to carry out research under his excellent supervision. His continuous guidance and support during this tenure helped me completing my research work successfully. I sincerely thank you for your mentorship & encouragement.

I am thankful to my co-supervisor, Dr Anjani Kumar Tiwari, Associate Professor, Baba Bhimrao Ambedker University (BBAU), Lucknow, for his continuous guidance, expert advice, constructive criticism and supervision during my entire Ph.D. tenure. His invaluable ideas and creative intellectual support immensely helped become more productive during the research work.

Words elude me in expressing my special thanks to Dr A. K. Singh, Director General, Defense Research and Development Organization, Life Science for permitting me to carry out Ph.D. I also thank him for his constant support and endless encouragement during the entire tenure.

I wish to place on record my grateful thanks to Dr Tarun Sekhri, Director, Institute of Nuclear Medicine & Allied Sciences (INMAS), for providing access to all the necessary facilities in the institute during my research.

I would like to express my kind regards to Vice Chancellor Prof. Yogesh Singh, Delhi Technological University (DTU) for allowing me to be a member of Delhi Technological University.

I am grateful to Prof. Jai Gopal, Head Department of Biotechnology, DTU, to enroll me for the Ph.D. programme in his department.

My thanks are due to Dr Rajnish Sharma, Scientist 'G' and Head of the Division (Department of Combat Sciences & Nuclear Medicine), INMAS, for providing the

access to facilities in division, His appreciation for my work has boosted my confidence to carry out research work more effectively.

Further, I pay my regards and thanks Dr A. K. Mishra, Head, Department of Cyclotron and Radiopharmaceuticals, INMAS to allow me to use the facilities in his department.

I profoundly thank Dr Gaurav Mittal, Head, Department of Combat Sciences, INMAS, for his encouraging support that helped me speed up my work effectively.

I would also like to thank Dr Dipti Kakkar, Scientist E, INMAS who extended advice, suggestions and assistance whenever I approached her which immensely helped me during my Ph.D. work.

I am grateful to Dr Ankur Kaul, Dr Himanshu Ojha, Dr Anant Narayan Bhatt, Dr Lalita Mehra, and Dr Sonia Gandhi for their support during experiments.

Mr Sunil Pal, Mr Pankaj Yadav, Mr Harish Rawat, Mrs Mita Datta, and Ms Shaalu, Mr. Chail Bihari, and Mr. Jitendra deserve my special thanks for their invaluable technical support.

I sincerely appreciate my colleagues at INMAS Dr Amit Tyagi, Mrs M. Memita Devi, Mr Chandrasekhar Beniwal, Dr Anupama Datta, Dr. Puja Panwar, Dr Rashi Mathur, Dr Shweta Singh, Dr Shubra Chaturvedi, Dr Aruna Kaushik, Mr. Dharmendra Kumar, and Dr Raunak for maintaining the cordial, academic and friendly environment throughout the research period.

Special regards are due to Dr Rashmi Ambastha for her loving encouragement and valuable suggestions.

It is a pleasure to acknowledge the enthusiastic support and assistance given to me by my colleagues in DTU Mr. Dhiraj Kumar, Rohan Gupta, Dr Saurabh Jha, Dr Niraj Jha, and Dr Renu Sharma.

Further, I would also like to express thanks to all the administrative and technical members at INMAS and Department of Biotechnology, Delhi Technological University.

Moral support and affectionate advice received from my loving husband Mr. Hemant Shrivastava and dear son Aryaman worked as a catalyst in accomplishing this work.

My father late Dr. G. Lal has always been source of tremendous inspiration. He used to always set ambitious goals for me and was a proud father. This accomplishment would have made him even more proud.

My immeasurable gratitude is due to my mother Smt. Malti Shrivastava who has been a constant driving force behind all my achievements. Her continuous loving care and guidance made my all successes since my childhood.

Special thanks to my father in law Mr. Suresh Kumar Shrivastava and mother in law Mrs. Pushpa Shrivastava for their support and blessings.

Finally, my heartfelt thanks are due to my sister Dr. Parul Shrivastava, brother in law Dr. Naveen Shrivastav and brother Parijat Shrivastava for their continuous appreciation and encouragement.

Pooja Shrivastava

ABSTRACT

The translocator protein (TSPO, 18 kDa) and highly conserved protein during evolution, has been studied for its importance in various life essential functions. TSPO is mainly found on the outer surface of mitochondria in central nervous system and in peripheral tissues. It is an intracellular protein complexed with voltage dependent anion channel (VCAD) having molecular weight 32 kDa as well as adenine nucleotide translocator (ANT) having molecular weight 30 kDa in mitochondria. TSPO has been investigated as biomarker for inflammatory conditions of lungs, liver, kidneys and brain etc. Its role has been studied in other disorders such as depression, anxiety, and neurodegenerative disorders. Therefore, high affinity TSPO ligands can find applications for non-invasive disease evaluations and for the drug delivery to the pathologically affected tissues. This led to the development of TSPO ligands as diagnostic ligands.

There are few classical ligands available such as PK11195, Ro5-4864 and FGIN-127 which are isoquinoline carboxamide, benzodiazepine and indole derivatives, respectively. All of them showed compatibility to tetrapyrrole protoporphyrin IX (PPIX) structure which is a well-known endogenous TSPO ligand.

^{11}C (R) PK11195 ligand is most widely studied positron emission tomography (PET) TSPO ligand from first generation which has limitation of high lipophilicity and low *in vivo* specific binding. These limitations were overcome by second generation TSPO ligands for improved imaging. Some of the TSPO ligands used in clinical human studies are [^{18}F]FEDAA, [^{11}C]DAA, [^{11}C]PBR28, [^{18}F]DPA714 and [^{11}C]AC-5216.

These second-generation ligands have the problem of intersubject variability. A new skeleton acetamidobenzoxazolone (ABO), which has been derived from Ro5-4864 by opening the diazepine ring and reorganizing it, that can overcome the problems of intersubject variability and non-specific binding.

In the present study, acetamidobenzoxazolone (ABO) was chosen as lead skeleton for modification and investigation as Technetium-99m (^{99m}Tc) complexed TSPO ligands for single photon emission computed tomography (SPECT) application. This skeleton was chosen as it has recently shown to overcome non-specificity and polymorphism issues, the limitations of TSPO ligands from first two generations. Recently, our group has developed acetamidobenzoxazolone (ABO) moiety which has been reported for PET application with improved properties.

Firstly, pharmacophore modelling was performed taking 51 acetamidobenzoxazolone based TSPO derivatives from literature. The best four featured pharmacophore hypothesis AAAR (three acceptors and one aromatic group) was used for designing the TSPO ligands for diagnostic application. Besides that, computational ligand-protein interactions (PDB used: 4RYQ, 2MGY and 4UCI) and ADME (absorption, distribution, metabolism, and excretion) properties have also been compared to known TSPO ligands to get more insight into the complete pharmacokinetics of ^{99m}Tc -ABEO-Br/Cl skeleton for SPECT application.

Six new halogenated acetamidobenzoxazolone-amino acid methyl esters (ABEO-Br/Cl) falling in three categories on the basis of amino acids chosen (tryptophan, phenylalanine and methionine) were synthesized and tested for their ability to bind with ^{99m}Tc . The stability of radiocomplexes were >93% and >87% in saline and

human serum, respectively over 24 h. ABO was modified to ABEO-Br/Cl for SPECT application using tryptophan methyl ester, phenylalanine methyl ester and methionine methyl ester to provide skeleton for ^{99m}Tc and improve pharmacokinetics. Amino acid esters were used for modification as they are biocompatible and/or provide pharmacophoric features. As per literature, halogen substitution at 5th position of acetaminodobenzoxazolone was important for TSPO affinity, therefore bromo and chloro analogs were synthesized. The radiocomplexes were evaluated as SPECT imaging agents for targeting TSPO through *in vitro*, *ex vivo* and *in vivo* means. PK11195 was used for proving the specificity of the radioligands towards TSPO in normal mice. These studies demonstrated significant decrease in uptakes of radioligands in TSPO rich organs when PK11195 was injected 10 min prior to radioligand injection in mice. Thereafter, these novel TSPO radioligands were compared with each other in terms of *ex vivo* biodistribution and *in vivo* radioactivity uptake in TSPO enriched organs. All the radiocomplexes demonstrated uptakes majorly in organs rich in TSPO, such as kidneys, lungs, heart, livers, spleen and brain. The uptakes in brain were minimal in normal mice and rabbits as TSPO is present in minimal concentration in normal brain. All the analogs were able to cross blood brain barrier. The blood kinetics were fast leading to good contrast as seen under *in vivo* studies of mice and rabbits. As per biodistribution pattern, there is preference of ^{99m}Tc -ABTO analogs for lungs, ^{99m}Tc -ABPO analogs for spleen and ^{99m}Tc -ABMO analogs for brain. The release kinetics of these tracers were compared to see their retention under *in vivo* conditions. Both *ex vivo* studies in mice and *in vivo* studies in rabbits demonstrated fast release still providing significantly long window for diagnostic applications in case of all the radioligands.

The ^{99m}Tc -ABTOs, being most potential candidates for lungs, were further studied for cell uptake in A549 human lung tumor cell lines, A549 xenograft nude mice model and lung inflammation model with and without PK11195. These studies further proved their potential as TSPO imaging agents for SPECT.

CONTENTS

	<i>Page No.</i>
List of Figures	i
List of Tables	vi
List of Schemes.....	vii
List of Abbreviations	viii
List of Symbols and Units.....	xi
Overview of the thesis	xiii
Chapter 1: Introduction and literature review	1-39
1.1 Radiation	1
1.1.1 History.....	1
1.1.2 Interaction between radiation and matter.....	2
1.1.3 Interaction between charged particles and matter.....	2
1.1.4 Interaction between γ -radiation and matter.....	3
1.2 Molecular imaging	3
1.2.1 Principles of molecular imaging	6
1.2.2 Selection criteria of imaging modalities	7
1.2.2.1 Computed tomography (CT).....	8
1.2.2.2 Magnetic resonance imaging (MRI)	9
1.2.2.3 Nuclear medicine modalities (PET & SPECT).....	12
1.2.2.3.1 Tomographic imagers	13
1.2.2.3.2 Positron emission tomography (PET).....	14
1.2.2.3.3 Single photon emission computed tomography (SPECT).....	18
1.3 Type of radiopharmaceuticals.....	23
1.4 PET molecular imaging probes for the central nervous system (CNS).....	24
1.4.1 Imaging agents for Dopaminergic Neurotransmission	24
1.4.2 Imaging agents for Serotonergic Neurotransmission.....	25
1.4.3 Imaging agents for Cholinergic Neurotransmission	26
1.4.4 Imaging agents for β -Amyloid.....	27
1.4.5 Imaging agents for Glutamatergic Neurotransmission	28

	<i>Page No.</i>
1.5	Currently used SPECT molecular imaging probes for brain imaging29
1.6	Traumatic brain injury (TBI) imaging30
1.7	Translocator protein (TSPO).....31
1.7.1	Endogeneous TSPO ligands.....33
1.7.2	Tissue distribution and subcellular location of TSPO34
1.7.3	Second and third generation TSPO radiotracers in neurologic diseases35
1.7.4	Limitations of new TSPO radiotracers37
1.8	Aims and objectives of present study38
1.9	Plan of work.....38
Chapter 2:	Materials and Methods 40-53
2.1	Introduction.....40
2.2	<i>In silico</i> techniques40
2.2.1	Pharmacophore hypothesis generation40
2.2.2	ADME studies41
2.2.3	Preparation of ligands42
2.2.4	Protein preparation.....43
2.2.5	Docking.....43
2.3	Synthesis and characterization.....46
2.3.1	Chemicals.....46
2.3.2	Instrumentation47
2.4	<i>In vitro</i> techniques.....47
2.4.1	MTT cell viability studies.....47
2.5	Radiolabelling protocol48
2.6	Stability studies of radioligands.....48
2.6.1	Stability in saline48
2.6.2	<i>In vitro</i> human serum stability assay49
2.7	<i>In vitro</i> cell uptake of ^{99m} Tc-radioligand in A549 human lung tumor cell.....49
2.8	Animal studies49
2.8.1	<i>Ex vivo</i> studies.....50

	<i>Page No.</i>
2.8.1.1	Blood kinetic studies in New Zealand rabbits50
2.8.1.2	Biodistribution studies in Balb/c mice50
2.8.2	<i>In vivo</i> studies51
2.8.2.1	Gamma camera design51
2.8.2.2	Biodistribution in New Zealand rabbits51
2.8.2.3	Biodistribution and blocking studies in normal Balb/c mice52
2.8.3	Blocking studies in animal model52
2.8.3.1	LPS induced lung inflammation model52
2.8.3.2	Lung tumor xenograft model53

**Chapter 3: Designing of Acetamidobenzoxazolone based TSPO ligands
for Single Photon Emission Computed Tomography..... 54-94**

3.1	Introduction.....54
3.2	Literature review of computational studies for TSPO ligands.....55
3.2.1	QSAR studies.....55
3.2.2	3D-QSAR studies.....58
3.2.3	Virtual screening: a pharmacophore and 3D-QSAR studies61
3.2.4	Docking studies.....62
3.3	Properties of CNS imaging probes63
3.3.1	Selectivity for the receptor.....63
3.3.2	Specific radioactivity64
3.3.3	Metabolism and position of label.....65
3.3.4	Blood-brain barrier permeability65
3.3.5	Clearance rate, protein binding, and non-specific binding66
3.4	Result and discussion.....66
3.4.1	Pharmacophore modelling and 3D QSAR studies.....66
3.4.2	Design of new TSPO skeletons.....74
3.4.3	ADME properties.....76
3.4.3.1	Assessment of drug-likeness76
3.4.3.2	Prediction of bioavailability78

	<i>Page No.</i>
3.4.3.3 Penetration of blood-brain barrier (BBB)	82
3.4.3.4 Plasma protein binding	82
3.4.3.5 Human ether-a-go-go-related gene potassium (HERG K ⁺) channel	83
3.4.3.6 Molecular Volume	84
3.4.4 Docking studies.....	85
3.5 Conclusion	93
Chapter 4: Synthesis, characterization and cytotoxicity studies	95-128
4.1 Synthesis	95
4.1.1 Procedure for synthesis of 2-(2-(5-bromo benzoxazolone) acetamido)-3-(1 <i>H</i> -indol-3-yl) propanoate, ABTO-Br	95
4.1.2 General procedure for synthesis of 5-chloro/bromo benzoxazol- 2(3 <i>H</i>)-one, ABO-Br/Cl	96
4.1.3 General procedure for chloroacetylation of methyl ester of amino acid.....	96
4.1.4 General procedure for synthesis of Br/Cl-ABO-Amino Acid ester (ABEO-Br/Cl).....	96
4.2 Result and discussion.....	101
4.3 Characterization	103
4.3.1 Characterization of 5-chloro benzoxazol-2(3 <i>H</i>)-one (ABO-Cl).....	103
4.3.2 Characterization of 5-bromo benzoxazol-2(3 <i>H</i>)-one (ABO-Br)	105
4.3.3 Characterization of methyl 2-(2-chloroacetamido)-3-(1 <i>H</i> -indol-3- yl) propanoate (T-Cl)	107
4.3.4 Characterization of methyl 2-(2-chloroacetamido)-3- phenylpropanoate (P-Cl).....	110
4.3.5 Characterization of 2-(2-chloro-acetylamino)-4-methylsulfanyl- butyric acid methyl ester (M-Cl).....	112
4.3.6 Characterization of 2-(2-(5-bromo benzoxazolone)acetamido)-3- (1 <i>H</i> -indol-3-yl) propanoate (ABTO-Br).....	113

4.3.7	Characterization of 2-(2-(5-bromo benzoxazolone)acetamido)-3-(1 <i>H</i> -indol-3-yl) propanoate (ABTO-Cl)	116
4.3.8	Characterization of methyl 2-(2-(5-chloro-2-oxobenzooxazol-3(2 <i>H</i>)-yl)acetamido)-3-phenylpropanoate (ABPO-Cl).....	118
4.3.9	Characterization of methyl 2-(2-(5-bromo-2-oxobenzooxazol-3(2 <i>H</i>)-yl)acetamido)-3-phenylpropanoate (ABPO-Br)	121
4.3.10	Characterization of 2-[2-(5-chloro-2-oxo-benzoxazol-3-yl)-acetylamino]-4-methylsulfanyl-butyric acid methyl ester (ABMO-Cl).....	122
4.3.11	Characterization of 2-[2-(5-bromo-2-oxo-benzoxazol-3-yl)-acetylamino]-4-methylsulfanyl-butyric acid methyl ester (ABMO-Br).....	124
4.4	<i>In vitro</i> toxicity evaluation.....	126
4.5	Conclusion	128

Chapter 5: Radiosynthesis and biological evaluation of ^{99m}Tc-ABEO-

Br/Cl..... 129-169

Part A: Radiosynthesis and biological evaluation of ^{99m}Tc-ABTO-Br/Cl129

5.1.1	Radiosynthesis and stability studies of radiocomplexes.....	129
5.1.2	<i>In vitro</i> studies	131
5.1.2.1	Cell uptake of ^{99m} Tc-radioligand in A549 human lung tumor cells.....	131
5.1.3	<i>Ex vivo</i> studies.....	132
5.1.3.1	Blood kinetic studies in New Zealand rabbits.....	132
5.1.3.2	Biodistribution studies in Balb/c mice	132
5.1.3.3	Biodistribution studies of ^{99m} Tc-ABTO-Br in lung inflamed model of Balb/c mice	135
5.1.4	<i>In vivo</i> studies	136
5.1.4.1	Biodistribution and blocking studies of ^{99m} Tc-ABTO-Br/Cl in normal Balb/c mice	136

5.1.4.2 Biodistribution studies of ^{99m}Tc -ABTO-Br in New Zealand rabbits	137
5.1.4.3 Biodistribution and blocking studies of ^{99m}Tc -ABTO-Cl in lung inflamed model of Balb/c mice.....	139
5.1.4.4 Biodistribution and blocking studies of ^{99m}Tc -ABTO-Br in lung tumor xenograft model in nude mice	141
5.1.5 Conclusion	142
Part B: Radiosynthesis and biological evaluation of ^{99m}Tc-ABPO-Br/Cl.....	143
5.2.1 Radiosynthesis and stability studies of radiocomplexes.....	143
5.2.2 <i>Ex vivo</i> studies.....	144
5.2.2.1 Blood kinetic studies in New Zealand rabbits.....	144
5.2.2.2 Biodistribution studies in Balb/c mice	145
5.2.3 <i>In vivo</i> studies	148
5.2.3.1 Biodistribution and blocking studies of ^{99m}Tc -ABPO-Br/Cl in normal Balb/c mice	148
5.2.3.2 Biodistribution studies of ^{99m}Tc -ABPO-Br in New Zealand rabbits	149
5.2.4 Conclusion	151
Part C: Radiosynthesis and biological evaluation of ^{99m}Tc-ABMO-Br/Cl.....	153
5.3.1 Radiosynthesis and stability studies of radiocomplex	153
5.3.2 <i>Ex vivo</i> studies.....	155
5.3.2.1 Blood kinetic studies in New Zealand rabbits.....	155
5.3.2.2 Biodistribution studies in Balb/c mice	156
5.3.3 <i>In vivo</i> studies	158
5.3.3.1 Biodistribution and blocking studies of ^{99m}Tc -ABMO-Br/Cl in normal Balb/c mice	158
5.3.3.2 Biodistribution studies of ^{99m}Tc -ABMO-Br/Cl in New Zealand rabbits	158
5.3.4 Conclusion	160

Part D: Comparative evaluation of ^{99m}Tc-ABEO-Br/Cl analogues	161
5.4.1 Comparative analysis of stability of radiocomplexes	161
5.4.2 <i>Ex vivo</i> blood kinetic studies in New Zealand rabbits	162
5.4.3 <i>Ex vivo</i> biodistribution studies in Balb/c mice.....	162
5.4.4 <i>In vivo</i> images of radiocomplexes in New Zealand rabbits	166
5.4.5 Conclusion	169
Chapter 6: Summary, discussion and future perspective	170-172
References	173-198
Publications	199-200
Curriculum Vitae	

LIST OF FIGURES

<i>Figure No.</i>		<i>Page No.</i>
Figure 1.1	Schematic of main steps involved in molecular imaging	5
Figure 1.2	<i>In vivo</i> principles/function of PET isotope	15
Figure 1.3	Integrated or metal essential radiopharmaceuticals	23
Figure 3.1	TSPO ligands	54
Figure 3.2	Schematic TSPO models' representation on a) 6-arylpyrrolo[2,1-d][1,5]benzothiazepines analogues; b) quinolone, isoquinoline, pyrrolobenzoxazepine, pyrrolopyridin-5-one, and pyrroloquinolin-1-one derivatives; c) pyrrolobenzoxazepine derivatives; d) 2-arylpyrazolo[1,5-a]pyrimidin-3-yl acetamides analogues	59
Figure 3.3	TSPO ligands identified through virtual screening of Maybridge database	62
Figure 3.4	Frame of total 51 compounds	72
Figure 3.5	pharmacophore model AAAR: presenting the best model of the study	73
Figure 3.6	Scattering plot of predicted vs experimental activities of TSPO ligands as per the 3D-QSAR model for the best four-featured pharmacophore model	73
Figure 3.7	2D and 3D interaction diagrams of ABTO-Br with PDB 4RYQ	88
Figure 3.8	2D and 3D interaction diagrams of ABTO-Br with PDB 4UC1	89
Figure 3.9	2D interaction diagrams of FPBMP with PDBs a) 2MGY, b) 4RYQ and c) 4UC1	90
Figure 3.10	2D interaction diagrams of i) DAA1106 and ii) Diazepam with TSPO PDB 2MGY	90
Figure 3.11	2D and 3D interaction diagrams of ABMO-Br with PDBs a) 4RYQ and b) 4UC1	91
Figure 3.12	2D and 3D interaction diagrams of i) ABPO-Br and ii) ABPO-Cl with PDBs a) 2MGY, b) 4RYQ and c) 4UC1	93
Figure 4.1	Mass spectrum of ABO-Cl	104
Figure 4.2	¹ H-NMR spectrum of ABO-Cl	104
Figure 4.3	¹³ C-NMR spectrum of ABO-Cl	105
Figure 4.4	Mass spectrum of ABO-Br	105
Figure 4.5	¹ H-NMR spectrum of ABO-Br	106
Figure 4.6	¹³ C-NMR spectrum of ABO-Br	106

<i>Figure No.</i>		<i>Page No.</i>
Figure 4.7	Mass spectrum of T-Cl	108
Figure 4.8	¹ H-NMR spectrum of T-Cl	108
Figure 4.9	¹³ C-NMR spectrum of T-Cl	109
Figure 4.10	HPLC profile of T-Cl	109
Figure 4.11	Mass spectrum of P-Cl	110
Figure 4.12	¹³ C-NMR spectrum of P-Cl	111
Figure 4.13	HPLC profile of P-Cl	111
Figure 4.14	¹ H-NMR spectrum of M-Cl	112
Figure 4.15	¹³ C-NMR spectrum of M-Cl	112
Figure 4.16	Mass spectrum of ABTO-Br	114
Figure 4.17	¹ H-NMR spectrum of ABTO-Br	114
Figure 4.18	¹³ C-NMR spectrum of ABTO-Br	115
Figure 4.19	HPLC profile of ABTO-Br	115
Figure 4.20	Mass spectrum of ABTO-Cl	116
Figure 4.21	¹ H-NMR spectrum of ABTO-Cl	116
Figure 4.22	¹³ C-NMR spectrum of ABTO-Cl	117
Figure 4.23	HPLC profile of ABTO-Cl	117
Figure 4.24	Mass spectrum of ABPO-Cl	119
Figure 4.25	¹ H-NMR spectrum of ABPO-Cl	119
Figure 4.26	¹³ C-NMR spectrum of ABPO-Cl	120
Figure 4.27	HPLC profile of ABPO-Cl	120
Figure 4.28	Mass spectrum of ABPO-Br	121
Figure 4.29	¹ H-NMR spectrum of ABPO-Br	121
Figure 4.30	¹³ C-NMR spectrum of ABPO-Br	122
Figure 4.31	Mass spectrum of ABMO-Cl	123
Figure 4.32	¹ H-NMR spectrum of ABMO-Cl	123
Figure 4.33	¹³ C-NMR spectrum of ABMO-Cl	124
Figure 4.34	Mass spectrum of ABMO-Br	124
Figure 4.35	¹ H-NMR spectrum of ABMO-Br	125
Figure 4.36	¹³ C-NMR spectrum of ABMO-Br	125
Figure 4.37	HPLC profile of ABMO-Br	126

<i>Figure No.</i>		<i>Page No.</i>
Figure 4.38	Effect of ABEO-Br/Cl analogues on cell viability in RAW 264.7 cell line	127
Figure 5.1.1	Labelling efficiency (%LE) of a) ABTO-Br and b) ABTO-Cl with ^{99m}Tc	130
Figure 5.1.2	Serum stability studies in terms of labelling efficiency (%LE) of a) ^{99m}Tc -ABTO-Br and b) ^{99m}Tc -ABTO-Cl over 24 h	130
Figure 5.1.3	Uptake kinetics of a) ^{99m}Tc -ABTO-Br and b) ^{99m}Tc -ABTO-Cl in A549 cells in the presence (blue) and absence (red) of PK11195	131
Figure 5.1.4	Time-activity curves showing blood clearance of a) ^{99m}Tc -ABTO-Br and b) ^{99m}Tc -ABTO-Cl post injection in New Zealand rabbit	132
Figure 5.1.5	Biodistribution patterns of a) ^{99m}Tc -ABTO-Br and b) ^{99m}Tc -ABTO-Cl in normal Balb/c mice	134
Figure 5.1.6	^{99m}Tc -ABTO-Br <i>ex vivo</i> biodistribution in lungs, liver, spleen and kidneys of lung inflamed mice at 40 min post i.v. injection with 10 min preadministration of 2.5/5/10 mg/kg PK11195 as blocking agent	136
Figure 5.1.7	<i>In vivo</i> SPECT images of ^{99m}Tc -ABTO-Cl a(i) without and a(ii) with PK11195 preadministration and ^{99m}Tc -ABTO-Br b(i) without and b(ii) with PK11195 preadministration at 40 min post injection of radioligand	137
Figure 5.1.8	<i>In vivo</i> biodistribution of a) ^{99m}Tc -ABTO-Br and b) ^{99m}Tc -ABTO-Cl in New Zealand rabbits (Dynamic studies for 30 min)	138
Figure 5.1.9	<i>In vivo</i> SPECT images showing activity distribution of ^{99m}Tc -ABTO-Cl in inflamed mice a) without and b), c) with blocking at 40 min post i.v. injection with 10 min preadministration of 5/10 mg/kg PK11195 as blocking agent in lung inflammation model of Balb/c mice	139
Figure 5.1.10	^{99m}Tc -ABTO-Cl <i>in vivo</i> biodistribution in lungs, main organs (lungs, liver, heart, kidneys and spleen) and total body uptakes at 40 min post i.v. injection with 10 min preadministration of 5/10 mg/kg PK11195 as blocking agent in lung inflammation model of Balb/c mice	140
Figure 5.1.11	Localization of ^{99m}Tc -ABTO-Br in lung tumor xenograft model in a) unblocked b) blocked with PK11195 and c) blocked with MBMP precursor at i) 1h and ii) 3 h	141
Figure 5.2.1	Labelling efficiency (%LE) of a) ABPO-Br and b) ABPO-Cl with ^{99m}Tc	143

<i>Figure No.</i>		<i>Page No.</i>
Figure 5.2.2	Serum stability studies in terms of labelling efficiency (%LE) of a) ^{99m}Tc -ABPO-Br and b) ^{99m}Tc -ABPO-Cl over 24 h	144
Figure 5.2.3	Time-activity curves showing blood clearance of a) ^{99m}Tc -ABTO-Br and b) ^{99m}Tc -ABTO-Cl post injection in New Zealand rabbits	144
Figure 5.2.4	Biodistribution patterns of a) ^{99m}Tc -ABPO-Br and b) ^{99m}Tc -ABPO-Cl in normal Balb/c mice	145
Figure 5.2.5	<i>In vivo</i> SPECT images of ^{99m}Tc -ABPO-Br without a(i) and with a(ii) PK11195 preadministration and ^{99m}Tc -ABPO-Cl without b(i) and with b(ii) PK11195 preadministration at 40 min post injection of radioligand	148
Figure 5.2.6	<i>In vivo</i> biodistribution of ^{99m}Tc -ABPO-Br in New Zealand rabbit (Dynamic studies for 30 min)	149
Figure 5.2.7	<i>In vivo</i> biodistribution of ^{99m}Tc -ABPO-Cl in New Zealand rabbit (Dynamic studies for 30 min)	150
Figure 5.3.1	Labelling efficiency (%LE) of a) ABMO-Br and b) ABMO-Cl with ^{99m}Tc	153
Figure 5.3.2	Serum stability studies in terms of labelling efficiency (%LE) of a) ^{99m}Tc -ABMO-Br and b) ^{99m}Tc -ABMO-Cl over 24 h	153
Figure 5.3.3	Comparative stability of ^{99m}Tc -ABMO-Br and ^{99m}Tc -ABMO-Cl in saline	154
Figure 5.3.4	Comparative stability of ^{99m}Tc -ABMO-Br and ^{99m}Tc -ABMO-Cl in human serum	154
Figure 5.3.5	Time-activity curves showing blood clearance of ^{99m}Tc -ABMO-Br and ^{99m}Tc -ABMO-Cl postinjection in New Zealand rabbits	155
Figure 5.3.6	Biodistribution patterns of a) ^{99m}Tc -ABMO-Br and b) ^{99m}Tc -ABMO-Cl in normal Balb/c mice	156
Figure 5.3.7	<i>In vivo</i> SPECT images of ^{99m}Tc -ABMO-Br without (ai) and with (aii) PK11195 preadministration and ^{99m}Tc -ABMO-Cl without (bi) and with (bii) PK11195 preadministration at 40 min post injection of radioligand	158
Figure 5.3.8	<i>In vivo</i> biodistribution of a) ^{99m}Tc -ABMO-Br and b) ^{99m}Tc -ABMO-Cl in New Zealand rabbits (Dynamic studies for 30 min)	160
Figure 5.4.1	Time-activity curves showing blood clearance of ^{99m}Tc -ABEO-Br/Cl analogues in New Zealand rabbits	162
Figure 5.4.2	Biodistribution (%ID/g, Mean) data of ^{99m}Tc -ABEO-Br/Cl for a) Kidneys and b) Liver	163
Figure 5.4.3	Biodistribution (%ID/g, Mean) data of ^{99m}Tc -ABEO-Br/Cl for a) Brain and b) Spleen	163

<i>Figure No.</i>		<i>Page No.</i>
Figure 5.4.4	Biodistribution (%ID/g, Mean) data of ^{99m}Tc -ABEO-Br/Cl for a) Heart and b) Lungs	164
Figure 5.4.5	Biodistribution (%ID/g, Mean) data of ^{99m}Tc -ABEO-Br/Cl for a) Stomach and b) Intestine	164
Figure 5.4.6	Biodistribution (%ID/g, Mean) data of ^{99m}Tc -ABEO-Br/Cl for Blood	165
Figure 5.4.7	<i>In vivo</i> images of ^{99m}Tc -ABEO-Br/Cl in New Zealand rabbits	168

LIST OF TABLES

<i>Table No.</i>		<i>Page No.</i>
Table 1.1	Features of imaging modalities	4
Table 1.2	Main physical characteristics of medically important PET isotopes	17
Table 1.3	Examples of PET radiopharmaceuticals	17
Table 1.4	Main physical characteristics of medically important SPECT isotopes	19
Table 1.5	Examples of SPECT radiopharmaceuticals	21
Table 3.1	List of TSPO ligands used in pharmacophore modelling	67
Table 3.2	Chemical structures of designed ligands	77
Table 3.3	Molecular descriptors and their components	80
Table 3.4	Predictive values of properties of known and designed TSPO ligands	81
Table 3.5	Glide XP docking results of known and acetamido-benzoxazolone- amino acid ester based designed ligands (ABEO-Br/Cl) with PDBs of TSPO: 2MGY, 4RYQ, and 4UC1	86
Table 5.2.1	Ratio of uptake at 120 min with respect to highest uptake	147
Table 5.4.1	Stability in saline and serum at 24 h	161

LIST OF SCHEMES

<i>Scheme No.</i>		<i>Page No.</i>
Scheme 1:	Synthesis of 2-(2-(5-bromo benzoxazolone)acetamido)-3-(1 <i>H</i> -indol-3-yl) propanoate (ABTO-Br)	97
Scheme 2:	Synthesis of 2-(2-(5-bromo/chlororbenzoxazolone)acetamido)-3-(1 <i>H</i> -indol-3-yl) propanoate (ABTO-Br/Cl)	98
Scheme 3:	Synthesis of methyl 2-(2-(5-bromo/chloro-2-oxobenzoxazol-3(2 <i>H</i>)-yl) acetamido)-3-phenylpropanoate (ABPO-Br/Cl)	99
Scheme 4:	Synthesis of 2-[2-(5-bromo/chloro-2-oxo-benzoxazol-3-yl)-acetylamino]-4-methylsulfanyl-butyrac acid methyl ester (ABMO-Cl/Br)	100

ABBREVIATIONS

%	:	Percentage
%LE	:	Percentage Labelling Efficiency
2-D	:	Two-Dimensional
3-D	:	Three Dimensional
ANC	:	30 kDa Adenine nucleotide carrier
BBB	:	Blood brain barrier
CADD	:	Computer Aided Drug Design
CNS	:	Central Nervous System
CO ₂	:	Carbon Dioxide
CT	:	Computed Tomography
CDCl ₃	:	Deuterated Chloroform
D ₂ O	:	Deuterated Oxide
CD ₃ OD	:	Deuterated Methanol
DMSO- <i>d</i> ₆	:	Deuterated Dimethylsulfoxide
DBT	:	Diazepine binding inhibitor
DMEM	:	Dubecco's modified Eagle medium
EDTA	:	Ethylenediaminetetraacetic acid
ENP	:	Eicosa neuro peptide
ESI	:	Electron Spray Ionization
FBS	:	Fetal Bovine Serum
FDA	:	Food and Drug Association
G _{solv}	:	Solvation energy
HAS/BSA	:	Human Serum Albumin/Bovine Serum Albumin
HPLC	:	High Performance Liquid Chromatography
HTVS	:	High throughput virtual screening
i.v.	:	Intravenous
ITLC-SG	:	Instant Thin Layer Chromatography-Silica Gel
K ₂ CO ₃	:	Potassium Carbonate
LCMS	:	Liquid Chromatography-Mass Spectroscopy
MM-GBSA	:	Molecular mechanics-generalized Born and surface area
MRI	:	Magnetic Resonance Imaging
MS	:	Multiple Sclerosis
MTT	:	3-(4,5-Dimethylthiazole-2-yl)-2,5-diphenyl-2H-tetrazolium bromide

NaHCO ₃	:	Sodium Bicarbonate
NMR	:	Nuclear Magnetic Resonance
ODN	:	Octadecaneuro peptide
PAP7	:	Protein kinase A associated protein 7
PBS	:	Phosphate Buffer Solution
PDB	:	Protein Data Bank
PET	:	Positron Emission Tomography
rCBF	:	Regional cerebral blood flow
RCSB	:	Research Collaboratory of Structural Bioinformatics
RMSD	:	Root Mean Square Deviation
SASA	:	Solvent accessible surface area
SBDD	:	Structure Based Drug Design
SP	:	Standard precision
SPECT	:	Single Photon Emission Computed Tomography
StAR	:	Steroidogenic acute regulatory protein
TBI	:	Traumatic brain injury
TLC	:	Thin Layer Chromatography
TSPO	:	18 kDa Translocator protein
TTN	:	Triakonta tetra neuro peptide
UV	:	Ultraviolet
VDAC	:	32 kDa Voltage-dependent anion channel
WBC	:	White blood counts
XP	:	Extra precision
XP/SP	:	Extra Precession/Standard Precession
NFT	:	Neuro fibrillary tangles
FTLD	:	Frontotemporal lobar degeneration
IT	:	Isomeric transition
ITLC-SG	:	Instant thin layer chromatography- Silica gel
EAF	:	Experimental animal facility
CPCSEA	:	Committee for the purpose of control and supervision of experiments on animals
TOF	:	Time of flight
PIB	:	Pittsburgh Compound-B
DOPA	:	Dihydroxyphenylalanine
FES	:	Fluoroestradiol

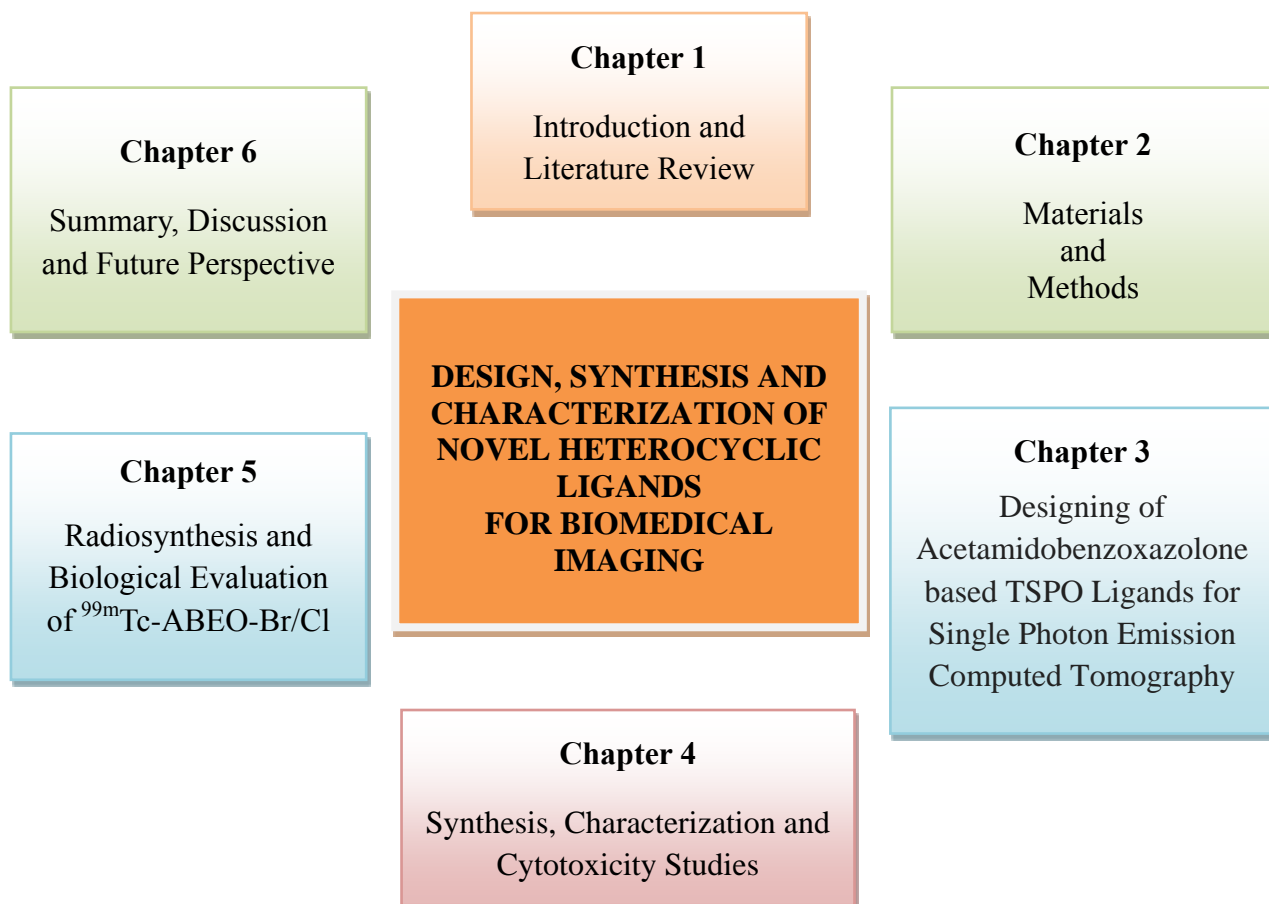
MISO	:	Fluoromisonidazole
FAZA	:	Fluoro-azomycin- α -arabinoside
FDG	:	fluoro deoxy-glucose
HBG	:	Hydroxymethyl-butyl guanine
mAb	:	Monoclonal antibodies
ASTM	:	American Society for Testing and Materials
RGD	:	Arginyl-glycyl-aspartic acid
MW	:	Molecular weight
FP-CIT	:	Ioflupane
MIBG	:	Meta-iodobenzylguanidine
HyNIC-TOC	:	Hydrazinonicotinyl-Tyr ³ -Octreotide
CZT	:	Cadmium zinc telluride
CNS	:	Central Nervous System
PD	:	Parkinson's disease
EDDA	:	ethylenediamine diacetic acid
AD	:	Alzheimer's disease
D ₁ -D ₅	:	Dopamine receptor subtypes
5HT	:	Serotonergic receptor
nAChRs	:	Nicotinic acetylcholine receptors
mAChRs	:	Muscarinic acetylcholine
FLT	:	3'-deoxy-3'-[¹⁸ F]fluorothymidine
ADC	:	Apparent diffusion coefficient

LIST OF SYMBOLS AND UNITS

Mm	:	Millimeter
γ	:	Gamma
$^{\circ}$:	Degree
\AA	:	Angstrom
pH	:	Protonation constant
λ	:	Wavelength
ν	:	Frequency
Hz	:	Hertz
nm	:	Nanometer
kcal	:	Kilocalorie
L	:	Litre
mol	:	Number of moles
cm	:	Centimeter
kDa	:	Kilodalton
gm	:	Gram
h	:	Hour
α	:	Alpha
β	:	Beta
keV	:	Kilo electron volt
y	:	Year
M	:	Molar
mmoles	:	Millimoles
mg	:	Milligram
μL	:	Microlitre
min	:	Minute
δ	:	Chemical shift
ppm	:	Parts per million
t_R	:	Retention time
Kg	:	Kilogram

MBq	:	Mega becquerel
ID	:	Injected dose
$t_{1/2}$:	Half life
IC ₅₀	:	50% inhibited concentration
μ M	:	Micromolar
$^{\circ}$ C	:	Degree centigrade
dl	:	Decilitre
mEq/l	:	Milliequivalent/litre
s	:	Second
h	:	Hour
mL	:	Millilitre
%	:	Percentage
rpm	:	Rotation per minute
Cps/Bq	:	Counts per second/Becquerel
mSv	:	Millisievert
B _{max}	:	Maximum number of binding sites
Pmol/g	:	Picomoles/gram
v/v	:	Volume/volume
%ID/g	:	Percentage administered dose per gram
μ Ci	:	Microcurie
Log P	:	Partition coefficient
SA	:	Specific activity
N	:	Number of atoms
mol	:	Number of Moles

OVERVIEW OF THESIS



Chapter 1
Introduction and Literature Review

CHAPTER 1

INTRODUCTION AND LITERATURE REVIEW

1.1 Radiation

1.1.1 History

In 1896, there was a phenomenal discovery of the nuclear radiation by Antoine Henri Becquerel that led to the development of its diverse applications ranging from atom bomb to nuclear medicine. He named the natural radiations emitted by uranium radionuclide as “U-rays”. In the following years, Pierre and Marie Curie contributed significantly in the discovery of radioactivity and radioactive isotopes. Marie Curie demonstrated radioactive nature of thorium like uranium. In 1898, Pierre and Marie Curie successfully isolated polonium, a new material which was a million times more radioactive than uranium. Several tons of pitchblende ore was used by Pierre and Marie to extract few milligrams of radium, a new material with 2.5 million times more radioactive than uranium. In 1933, Irene Curie and Frederick Joliot, discovered artificial radioisotopes (Froman 1996).

First ever application of radioisotopes in biology was rationalized by George Hevesy. In 1935, he first used radiophosphorus in rats for metabolic studies. This was beginning of use of trace amount of radioisotopes to study physiological functions and to treat diseases in animals and humans (Hevesy 1939).

In the last 40 years, a new area of medical research for diagnosis has flourished by using metal complexes. By the end of World War II, nuclear technology for medical purposes

was in use and radioisotopes were produced for medical purpose through nuclear reactors, accelerators and cyclotrons. In 1946, ^{131}I was the first isotope used as medicine for the treatment of cancer (thyroid). In 1959, $^{99}\text{Mo}/^{99\text{m}}\text{Tc}$ generator was developed by Brookhaven National Laboratory, New York, USA and in 1964, $^{99\text{m}}\text{Tc}$ was used for first time in tracers by Argonne National Laboratory, Lemont, USA. In the current scenario, $^{99\text{m}}\text{Tc}$ is a radio nucleotide with wide utility for diagnostic application and development of its pharmaceuticals has started the study of coordination chemistry for diagnostic imaging (Morais *et al.*, 2012; Liu and Edwards 1999).

1.1.2 Interaction between radiation and matter

Radiations are either particulates such as α and β particles, or non-particulate such as X-rays and γ -rays, and are of ionizing nature that interacts with matter through different modes.

1.1.3 Interaction between charged particles and matter

When energetic charged particle passes through matter, there is a loss of energy due to interaction with the electrons in the orbital of the matter's atoms. This encounter ionizes the atoms through electron's ejection or excites atoms through electron's movement to a higher state of energy. These processes of ionization and excitation may rupture chemical bonds of the molecules forming other molecules.

β -particles which are lighter in weight with charge move in zigzag form and the α particles like heavier moieties move in straight line. The traversed straight path of

charged particle is called as range R. This increases with increase in energy and charge, and decreases with increase in matter density and particle mass.

The positrons pass through an absorber demonstrate a unique situation of loss in their energy through combination of electrons of the atoms of the absorber resulting in annihilation of both antiparticles producing two photons emitted in opposite directions.

1.1.4 Interaction between γ -radiation and matter

γ -radiation are considered as radiation with high-frequency in electromagnetic radiation spectrum which uses different mechanisms such as photoelectric effect, Compton effects, and pair production for the interaction with matter (Nikjoo, 2012).

1.2 Molecular imaging

The developments in the field of genomics and molecular biology in the previous decades provided better insight of diseases, resulting in specific targeting of abnormal molecular pathways for new diagnostic and therapeutic strategies (Williams 2008; Willmann *et al.*, 2008). Although several drugs can have therapeutic effect by stopping or modulating molecular processes which is still based upon late symptoms like size of the tumor, the development of diagnostic process at molecular level could facilitate early stage detection and effective therapeutic assessment. Furthermore, molecular diagnostic techniques can assist the new therapeutic development. In the long run, the development of molecular therapy or diagnosis could enable prevention

or cure of diseases at early stage through assessment of disease-specific molecular information (Weissleder 2006; Weissleder and Pittet 2008; Massoud and Gambhir 2003).

Molecular imaging aims to develop specific molecules for the molecular target to enhance image contrast. All imaging techniques used for diagnosis, like ultrasound, magnetic resonance imaging, optical imaging and nuclear imaging can be applied for molecular imaging purpose. A comparative table for their primary uses and instrumental features are shown in Table 1.1.

Table 1.1: Features of imaging modalities

Sensitivity	Modality	Resolution (Temporal)	Resolution (Spatial)	Penetration depth	Type of radiation	Primary uses
nM	Nuclear					
	SPECT	min	Preclinical: 1-2 mm Clinical: 8-10 mm	Limitless	Ionizing	Protein labelling
	PET	sec-min	Preclinical: 1-2 mm Clinical: 5-7 mm	Limitless	Ionizing	Drug development, gene expression
μ M	MRI	min-h	Preclinical: 25-100 μ Clinical: ~1 mm	Limitless	Non ionizing	Central Nervous System (CNS), prostate, heart, breast
	Ultrasound	sec-min	For superficial: 0.01-0.1 mm (few mm depth) For deeper: 1-2 mm (few cm depth)	mm-cm	Ionizing	Drug delivery, gene transfection
	CT	min	Preclinical: 50-100 μ m Clinical: 0.5-1 mm	Limitless	Ionizing	Bone, blood vessel, soft tissues

Modern imaging technologies are increasingly facilitating measurement of physical parameters like concentration, surface area, properties of tissues and insight in biological functions. Molecular probe can be either for diagnostic or for therapeutic applications. The advancement of spatial and temporal resolution has facilitated the monitoring of protein and substrate dynamics. The validation of model created is possible through segmentation and registration for imaging at different times to identify the region of interest and its acquisition. These time series data are useful for validating system biology models which along with imaging provides understanding of biological systems. With the wide use of imaging tools and understanding of biological processes, systems biology models will be more productive. This is further assisted by computational science and imaging science.

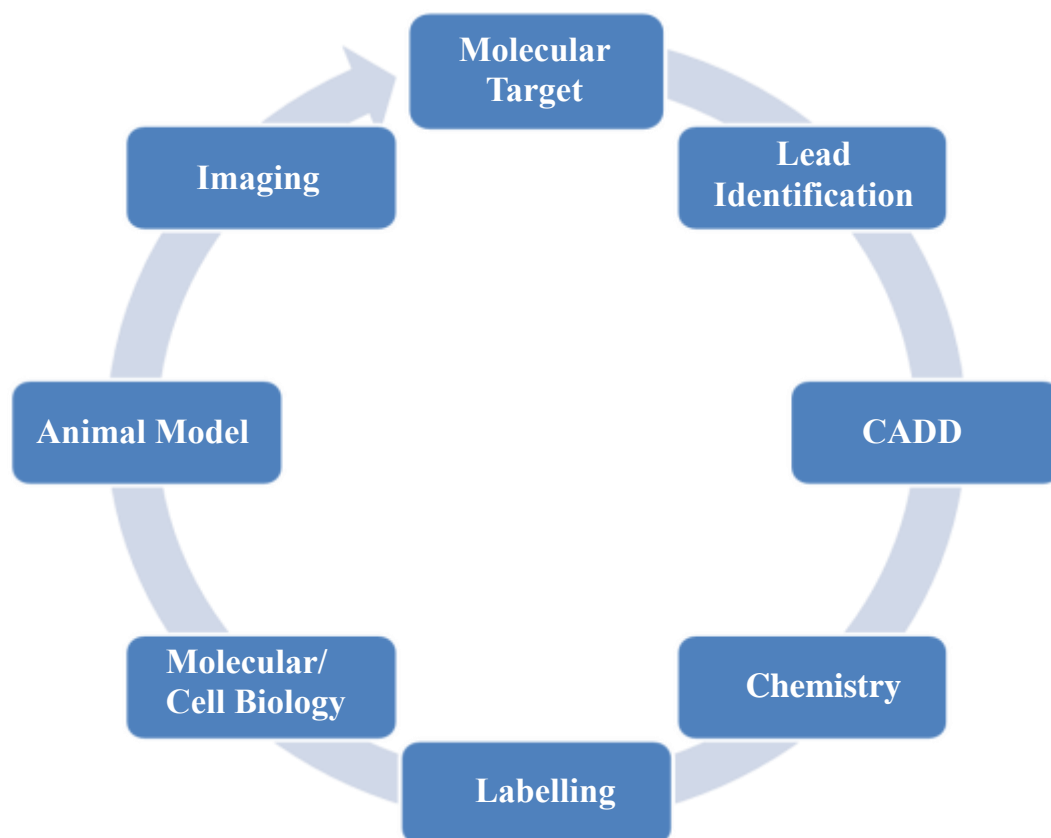


Fig. 1.1: Schematic of main steps involved in molecular imaging

Molecular imaging in addition to anatomical imaging gives various opportunities for the process of more efficient drug development and therapy. Various non-invasive molecular imaging techniques enable quantitative imaging for preclinical and clinical application along with validation of new molecules. The steps involved in development of molecular imaging ligands is shown in Fig.1.1 which starts from molecular target identification, computational screening, wet chemistry, and their tagging/complexation before biological (*in vitro* & *in vivo*) evaluation.

1.2.1 Principles of molecular imaging

At early stage, there are several pathological features demonstrated in diseased cells. There could be mutation in gene or variation in gene expression resulting in up/down-regulation of related molecule. Quantification and detection of these molecules directly or through targeted agents result in imaging of molecules.

Generally, detection of molecular target is possible through two ways of targeted agents' interaction. First one is through selective binding of a targeted agent with the molecular target as in case of cell receptor. There is same concentration of agent as receptor once the contrast agents which are not bound are cleared resulting in determination of receptor density through imaging. Second one is entrapment of contrast agent such as enzymes for its internalization in cells. This is advantageous as an enzyme can entrap various targeted agents through this mechanism. The imaging targets are defined on the understanding of the disease on the scientific basis. In few cases, targets as well as their suitable ligands can be available in literature. In order to

find the biomarkers i.e. molecules that are up or down regulated in diseased condition, high-throughput screening techniques can be utilized by incorporating genomic and proteomic data. As several diseases have involvement of genes and proteins which are influenced by genetic, environmental and immune factors. The dynamic process of varying concentration of biomarkers reflects different stages of diseases.

The availability of specific targets is key aspect to develop diagnostic and therapeutic agents. Currently, there is availability of drugs for around 500 molecular targets involving receptors (45%) and enzymes (30%). There are more than 5,000-10,000 drug-targets available for future drug development. In general, imaging agents should have proper target-ligand interaction as well as its suitable physicochemical properties.

Molecular imaging has enhanced the visualization in real time and non-invasive investigation of complex biochemical processes at the molecular and cellular level in living system. Broadly, sophisticated bio-instruments with or without imaging agents have shown prospects for diagnosis, monitoring of therapy, and drug discovery by understanding of biological processes, identification of pathological regions and insight of disease related mechanism.

1.2.2 Selection criteria of imaging modalities

The use of an appropriate modality dependent on the type of imaging data required and the biochemical process needs to be visualized. The factors considered for selection of modality are as follows:

- Requirement of spatial resolution
- Level of sensitivity
- Need of dynamic information
- Whether whole body or small region imaging
- Requirement of temporal resolution
- Whether depth of penetration important
- Requirement of quantitative data
- Requirement of repeated or multiple studies
- Requirement of multiple molecular targets' visualization simultaneously
- Whether clinical translation required

1.2.2.1 Computed tomography (CT)

CT produces anatomical image on the basis of tissues' differential attenuation of X-ray inside the body.

Basic principles of CT

CT produces 3D anatomical images with the help of imaging by sections i.e tomography. This makes it different from traditional X-ray. The X-ray source and detector both can simultaneously rotate around the subject. During scan, strongly and poorly absorbed X-rays tissues or media appear white and black, respectively. This displays detailed morphological information with the help of high-contrast images. Software is used for interpretation of efficient scan. A contrast agent with iodine is often used for CT imaging that improves soft tissue contrast and spatial resolution.

CT has been found useful in assessing several medical conditions such as brain injury (Dubroff and Newberg 2008), tumors (Vlychou and Athanasou 2008) and ischemia (Mallo *et al.*, 2005). Miniaturized and cost-effective CT scan is also available for preclinical research on animals which allows real time assessment for various diseases and response to therapy.

Key strengths and limitations

Fast acquisition time, high spatial resolution, relative simplicity, clinical utility, availability, and cost effectiveness are few of the advantages of CT. Due to relatively high energy of X-rays, it can penetrate through the body. High radiation exposure in case of CT is one of the main limitations for limiting the number of scan on the same patient in a given duration. Additionally, its tissue contrast quality is low.

1.2.2.2 Magnetic resonance imaging (MRI)

MRI, a versatile modality for imaging, is utilized to visualize soft tissue morphology and internal structure of the body using powerful magnet and radio frequency. The basic principles of MRI and Nuclear Magnetic Resonance (NMR) are similar allowing atomic nuclei imaging of the body.

Basic principles of MRI

The MR signal depends on gyromagnetic ratio, concentration of nuclei, polarization, magnetically active isotope and its abundance. ^1H being most abundant is the most common nucleus for MRI in clinical application. Hydrogen of water in tissues with 80 Molar concentrations in body is used for anatomical imaging. The other nuclei of interest are ^{31}P , ^{13}C , ^{23}Na , ^{19}F and ^{17}O whose imaging is achieved through Magnetic

Resonance Spectroscopy i.e. MRS. The advent of MRS with hyper-polarization has led to significant advances in imaging of these nuclides. Some of the important parts of MRI are coils for homogeneous magnetic field, gradient coils to produce variations in the X, Y, and Z directions for localizing the source of the magnetic signal, and RF coils to alter the magnetic dipoles' alignment. Post RF pulse, magnetic dipoles shift from equilibrium and relaxes back through longitudinal (spin-lattice) and transverse (spin-spin) relaxation and the different time taken in relaxation for each tissue results in the generation of contrast of that tissue (Faulkner 1996).

Some specialized MRI techniques can provide physiological information along with anatomical information with different variaents of MRI such as BOLD (blood oxygen level dependent), DCE (dynamic contrast-enhanced), and DW (diffusion weighted). MRI contrast agents produce disturbance in magnetic field through their presence to enhance the contrast. The common DCE-MRI contrast agents are Gd complexes (Padhani and Husband 2001), and super paramagnetic iron oxides (SPIOs) (Thorek *et al.*, 2006) which are positive (shortens the relaxation time, T_1) and negative contrast agents (shortens the relaxation time, T_2), respectively. DCE-MRI can have application for imaging of tumor (Turkbey *et al.*, 2009) and rheumatoid arthritis (Hodgson *et al.*, 2007).

Diffusion weighted (DW) MRI can detect the apparent coefficient of diffusion of water present in tissue that measures cellularity through molecular water movement in the interstitial space, showing high apparent diffusion coefficient (ADC) for low

cellularity and vice versa. Diffusion weighted imaging (DWI) can have application in diagnosis as well as maintenance of various pathological states such as tumor and ischemic stroke.

Blood-oxygen-level dependent (BOLD) imaging, a functional MRI (fMRI), is extensively used for studying normal and diseased brain. It is based on alteration in deoxygenated haemoglobin which is endogenous and paramagnetic. Oxyhemoglobin does not have paramagnetic behaviour. Therefore, presence of oxyhemoglobin results in more intense image in T_2 weighted images and could be applied in assessing increased activity of neuronal region of brain and in brain functions like memory. (Ziemus *et al.*, 2007; Azulay *et al.*, 2009), cognition (Fink 2004), and depression (Siegle *et al.*, 2007). Usefulness of BOLD is in measurement of deoxyhemoglobin differences in organs such as kidney and oxygenation level in red blood cells in perfused tumor.

Although availability of specialized MRI techniques provides important physiological information, but they have limitation of being relatively non-specific and are not able to provide receptor/biochemical information. To overcome this limitation Gadolinium (Gd) based complexes for molecular imaging were developed but they have limitations in terms of quantification and sensitivity. Recently, CEST (chemical exchange saturation transfer) (De Leon-Rodriguez *et al.*, 2009) and PARACEST (paramagnetic-chemical exchange saturation transfer) (Zhang *et al.*, 2003) contrast agents have been explored to probe specific molecular and physiological events. They

are promising agents but they are at their early stage of development. The other advancement in MRI contrast agent is targeted contrast agents to visualize markers at molecular level and their biochemical events. Few specific examples are SPIOs with specific peptide for matrixmetalloprotease-2 and Gd containing liposome for $\alpha_v\beta_3$ integrin imaging.

Key strengths and limitations

MRI is advantageous over other modalities for imaging in terms of penetration depth, high spatial resolution, use of non-ionizing radiation, superior tissue contrast than CT imaging, concurrent collection of metabolic and physiological data with anatomical images, molecular information through MR contrast agents and excellent clinical utility.

However, it is an expensive technique with poor sensitivity as compared to other modalities used for molecular imaging and temporal resolution. The poor sensitivity leads to the requirement of large amount of imaging agents which could be problematic due to toxicity and/or likely change in biological system through pharmacological effects. In spite of not having favourable sensitivity and being relatively expensive, MRI has revolutionized the medical diagnosis and basic research.

1.2.2.3 Nuclear medicine modalities (PET & SPECT)

Nuclear properties of radioactive nuclides are utilized in nuclear medicine for diagnosis to evaluate anatomical and physiological conditions and/or treat using radioactive sources. It has gained universal acceptance as a powerful discipline for non-invasively diagnose the diseases since it not only finds out the location and size

of the lesion but also evaluates its functional status. Nuclear medicine incorporates the use of radiopharmaceuticals, both for diagnostic as well as therapeutic applications.

A radiopharmaceutical which is used as an imaging agent must give a better visual representation of the target tissue with least radiation exposure to the non-target tissues. The main objective of developing an imaging agent thus lies in selective localization of target coupled with its fast clearance from the body.

Among the various clinical syndromes where nuclear medicine paved its way, neurology, cardiology and oncology have been nourished the most by this field.

1.2.2.3.1 Tomographic imagers

A basic limitation of the scintillation camera is depiction of three dimensional activity distributions in two dimensional forms. The third dimension structure and depth are underlying and overlying which makes its understanding difficult. This problem can be partially solved through image capture from various angles. This strategy was not very successful due to complex environment of region to be diagnosed.

In present scenario, techniques of tomography are applied for delineation of the imaging object's depth using rigorous mathematical algorithms for reconstruction of the images at different slices (Saha & Saha, 2004).

1.2.2.3.2 Positron emission tomography (PET)

PET can image the functional aspect to study the physiological, biochemical and pharmacological process in vivo. A chemical structure designed to bind biological molecule of interest is labelled with an isotope which can emit positron i.e. ^{11}C , ^{18}F , ^{13}N , ^{15}O , ^{82}Rb and ^{68}Ga . In principle, it is possible to label the majority of natural substrates that are chemically not distinguishable from their unlabeled counterpart as oxygen, carbon and nitrogen are included in most organic molecules. In practice, the brief physical half-life of PET isotopes can make the radiosynthesis difficult.

Basic Principle of PET

β^+ emitted by decaying nucleus collides with an e^- of a nearby atom after travelling a short distance. The emitted positron loses its kinetic energy in matter mostly by exchanging energy with electrons that causes ionizations and excitations in a similar manner to that of a normal electron. Consequently, the distance travelled by a positron depends on its energy. Positron stops and combines with ordinary electron of nearby atom, forming positronium as an intermediate.

On interaction of a positron with an electron, annihilation turns the mass into two 511 keV gamma-rays energy which emit at 180° apart, escaping from the body. These photons are recorded by external detectors for imaging purpose.

As an annihilation radiation consists of two photons of 511 keV emitted simultaneously and travelling co-linearly in opposite directions, it provides a special detection method called coincidence detection. (Fig 1.2) The basis of detection is that two detectors placed on each side of annihilation point may register these photons

reaching the detector crystal almost simultaneously. The registered coincidence means that a positron has been emitted somewhere between the two detectors on a line. The PET camera has several coincidence detectors arranged in rings and connected to a computer for data collection (Wernick and Aarsvold 2004). The reconstruction of data by computer will yield a description of distribution of the radioactivity.

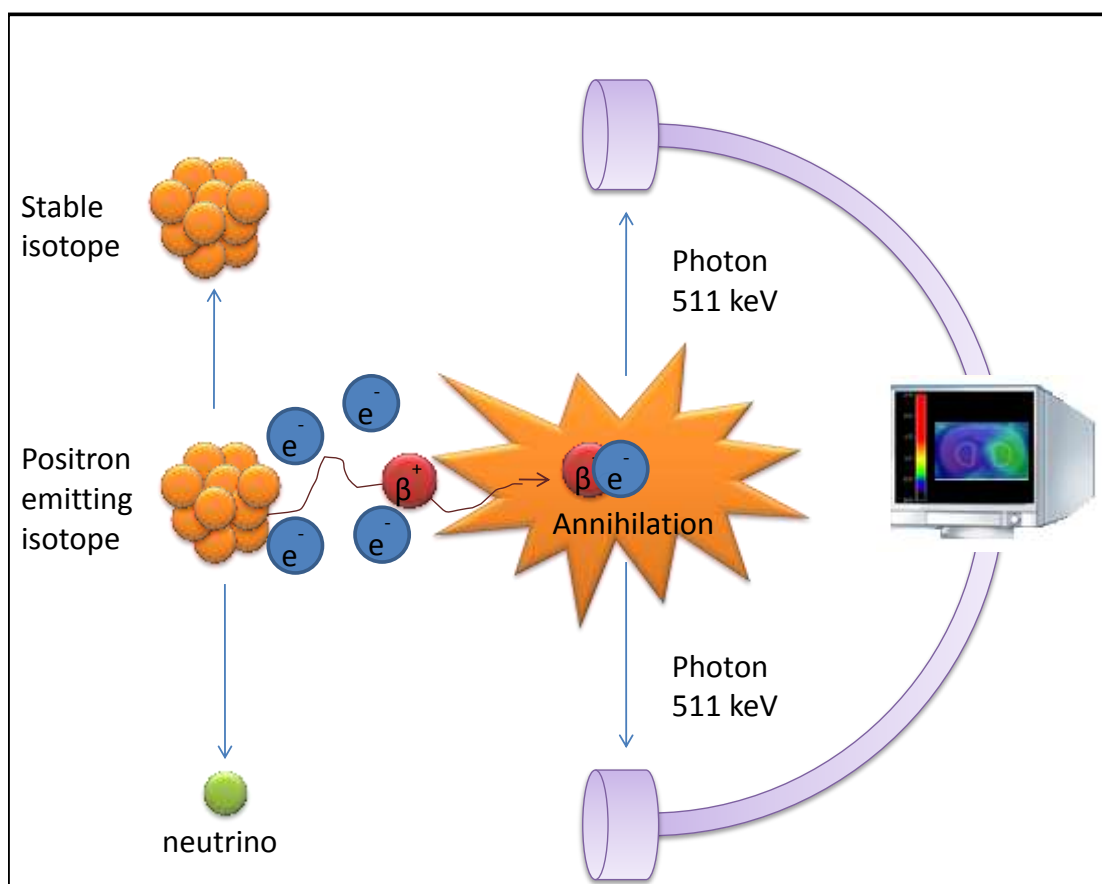


Fig. 1.2: In vivo principle/function of PET isotope

NaI(Tl), GSO (gadolinium oxyorthosilicate), LYSO (lutetium yttrium oxyorthosilicate), LSO (lutetium oxyorthosilicate), or BGO (bismuth germinate) are primarily used to make detectors. PET system consists of multiple detectors having rings with different shapes like circle, octagon or hexagon and 2 to 8 in number. There are two detector attached

opposite to each other to simultaneously acquire coincidence signals from several slices of the person. Another variety of camera named dual head camera can be used in PET as well as in SPECT having two detectors that rotates. The coincidence data acquisition takes place in PET and collimators are utilized in SPECT.

Sensitivity of PET

The PET sensitivity depends on two types of efficiencies: detection and geometrical. The PET differs with SPECT in terms of involvement of two coincidence detectors with no collimator. The sensitivity of the PET is dependent on the intrinsic efficiency of critical component in the detector material. In terms of geometric efficiency, PET is more efficient than SPECT due to the larger coverage of the total space angle through single and multi-detector rings. In addition to this, more γ rays in PET can be detected due to their higher energy (511 keV) leading to less relevant tissue absorption. For a source with small volume, the overall sensitivity of PET systems is 0.005 cps/sec and upto 0.1 cps/Bq for a single ring system and 3-D acquisition in a multi ring system, respectively.

The signal to noise ratio (SNR) can also be improved by measuring and exploiting the gap in times of arrival of γ rays. This PET technique with time-of-flight (TOF) locates the event having emission within 4-10 cm. The statistical uncertainty can be reduced in the reconstructed image by including this information with a higher signal to noise ratio, which could be higher than that of conventional PET (Phelps 2000).

Although there is large number of positron emitting radionuclide available, only a few of them qualifies for PET application.

Table 1.2: Main physical characteristics of medically important PET isotopes

Isotopes	Half life (min)	Maximum positron energy (keV)	% of positron decay
^{11}C	20.4	970	99.8
^{13}N	10.0	1190	100
^{15}O	2.05	1720	99.9
^{18}F	109.7	635	97
^{68}Ga	67.8	1899, 821	87.7, 1.2
^{82}Rb	1.3	3378, 2601	81.8, 13.1
^{64}Cu	12.7 h	653	17.5

Both PET and SPECT can generate 3-D images detecting activities at molecular level which are complimented through structure produced from CT or MRI (Halldin *et al.*, 2001).

PET radiopharmaceuticals

Table 1.3: Examples of PET radiopharmaceuticals

$[^{11}\text{C}]$ -PET Radiopharmaceutical	Applications in clinics
1. ^{11}C -acetate	Cancer (Grassi <i>et al.</i> , 2012)
2. ^{11}C -choline	Cancer (Reske <i>et al.</i> , 2006)
3. ^{11}C -methionine	Parathyroid, lymphoma, neuroblastoma (Singhal <i>et al.</i> , 2008)
4. ^{11}C -PIB	Alzheimer's disease (Rabinovici <i>et al.</i> , 2007)
5. ^{11}C -raclopride	Parkinson's disease (Hirvonen <i>et al.</i> , 2003)
6. ^{11}C -palmitate	Viability of myocardia (de Jong <i>et al.</i> , 2009)
7. ^{11}C -O-methyl-L-tyrosine	Breast cancer chemotherapy monitoring in research (Ishiwata <i>et al.</i> , 2004)
8. ^{11}C -PK11195	Alzheimer's disease, multiple sclerosis, Huntington's disease (Dupont <i>et al.</i> , 2017)
9. ^{11}C -Flumazenil	Cerebrovascular disease, anxiety, epilepsy (Froklage <i>et al.</i> , 2012)
10. ^{11}C -nicotine	Alzheimer's disease (Kadir <i>et al.</i> , 2006)

[¹⁸F]-PET Radiopharmaceutical	
1. ¹⁸ F-fluoroDOPA	Neuroendocrine tumors and Parkinson's disease (Morrish <i>et al.</i> , 1998)
2. ¹⁸ F-fluoride	Bone metastasis (Ramos 2015)
3. ¹⁸ F-FES	Cancer (Dixit <i>et al.</i> , 2013)
4. ¹⁸ F-FLT	Cell proliferation (Bollineni <i>et al.</i> , 2016)
5. ¹⁸ F-FMISO	Hypoxia imaging (Rajendran and Krohn 2015)
6. ¹⁸ F-fluoromethylcholine	Cancer (Brogsitter <i>et al.</i> , 2013)
7. ¹⁸ F-FAZA	Hypoxia (Zheng <i>et al.</i> , 2015)
8. ¹⁸ F-FDG	Cancer (Petriev <i>et al.</i> , 2016)
9. ¹⁸ F-FHBG	Receptor gene therapy (Min and Gambhir 2008)
10. ¹⁸ F-Galacto-RGD	Cancer (Beer <i>et al.</i> , 2005)
[¹³N]-PET Radiopharmaceutical	
¹³ N-ammonia	Myocardial perfusion (Beer <i>et al.</i> , 2006)
[¹⁵O] PET Radiopharmaceutical	
¹⁵ O-oxygen	Oxygen metabolism (Herzog <i>et al.</i> , 2009)
¹⁵ O-carbon monoxide	Blood volume (Frackowiak <i>et al.</i> , 1980)
¹⁵ O-carbon dioxide	Blood flow (Iida <i>et al.</i> , 1995)
¹⁵ O-water	Blood flow (Kaufmann <i>et al.</i> , 1999)
[¹²⁴I] PET Radiopharmaceutical	
¹²⁴ I-G250-mAb	Cancer (Lin <i>et al.</i> , 2015)
[⁶⁴Cu]-Radiopharmaceutical	
[⁶⁴ Cu]-ATSM	Cancer (Lewis <i>et al.</i> , 2008)

1.2.2.3.3 Single photon emission computed tomography (SPECT)

SPECT utilizes gamma rays for imaging which is capable of providing 3-D information. Gamma camera captures SPECT images that capture several 2-D images from various angles. Thereafter, 3-D dataset is obtained by applying algorithm of a tomographic reconstruction on multiple projections using computer. This data set may demonstrate thin slices of the body along any axis similar to tomographic images from other imaging techniques like MRI, CT and PET.

SPECT radiotracers are gamma emitting isotope containing small molecules with molecular weight < 2000. Radiopharmaceuticals for SPECT are developed through incorporation of clinically useful SPECT radioisotopes into molecules that can reach the target with selectivity and specificity. In general, SPECT isotopes emit gamma energy of medium value (100 to 400 keV) with suitable physical half-lives as mentioned in Table 1.4. Out of these, the most commonly utilized isotopes are ^{99m}Tc and ^{123}I .

There are several reactions which have radio-iodination such as oxidative iodination and aniododestannylation. Availability of ^{123}I is a major drawback for using its compounds in routine due to requirement of cyclotrons or accelerators. In contrast, ^{99m}Tc is a commonly used radionuclide in nuclear medicine which has various advantages such as favourable physical characteristics, suitable half-life ($t_{1/2} = 6.02$ h), a gamma ray emitter with 140 keV energy and wide availability due to production through $^{99}\text{Mo}/^{99m}\text{Tc}$ generators and easy preparation procedures for various ^{99m}Tc based radiopharmaceuticals through simple kit formulations.

Table 1.4: Main physical characteristics of medically important SPECT isotopes

Radionuclide	Half life	Energy (in keV)	Decay mode
^{99m}Tc	6.02 h	140	Isomeric Transition (100%)
^{131}I	8.03 d	364	β^- (100%)
^{123}I	13.22 h	159	Electron Capture (100%)
^{111}In	2.8 d	171	Electron Capture (100%)

Mode of action

In SPECT, there is an accumulation of injected radiopharmaceuticals in suspicious part of the body. When radionuclide decay happens, there are emissions of gamma rays in all directions. In the body, there is scattering and attenuation for some gamma rays. These gamma rays are captured using a gamma camera rotating around the patient. The basic gamma camera has collimator, scintillation crystal and several photomultipliers. The collimator captures gamma rays at 90° angle trajectory to the plane of detector and blocks rest. There are lead walls in honeycombed array of holes to prevent gamma rays' penetration from one hole to another. Mostly parallel-hole collimator is used. The magnification of object size in image can be the purpose of using other types of collimators. A pinhole collimator is converging collimator that allows magnification of closely placed objects of small size. The low efficiency of gamma ray utilization is major disadvantage of collimators.

The collimator converts passing gamma rays into a detectable signal which is detected through detector usually made of thallium doped single sodium iodide crystal. On striking the scintillation crystal, there is a loss of energy of gamma ray due to photoelectric interactions and light emission thereafter. The photomultipliers are coupled with the scintillation crystal to produce electrical signal from light signal. Anger position network is used for the positioning of the scintillation based on outputs of the relative signal of the photomultipliers.

In SPECT, the spatial resolution is dependent on several aspects. The intrinsic resolution of scintillator-photomultiplier is around 3 mm, collimator is the limiting factor for the practical resolution of the gamma cameras. However, the spatial resolution of SPECT in clinics is in the range of about 1-2 cm which is dependent on

collimator type and distance between collimator and gamma ray source. In animal systems, resolution is about <3 mm and pinhole collimators type of special collimators are used.

The commonly used SPECT systems consist of one to three NaI(Tl) detector head containing gamma camera, computer for online data acquisition and processing along with a system for display. The rotation of detector head is at small angle increments (3° to 10°) for 180° or 360° angular sampling around the patient's long axis. The data are stored in the computer in a 64×64 or 128×128 matrix which is utilized to reconstruct the slice of interest i.e. images of plane. The collected data can be used to reconstruct transverse, sagittal, and coronal images (Khalil *et al.*, 2011).

SPECT radiopharmaceuticals

Table 1.5: Examples of SPECT radiopharmaceuticals

^{123}I- radiopharmaceutical	
1. ^{123}I -FP-CIT	Parkinson's disease (Benamer <i>et al.</i> , 2000)
2. ^{123}I -CLINDE	Alzheimer's disease, Multiple Sclerosis, Huntington's disease (de Vries <i>et al.</i> , 2006)
3. ^{123}I -MIBG	Heart failure, cardiac sympathetic dysfunction (Miyamoto <i>et al.</i> , 2008)
$^{99\text{m}}\text{Tc}$-Radiopharmaceutical	
1. $^{99\text{m}}\text{Tc}$ -TRODAT	Parkinson's disease, depression (Huang <i>et al.</i> , 2001)
2. $^{99\text{m}}\text{Tc}$ - EDDA/HyNIC-TOC	Cancer (Lin <i>et al.</i> , 2015)
3. $^{99\text{m}}\text{Tc}$ -Annexin V	Apoptosis, cancer, cardiovascular risk, transplant rejection (Kuge <i>et al.</i> , 2004)
4. $^{99\text{m}}\text{Tc}$ -Rituximab	Cancer (Wang <i>et al.</i> , 2006)
^{111}In-radiopharmaceutical	
1. [^{111}In]-DOTAZ(HER2:342-pep2)-affibody	Cancer (Orlova <i>et al.</i> , 2007)
2. [^{111}In]-panitumumab-affibody	Cancer (Gong <i>et al.</i> , 2014)

Sensitivity of gamma-cameras (SPECT)

The higher absorption efficiencies can be achieved through the development of new detector crystals. A crystal with a large atomic number and a high density will be ideal for a high detection efficiency of γ ray. A high level of light output and a large optical transparency is a must for efficient light transmission. Another approach is the using semiconductor based detectors, such as CZT (cadmium zinc telluride), which can generate electronic signal from γ -ray. These solid-state type detections eliminate Compton-scattering to provide an improved resolution of energy.

Key strengths and limitations of PET and SPECT

These nuclear imaging modalities are advantageous over anatomical capturing modalities like MRI and CT as in disease, changes at biochemical level occur before changes at anatomical level. However, PET and SPECT are disadvantageous, due to non availability of anatomical frame of reference. Multimodality imaging combines the instrument of different modality to combine the strength of each modality and overcome the weaknesses of each modality. For example, PET/SPECT with CT/MRI can provide molecular and anatomical information in a single scan.

Additionally, radionuclide imaging techniques has safety aspect also. Both PET and SPECT use ionizing radiation limiting the number of scans per year through these modalities. The maximum exposure for the general public and radiation workers are 5 mSv per year and 50 mSv per year, respectively which is considered while planning of clinical studies.

The excellent sensitivity, quantitative capabilities, and limitless penetration depth are the key strengths of PET. In a nut shell, both modalities are very useful modalities to

investigate processes at molecular level in living beings and are used in clinics and in research for imaging diseased state and biological processes.

1.3 Type of radiopharmaceuticals

Radiopharmaceuticals can be divided into two classes of drugs: metal essential (integrated radiopharmaceuticals) and metal tagged (biomolecule-based radiopharmaceuticals).

In nuclear medicine, radionuclides are mostly used in various chemical compounds that are applicable due to their favourable physiological, biochemical and metabolic properties. In metal-based radiopharmaceuticals, the presence of a particular metal is essential for the desired biodistribution in body. Each metal complex has its unique distribution because of its affinity for particular receptors and distribution of those receptors in body or its unique biochemical and biophysical properties. A metal may be incorporated into bioligand without affecting its biochemical properties. This is called integrated approach for radiopharmaceutical preparation. (Fig. 1.3) In this approach, a metal is present in a part of ligand with high affinity towards receptor. There is minimal change in structure, shape, and size. Ideally not much effect on binding affinity of ligand should be there but it is a challenge to synthetically come up with such target molecule without compromising its binding affinity.

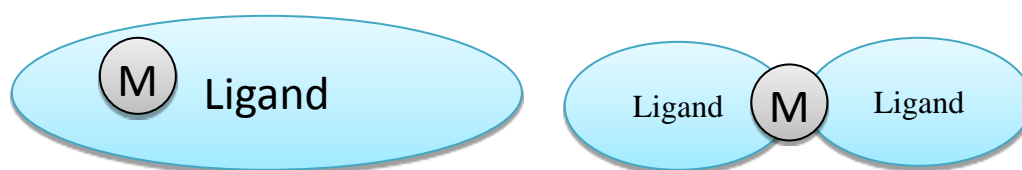


Fig. 1.3: Integrated or metal essential radiopharmaceuticals

Metal complexes of Technetium, Rhenium, Indium, Thallium, Chromium, and Gallium have been explored and some have been approved for clinical studies. Among these, Technetium complexes have been the most explored and maximum of the approved radiopharmaceuticals are from this metal. When the coordination property of the Technetium and its resultant complex decides the localization in biological system, the complex is called “technetium essential” radiopharmaceuticals. (Fig. 1.3) Technetium form complexes with various coordination geometries (IV-IX) and several ligand-types can coordinate with it. Therefore designing of specific ligand for ^{99m}Tc containing radiopharmaceuticals is possible. In certain cases, the ligand will have the properties of the complex defining its biological properties. For example, the technetium diphosphonate skeletal based imaging agents deposit on growing bone site due to diphosphonate’s high affinity towards bone which is growing actively.

1.4 PET molecular imaging agents for central nervous system

1.4.1 Imaging agents for the Dopaminergic Neurotransmission

The dopaminergic system is involved in various disorders of brain for example, Parkinson’s disease and Schizophrenia. There are five subtypes of dopamine receptor (D_1 - D_5) which are divided in two families (Jaber *et al.*, 1996; Seeman and Van 1994). D_1 family (D_1 and D_5) and D_2 family (D_2 , D_3 , and D_4). D_1 and D_2 subtypes are relatively more abundant in the striatum with B_{max} values being 50 and 20 pmol/g tissue, respectively making it better target for developing probes for molecular imaging. (Hall *et al.*, 1994) D_2 receptor was the first receptor which was visualized in human brain through PET agent with [^{11}C]-3-N-methylspiperone, a derivative of butyrophenone (Wagner *et al.*, 1984). However, butyrophenones lacks in sensitivity

which binds with D₂ receptor subtype as well as 5-HT₂ (subtype-2 of 5-hydroxytryptamine) receptors with high affinity. Also there is irreversible binding not allowing equilibrium studies. The derivative of other compound i.e. benzamide are relatively more selective as well as demonstrate binding in reversible manner. [¹¹C]-raclopride, a PET ligand of benzamide derivative, is widely utilized for investigating D₂/D₃ receptor subtypes in the patients of PD, HD and Schizophrenia (Farde *et al.*, 1986; Dewey *et al.*, 1993; Breier *et al.*, 1997; Nyberg *et al.*, 1998; Talbot and Laruelle 2002). Examples of structural analogues for visualization of D₂ subtype as PET agents using ¹⁸F and ¹¹C radionuclide are Fallypride (Mukherjee *et al.*, 1999) and FLB (Aalto *et al.*, 2005), respectively. For the assessment of D₁ receptor subtype, [¹¹C]-SCH23990 (Farde *et al.*, 1987) and [¹¹C]-NNC112 (Halldin *et al.*, 1998) are used. Currently, there is no PET radioligand available for the subtype D₃ and D₄.

There are ¹¹C and ¹⁸F labelled cocaine congeners such as [¹¹C]-PE21 (Francken *et al.*, 1998) [¹⁸F]-CFT (Laakso *et al.*, 1998), and [¹⁸F]-FECNT (Goodman *et al.*, 2000) developed for dopamine transporters (DATs) which is used in clinics to assess the altered DAT concentration in PD. DAT ligands are also developed for therapy in brain disorders.

1.4.2 Imaging agents for the Serotonergic Neurotransmission

The serotonergic system is implicated in several psychiatric and neurological disorders such as schizophrenia, AD, depression, and anxiety. There are 16 subtypes of receptor but imaging probes for PET are available for 5-HT_{1A} and 5-HT_{2A} subtypes. 5-HT_{1A} and 5-HT_{2A} are present in the hippocampus and neocortical of the brain in high concentration.

[¹¹C]-WAY100635 is highly selective for the subtype 5-HT_{1A} receptor in humans (Farde *et al.*, 1998; Rabiner *et al.*, 2001) which is used to demonstrate reduction in density of 5-HT_{1A} in case of major depression (Drevets *et al.*, 2000). The analogues of WAY100635 with fluorine are [¹⁸F]-p-MPPF (Passchier *et al.*, 2000) and [¹⁸F]-FCWAY (Carson *et al.*, 2000) are potential 5-HT_{1A} receptors' imaging probes. Some other probes for subtype are [¹¹C]-NAD-299 for 5-HT_{1A} (Sandell *et al.*, 2002) [¹¹C]-MDL100907 (Ito *et al.*, 1998), [¹⁸F]-Altanserin (Biver *et al.*, 1997), and [¹⁸F]-Setoperone (Blin *et al.*, 1990) for 5-HT_{2A}.

(+)[¹¹C]McN-5652 was the first promising tracer of the serotonin transporter (SERT) (Frankle *et al.*, 2005). It shows slow kinetics and high non-specific binding. This PET ligand has demonstrated that SERT density significantly increases in the thalamus region during depression (Ichimiya *et al.*, 2002). Some of the highly promising and recently developed diarylsulfide derivatives as PET agents for SERT are [¹¹C]-DASB (Houle *et al.*, 2000), [¹¹C]-MADAM (Lundberg *et al.*, 2005), and [¹¹C]-HOMADAM (Jarkas *et al.*, 2005).

1.4.3 Imaging agents for the Cholinergic Neurotransmission

The association of cholinergic system is with various psychiatric and neurological disorders such as cognitive, depression and memory disorders. Nicotinic and muscarinic are two known acetylcholine receptors classes. Few [¹¹C]4-NMPB (Zubieta *et al.*, 2001; Mulholland *et al.*, 1995), [¹¹C]3-NMPB (Tsukada *et al.*, 2001; Takahashi *et al.*, 1999), and [¹¹C]-bezotrope (Dewey *et al.*, 1990) are few PET ligands which are used for muscarinic receptors. They lack selectivity for subtypes of receptor. PET ligand [¹¹C]4-NMPB correlated decrease in muscarinic receptor density with normal aging. The PET agent for nicotinic receptor is [¹¹C]-Nicotine but are

highly non-specific in binding (Nyback *et al.*, 1994; Muzic *et al.*, 1998). Several derivatives of epibatidine demonstrated high specific binding and have been utilized as PET imaging agent. Epibatidine as well as some of its analogues demonstrated were never utilized on human due to extremely high toxicity. The nontoxic imaging probes for subtype R42 receptor are [¹⁸F]2-F-A-85380 (Koren *et al.*, 1998; Gallezot *et al.*, 2005) and [¹⁸F]6-A-85380 (Horti *et al.*, 2000; Ding *et al.*, 2004). They are under investigation for human use. Studies demonstrated correlation of R42 density reduction with disease severity (Kendziorra *et al.*, 2006).

For central acetylcholinesterase activity measurement, the potential PET imaging agents are [¹¹C]MP3A and [¹¹C]MP4A. PET studies demonstrated reduction in AD patients (Iyo *et al.*, 1997).

1.4.4 Imaging agents for β -amyloid

In case of AD, brain has extracellular β amyloid-rich β amyloid plaques as well as phosyperphosphorylated tau filaments in intracellular neuro fibrillary tangles (NFTs). [¹⁸F]-FDDNP is a naphthalene derivative which is lipophilic PET imaging probes for β -amyloid plaques and NFTs which can identify mild cognitive impairment in AD patients (Shoghi *et al.*, 2002; Rowe *et al.*, 2007). ¹¹C-labeled PET agents Pittsburgh Compound B ([¹¹C]PIB) and [¹¹C]SB-13 showed potential for human application in imaging of β amyloid plaques. [¹¹C]PIB demonstrated higher uptake in AD patient as compared to healthy controls. Its uptake was correlated with distribution of β amyloid plaque in histopathological studies in aging but not with severity of dementia in AD (Verhoeff *et al.*, 2004). A F-18 based PET agent for β amyloid plaques [¹⁸F]-BAY, with high affinity binding, has found its usefulness in early detection of β amyloid in disease and in discriminating well in AD patients and healthy individuals (Rowe *et*

al., 2007). These results demonstrated that potential imaging agents for β amyloid can provide better insights into AD progression.

1.4.5 Imaging agents for the Glutamatergic Neurotransmission

Glutamate regarded as the neurotransmitter with major excitatory ability in the CNS. Metabotropic glutamate receptors (mGluRs) and ionotropic glutamate receptors mediate its effect. The ionotropic glutamate receptors are AMPA (R-amino-3-hydroxy-5-methylisoxazole-4-propionate), NMDA (N-methyl-D-aspartate), and kainite receptors. The mGluRs are involved in the activation of intracellular systems of secondary messenger when bind with glutamate, its physiological ligand. The eight subtypes of metabotropic glutamate receptor are placed in three groups: mGluRs 1 and 5 in Group I; mGluRs 2 and 3 in Group II; and mGluRs 4, 6, 7, and 8 in group III. Group I regulates neuron excitation through fluctuation, group II and group III are involved in inhibition of adenylatecyclase and reduction of synaptic transmission thereafter (Meador *et al.*, 2002).

Ionotropic glutamate receptors are possibly involved in cognitive functions like learning and memory, and a variety of diseases related to brain such as depression (Tatarczynska *et al.*, 2001), anxiety (Spooren *et al.*, 2000), schizophrenia (Ohnuma *et al.*, 1998), PD (Rouse *et al.*, 2000), addiction with drug (Chiamulera *et al.*, 2001), and various pain states (Sotgiu *et al.*, 2003; Walker *et al.*, 2001). No suitable ligand for PET is currently available to image the ionotropic glutamate receptors (Blin *et al.*, 1991; Hartvig *et al.*, 1995; Ametamey *et al.*, 2002). Recently, three new compounds with fluorine are reported for PET application to image mGluR₅ although their human use is not clear (Hamill *et al.*, 2005; Simeon *et al.*, 2007). A novel antagonist of

mGluR₅, with selectivity and high-affinity is a promising PET radioligand to image mGluR₅ for application in humans (Ametamey *et al.*, 2006; Ametamey *et al.*, 2007). One more novel compound, [¹¹C]-ABP688, demonstrated its uptake in region of mGluR₅ in human brain and is being explored for diagnosis of neurological and psychiatric disorders (Verhaeghe *et al.*, 2018).

1.5 Currently used SPECT molecular imaging probes for brain imaging

^{99m}Tc-Hexamethylpropyleneamineoxime (^{99m}Tc-HMPAO)

As radiotracer, ^{99m}Tc-HMPAO demonstrates relative flow of blood (increased or decreased) in different regions of brain depending upon the disease. It finds application in clinical problems such as AD, depression, acute leukemia associated CNS toxicity and brain death imaging.

²⁰¹Tl Chloride

²⁰¹Tl chloride is potassium analogue and utilizes K pump for measurement of metabolic activity. Its distribution in CNS is dependent on BBB breakdown and relative flow of blood in CNS. SPECT images 2 h post injection demonstrated its increased retention in malignancies such as lymphoma and glioblastoma.

^{99m}Tc-ECD

SPECT imaging using ^{99m}Tc-ECD tracks metabolic activity. It provides cerebral blood flow map which is not quantitative. It has found application in following symptoms of psychosis in PD, detecting the seizure activity foci post febrile seizures, and revealing abnormalities in specific brain in case of seizure activity.

[¹²³I]-Ioflupane

[¹²³I]-Ioflupane is an FDA approved SPECT agent (DaTscanTM) for imaging DAT and has been utilized in assisting the development of compounds for PD diagnosis showing reduced striatum uptake in comparison with healthy individuals.

^{99m}Tc-TRODAT

The technetium-labelled agent, ^{99m}Tc-TRODAT for DAT imaging showed good difference in uptake in healthy individuals and PD patients. But its low target to background ratio proved hindrance in follow up of PD. This can have wide use in clinics as technetium is easily available. However, slight changes can be detected with [¹⁸F]-dihydrotrabenazine (DTBZ) (AV-133).

1.6 Traumatic Brain Injury (TBI) imaging

TBI, a heterogeneous disease, is differentiated on the basis of severity, pathophysiology and injury mechanism. Pathophysiological differentiation is primary and secondary traumatic brain injury. In primary traumatic brain injury, there will be traumatic event of initial stage and as per severity, may have extra/intra parenchymal hemorrhages. Clinically, CT and MRI are used for the evaluation. In secondary TBI, molecular level changes are observed which involve inflammatory responses, apoptosis, and excitotoxicity mediated by neurotransmitter. These initial trauma initiated events may persist for extended time period. In 1980s, ¹⁸F-FDG was used to image hypometabolism in patients with TBI through PET reflecting disturbances in metabolism of glucose in addition to abnormalities in structure demonstrated through

MRI and CT. In 1990s SPECT using ^{99m}Tc -HMPAO evaluated the effects of brain trauma on rCBF. In TBI patients, SPECT using ^{99m}Tc -HMPAO could identify more focal areas in comparison to CT or MRI.

Recently, a study demonstrated that brains of TBI and AD patient have similarities and both tend to accumulate amyloid plaques. Current research focuses to image secondary TBI pathophysiological neuroinflammation, particularly microglia activation. Several neurodegenerative diseases are associated with chronic microglia activation. There was increased [^{11}C]-(*R*) PK11195-TSPO binding, expressed by the activated microglial mitochondria, in the putamen, occipital cortices, thalami, and posterior limb in TBI patients. There was a correlation i.e. more the severe cognitive impairment, higher the binding in the thalamus.

Imaging of TBI may provide more information to discover novel diagnostic agents. [^{18}F]-FDG-PET can indicate injured region through hyper metabolism and ^{99m}Tc -HMPAO-SPECT through hypo perfusion.

Primarily, the TSPO agents are applied for imaging in research and suffer with the limitation of genotyping requirement as there is variable binding affinity towards TSPO due to TSPO polymorphism. Recently developed agents are at various stages of development.

1.7 Translocator protein (TSPO)

The translocator protein (TSPO, 18 kDa), originally designated as the peripheral benzodiazepine receptor, has 169 amino acids which is rich in tryptophan and highly

hydrophobic (Casellas *et al.*, 2002). TSPO is present in several tissues in the body and up-regulated under inflammatory conditions. The healthy brain has low TSPO expression on microglia which is found in CNS as the primary immune cells. However, injured brain activates microglia; in response expression of TSPO is up-regulated. Therefore, TSPO expression is considered as neuroinflammatory marker. Even various neurological diseases also reflect its increased expression in brain. Imaging TSPO with nuclear imaging modalities is potential tool for clinical assessment of neuroinflammation which in turn can increase the correlation of neuroinflammation with diseased brain as well as assess the efficacy of therapy. The sequence homology present in cDNA that encode TSPO in several species for example humans, bovine and rodents are 80% (Garnier *et al.*, 1994; Chang *et al.*, 1992; Parola *et al.*, 1991). TSPO (18kDa), voltage-dependent anion channel (VDAC, 32 kDa) and the adenine nucleotide carrier (ANC, 30 kDa) forms a multimeric complex in the outer membrane of mitochondria (Papadopoulos *et al.*, 1997; McEnergy *et al.*, 1992; Anholt *et al.*, 1986). The 3-D modelling studies revealed that TSPO has a 5α -helices structure present on the membrane of mitochondria (Bernassau *et al.*, 1993). TSPO is also associated with two proteins steroidogenic acute regulatory protein (StAR) and kinase A associated protein 7 (PAP7) which is located in steroidogenic tissue and participate in steroid synthesis. Furthermore, an acylCoA motif is present in PAP7 that is in sequence to DBI (diazepine binding inhibitor), predicting a common interaction site between TSPO, DBI and PAP7 (Lacapere and Papadopoulos, 2003).

1.7.1 Endogenous TSPO ligands

Several of endogenously present TSPO ligands has been recognized. DBI (Diazepam binding inhibitor) is predominantly present in CNS and in peripheral organs (Guidotti *et al.*, 1983). It also has affinities for CBR and TSPO in micromole (μM). The cleavage of DBI, 86 amino-acids containing peptide of 10 kDa, into biologically active fragments such as eicosa neuro peptide (ENP), octadecaneuro peptide (ODN), and triakonta tetra neuro peptide (TTN). On comparison with DBI, TTN has similar affinity but more selectivity, and ODN has less potency (Slobodyansky *et al.*, 1989; Ferrero *et al.*, 1986). Steroidogenesis can be stimulated by DBIs and and neurosteroid synthesis can be stimulated by TTN as found in cells of C6 glioma through TSPO interaction (Papadopoulos *et al.*, 1991). One more endogenous TSPO ligand is Cholesterol which has nanomolar (nM) affinity towards TSPO (Lacapere *et al.*, 2001). Supposedly steroidogenesis happens through transportation of cholesterol to the inner membrane of mitochondria by binding to the CRAC (Li *et al.*, 2001). Few other endogenously present ligands, exhibiting high affinities towards TSPO (in nM range) but not for CBR, are the porphyrins (ehemin, mesoporphyrin IX, protoporphyrin IX and deuteroporphyrin IX) (Snyder *et al.*, 1987). The tetrapyrrolic pigments porphyrins are synthesized in the pathway of biosynthesis of hemoglobin, mitochondrial cytochrome, heme, and few more heme proteins. The heme biosynthesis and occurrence of initial and final steps of biosynthesis of porphyrin in mitochondria fits in the concept of porphyrins as endogenous ligands (Verma and Snyder, 1989).

1.7.2 Tissue distribution and subcellular location of TSPO

Primarily, the localization of TSPO on subcellular level is on the outer mitochondrial membrane which was performed through binding studies on rat using the [³H]-PK11195, as elective ligand. TSPO are found in kidneys, lungs, liver, heart, adrenal glands, testis, and skeletal muscle of rat (Anholt *et al.*, 1986; Antkiewicz- Michaluk *et al.*, 1988). These findings were confirmed by immunohistochemistry for TSPO using electron microscopy and confocal microscopy (Bribes *et al.*, 2004; Garnier *et al.*, 1994). One study showed TSPO presence in red blood cells which do not have mitochondria, indicating non-mitochondrial presence of TSPO (Olson *et al.*, 1988). In few studies in organs like liver, small quantity of TSPO may be present on plasma membrane (Woods *et al.*, 1996). Additionally, human cancer cells such as breast cancer, hepatic tumor, and glioma demonstrate presence of TSPOs in perinuclear and nuclear area (Hardwick *et al.*, 1999; Corsi *et al.*, 2005; Brown *et al.*, 2000). Anatomical distribution of TSPO in the body has been demonstrated through autoradiography and radioligand binding assays using selective TSPO ligands PK-11195 or Ro5-4864 labelled with tritium. The TSPO is found in abundance in secretory and glandular tissues for example pineal gland, adrenal glands, olfactory epithelium, gonads, and salivary glands, at intermediate level in myocardial and renal tissue and at relatively low level in brain (Gavish *et al.*, 1999). Within a given organ, TSPO is not homogeneously distributed. In the adrenal glands, there is high density of TSPO in adrenal cortex and no TSPO in medulla in rat liver (Anholt *et al.*, 1986). TSPO is found in hepatocytes as mitochondrial form and in biliary epithelial cells as non-mitochondrial form (Woods *et al.*, 1996). The expression of TSPO is in blood

cells with polymorphonuclear neutrophils and monocytes having the highest concentrations (Canat *et al.*, 1993).

^{11}C -PK11195, a derivative of isoquinoline carboxamide and TSPO antagonist, is the most widely used PET radioligand for TSPO. Initially, racemic ^{11}C -PK11195 was used but later R-enantiomer demonstrated almost double binding affinity as compared to the S-enantiomer resulting in use of ^{11}C -(R)-PK11195 for subsequent PET studies for neuroinflammation and oncologic diseases. However, ^{11}C -PK11195 is widely used but restricted to the neuroinflammation imaging due to its major limitations. ^{11}C -PK11195 has relatively high non-specific and plasma protein binding and low brain permeability that resulted in PET images with a low specificity and low signal-to-noise ratio. Therefore, detection of slight alterations in neuroinflammation and accurate tracking of neuroinflammation is not possible with ^{11}C -PK11195. Also, ^{11}C requires on-site cyclotron due to its short half-life for the use of this radiotracer. This, resulted in the fluorine (^{18}F) based TSPO radiotracers development, which does not require on-site cyclotron as ^{18}F based TSPO ligands have improved access of the radio isotope to clinicians and researchers as well as reduced costs.

1.7.3 Second and third generation TSPO radiotracers for neurologic diseases

With the synthesis of various TSPO-specific fluorinated radiotracers, several studies on neurological and oncological diseases have been carried out. The glioma models on rat have demonstrated high uptakes of ^{18}F -DPA714 and ^{18}F -PBR06 in tumor than the contralateral hemisphere with high degree of specific binding to TSPO (Buck *et al.*, 2011, Tang *et al.*, 2012). However, the major limitation of TSPO imaging of brain tumor is lack of differentiation between tumor cells and inflammatory cells around the

tumor. Preclinical and clinical studies of TSPO expression in AD has also been investigated using PET in which microglial activation takes place (James *et al.*, 2012; Lyoo *et al.*, 2015). Stroke researchers have also imaged TSPO for investigation of purpose of neuroinflammation after acute cerebral infraction using PET. Imaging of periinfarction as well as core areas in ischemic model of rat have been performed through various TSPO radiotracers. These studies demonstrated specific uptake in the ischemic infarct region which is in agreement with studies performed by ex vivo autoradiography (Varrone *et al.*, 2013).

In vivo imaging of TSPO using PET of neuroinflammation in patients with MS is possibly the greatest opportunity in clinical condition. Both acute as well as chronic neuroinflammation have been therein the clinical manifestation and pathogenesis of multiple sclerosis; however, lack of assessment of neuroinflammation in vivo made this correlation difficult (Yui *et al.*, 2010). On comparison with control, the expression of TSPO was observed in these mice-brains which were correlated with ex vivo autoradiography and immunohistochemistry studies (Xie *et al.*, 2012). In future, the TSPO radiotracers for PET can be used for evaluation and monitoring of MS as demonstrated in the study i.e. reduced the radiotracer uptake post immune suppressant drug treatment (Xie *et al.*, 2012; Airas *et al.*, 2015). The potential utility of TSPO radiotracers for PET ^{18}F -PBR111 and ^{11}C -PBR28 has been demonstrated on patients with MS with increased uptake of radiotracer in white matter of lesional and perilesional region as compared to that of non-lesional region. There is positive correlation between radiotracer uptake with disease severity or duration (Colasanti *et al.*, 2014; Oh *et al.*, 2011).

1.7.4 Limitations of new TSPO radiotracers

New radiotracers for TSPO have shown promise for several application of evaluation and monitoring, still there are several issues that may limit clinical use in routine. Based on TSPO affinity, three binding groups are defined: high-, mixed- and low-affinity binder on the basis of binding affinity of second generation of TSPO tracers such as ^{11}C -PBR28 (Owen *et al.*, 2011). This non-binding issue is a major limitation, which has been attributed to a single polymorphism (rs6971) present in the TSPO gene in which threonine is substituted by alanine (Owen *et al.*, 2012). The Ala/Ala, Ala/Thr and Thr/Thr are present is present in high-, mixed- and low-affinity binders, respectively (Guo *et al.*, 2013). However, in patients with low-affinity binders, the clinical usefulness of PET for TSPO is limited as images are of low quality.

The ligand from first generation, PK11195 is not having problem of non-binding issue but it is non-specifically binds. The second generation TSPO ligands are specific but have non-binding issues. The other aspect for TSPO ligands is limited specificity towards activated microglia (Lavisse *et al.*, 2012). The limitations of existing ligands need to be taken care to get better ligands for TSPO as a biomarker are required for the imaging of immune cells. More selective ligands would be useful for the qualitative as well quantitative analysis of neuroinflammation. The existing PET ligands are showing limitation in terms of TSPO ligand but also in terms of cost and infrastructural requirements of cyclotron. This reduces the reach of the TSPO ligands for various applications. The ligand with good selectivity for TSPO along with its ability for more widely used modality could be of great value for diagnostic applications.

Therefore, there is a need of a ligand to have more specificity, biocompatibility, easy availability, lipophilicity, and free from non-binding issues.

1.8 Aims and objectives of present study

Aim: Development of acetamidobenzoxazolone based TSPO ligand for SPECT application

Objectives of the study: In order to fulfil the aim of the present work, the following objectives were outlined:

- a. To develop *in silico* pharmacophore based on acetamidobenzoxazolone
- b. To design molecules on the basis of pharmacophore developed and *in silico* validation
- c. To synthesize and characterize the designed ligands
- d. Radiocomplex with ^{99m}Tc and their stability measurement
- e. To validate the specificity and selectivity of radioligands towards TSPO through tracer technique

1.9 Plan of Work

The present work was divided into various sections to achieve the following objectives:

- I. Design of potential candidates to target TSPO using *in silico* tools and techniques
 - A. Identification of lead skeleton and pharmacophore modelling using lead skeleton based TSPO ligands and their binding affinity from literature
 - B. Incorporating various identified pharmacophoric features on lead skeleton in order to design TSPO ligands for metal complexation

- C. Screening the molecules for pharmacokinetic properties through ADME analysis and interaction with TSPO through docking and known TSPO ligands were taken as reference
- II. Synthesis of SPECT ligands
- A. Synthesis of designed ligands
 - B. Characterization of synthesized ligands through various spectroscopic techniques
 - C. Cytotoxicity study of ligands on RAW264.7 cell line
 - D. Radiocomplexation of ligands with ^{99m}Tc
 - E. Stability studies of radioligands over 24 h
- III. Validation of radioligands as TSPO ligands
- A. *In vitro* studies on A549 cell line to assess specificity using PK11195 as blocking agent
 - B. *Ex vivo* blood kinetic studies on New Zealand rabbits
 - C. *Ex vivo* biodistribution pattern of TSPO in Balb/c mice
 - D. *In vivo* biodistribution studies on Balb/c mice and New Zealand rabbit to assess their selectivity
 - E. Radioligand specificity by blocking agent in Balb/c mice
 - F. Lung inflammation model and A549 human lung tumor xenograft models to assess the specificity of the most potential skeleton for lung application

The experimental procedures employed in carrying out the above-mentioned objectives have been elaborated in the next chapter.

Chapter 2
Materials and Methods

CHAPTER 2

MATERIALS AND METHODS

2.1 Introduction

This chapter contains the detailed information about the tools, techniques and reagents used for design, synthesis, characterization as well as biological evaluation of acetamidobenzoxazolone based TSPO ligands. The experimental procedures employed in cell lines, normal animal, and modelled animal as well as model preparation methods are described.

2.2 *In silico* techniques

2.2.1 Pharmacophore hypothesis generation

For developing the pharmacophore hypothesis 51 acetamidobenzoxazolone based TSPO ligands were taken from the literature and aligned for their pharmacophoric features (Fukaya *et al.*, 2012; Fukaya *et al.*, 2013) using PHASE of Schrödinger, Maestro LLC 9.1 software. The conformers were generated by MacroModel ConfGen using OPLS2005 force field with rapid torsional search. The score for hypothesis was generated through alignment of geometric site points in the active molecules to that of the hypothesis. The hypothesis was generated for each conformer of active molecule. The pharmacophore hypothesis was evaluated by carrying out PLS analysis. For that, atom-based PHASE QSAR models were generated with three PLS factors as maximum for every pharmacophore type. The TSPO ligands were designed further on the basis of the best hypothesis.

2.2.2 ADME studies

A promising lead should have potency and attractive ADME profile both. The incorporation of desired ADME properties at early stages of drug discovery using computer aided drug design methods reduces the chances of failure of compound at later stages. The drug-like behavior of all the designed molecules and few known TSPO ligands were predicted through the analysis of pharmacokinetic profiles of the molecules prepared by LigPrep module using QikProp module of Schrödinger. The method of Jorgensen was utilized by the program QikProp to compute pharmacokinetic properties and descriptors. QikProp provides ranges for all the properties of 95% of known drugs for comparison purpose.

In the present study, QikProp derived physico-chemical properties used for ADME properties are number of hydrogen bond acceptors/donors, partition coefficients, molecular volume, molecular weight, and number of rotatable bonds etc which, in turn, predict the properties for assessing drug likeliness, bioavailability, plasma protein binding, metabolism, and toxicity. As we are targeting the receptors/proteins which are found on outer mitochondrial surface of glial cells, our molecules should be able to reach glial cells of brain. This means their capability for crossing blood brain barrier is essential and their lipophilicity must be high as lipophilic substances have ability to cross the BBB. During this process, transportation/binding pattern with human serum and toxicity are also important for consideration. That's why we have considered following predictive properties:

- QPlogPoctanol/water
- QPlogS -aqueous solubility

- QPlogS-Conformation independent aqueous solubility
- QPlogK_{h_{sa}} Serum protein binding
- QPlogBB for blood brain
- No of primary metabolites
- HERG K⁺ Channel blockage
- LogIC₅₀
- Apparent Caco-2 permeability (nm/s)
- Apparent MDCK permeability (nm/s)
- Qualitative model for human oral absorption
- % Human oral absorption in GI

Other standard rules considered for evaluation of ligand for drug likeliness or capability for becoming a good drug candidate for clinical application and bioavailability are Lipinski rule of five and Jorgensen rule of three.

2.2.3 Preparation of ligands

The lead skeleton was taken from our previous work which proved its potential for TSPO targeting. Further new designed ligands were drawn using chemdraw Ultra 10.0 and were checked for drug likeliness using Lipinski rule and other properties mentioned above as filter. These analogues are geometrically optimized and energetically minimized to obtain in .mol format which were used as input structures for processing in LigPrep, Schrödinger, Maestro LLC 9.1 software. A series of steps involved in the LigPrep process are as follows: performing conversions, corrections application to the structures, generation of structural variations, unwanted structures' elimination and finally the structural optimization.

2.2.4 Protein preparation

Prior to docking, identification of the binding sites in the target protein is important. This information was taken through the structures of the complexes of the TSPO proteins with its substrate PK11195. The PDB structure files of the proteins were imported and prepared through protein preparation wizard, Schrodinger utilizing the OPLS2005 force field. In the process of protein preparation the steps involved were processing, optimization and minimization.

The validation of docking protocol was performed through docking back after removing the PK11195 from active site.

For the current study PDB structures were taken from RCSB Protein Data Bank (PDB) and the PDBs used were 2MGY (wild type TSPO), 4RYQ (wild type TSPO, resolution 1.7 Å) and 4UC1 (Mutant TSPO, resolution 1.8 Å).

2.2.5 Docking

After designing the ligands and screening them for their ADME properties, they were validated for binding/affinity towards TSPO through docking studies to understand their preferred orientation of protein ligand interaction by forming a complex with high stability. Molecular docking can now be readily used for *in silico* validation of designed TSPO ligands as recent advancement has made TSPO protein structures available using nuclear magnetic resonance (NMR) spectroscopy or X-ray crystallography. 2MGY (Jaremko *et al.*, 2014) and 4RYQ (Guo *et al.*, 2015) are crystal structure of mTSPO and BcTSPO, respectively. 4UC1 (Li *et al.*, 2015) is crystal structure of TSPO from *Rhodobacter sphaeroids* (A139T Mutant) with resolution 1.8 Å. All these PDBs of TSPO are derived through X-ray crystallography

techniques and have 181 residue counts. 4RYQ and 4UC1 with resolution $< 2 \text{ \AA}$ have been published in 2015. This has facilitated docking studies more efficiently. Prior to that docking was performed for TSPO ligands using homology modelling using PDB such as 2MGY (Tiwari *et al.*, 2014).

As the TSPO crystal structures are from two bacteria which are unrelated their comparison and contrast were assessed in literature. In all TSPO structures, the protein monomer forms a structure of helical bundle with five transmembrane helices (TM1, TM2, TM3, TM4 and TM5) which was predicted by several methods. LP1, a long loop, connecting TM1 and TM2 were present as well-defined structure (Guo *et al.*, 2015). In spite of the TSPO crystal structures from two distinct sources i.e. Gram-negative (*R. sphaeroides*) and Gram-positive (*Bacillus cereus*) bacterias with 23% sequence identity, their structural fold are strongly conserved during evolution as demonstrated by remarkable similarity, without and with ligand. The transmembrane helices of the *Bc*TSPO and *Rs*TSPO overlap well along with similar structural adaptation of LP1 and a short middle helix (Jaremko *et al.*, 2015).

A structure-based optimization process makes use of the ligand-protein interactions for assessing the affinity of ligand in rational and efficient way. The knowledge of interaction is the best obtained by the protein–ligand complex through molecular docking methodology which is predictive and rapid at this stage. It explores the interaction of small molecules with target protein at its binding site. There is continuous improvement brought to the docking programs.

Glide module of Schrodinger software is reported to be one of the best in terms of top-ranked docking solutions with minimal root mean square deviation (RMSD) and

binding scores (G_{score}) (Halgren *et al.*, 2004). Glide Score, an empirical score, approximates the free energy of ligand binding. It includes contribution from force field (vander Waals and electrostatic) and few other influencing ligand binding. It has been optimized for accuracy of docking, enrichment of database, and prediction of binding affinity. Glide score could rank different ligands' poses, such as for virtual screening and prediction of affinity for certain target in comparison to known ligands. G_{score} is simulation of binding free energy and more negative score represents better binding. XP Glide score has several terms in common with the SP Glide score and HTVS Glide score but they have significant differences and separate optimization have been performed therefore cannot be directly compared (Pagadala *et al.*, 2017; Chaput *et al.*, 2017; Bhargavi *et al.*, 2017; www.Schrodinger.com).

The strain energy of the ligand is the difference between the energy of ligand in complex and the energy of the extracted ligand, minimized, starting from the geometry in the refined complex. This is 'local' strain energy used for comparison of different poses of the same ligand. Calculations to assess the strain were performed in implicit solvent.

The free energy approximation of ligand-receptor binding as per MM-GBSA approach involves energies of molecular mechanics (MM), solvation term both non-polar and polar, and entropy term as shown in the equations below:

$$\Delta G = \Delta E_{\text{MM}} + \Delta G_{\text{Solv}} - T \cdot \Delta S = \Delta E_{\text{bat}} + \Delta E_{\text{vdW}} + \Delta E_{\text{coul}} + \Delta G_{\text{Solv,p}} + \Delta G_{\text{Solv,np}} - T \cdot \Delta S$$

E_{MM} consists of E_{bat} (combined term of bond, and torsion), E_{vdw} (term of vander Waals), and E_{coul} (a term of coulombic force). The generalized Born (GB) approximation is usually used for computing $\Delta G_{\text{Solv,p}}$ i.e. contribution due to polaristy to the solvation-free

energy and a linear function of the solvent accessible surface area (SASA) often computes $G_{\text{solvp,np}}$ i.e. non-polar solvation energy (www.Schrodinger.com).

All the newly designed analogues as well as few well known TSPO ligands were subjected to docking in GLIDE of Schrödinger, Maestro LLC 9.1 with translocator protein. All the molecules were docked with negative G_{Score} and were ranked on the basis of their interaction energies. Overall, the maximum contribution to the interaction energy was from Vander Waals energy but the greatest variation was due to electrostatic energy, making it main deciding factor for the ranking of molecules. The XP form of G_{score} has more physical accuracy. The XP protocol involves ligand flexibility by multiple conformers docking in a rigid receptor, and ranking them on the basis of XP Glide scores.

2.3 Synthesis and characterization

The acetamidobenzoxazolone-amino acid ester (ABEO) skeletons were synthesized by carrying out two parallel reactions to synthesize the intermediates chloro acetylated amino acid ester and 5-chloro/bromo benzoxazol-2(3*H*)-one. These intermediates were combined through alkylation reaction in the final step.

2.3.1 Chemicals

The solvents and chemicals used in the reactions procured were from Merck and Sigma-Aldrich which were used without further purification. For column chromatography, MN60 silica having mesh size 60-120 was used to purify the synthesized compounds and for thin layer chromatography (TLC), silica gel 60 F₂₅₄ coated on aluminium plates were utilized to monitor the reaction.

2.3.2 Instrumentation

^1H and ^{13}C Nuclear Magnetic Resonance Spectroscopy (NMR) were recorded on Bruker Avance III 600 MHz system at 600 MHz and 150 MHz, respectively. Mass spectroscopy was performed on Agilent 6310 system using ESI. High performance liquid chromatography (HPLC) was carried out on 1200 series of Agilent using analytical T3 Waters column (4.6X250 mm) for analysis.

2.4 *In vitro* techniques

2.4.1 MTT cell viability studies

MTT assay i.e 3-(4, 5-dimethylthiazole-2-yl)-2,5-diphenyl-2H-tetrazolium bromide assay was performed for determining cytotoxicity. A 96-well micro titre plate was used for plating of 4000 cells of exponentially growing RAW 264.7 cells per well 24 h prior to the treatment with different drug concentration of ABTO-X/ABPO-X/ABMO-X (1 nM-100 μM) for 24 h. Thereafter, MTT assay was performed 24 h post treatment.

For MTT assay, untreated (negative control) and cells treated with compounds were incubated with 10% solution taken from 5 mg/mL stock solution of MTT in PBS for 2 h at 37°C. The cells were lysed after treatment and 150 μL DMSO was used for dissolving formazan crystals. For absorbance measurement, 570 nm using 690 nm of reference filter was used on multiwell plate reader from Biotek life Science Instruments of USA. The activity of mitochondria was determined by calculating cell viability in terms of percentage in comparison to negative control. After determining survival fraction, it was plotted as a function of time against concentration.

2.5 Radiolabelling protocol

The radioactive element containing compounds of ligands are called radiopharmaceuticals which can find application in the assessment of the state of disease and health. We have developed few TSPO ligands that can be tagged with ^{99m}Tc to convert it as SPECT agent for diagnostic application. The gamma rays of 140 KeV emitted by ^{99m}Tc , were acquired for imaging which were processed and interpreted by highly sophisticated gamma cameras.

$\text{SnCl}_2 \cdot 2\text{H}_2\text{O}$ (1×10^{-2} M) was added to 200 μl ligand solution having 0.2 mg. Then 74-110 MBq sodium pertechnetate in 100 μl saline was added. NaHCO_3 (0.1-0.5 M) was used for pH adjustment to 6.5-7.0 and then content was manually shaken and kept at room temperature for 15-30 min. ITLC-SG strip as stationary phase and acetone and PAW (pyridine, acetic acid and water in 3:5:1.5 ratio) as mobile phase were used to determine complexation with ^{99m}Tc and purity of the labelled compound. Count measurement was done by cutting ITLC into 0.1 cm segments.

2.6 Stability studies of radioligands

2.6.1 Stability in saline

The ^{99m}Tc -labelled complexes of synthesized TSPO ligands were incubated with saline at 37°C. ITLC-SG was used for the analysis of samples at different time points. Time dependent percentage dissociation of the complex in saline was measured using acetone and PAW (pyridine, acetic acid and water in the ratio of 3:5:1.5) as mobile phases.

2.6.2 *In vitro* human serum stability assay

Blood, collected from healthy volunteers and clotted in humidified incubator at 37°C for 1 h under 5% CO₂ and 95% air, was used in preparation of serum. Sample was centrifuged at 400 rpm and 0.22 µm filter was used for filtration. Sterile plastic culture tube was used for collection of filtrate. ^{99m}Tc-labelled complexes of synthesized compounds were incubated with freshly prepared serum at 37°C (100 nM/mL conc). Samples were analyzed at different time point using ITLC-SG. Time dependent percentage dissociation of the complex in serum was assessed using acetone as mobile phase.

2.7 *In vitro* cell uptake of ^{99m}Tc-radioligand in A549 human tumor cells

Human lung carcinoma A549 cells were cultured as per protocol in literature (Choi *et al.*, 2016). A549 cells were maintained in RPM1 medium which was supplemented with heat inactivated fetal bovine serum (10% (v/v)), L-glutamine (2 mM) and penicillin-streptomycin (100 U ml⁻¹) kept in a incubator in 5% CO₂ humidified at 37 °C. The incubation of 1x10⁶ A549 cells per well with ^{99m}Tc-labelled complex (in 10% ethanol, 5% tween 20 and 85% water) for 10, 30 and 60 min were carried out. In an inhibition study for specificity, 300 mM solution of PK11195 was added to the cells prior to incubation and the cells were washed with PBS after 1 h. Thereafter, radiocomplex was added and its cell uptake was studied at 10, 30 and 60 min with the help of a gamma counter.

2.8 Animal studies

Animal protocols were approved by the Institutional Animal Ethics Committee (INM/DASQA/IAEC/09/015). Balb/c mice were used for *ex vivo/in vivo* biodistribution studies, SPECT imaging, blocking studies in normal and inflammation models. Lung

tumor xenograft model was prepared on nude mice. Blood kinetics and biodistribution studies under *in vivo* condition were carried out on New Zealand rabbits.

Animals were supplied by experimental animal facility (EAF) of INMAS, Delhi. The regulations of the CPCSEA (Committee for the Purpose of Control and Supervision of Experiments on Animals) were implemented for maintenance of animals. Animals were maintained on standard diet (Hindustan Lever Ltd, Mumbai, India). They were kept in the animal house of the institute which was maintained at $22 \pm 2^\circ\text{C}$ and 50% humidity under a 12 h dark/light cycles. Mice were housed in sterile and pathogen free plastic cages. For *in vivo* biodistribution and blocking studies, SPECT imaging was performed. The *ex vivo* biodistribution was done after sacrificing the animals.

2.8.1 *Ex vivo* studies

2.8.1.1 Blood kinetic studies in New Zealand rabbits

Normal New Zealand rabbits (2-2.5 Kg, n=3) were used to perform blood clearance studies of $^{99\text{m}}\text{Tc}$ -labelled complex. 0.1-0.2 mCi of radiocomplex was administered intravenously via dorsal ear veins of rabbits. Blood samples (200 μL) were taken at different time intervals. The well counter was used for activity measurement in blood samples to assess the percentage of dose administered at different time points to generate the time activity curve.

2.8.1.2 Biodistribution studies in Balb/c mice

Initial assessment of $^{99\text{m}}\text{Tc}$ -radiocomplexes under *ex vivo* condition was carried out on Balb/c mice. Radioactivity was measured in specific organs of the mice at different time points after injecting 100 μCi of radioligands via vein of the tail as percentage

administered dose per gram (%ID/g) of tissue. Three sets of experiments were performed at every time point. Blood was collected, and organs were dissected for analysis. Radioactivity in organs was measured by gamma counter. Radioactivity injected in each mouse was found out by subtracting the activity left in tail from the activity injected. Total blood volume was calculated as 7% of the total body weight.

2.8.2 *In vivo* studies

2.8.2.1 Gamma camera design

For SPECT images of ^{99m}Tc -labelled complexes in animal, a gamma camera at INMAS (Symbia, T2, True point SPECT/CT Siemens) having dual head, high resolution, low energy and parallel-hole collimator was used which has an interface to a computer network system. For image acquisition, animal was fixed on a mechanical support for standardization of orientation and position.

2.8.2.2 Biodistribution in New Zealand rabbits

Ketamine/xylazine (50 mg/kg & 5 mg/kg, respectively) were used for sedating animals. SPECT images were taken after 0.2-0.3 mCi of radiocomplex injection intravenously through ear of New Zealand rabbit. Images were acquired at defined time point in case of static imaging. For dynamic imaging, acquisition was done for 30 min immediately after injection. Anterior images for 30 min with 2 sec/frame, 10 sec/frame, 15 sec/frame and/or 60 min/frame were acquired for different time intervals. A 15% window centred on 140 KeV i.e. ^{99m}Tc peak was used with zoom of factor 1. The dynamic and static imaging used matrices 128X128 and 256X256, respectively.

Pegasys workstation was used for data extraction and analysis to have SPECT image. Once image is acquired, ROI (region of interest) were considered over desired organs and the total field of view.

2.8.2.3 Biodistribution and blocking studies in normal Balb/c mice

Balb/c mice (22-28 g) were used for blocking studies in normal mice. PK11195, a known TSPO ligand, was taken as blocking agent. Ketamine/xylazine (50 mg/kg & 5 mg/kg, respectively) were used for sedating animals. In control, 100 μCi $^{99\text{m}}\text{Tc}$ -labelled complex was administered which provided *in vivo* biodistribution. For blocking, 5 mg/kg unlabeled PK11195 was administered 10 min prior to injection of 100 μCi $^{99\text{m}}\text{Tc}$ -labeled complexes and was imaged after 40 min. PK11195 was dissolved in minimal amount of DMSO which is acceptable for injection in saline and administered intravenously.

2.8.3 Blocking studies in animal model

2.8.3.1 LPS induced lung inflammation model

A lung inflammation model was prepared in Balb/c mice by delivery of lipopolysaccharide (LPS) intranasally as well as intratracheally. For intranasal delivery, 40 μl of 0.5 mg/ml of LPS solution was used in Balb/c mice (10 weeks, male). For intratracheal delivery, Balb/c mice (6-8 weeks, male) were anesthetized by isoflurane sedation. While anesthetized, an incision was made around the thoracic region in mice and intratracheally delivered LPS dose was 100 μl of 0.5 mg/mL. After 24 h, the mice were used for experimental purpose to validate the uptake of radioligand in inflamed lungs, overexpressing TSPO receptors. The blocking studies

were performed in these models by preadministering 2.5 mg/kg, 5 mg/kg and/or 10 mg/kg unlabelled PK11195, 10 min prior to 100 μCi $^{99\text{m}}\text{Tc}$ -labelled complex was injected and was imaged/sacrificed 40 min post radioligand injection. The tracer technique was used to assess the lung model by comparing biodistribution of radiocomplex in lung modelled mice and normal mice.

2.8.3.2 Lung tumor xenograft model

A549 cells were maintained in medium (RPM1) which was supplemented with heat inactivated fetal bovine serum (10% (v/v)), penicillin-streptomycin (100 U mL^{-1}), L-glutamine (2 mM) and in a humidified incubator at 37°C in 5% CO_2 . 2×10^6 A549 cells in 100 μl were injected subcutaneously into the left side of the nude mice. After 3 weeks, the mice models were utilized for the studies.

Chapter 3
Designing of Acetamidobenzoxazolone
based TSPO ligands for Single Photon
Emission Computed Tomography

CHAPTER 3

DESIGNING OF ACETAMIDOBENZOXAZOLONE BASED TSPO LIGANDS FOR SINGLE PHOTON EMISSION COMPUTED TOMOGRAPHY

3.1 Introduction

As TSPO is involved in physiological processes of different organs and its association is with pathological states, therefore it is a promising diagnostic and therapeutic target for a number of diseases (Beurdeley *et al.*, 2000; Lartey *et al.*, 2014; Veenman *et al.*, 2015; Morin *et al.*, 2016). Therefore, the development of specific and selective ligand for TSPO is an important area of research which could quantify TSPO concentration (Hatty and Banati, 2015). Computational tools can provide a general approach to create new small TSPO binding molecules and help predicting their activity.

Different basic skeletons developed as TSPO ligands have one hydrogen bond acceptor, two aromatic regions as well as one lipophilic region such as isoquinoline carboxamides, imidazopyridine acetamides, benzothiazepines, benzoxazepines, indol-3-ylglyoxylamides, indole acetamides, pyrazolopyrimidine acetamides (Cappelli *et al.*, 1997). Few representative or clinically known TSPO ligands are shown in Fig. 3.1.

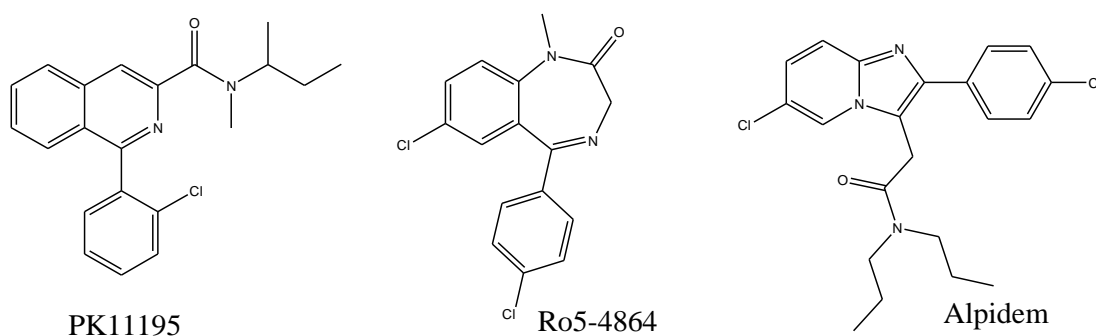


Fig. 3.1: TSPO ligands

Recently, theoretical models could predict the TSPO ligand affinity quantitatively by applying ligand-based methods for virtual screening of scaffold with sub-micro molar affinities (Tuccinardi *et al.*, 2009). Further QSAR/3D-QSAR and pharmacophoric modelling were applied for lead optimization. The availability of TSPO can provide insight about interaction of receptor with ligand along with effect of ligand substitutions on it. The selectivity analysis of TSPO ligand can be more reliable with the combined approach of ligand-based as well as receptor-based *in silico* techniques.

3.2 Literature review of computational studies for TSPO ligands

3.2.1 QSAR studies

In 1997, the twenty one synthesized PK11195 (1-(2-chlorophenyl)-*N*-methyl-*N*-(1-methylpropyl)-3-isoquinolinecarboxamide) analogues were reported along with their biological outcome (Cappelli *et al.*, 1997). The adhoc defined size and shape descriptors for QSAR model with $r=0.912$, $s=0.462$ and $F=111.09$, was found to be the best model but the incorporation of reactivity and electronic indexes resulted in inferior outcomes. Three high affinity TSPO ligands were selected for predicting properties of binding site of TSPO in terms of the conformational freedom and the shape. This was for the constitution of skeleton which was superimposed on their common nucleus. For computation of V_d , which is an adhoc descriptor based on shape as well as size, the formulas: $V_d = (V_{in} - V_{out}) / V_{sup}$, where V_{in} , V_{out} and V_{sup} are intersection vander Waals volume, Outer vander Waals volume and supermolecular vander Waals volume of the ligands, respectively. V_{in} mimics repulsive and V_{out} mimics attractive interactions of short range with the receptor (De Bebedetti *et al.*, 1994). Two QSAR models of derivatives of quinolone and isoquinoline carboxamide

were obtained correlating V_{out} and V_{in} , reflecting direct correlation of the shared molecular volume between a supermolecule and a ligand, and the amide substituent's molecular shape with the binding affinities.

In 2001, further description of derivatives of quinoline and isoquinoline carboxamide were used with the same method (Anzini *et al.*, 2001; Trapani *et al.*, 2005; Cruciani *et al.*, 2007; Samanta *et al.*, 2007; Goswami *et al.*, 2017). It could explain the ligands' affinities which were additional but not for ligands with quinoline nuclei having bulky substitution at 3rd position due to different structure from the supermolecule used. A different approach increased the predictability of molecules with different structure than the training set molecules: On the basis of pharmacophore common to representative ligands, a hypothesis of receptor was defined considering the required factors at the specified place but not the shape of the binding site. The scoring of the molecules included the number of matching functional groups and incomplete orientation or superimposition was used for the penalization.

In 2005, a QSAR study on 2-phenylimidazopyridine derivatives was carried out to understand the change in TSPO affinity with respect to changes in the structure on amide nitrogen. Several molecular descriptors, such as parameters of bulk (molecular refractivity, MR; molecular volume, MV) and lipophilicity (ClogP) were examined. In addition, variables accounting for chlorine substitution at phenyl group (I_{Z_1}) along with chlorine atom at 8th position of 2-phenylimidazopropanamide group (I_{Z_2}), di- or monosubstitution at the nitrogen of carboxamide (I), and the carbon atoms number in nitrogen substituents (alkyl) of carboxamide (N), and an acetamide or propanamide group (I_{CH_3}) were examined. The partial least square (PLS) algorithm was used to

correlate pIC_{50} values with the eight selected descriptors. The best computational model consisted of five predictors: ClogP, MR, MR^2 , I, and I_{CH_3} , with PLS factor 5, which could explain 75% of the variance in the binding affinity towards TPSO. The QSAR model demonstrated that the molar refractivity was a critical factor due to strict allowed range of values that did not hinder in interaction of carboxamide moiety with TSPO. Also, there seemed to have link between binding affinity and lipophilicity. Additionally, doubly substituted nitrogen of carboxamide and the presence of an acetamide moiety favored the affinity for TSPO.

In 2007, 2-phenylimidazo[1,2- α]pyridineacetamide derivatives were used to develop QSAR models (Trapani *et al.*, 2005), using quantum chemical and topological descriptors (Samanta *et al.*, 2007).

Two different models for TSPO were developed as ovary as well as cerebral cortex sources were used for testing these compounds as TSPO ligands. They used two parameters as properties indicating doubly substituted nitrogen on carboxamide nitrogen and acetamide moiety; the atomic charges at atom number 1, 6, 16 and 19; total energy and dipole moment. The model developed through cerebral cortex-based data explained binding affinity with variance upto 65.80% and pointed out position 6 and 19 as the important substituents' positions for the activity and di-substitution on nitrogen of carboxamide favoured the TSPO affinity, as pointed out by previous researcher (Greco *et al.*, 1994). This also reflected the effect of compounds' polarity in decreasing the TSPO affinity. The dipole moment contributed for the electronic and non-covalent TSPO-2-phenylimidazo[1,2- α]pyridineacetamides interaction. The ovarian membrane data-based model explained affinity data with variance up to 58.16% and proposed that acetamide group at 9 numbered atom and atomic charges at C_{19} atom favoured the affinities for TSPO.

A group based QSAR (GQSAR) model was developed that related 2D descriptors with the contribution of the site of substitution of 4-Phenylquinazoline-2-carboxamide derivatives. The GQSAR model considered for further studies had four descriptors which were as follows: 1) R1 volume; 2) R2-SsCH3E-index; 3) R3-SsCH3count; and 4) R5-Epsilon R with positive contribution from two and negative contribution from other two having $r^2 = 0.8259$, $q^2 = 0.6788$, and F-test = 37.9418 (Goswami *et al.*, 2017).

3.2.2 3D-QSAR studies

The first contribution of 3D-QSAR for TSPO was in 1994 (Greco *et al.*, 1994), in which analysis of the molecular fields of 42 compounds with 6-arylpyrrolo[2,1-d][1,5]benzothiazepines derivatives was done in order to find out molecular properties responsible for TSPO affinity. The efficacy of their CoMFA model in estimating binding affinity values was validated by applying it to set of 7 compounds as test set and the model was applied to find the highest TSPO affinity ligand among the pyrrolobenzothiazepine derivatives which were investigated. Ro5-4864 was taken as template for resulting alignment through superimposed ligands demonstrating four pharmacophoric points: 1) the centroid L1 placed on the benzene ring (fused), 2) the centroid L3 placed on the phenyl ring (pendant), 3) the lone pair H2 placed on the oxygen (carbonyl/ester), and 4) the centroid n1 placed on the pyrrole moiety (Fig. 3.2.a). The 3D-QSAR model developed was applied for prediction of binding affinity towards TSPO for the compounds of test set. The affinity was measured as pIC_{50} . The differences between values of observed and predicted pIC_{50} fall in the range of -0.76 and 0.70 with IC_{50} of best derivative being comparable to that of PK11195 (Greco *et al.*, 1994).

In 2000, a new pyrrolobenzothiazepine analogues-based model was generated with more diverse molecules such as quinolone, isoquinoline, pyrrolobenzoxazepine, pyrroloquinolin

-1-one derivatives and pyrrolopyridin-5-one (Fig. 3.2.b) (Cinone *et al.*, 2000). The active analogue approach based principle was used for the alignment of 130 analogues (Marshall *et al.*, 1979). For template, *N*-benzyl-*N*,3-dimethyl-4-phenylquinoline-2-carboxamide was taken due to its relatively low flexibility with high affinity.

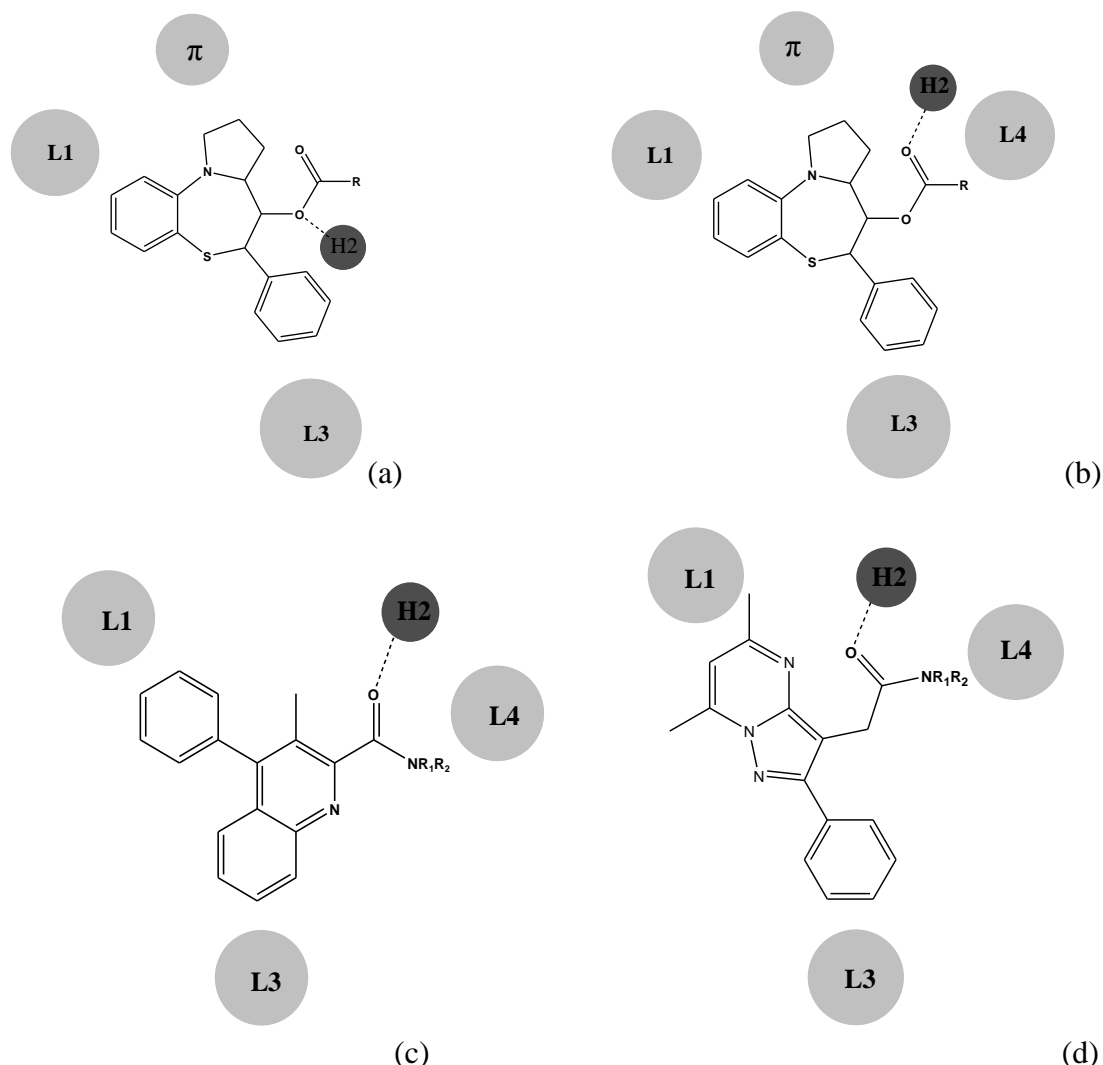


Fig. 3.2: Schematic TSPO models' representation on a) 6-arylpyrrolo[2,1-d][1,5]benzothiazepines analogues; b) quinolone, isoquinoline, pyrrolobenzoxazepine, pyrrolopyridin-5-one, and pyrroloquinolin-1-one derivatives; c) pyrrolobenzoxazepine derivatives; d) 2-arylpyrazolo[1,5-a]pyrimidin-3-yl acetamides analogues

In the interaction model, two centroids (L1 and L3) correspond to the aromatic rings and one carbonyl group containing lone pair (H2) and a lipophilic region L4 of the ester chains were defined. As compared to Greco's model (Greco *et al.*, 1994), the

common regions were L1 and L3, but there was a slight shift in H2 which was carbonyl group, not the oxygen of ester (Fig. 3.2.b). In 1996, similar findings of pharmacophoric studies were reported on a series of pyrrolobenzoxazepine derivatives (Fig. 3.2.c) (Campiani *et al.*, 1996). On trying different options for the correlation of 3-D molecular descriptors and dependent variables: the SRD-FFD (smart region definition along with fractional factorial design) method with the GRID lipophilic probe DRY produced the best model, representing 6 components with $r^2 = 0.898$ and $q^2 = 0.761$. This GRID/GOLPE study demonstrated the interactions in model which were hydrophobic in nature, specifically L4 region. With the aim to find out the common properties between endogenous peptides such as DBI, ODN, and TTN and synthetic ligands, the DRY MIFs were derived from these peptides based molecular models. Two compounds with high affinities were manually superimposed using DRY showed the most favoured interactions defining chemical features present in these ligands mimicking few amino acids present. On superpositioning with the best, L1, L3, and L4 regions were aligned with the Phe-Asp-Leu-Met, a common sequence.

In 2005, a new class of azaisosters Alpidem (2-arylpyrazolo[1,5-a]pyrimidin-3-yl acetamides) (Selleri *et al.*, 2001), reflecting high affinity and selectivity for TSPO ligands, was used for 3D-QSAR study to reveal the substitution effect on the acetamide with different moieties (Selleri *et al.*, 2005). Thirty eight pyrazolopyrimidines analogues were computed. The generated GRID/GOLPE model suggested that the binding sites of TSPO had cavities with variation in steric tolerance that could accommodate the two substituents (allyl) indicating the limitation of chain length with 4 to 5 C chains (Fig. 3.2.d). Moreover, this model could also explain the stereoselectivity and binding site

TSPO in terms of hydrophobic interactions. This supported the concept of site having two cavities which are different (Tuccinardi *et al.*, 2009).

In order to understand the physico-chemical and/or structural requirement for better selectivity of compound towards TSPO over central, QSAR study was performed on derivatives of [2-phenylimidazol[1,2-a]pyridine-3-yl]acetamide. Peripheral and central (from ovary and cortex) TPSO affinity binding data were used for the study (Roy *et al.*, 2003).

3.2.3 Virtual screening: a pharmacophore and 3D-QSAR studies

In 2009, based on 3D-QSAR, one pharmacophore hypothesis was chosen out of various considered hypotheses for TSPO ligands for virtual screening of the Maybridge database to identify new TSPO ligand. Out of 144 molecules (2-arylpyrazolo[1,5-a]pyrimidine acetamides, 2-phenylindolglyoxylamides, and 2-phenylimidazo[1,2-a]pyridineacetamides) were considered for generation of pharmacophore through PHASE software. Forty two and thirteen molecules with high and low TSPO affinities, respectively were chosen to generate pharamacophore. The 94 hypothesis obtained were divided into four groups AHRRR, AAHRR, AXRRR, and AXXRRR, where A was hydrogen bond acceptor, H was hydrophobic group, R was aromatic ring, and X was a customized feature combining hydrophobic group and aromatic ring. The best model was chosen out of each pharmacophoric types with the help of the atom-based QSAR model using PHASE. In order to provide better analysis for selection of the best pharmacophore, four 3D-QSAR models had been generated using four pharmacophoric hypotheses with the help of GOLPE software. The model AXRRR was found to be the best for predicting external test set ($q^2=0.70$ and SDEPTS (standard deviation of errors of predictions) = 0.60)). Though the pharmacophore building in this study used diverse structures, in comparison to the

precisely developed models on the pyrrolobenzothiazepine analogues (Selleri *et al.*, 2001; Selleri *et al.*, 2005), the L3 and L1 regions are also present in this model. Additionally, the alignment of the A could be with H2 and X could be with L4 regions. Finally, Maybridge database having 61785 compounds was virtually screened using AXRRR as pharmacophore model. This data base has 32 TSPO ligands with equal number of low and high TSPO affinity which were not included in 3D-QSAR and pharmacophoric studies. The compounds from database predicted to have high affinity were 38. Finally, 7 compounds were chosen and subjected to a TSPO binding assay that demonstrated TSPO affinity particularly two compounds, RJC02811 and NRB03635, mentioned in the Fig. 3.3 having K_i value 877 nM and 420 nM, respectively (Tuccinardi *et al.*, 2009).

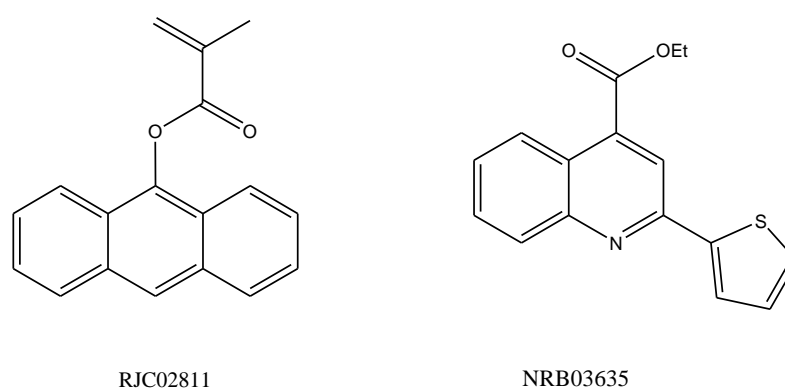


Fig. 3.3: Virtually screened compounds from Maybridge database

Till date, there are limited computational reports on benzoxazolone based TSPO ligands, although few correlations on the basis of experimental activity and their structures have been identified (Fukaya *et al.*, 2012; Fukaya *et al.*, 2013).

3.2.4 Docking studies

There were few studies reported for TSPO in literature for the identification of potential binding sites for TSPO ligands. The binding sites for known TSPO ligands were identified.

These were further differentiated as binding site with low- and high-affinity on TSPO (monomer as well as dimer) using 2MGY, a 3D structure of TSPO from mammalian source. In this, PK11195 was attached with a hydrophobic pocket (Bhargavi *et al.*, 2017).

In 2015, molecular docking of TSPO with cholesterol structure has been reported using *Rhodobacter sphaeroides* TSPO. Various binding conformations and orientations of cholesterol were docked on receptor grid generated at the binding site of CRAC. The most prominent anchoring points identified inside the binding cavity include Tyr152 of *Homo sapiens* TSPO, as well as Thr148 and Thr149 that could form favorable interactions with ligands (Papadopoulos *et al.*, 2015).

In the process of achieving high affinity towards TSPO, a number of lead skeletons for TSPO have been modified for improved affinity towards TSPO, most of them were CBR selective ligands modified to make them TSPO selective. For example, the benzodiazepine Ro5-4864 and the isoquinoline carboxamide PK11195 were structurally modified. This led to development of good ligands with affinity and selectivity towards TSPO. SAR data analysis was performed on the various TSPO ligands derivatives to come up with desired pharmacophoric requirements to develop new potent and selective TSPO ligands (Taliani *et al.*, 2011).

3.3 Properties of CNS imaging probes

There are several prerequisites for the usefulness of PET/SPECT probes as imaging agent under *in vivo* conditions which are derived from empirical research and provide guidance for designing of imaging probes. Some of these are as follows:

3.3.1 Selectivity for the receptor

The drug concentration that occupies fifty percent of receptors available is called equilibrium dissociation constant (K_d) of a drug complex with receptor. The

reciprocal of equilibrium dissociation constant is known as affinity and is the highest for the imaging target. The binding affinity of PET/SPECT probes for imaging should be in the range of sub nM as concentration of binding sites with maximum value (B_{\max}) for receptors in brain is mostly in the range of nano/mg to femtomoles/mg of tissue. The binding affinity of radioligands should not be too high as uptake is dependent on blood flow binding and high binding affinity makes uptake irreversible and equilibrium studies impossible. The B_{\max} and K_d are calculated by equilibrium assay of binding under *in vitro* condition and depends on the target protein and radiolabelled imaging agent, respectively. For example dopamine D_2 receptor has 10-30 pM density and PET/SPECT probes for D_2 are 1-10 nM. The binding potential is B_{\max}/K_d often gives predictive target to non-target ratio for *in vivo* condition. In reality this predicted value is much higher than the actual *in vivo* binding (Eckelman *et al.*, 2006).

3.3.2 Specific radioactivity

Specific radioactivity (SA) is defined by the amount of radioactivity per unit mass of a radioligand. The maximum value of theoretical specific radioactivity of radioligand is related to its physical half-life as per the following equation:

$$SA = (\ln 2/t_{1/2})N$$

Where, N and $t_{1/2}$ are the number of radionuclides and its physical half-life, respectively. Conversion of N to the moles can be done by its division with 6.023×10^{23} (Avogadro's number). The maximum value of theoretical SA can be calculated as per following equation:

$$SA \text{ (Bq/mol)} = 1.16 \times 1020/t_{1/2} \text{ (h)}$$

This implies that the shorter the half-life, higher the specific activity. For example, oxygen-15 has high theoretical specific activity as $t_{1/2}$ is short (2 min). Therefore, PET radioisotopes have requirement of low masses as their half-lives are relatively short. For example, doses in clinical setup i.e. 370 MBq of ^{18}F and ^{11}C are 1.0529 ng and 0.01186 ng, respectively. The mass requirement of imaging probes with ^{11}C - and ^{18}F -labelling are around 5-10 μg . For imaging of receptors in brain under *in vivo* condition, specific radioactivity of radiopharmaceuticals should be high. This would require low occupancy on binding sites. If radioligand is of low specific activity then significant binding site occupancy by radioligand may deteriorate signal to noise ratio and may be toxic.

3.3.3 Metabolism and position of label

PET/SPECT radiopharmaceuticals should not metabolize during image acquisition as these modalities are unable to differentiate between parent and metabolite which are radiolabelled. Sample of extract from target organs/blood can be used for analysis of metabolite using HPLC. The important factor of radiopharmaceutical is site of radiolabelling that needs to be chosen carefully at the design level as its loss through metabolism will restrict its ability as imaging agent.

3.3.4 Blood-brain barrier permeability

PET/SPECT probes for imaging CNS may be unsuccessful due to its inability to enter brain crossing blood brain barrier (BBB). There are two factors that are required in drug to assess the ability to cross BBB: 1) ability to form hydrogen bond with water

(< 8-10); and 2) molecular weight (<400-600 Da). For example, radiopharmaceuticals based of peptides form large number of hydrogen bonding but could not enter brain through BBB in considerable amount. There is molecular weight requirement as it is also linked with the volume of the molecule. The partition coefficient for octanol/water, P, is one of the properties to predict penetrating ability through BBB with optimal value of log P in the range 2-3.5 (Terasaki *et al.*, 2003; Abbott 2004). Among derivatives of same lead compound, the non-specific binding relates to log P for transport of compound through diffusion.

3.3.5 Clearance rate, protein binding, and non-specific binding

Some other important parameters are rapid blood clearance and binding to non-specific sites. There is a requirement of low plasma proteins binding of radiopharmaceutical as unbound drug in plasma may diffuse form vascular space to brain which provides better target to background ratio.

These properties may not assure a successful radiopharmaceutical for CNS still useful to design the molecular probes for imaging. Even successful drug may not be developed as imaging probe. For example, an anti-depressant drug fluoxetine is not appropriate candidate for serotonin transporter imaging due to its non-specific binding under *in vivo* condition (Shiue *et al.*, 1995).

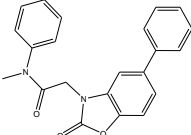
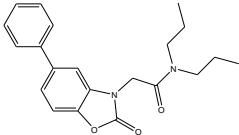
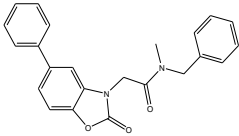
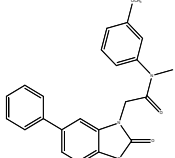
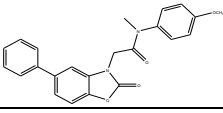
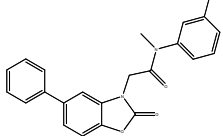
3.4 Result and discussion

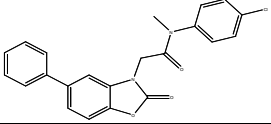
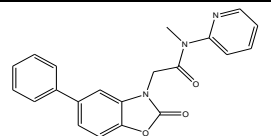
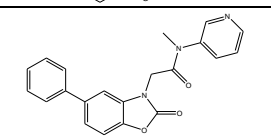
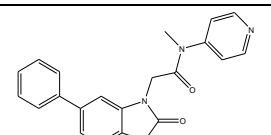
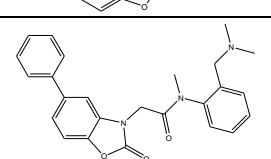
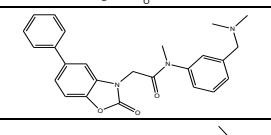
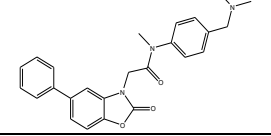
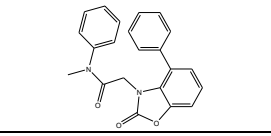
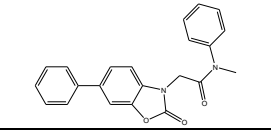
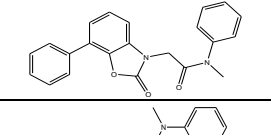
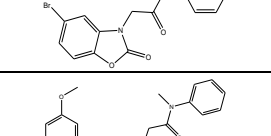
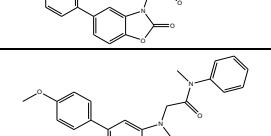
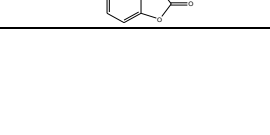
3.4.1 Pharmacophore modelling and 3D-QSAR studies

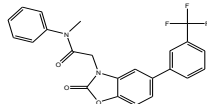
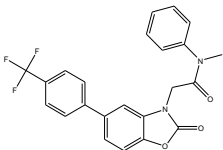
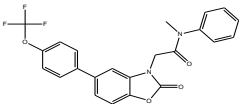
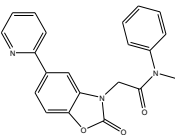
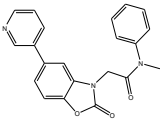
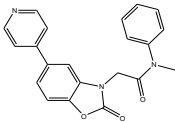
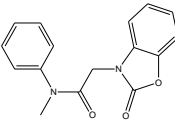
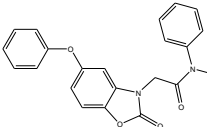
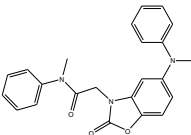
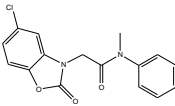
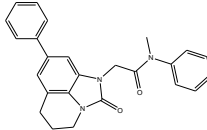
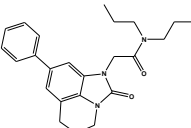
Among the recently published work considerable attention has been given to the benzoxazolone based TSPO ligands due to their affinity towards TSPO in nano molar range while avoiding the A147T mutation effect on affinity (Tiwari *et al.*, 2014). In the line to utilize these ligands for diagnostic purpose using different modalities, our

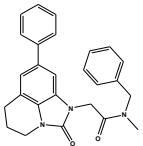
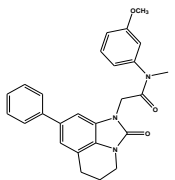
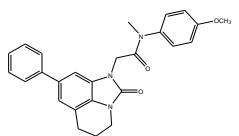
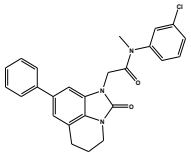
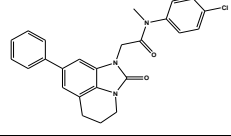
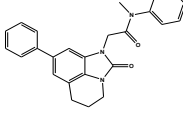
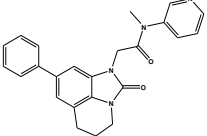
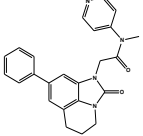
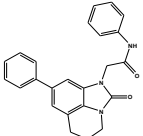
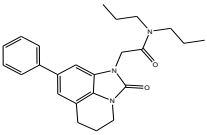
group has reported a new series of acetamidobenzoxazolone displaying similar affinity for both the mutants (Tiwari *et al.*, 2014; Tiwari *et al.*, 2014 (a); Tiwari *et al.*, 2015; Tiwari *et al.*, 2015(a)). In order to investigate the structural requirements of TSPO ligand and to come up with the predictive model that can find application in designing of novel ligands for TSPO targeting with selectivity, a common pharmacophore hypothesis generation followed by evaluation through 3D-quantitative structure-activity relationship (3D-QSAR) study was performed on the series of reported benzoxazolone derivatives for TSPO employing PHASE module of Schrodinger software. In order to understand the key responsible features for affinity, benzoxazolone based TSPO ligands were used for pharmacophore modelling.

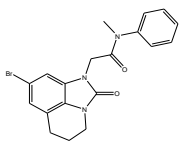
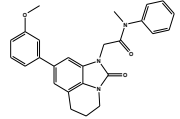
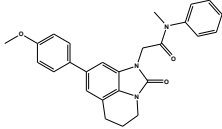
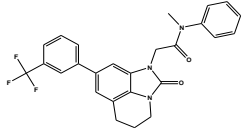
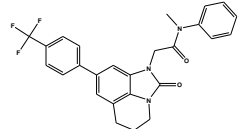
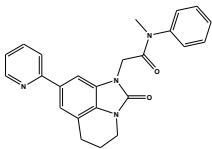
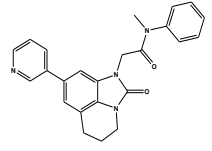
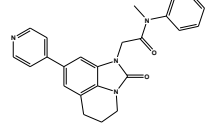
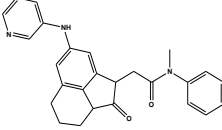
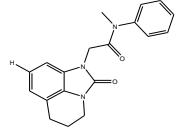
Table 3.1: List of TSPO ligands used in pharmacophore modelling

S. No	K _i (nM)	TSPO ligands	IUPAC Names
1	1.6		N-Methyl-2-(2-oxo-5-phenyl-benzoxazol-3-yl)-N-phenyl-acetamide
2	17		2-(2-Oxo-5-phenyl-benzoxazol-3-yl)-N,N-dipropyl-acetamide
3	13		N-Benzyl-N-methyl-2-(2-oxo-5-phenyl-benzoxazol-3-yl)-acetamide
4	0.9		N-(3-Methoxy-phenyl)-N-methyl-2-(2-oxo-5-phenyl-benzoxazol-3-yl)-acetamide
5	2.2		N-(4-Methoxy-phenyl)-N-methyl-2-(2-oxo-5-phenyl-benzoxazol-3-yl)-acetamide
6	0.79		N-(3-Chloro-phenyl)-N-methyl-2-(2-oxo-5-phenyl-benzoxazol-3-yl)-acetamide

S. No	K _i (nM)	TSPO ligands	IUPAC Names
7	0.21		N-(4-Chloro-phenyl)-N-methyl-2-(2-oxo-5-phenyl-benzoxazol-3-yl)-acetamide
8	23		N-Methyl-2-(2-oxo-5-phenyl-benzoxazol-3-yl)-N-pyridin-2-yl-acetamide
9	28		N-Methyl-2-(2-oxo-5-phenyl-benzoxazol-3-yl)-N-pyridin-3-yl-acetamide
10	270		N-Methyl-2-(2-oxo-5-phenyl-benzoxazol-3-yl)-N-pyridin-4-yl-acetamide
11	2		N-(2-Dimethylaminomethyl-phenyl)-N-methyl-2-(2-oxo-5-phenyl-benzoxazol-3-yl)-acetamide
12	12		N-(3-Dimethylaminomethyl-phenyl)-N-methyl-2-(2-oxo-5-phenyl-benzoxazol-3-yl)-acetamide
13	88		N-(4-Dimethylaminomethyl-phenyl)-N-methyl-2-(2-oxo-5-phenyl-benzoxazol-3-yl)-acetamide
14	11		N-Methyl-2-(2-oxo-4-phenyl-benzoxazol-3-yl)-N-phenyl-acetamide
15	120		N-Methyl-2-(2-oxo-6-phenyl-benzoxazol-3-yl)-N-phenyl-acetamide
16	29		N-Methyl-2-(2-oxo-7-phenyl-benzoxazol-3-yl)-N-phenyl-acetamide
17	9		2-(5-Bromo-2-oxo-benzoxazol-3-yl)-N-methyl-N-phenyl-acetamide
18	0.18		2-[5-(3-Methoxy-phenyl)-2-oxo-benzoxazol-3-yl]-N-methyl-N-phenyl-acetamide
19	0.49		2-[5-(4-Methoxy-phenyl)-2-oxo-benzoxazol-3-yl]-N-methyl-N-phenyl-acetamide

S. No	K _i (nM)	TSPO ligands	IUPAC Names
20	0.33		N-Methyl-2-[2-oxo-5-(3-trifluoromethyl-phenyl)-benzoxazol-3-yl]-N-phenyl-acetamide
21	0.29		N-Methyl-2-[2-oxo-5-(4-trifluoromethyl-phenyl)-benzoxazol-3-yl]-N-phenyl-acetamide
22	0.48		N-Methyl-2-[2-oxo-5-(4-trifluoromethoxy-phenyl)-benzoxazol-3-yl]-N-phenyl-acetamide
23	0.68		N-Methyl-2-(2-oxo-5-pyridin-2-yl-benzoxazol-3-yl)-N-phenyl-acetamide
24	0.65		N-Methyl-2-(2-oxo-5-pyridin-3-yl-benzoxazol-3-yl)-N-phenyl-acetamide
25	1.8		N-Methyl-2-(2-oxo-5-pyridin-4-yl-benzoxazol-3-yl)-N-phenyl-acetamide
26	11		N-Methyl-2-(2-oxo-benzoxazol-3-yl)-N-phenyl-acetamide
27	5.3		N-Methyl-2-(2-oxo-5-phenoxy-benzoxazol-3-yl)-N-phenyl-acetamide
28	3.8		N-Methyl-2-[5-(methyl-phenyl-amino)-2-oxo-benzoxazol-3-yl]-N-phenyl-acetamide
29	0.36		2-(5-Chloro-2-oxo-benzoxazol-3-yl)-N-methyl-N-phenyl-acetamide
30	2.5		N-Methyl-2-(2-oxo-8-phenyl-5,6-dihydro-4H-imidazo[4,5,1-ij]quinolin-1-yl)-N-phenyl-acetamide
31	0.06		2-(2-Oxo-8-phenyl-5,6-dihydro-4H-imidazo[4,5,1-ij]quinolin-1-yl)-N,N-dipropyl-acetamide

S. No	K _i (nM)	TSPO ligands	IUPAC Names
32	0.94		N-Benzyl-N-methyl-2-(2-oxo-8-phenyl-5,6-dihydro-4H-imidazo[4,5,1-ij]quinolin-1-yl)-acetamide
33	0.11		N-(3-Methoxy-phenyl)-N-methyl-2-(2-oxo-8-phenyl-5,6-dihydro-4H-imidazo[4,5,1-ij]quinolin-1-yl)-acetamide
34	0.3		N-(4-Methoxy-phenyl)-N-methyl-2-(2-oxo-8-phenyl-5,6-dihydro-4H-imidazo[4,5,1-ij]quinolin-1-yl)-acetamide
35	0.23		N-(3-Chloro-phenyl)-N-methyl-2-(2-oxo-8-phenyl-5,6-dihydro-4H-imidazo[4,5,1-ij]quinolin-1-yl)-acetamide
36	0.16		N-(4-Chloro-phenyl)-N-methyl-2-(2-oxo-8-phenyl-5,6-dihydro-4H-imidazo[4,5,1-ij]quinolin-1-yl)-acetamide
37	2.7		N-Methyl-2-(2-oxo-8-phenyl-5,6-dihydro-4H-imidazo[4,5,1-ij]quinolin-1-yl)-N-pyridin-2-yl-acetamide
38	3.3		N-Methyl-2-(2-oxo-8-phenyl-5,6-dihydro-4H-imidazo[4,5,1-ij]quinolin-1-yl)-N-pyridin-3-yl-acetamide
39	0.55		N-Methyl-2-(2-oxo-8-phenyl-5,6-dihydro-4H-imidazo[4,5,1-ij]quinolin-1-yl)-N-pyridin-4-yl-acetamide
40	2		2-(2-Oxo-8-phenyl-5,6-dihydro-4H-imidazo[4,5,1-ij]quinolin-1-yl)-N-phenyl-acetamide
41	1.7		2-(2-Oxo-8-phenyl-5,6-dihydro-4H-imidazo[4,5,1-ij]quinolin-1-yl)-N,N-dipropyl-acetamide

S. No	K _i (nM)	TSPO ligands	IUPAC Names
42	0.23		2-(8-Bromo-2-oxo-5,6-dihydro-4H-imidazo[4,5,1-ij]quinolin-1-yl)-N-methyl-N-phenyl-acetamide
43	0.28		2-[8-(3-Methoxy-phenyl)-2-oxo-5,6-dihydro-4H-imidazo[4,5,1-ij]quinolin-1-yl]-N-methyl-N-phenyl-acetamide
44	0.73		2-[8-(4-Methoxy-phenyl)-2-oxo-5,6-dihydro-4H-imidazo[4,5,1-ij]quinolin-1-yl]-N-methyl-N-phenyl-acetamide
45	0.44		N-Methyl-2-[2-oxo-8-(3-trifluoromethyl-phenyl)-5,6-dihydro-4H-imidazo[4,5,1-ij]quinolin-1-yl]-N-phenyl-acetamide
46	0.13		N-Methyl-2-[2-oxo-8-(4-trifluoromethyl-phenyl)-5,6-dihydro-4H-imidazo[4,5,1-ij]quinolin-1-yl]-N-phenyl-acetamide
47	2.5		N-Methyl-2-(2-oxo-8-pyridin-2-yl-5,6-dihydro-4H-imidazo[4,5,1-ij]quinolin-1-yl)-N-phenyl-acetamide
48	2.1		N-Methyl-2-(2-oxo-8-pyridin-3-yl-5,6-dihydro-4H-imidazo[4,5,1-ij]quinolin-1-yl)-N-phenyl-acetamide
49	15		N-Methyl-2-(2-oxo-8-pyridin-4-yl-5,6-dihydro-4H-imidazo[4,5,1-ij]quinolin-1-yl)-N-phenyl-acetamide
50	33		N-Methyl-2-[2-oxo-7-(pyridin-3-ylamino)-1,2,2a,3,4,5-hexahydro-acenaphthylen-1-yl]-N-phenyl-acetamide
51	994		N-Methyl-2-(2-oxo-5,6-dihydro-4H-imidazo[4,5,1-ij]quinolin-1-yl)-N-phenyl-acetamide

A data set of 51 TSPO ligands (Fukaya *et al.*, 2012; Fukaya *et al.*, 2013) with K_i values found under similar conditions with rat kidney membranes were considered for this purpose (Table 3.1). The compounds were divided as high and low affinity compounds for TSPO by putting threshold of K_i value as greater than 9.1 and lower than 8.5, respectively. This resulted in 19 compounds each in high and low affinity category for generating pharmacophore by PHASE. The list of variants with four-features was generated for the probable pharmacophore hypotheses.

The considered compounds were segregated in two sets, one for training and another for test i.e. external validation with 38 compounds and 13 compounds, respectively. Alignment of the compounds for training as well as test were performed on the pharmacophores and analysed through PLS with 3 factors. The best model for each type of pharmacophore was chosen on the basis of significant statistical data and predictability of the affinity of the external test set. The selected models were AAAR, AARR, AAAR, AHRR, ARRR and AAAR.

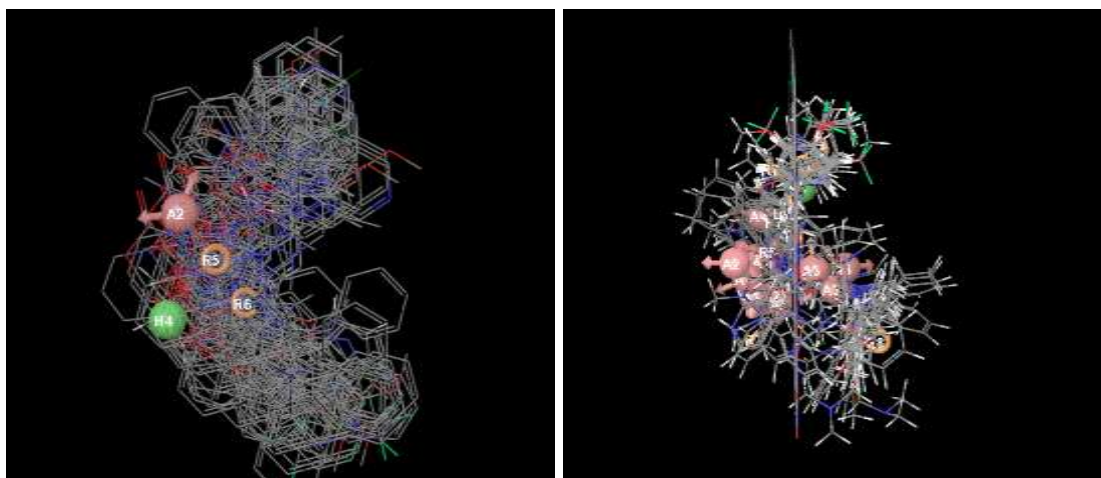


Fig. 3.4: Frame of total 51 compounds

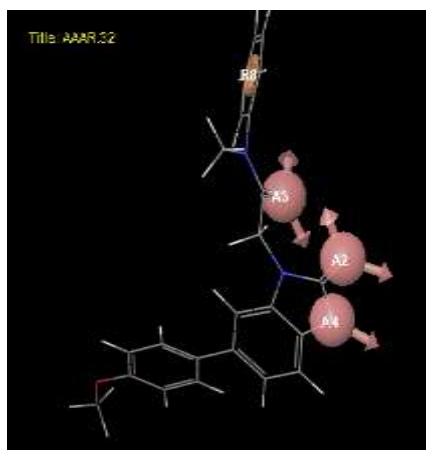


Fig. 3.5: Pharmacophore model AAAR: presenting the best model of the study

The best pharmacophore hypothesis was selected by applying 3D-QSAR methods which is an important step towards identification of pharmacophores. AAAR was found the best hypothesis on the basis of predictive ability as well as internal validation (Fig. 3.4, Fig. 3.5) with $R^2=0.95$ and standard deviation=0.237-0.760. Its scattering plot of predicted vs experimental activities is shown in Fig. 3.6. This was further utilized for designing the TSPO ligands having benzoxazolone moiety as a base skeleton.

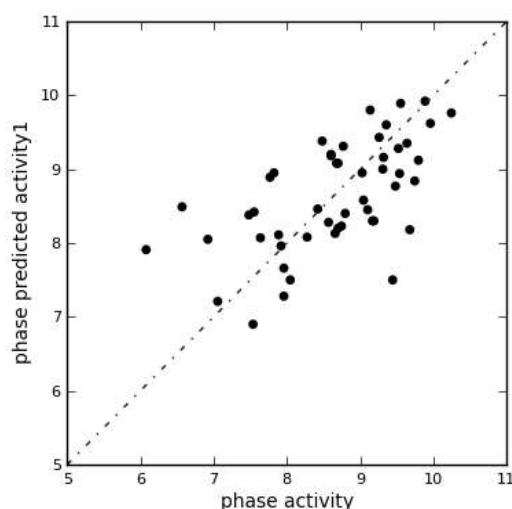


Fig. 3.6: Scattering plot of predicted vs experimental activities of TSPO ligands as per the 3D-QSAR model for the best four-featured pharmacophore model

3.4.2 Design of new TSPO skeletons

In the present work, the hypothesis of AAAR was applied for designing the TSPO ligands taking benzoxazolone as lead moiety, the three acceptor groups oxygen atom, carboxy of oxazolone moiety as well as carboxy group of acetamide were kept intact that forms acetamidobenzoxazolone moiety.

For the selection of R, amino acids were chosen as they are biological molecules. The selection of type of amino acids was done on the basis of several factors. Various amino acid analogues have been used in diagnosis of diseases as metabolic activity increases in various pathological situations such as cancer, increasing the requirement of amino acid uptake. The choice of amino acid was done to have aromatic/hydrophobic properties at a particular site. One of the factors was metabolic parameter. It has been reported that regulation of immune cell function is related to metabolic parameters. Therefore, the metabolism in inflammation plays important role for amino acids especially amino acids with aromatic group like phenylalanine and tryptophan. In addition, disturbed amino acids are associated with the acute and chronic conditions in neuropsychiatric conditions such as depression and cognitive impairment. The disease progression can be determined by biomarker such as TSPO for immune response along with monitoring of immunometabolic parameters such as amino acids before and during therapy (Strasser *et al.*, 2016).

Keeping the above mentioned points in mind, the resultant acetamidobenzoxazolone-amino acid esters (ABEO) skeleton ABO-AA was tried for four amino acid esters-methyl esters of tryptophan, phenylalanine, tyrosine and methionine. The tryptophan and phenylalanine are chosen as they are the important pharmacophores from

previous generation TSPO ligands i.e. indole of FGIN-127 and benzyl of AC-5216, respectively having affinity in nanomolar range. Presence of amino acid ester has also helped in reducing the log P values which is problem of FGIN-127 (6.94). Additionally presence of benzyl group in high affinity TSPO ligand AC-5216 has been explored for N-substituted 4-phenylquinazoline-2-carboxamides derivatives (Castellano *et al.*, 2014). These are the rationale behind our choice of tryptophan and phenylalanine esters as amino acid esters for conjugation.

Tyrosine and methionine are selected as they are positioned in the same class of amino acid as tryptophan and phenylalanine with hydrophobic side chain and both are widely used for diagnostic applications. In addition to this, presence of OH and S group in tyrosine and methionine would provide chelating arm for holding ^{99m}Tc . Tyrosine conjugated acetamidobenzoxazolone fulfils the requirements of AAAR hypothesis in addition to being benzyl analogue. Therefore, it is also worth analyzing. Though the choice of methionine is not as per pharmacophoric requirements, the requirement of three lipophilic pockets in the earlier studies with different structural skeletons encouraged us to explore this substitution.

Further, a substituent on the benzoxazolone derivative at C-5 position of phenyl ring that plays an important role in TSPO binding, has been incorporated at that position. Substitution by halogen in aromatic ring system at this position provides sub-nanomolar binding affinity (Fukaya *et al.*, 2012). This is the rationale behind selecting Br/Cl for C-5 position for designing the benzoxazolone ring. This has also been mentioned in literature that compound suffered from poor solubility due to phenyl substituent at acetamide side. We have tried biocompatible amino acid analogues at this position to solve solubility issue for better prospect in clinical application

3.4.3 ADME properties

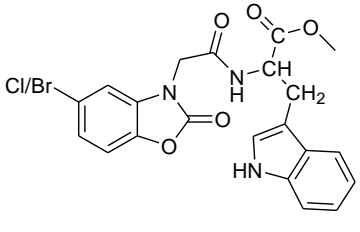
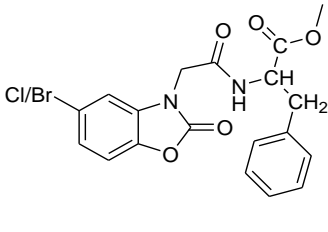
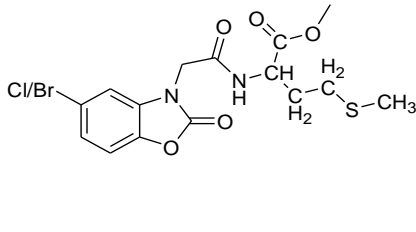
The acetamidobenzoxazolone-amino acid esters (ABEOs) were screened on the basis of ADME properties. It is important to know the pharmacokinetic profile of any ligand to be used under *in vivo* conditions which can be studied through ADME properties. ADME stands for adsorption, distribution, metabolism and excretion. Often drugs were unsuccessful because of their poor pharmacokinetic properties. A promising lead should have potency and attractive ADME profile both. Thus, it is imperative to design the compound with easy transportability to desired site, proper interaction at desired site, not or minimally metabolize before its action and finally excrete after expected action.

As we are targeting the receptors/proteins which are found on outer mitochondrial surface of glial cells, our molecules should be able to reach glial cells in brain. This means that their capability to cross BBB is essential and their lipophilicity must be high as lipophilic substances are required to cross the BBB. The contribution of different molecular descriptors towards various molecular properties such as $-\log S$, $\log P_{o/w}$, $\log PMDCK$ and $\log BB$ of known and ABEOs are mentioned below (Table 3.3). In case of ABEOs, the contributors for these properties are common with atleast one known ligand.

3.4.3.1 Assessment of drug-likeness

The drug-likeness or capability for becoming a good drug candidate for clinical application was predicted by Lipinski rule of 5 which is used in CADD analysis. All the six proposed ligands (2-(2-(5-bromo/chloro-benzoxazolone) acetamido)-3-(1*H*-indol-3-yl) propanoate (ABTO-Br/Cl), methyl 2-(2-(5-bromo/chloro-2-oxobenzoxazol-3(2*H*)-yl)acetamido)-3-phenylpropanoate (ABPO-Br/Cl) and 2-[2-(5-bromo/chloro-2-oxo-benzoxazol-3-yl)-acetylamino]-4-methylsulfonyl-butyric acid methyl ester (ABMO-Cl/Br) shown in the Table 3.2 follow all the 5 rules of Lipinski which reflect their drug like properties.

Table 3.2: Chemical structures of designed ligands

ABTO-Br/Cl	ABPO-Br/Cl	ABMO-Br/Cl
		

The molecular weight of known TSPO ligands (DAA1106, DPA-713, FGIN-127, PBR-06, PBR28, PBR111, PK11195, and Ro5-4864) as well as of designed ligands were < 500 as desired by Lipinski rule. Similarly, hydrogen bond donors for known and designed molecules were in between 0 and 1.25, following Lipinski rule requirement of < 5. Additionally, hydrogen bond acceptors were between 3 and 7.25 for known and for designed molecules which were well within the acceptable proposed limit of 10 for Lipinski rule. However, QPlogP, an important property for molecule to cross BBB which was followed by all the designed ligands and their values were in the range of 2.18-3.23, with the lowest value for ABMO-Br and the highest value for ABTO-Br. Few known TSPO ligands such as FGIN-127, PBR06, PBR111 and PK11195 showed one violation with QPlogP > 5, reflecting their high lipophilicity, reduced specificity and reduced bioavailability due to its interaction with plasma protein. The lipophilicity aspect of these known ligands needs correction through its reduction. All the proposed ligands had lower value but good enough to cross the BBB as per preference values from literature. They could possibly reduce non-specificity. Overall, the proposed ligands had drug like properties as per Lipinski rule and better than known ligands in terms of lipophilicity which were needed to be improved for better specificity and bioavailability (Table 3.4).

3.4.3.2 Prediction of bioavailability

Various factors affect compound's bioavailability such as liver-pass metabolism and processes of absorption. Solubility, permeability, transporters' interaction and enzymes' interaction (enzymes available on the wall of gut) are deciding factors for absorption. The oral absorption of compound depends on computed parameters such as conformation independent aqueous solubility, aqueous solubility, qualitative model for human oral absorption, % of human oral absorption in GI, and compliance of Jorgensen's rule of three.

Out of all the known ligands taken for comparison purpose, only two were violating this rule for QPlogS < -5.7 (-7.4 for FGIN-127 and -6.22 for PBR111). For designed ligands, the solubilities were in increasing order for ABMO, ABPO, and ABTO analogues with their QPlogS for aqueous solubility in the range of -5.4 to -3.72 which were better or comparable with the known ligands.

The Caco-2 permeability for designed ligands were between 198-477 and for known ligands between 2290-6015, all being much higher than 25 nm/s, the limit of poor permeability as mentioned by software.

The Qikprop can estimate the number of possible metabolites of a drug which determines its accessibility to the target post blood stream administration. This was in the ranges from 0-5 for known TSPO ligands and 2-3 for designed ligands. These molecules reflected that the designed molecules have limited possibilities to cleave or hydrolyze under *in vivo* condition.

All the designed ligands follow Jorgensen's rules with apparent Caco-2 permeability >22 nm/s, $\text{LogS}_{\text{wat}} < -5.7$, and primary metabolites <7 , predicting their bioavailabilities.

The other parameter responsible for absorption, conformation independent QPlogS values for designed molecules (-6.55 to -3.72) were comparable to that of known ligands (-7.17 to -4.44). Reasonably good absorption were also reflected by % human oral absorption in GI which were >85 for proposed ligands and 100 for known ligands. Even qualitative model for human oral absorption predicted high oral absorption for the proposed ligands. The permeability was determined by molecular size, lipophilicity, shape and flexibility. Molecular size and lipophilicity of designed ligands were comparable to known TSPO ligands. Molecular flexibility is related to number of rotatable bond which is connected to bioavailability that increases with the decrease in number of rotors. They were 6 or 7 in designed molecules which were comparable to known TSPO ligands such as DAA1106, PBR06 and PBR28. However, some known ligands have either high (12 for FGIN-127) or low (0 for Ro5-4864) rotatable bonds. There is requirement of optimum rotatable bonds to bind in the pocket of receptor as conformational restriction generates entropy loss on binding in case of flexible molecules. As the molecule is meant for diagnostic application, too low number of rotatable bonds may lead to stickiness to the target receptor. Therefore, designed ligands with 6 or 7 rotatable bonds as present in known ligands seemed to be reasonable for ligands for diagnostic purpose (Table 3.4).

Table 3.3: Molecular descriptor and their components

	DAA1106	DPA-713	FGIN-127	PBR06	PBR28	PBR111	PK11195	Ro5-4864	ABMO-Br	ABMO-Cl	ABPO-Br	ABPO- Cl	ABTO-Br	ABTO-Cl
log Po/w														
H-bond Donor	0	0	-0.3	0	0	0	0	0	-0.075	-0.075	-0.075	-0.075	-0.375	-0.375
H-Bond acceptor	-2.435	-2.8	-1.461	-2.435	-2.8	-2.557	-1.948	-1.948	-3.531	-3.531	-3.287	-3.287	-3.287	-3.287
Volume	7.579	7.834	9.794	7.831	7.333	8.528	7.371	6.142	7.287	7.333	7.652	7.468	8.226	7.871
Ac x Dn [^] .5/SASA	0	0	0.164	0	0	0	0	0	0.25	0.249	0.23	0.237	0.471	0.512
FISA	-0.165	-0.334	-0.308	-0.158	-0.299	-0.233	-0.246	-0.414	-0.965	-0.967	-1.039	-0.844	-1.128	-1.05
Non-con amides	0	-0.626	-0.626	0	0	-0.626	0	0	-0.626	-0.626	-0.626	-0.626	-0.626	-0.626
WASA & PISA	0.531	0.176	0.46	0.615	0.488	0.711	0.547	0.807	0.545	0.556	0.61	0.574	0.654	0.549
Constant	-0.705	-0.705	-0.705	-0.705	-0.705	-0.705	-0.705	-0.705	-0.705	-0.705	-0.705	-0.705	-0.705	-0.705
Total	4.805	3.546	7.019	5.148	4.017	5.118	5.019	3.882	2.18	2.23	2.76	2.741	3.23	2.89
-log S														
H-bond donor	0	0	-0.402	0	0	0	0	0	-0.1	-0.1	-0.1	-0.1	-0.502	-0.502
H-Bond acceptor	-2.618	-3.011	-1.571	-2.618	-3.011	-2.749	-2.094	-2.094	-3.796	-3.796	-3.534	-3.534	-3.534	-3.534
SASA	11.381	12.317	15.341	12.179	11.863	13.797	11.661	10.369	12.189	12.224	12.353	11.981	143.47	12.38
Ac x Dn [^] .5/ SASA	0	0	0.37	0	0	0	0	0	0.563	0.562	0.518	0.534	1.061	1.155
Rotor bonds	-1.14	-0.814	-1.954	-1.14	-0.977	-1.14	-0.651	0	-1.14	-1.14	-0.977	-0.977	-0.977	-0.977
Non-con amides	0	-0.743	-0.773	0	0	-0.409	0	0	-0.631	-0.639	-0.73	0.666	-0.636	-0.675
WPSA	0.205	0	0.147	0.196	0	0.503	0.186	0.624	0.467	0.482	0.314	0.268	0.317	0.209
Constant	-3.783	-3.783	-3.783	-3.783	-3.783	-3.783	-3.783	-3.783	-3.783	-3.783	-3.783	-3.783	-3.783	-3.783
Total	4.046	3.966	7.376	4.834	4.093	6.22	5.319	5.117	3.77	3.809	4.06	3.723	5.416	4.273
log BB														
Hydrophilic SASA	-0.201	-0.455	-0.484	-0.211	-0.413	-0.346	-0.326	-0.553	-1.419	-1.418	-1.471	-1.161	-1.723	-1.437
WASA	0.115	0	0.083	0.11	0	0.283	0.105	0.351	0.263	0.271	0.177	0.151	0.179	0.118
Rotor bonds	-0.422	-0.301	-0.723	-0.422	-0.362	-0.422	-0.241	0	-0.422	-0.422	-0.362	-0.362	0.362	-0.362
Constant	0.564	0.564	0.564	0.564	0.564	0.564	0.564	0.564	0.564	0.564	0.564	0.564	0.564	0.564
Total	0.056	-0.193	-0.561	0.041	-0.211	0.068	0.102	0.362	-1.014	-1.005	-1.092	-0.808	-1.343	-1.118
log PMDCK														
Hydrophilic SASA	-0.244	-0.494	-0.456	-0.234	-0.443	-0.346	-0.364	-0.613	-1.429	-1.432	-1.539	-1.251	-1.67	-1.555
WPSA	0.257	0	0.185	0.246	0	0.632	0.234	0.785	0.587	0.605	0.395	0.337	0.399	0.262
Constant	3.771	3.771	3.771	3.771	3.771	3.771	3.771	3.771	3.771	3.771	3.771	3.771	3.771	3.771
Total	3.784	3.276	3.499	3.783	3.328	4.057	3.641	3.942	2.929	2.944	2.626	2.857	2.499	2.478

Only contributing parameters are mentioned in the table. Zero contributors are non-con amines for log $P_{o/w}$, N-protonation for $-\log S$, N-protonation and FOSA for logBB and rotor bonds, non-con amines and COOH/SO₃H acids for logPMDCK.

Table 3.4: Predictive values of properties of known and designed TSPO ligands

Predictions for Properties:	(Range 95% of Drugs)	DAA1106	DPA-713	FGIN-127	PBR06	PBR28	PBR111	PK11195	Ro5-4864	ABMO-Br	ABMO-Cl	ABPO-Br	ABPO-Cl	ABTO-Br	ABTO-Cl
QP log P for octanol/water	(-2.0 / 6.5)	4.805	3.546	7.019	5.148	4.017	5.118	5.019	3.315	2.18	2.236	2.76	2.741	3.23	2.89
QP log K _{hsa} Serum Protein Binding	(-1.5 / 1.5)	0.356	0.032	1.318	0.468	0.088	0.39	0.658	0.281	-0.5	-0.48	-0.181	-0.256	0.126	0.008
QP log BB for brain/blood	(-3.0 / 1.2)	0.056	-0.193	-0.561	0.041	-0.211	0.068	0.102	0.362	-1.014	-1.005	-1.092	-0.808	-1.343	-1.118
No. of Primary Metabolites	(1.0 / 8.0)	4	4	1	5	5	2	0	1	2	2	3	3	3	3
HERG K ⁺ Channel Blockage: log IC ₅₀	(concern below -5)	-4.746	-3.454	-5.015	-5.767	-6.188	-4.59	-5.483	-5.037	-3.795	-3.772	-4.352	-4.177	-5.021	-4.258
Apparent Caco-2 Permeability (nm/sec)	(<25 poor, >500 great)	5888	2290	2441	6015	3854	3783	4561	2683	332	329	248	477	198	248
Apparent MDCK Permeability (nm/sec)	(<25 poor, >500 great)	6080	1889	3154 M	6062	2126	10000	4375	8755	849	879	422 M	719	315 M	300
Lipinski Rule of 5 Violations	(maximum is 4)	0	0	1	1	0	1	1	0	0	0	0	0	0	0
Jorgensen Rule of 3 Violations	(maximum is 3)	0	0	1	0	0	1	0	0	0	0	0	0	0	0
% Human Oral Absorption in GI (+20%)	(<25% is poor)	100	100	100	100	100	100	100	100	85	85	86	91	87	87
QP Polarizability (Angstroms ³)	(13.0 / 70.0)	38.710 M	40.130 M	48.922 M	41.007 M	38.961M	43.870M	39.624 M	33.649 M	35.157 M	35.435 M	39.670 M	38.568 M	43.524 M	41.263 M
QP log P for hexadecane/gas	(4.0 / 18.0)	11.087 M	10.775 M	14.593 M	11.916 M	11.901M	12.463M	11.599 M	9.931 M	11.188 M	11.276 M	12.754 M	12.244 M	14.196 M	13.323 M
QP log P for octanol/gas	(8.0 / 35.0)	15.550 M	15.879 M	19.002 M	16.433 M	15.865M	17.762M	15.462 M	13.924 M	17.126 M	17.317 M	18.031 M	17.936 M	21.015 M	20.768 M
QP log P for water/gas	(4.0 / 45.0)	6.765 M	8.856 M	7.408 M	7.394 M	8.697 M	7.852 M	6.746 M	6.946 M	10.415 M	10.434 M	11.606 M	11.243 M	13.327 M	13.135 M
J _m , max transdermal transport rate	(micrograms/cm ² -hr)	21.007	1.582	0.012	6.736	15.082	0.056	0.393	0.035	0.062	0.062	0.075	0.496	0.003	0.053

3.4.3.3 Penetration of blood-brain barrier (BBB)

The molecules proposed have potential application for brain that makes it mandatory for them to cross the BBB. Too polar molecules may not be able to cross the BBB. To assess the access of drug to the brain, blood-brain partition co-efficient (QPlogB/B) is computed. The values for known TSPO ligands from first and second generation and designed ligands were in between -1.34 to 0.362. This range was permissible limit for crossing blood brain barrier.

The Madin-Darby canine kidney (MDCK) estimates for absorption via oral route by monolayers as these cells have expression of transporter proteins with very low levels of metabolizing enzymes, is used as an additional BBB penetration prediction criterion. The calculated MDCK cell permeability is considered as non-active transport for blood brain barrier.

The values of MDCK were >1889 for all the considered known TSPO ligands and >500 for all the designed ligands except 300 for ABTO-Cl. These values were much higher than 25 nm s⁻¹ which was recommended limit for poor penetration. The QPlogBB and MDCK calculations and comparison of known and designed ligands reflect the prospects of proposed ligands to cross BBB (Table 3.4).

3.4.3.4 Plasma protein binding

The degree of binding to the blood plasma proteins (like human serum albumin, glycoprotein, lipoproteins, alpha, beta and gamma globulins) affects the efficiency of a drug as it greatly reduces the drug quantity in circulation of blood which passes through traverse cell membranes or diffuses less efficiently. Therefore, the abilities of

all the designed molecules were predicted to act on human serum albumin through $QPlogK_{hsa}$. Their values for designed ligands were between -0.48 and 0.126 which were well within limit (-1.5 to 1.5) defined for 95% of the drug-database of Schrodinger. For known ligands considered, this range was from 0.032 to 1.31 but on a positive side. For PK11195, its value was quite high i.e. 0.65 resulting in its non-specific binding and responsible for poor ratio of signal to noise in case of radiolabelled ligands for PET. Out of the ligands chosen for comparison purpose, DPA-713 and DAA1106 were better with values being 0.03 and 0.35, respectively that reflects their improved signal to noise ratio. For all the designed molecules, ABMO-Br/Cl had least interaction with serum protein with -0.50 and -0.48, respectively. The other designed ligands ABPO-Br/Cl (-0.18 & -0.26, respectively) and ABTO-Br/Cl (0.13 & 0.01, respectively) had moderate interaction. All the proposed ligands are better than all other known ligands in terms of plasma protein binding. As protein binding influences the biological half-life of drug and free fraction is important for in vivo activity, relatively lower value for all newly designed ligand in comparison to known ligands predict their improved availability, reduced non-specific binding and better selectivity (Table 3.4).

3.4.3.5 Human ether-a-go-go-related gene potassium (HERG K⁺) channel

The HERG reflects the heart's electrical activity for coordinating its beating and act as the molecular target in case of various therapeutic drugs causing cardiac toxicity. HERG also modulates the function of some of the nervous systems cells through establishment and maintenance of cancer-type properties in leukemic cells. Therefore,

HERG K⁺ channel blocking agents are potentially toxic and cardiac toxicity of drugs can be reasonably predicted by logIC₅₀ at the design level. In this work, predicted logIC₅₀ has been used to assess the blocking capacity of molecule *in silico* whose recommended range was <-5. The predicted logIC₅₀ (HERG K⁺) values were in the range -6.18 to -3.45 for known ligands and -5.02 to -3.77 for designed ligands. As all the designed molecules have toxicity comparable or less than known ligands and < -5, they could be predicted as non-toxic (Table 3.4).

3.4.3.6 Molecular Volume

Molecular volume of drug is also responsible for its binding with receptor. The volume of ligand and that of active site should match for perfect interaction. To assess the structural compatibility of molecule at active site, molecular volume has been analyzed. For known ligands their values were observed to be 941 and 1502 for Ro5-4864 and FGIN-127, respectively. However, the rest of the known ligands were in the range of 1129-1201 with one exception of 1307 for PBR111. All the designed molecules were also falling in the range 1116-1260 in which most of the known ligands were lying. This predicted that proposed ligands have sufficient molecular volume for ligand-protein interaction.

On comparison of proposed ligands with known ligands, it was found that the ABEOs were small lead like molecules which were benzoxazolone analogues. As the ligands have been designed for their application for TSPO targeting which can found application in brain in addition to peripheral organs; drug-likeness, bioavailability, crossing of blood brain barrier, plasma protein binding, and metabolism were predicted. They have attractive predictive pharmacokinetic profiles/ADME properties,

and toxicity permissible for *in vivo* application. These findings suggested that these ligands can be further considered for synthesis and *in vitro/in vivo* analysis.

3.4.4 Docking studies

To illustrate the binding efficiency and mode of interaction with TSPO protein, ligands ABTO-Cl/Br, ABPO-Cl/Br, ABMO-Cl/Br and ABTyO-Cl/Br were analyzed in detail. The docked poses demonstrated that aromatic moieties present in benzoxazolone were involved in pi-pi interactions for ABTO-Cl/Br and ABMO-Cl/Br. However, in ABPO-Br/Cl the aromatic moiety of phenylalanine were involved in pi-pi interaction. Overall, Glide scores showed binding affinities which were also compared with the known TSPO ligands (Table 3.5).

Proteins from different sources were taken for analysis of interaction to validate the idea through “the wisdom of crowds” for reaching a global solution by collecting wisdom from different sources in case of too many possibilities as applied in social sciences. Here, this collection was done by gathering the information of interaction scores from different PDBs of TSPO using Glide scores (Table 3.5). Although there are some significant discrepancies in TSPOs of these sources, the central cavities of these structures provide important ligand binding sites. The TSPO ligands from first generation such as PK11195 non-specifically bind with TSPO. The ligands from second generation could specifically bind, overcoming this limitation of first generation ligands but suffer from inter-subject variability aspect due to single nucleotide polymorphism at 147 position of human TSPO replacing alanine with

threonine. This aspect was also studied for designed TSPO ligands using mutated TSPO. We have chosen wild type PDBs (4RYQ and 2MGY) as well as mutant PDB (4UC1) for docking studies from different sources such as BcTSPO, mTSPO and RsTSPO, respectively. Out of these 4RYQ and 4UC1 were derived from X-ray crystallography and 2MGY was reported as NMR structure with PK11195 ligand.

Table 3.5: Glide XP docking results of known and acetamidobenzoxazolone-amino acid ester based designed ligands (ABEO-Br/Cl) with PDBs of TSPO: 2MGY, 4RYQ, and 4UC1

	2MGY	4RYQ	4UC1
ABTO-Br	-8.50	-6.92	-9.61
ABTO-Cl	-6.65	-8.99	-9.30
ABMO-Br	-8.09	-8.31	-8.19
ABTyO-Br	-7.99	-6.68	-8.84
ABTyO-Cl	-7.70	-5.86	-7.84
FPBMP	-10.50	-6.28	-9.75
MBMP	-10.28	-6.13	-7.70
FEBMP	-10.06	-5.53	-8.07
PK11195	-8.37	-7.17	-8.25
DAA1106	-7.39	-7.06	-6.79
Alpidem	-7.03	-8.19	-7.90
DPA714	-6.83	-5.99	-6.09
SSR180575	-5.45	-6.28	-7.07
PBR28	-4.96	-7.14	-7.80
Diazepam	-8.91	-7.20	-6.60

The validation of docking protocol was done before docking the compounds with PDBs. The ligand present in co-crystallized PBD was removed and docked with binding site. The root mean square deviation between predicted and observed X-ray

crystallographic/NMR conformers was found to be around 0.5 Å predicting the reproduction of binding mode of docked compound using this docking protocol.

The key interactions were present in the regions of 19 to 55 and 87 to 143 amino acid residues which were there in all the ligands though the interacting amino acids were different. This was in agreement with the earlier reported binding modes BcTSPO-PK11195 model which showed interaction between oxygen of carbonyl group of PK11195 with indole groups of Try51 and Try138, vander Waal interaction with Ser22, Tyr32, Pro42, Ile47, Phe55, Asn87, Phe90, Ser91, Gln94, Cys 107, Ala142 and Leu 145. Interaction of PK11195 as on Ser22, Try32, Phe55, Phe90, and Ser91 were similar to ABTO-Br/Cl interactions.

2MGY-PK11195 complex displayed interactions (hydrophobic) with residues of amino acid Ala23, Val26, Leu49, Ala50, Ile52, Trp107, Ala110, Leu114, Ala147, and Leu150 (Jaremko *et al.*, 2014; Okubo *et al.*, 2004).

In addition to favourable vander Waals forces and hydrophobic forces, in several cases hydrogen bonds and pi-pi interaction with highly conserved amino acids residues such as Trp53 of TM2 and Trp143 of TM5 were also observed.

All the ABEO ligands showed comparable/better TSPO affinity (-5.86 to -9.61) as compared to known ligands for TSPO (-4.96 to -10.50). G_{score} for known ligands on docking with TSPO PDBs- 2MGY, 4RYQ, and 4UC1 are shown (Table 3.5). Although the values of G_{score} of ABEOs with 2MYG were slightly lower than those of other acetamidobenzoxazolone (ABO) derivatives from literature, still better/comparable to the G_{score} of other non-benzoxazolone based derivatives. In case

of 4RYQ and 4UC1 these values were relatively better for ABEOs than known ABO ligands. Out of all types of ABEO ligands, G_{score} were higher for ABTO-Br/Cl than those of ABMO-Br/Cl and ABTyO-Br/Cl for at least with two TSPO PDBs out of 2MGY, 4RYQ, and 4UC1. ABTO-Cl showed relatively lower G_{score} value than those of ABTyO-Cl/Br with 2MGY but relatively higher G_{score} with 4RYQ (-8.99 vs -6.68/-5.86) and 4UC1 (-9.30 vs -8.84/-7.84). During docking it was observed that the known ABO moieties were sitting in site with majority of hydrophobic amino acids.

We also tried to predict the intersubject variability aspect of ABEO ligands, a major concern in development of TSPO ligands. Similar affinities towards wild type as well as A147T TSPO were observed with PK11195, but different affinities with several second generation radioligands. ABO based TSPO ligands such as MBMP, FEBMP, and FPBMP demonstrated similar affinities towards both the variants of human TSPO. This comparison predicted that the ABEO ligands might not be affected by this aspect.

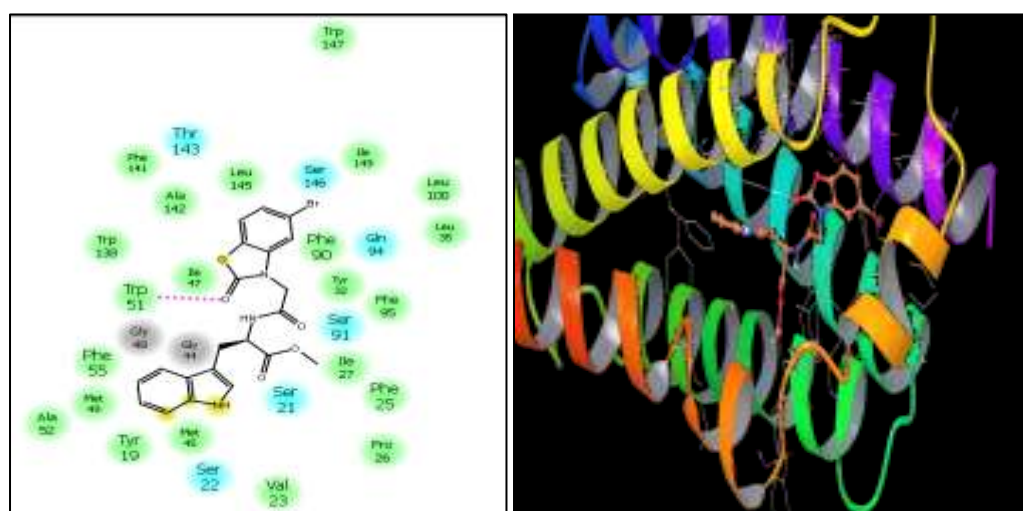


Fig. 3.7: 2D and 3D interaction diagrams of ABTO-Br with PDB 4RYQ

The compound ABTO-Cl and ABTO-Br shared the same skeleton with variation in bromo and chloro groups at 5th position of benzoxazolone moiety. These analyses showed that ABTO-Cl/Br were sitting at similar site of 4RYQ interacting with Phe (55, 90, 95, 141), Try (51, 138), Tyr (19, 32), Ser (21, 22, 91, 146) and Gly (44, 48) with similar type of interaction except pi-pi interaction at Phe91 present in chloro analogue (Fig. 3.7). H-bond with C=O at Trp51 were common interaction for both the ligands. This was reflected in the G_{score} with ABTO-Cl (-8.99) having higher value than ABTO-Br (-6.92).

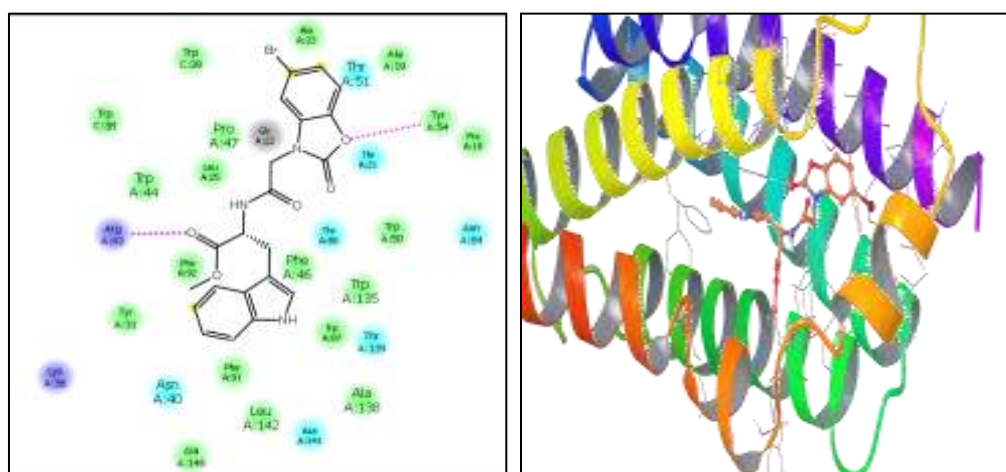


Fig. 3.8: 2D and 3D interaction diagrams of ABTO-Br with PDB 4UC1

The ABTO-Cl/Br, on docking with 4UC1, shared interactions with Ala (19, 23, 138, 146), Tyr (31, 54), Trp (38, 50, 87), and Phe (55, 90, 95, 141) amino acids. ABTO-Br had two hydrogen bonds and ABTO-Cl had one hydrogen bond with G_{score} higher for ABTO-Br as compared to ABTO-Cl (Fig. 3.8).

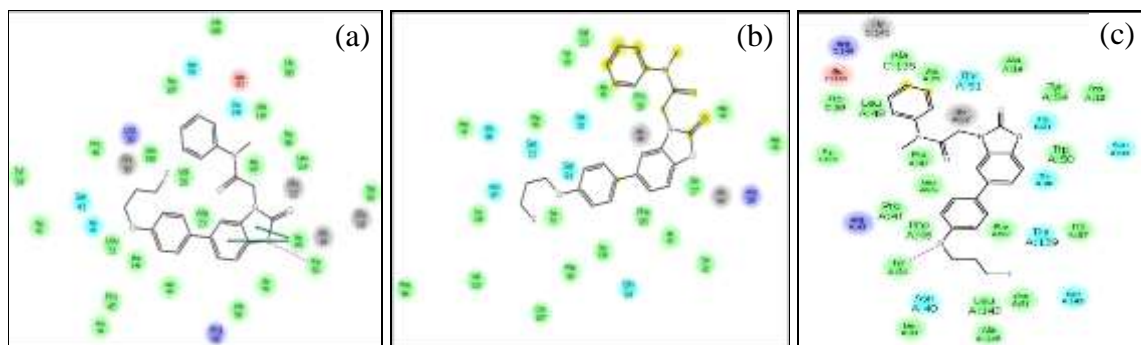


Fig. 3.9: 2D interaction diagrams of FPBMP with PDBs a) 2MGY, b) 4RYQ and c) 4UC1

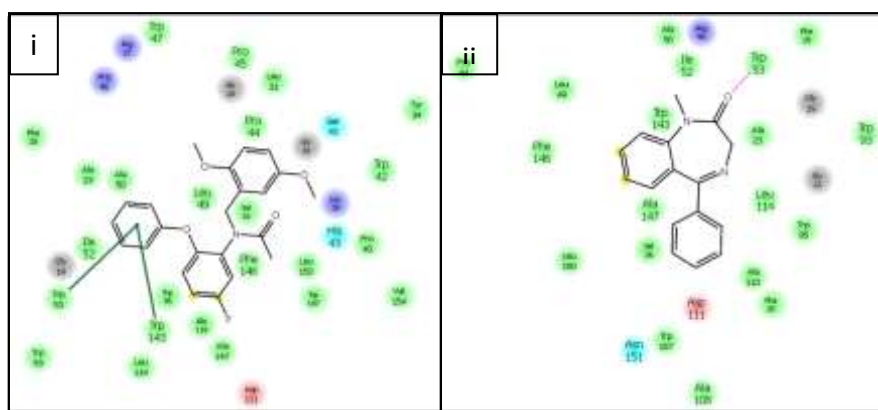


Fig. 3.10: 2D interaction diagrams of i) DAA1106 and ii) Diazepam with TSPO (PDB 2MGY)

On comparing, all the receptor-ligand interactions with TSPO PBDs 4RYQ and 4UC1 were in the range of 19-55 and 87-146. H-bond with benzoxazolone and amino acid around 50-54 were present in all the four interactions. As different amino acids were present at same positions still majorly the ligands were interacting with hydrophobic amino acids. Even few known TSPO ligands were also having interaction of almost similar regions and similar types with several ligands having Trp51 and Trp143 involved in H- bonding/pi-pi bonding (Fig. 3.9, 3.10). Some interactions of ABTO-Br/Cl with TSPO were present in BcTSPO-PK11195 interaction such as Ser22, Tyr32, Phe55, Phe90, and Ser91.

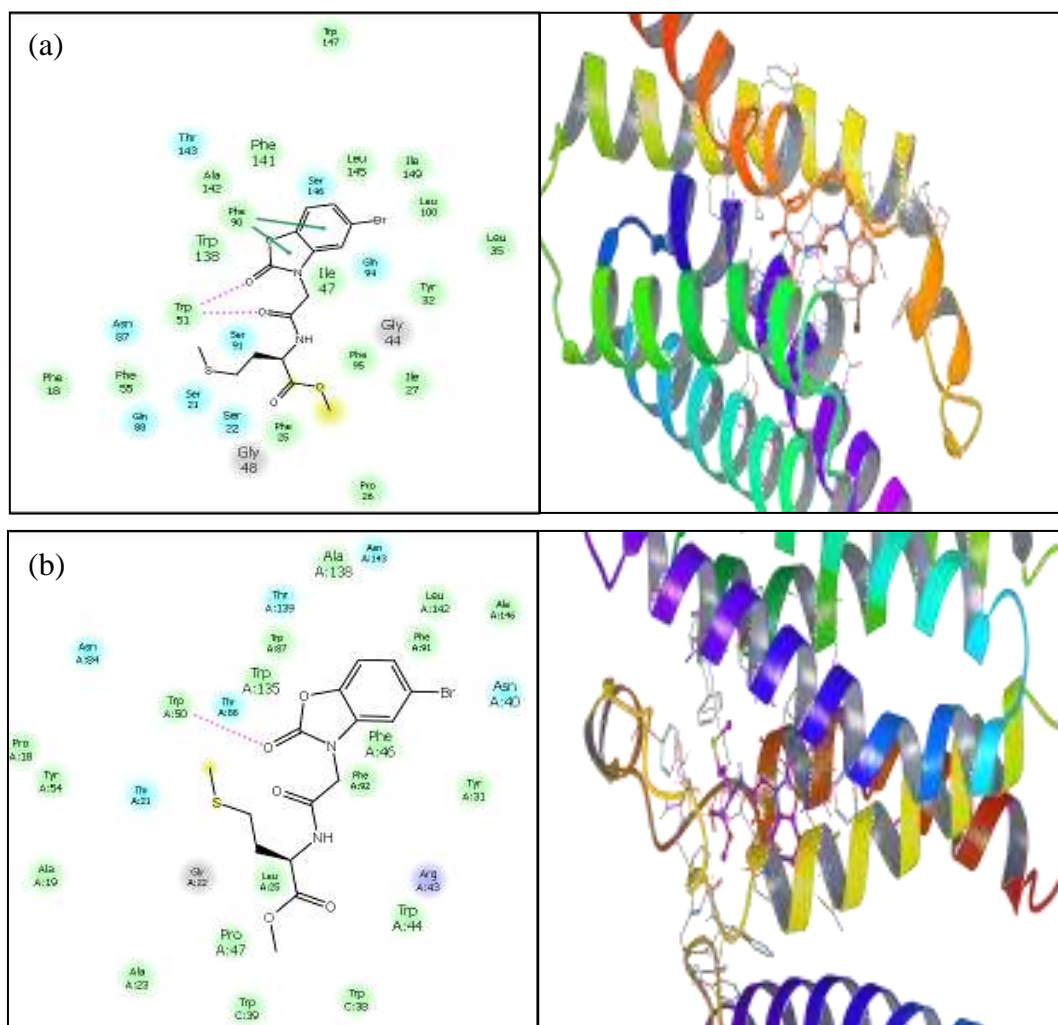
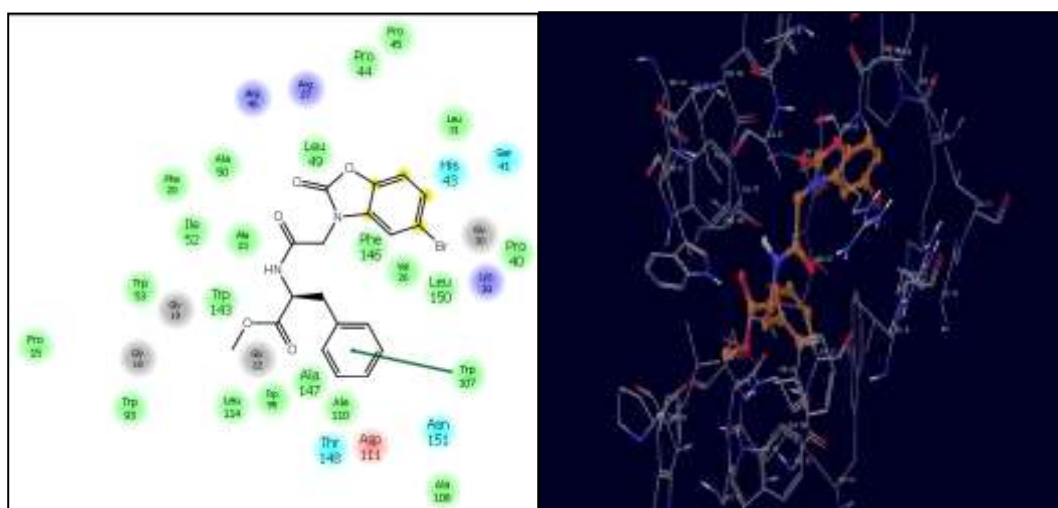
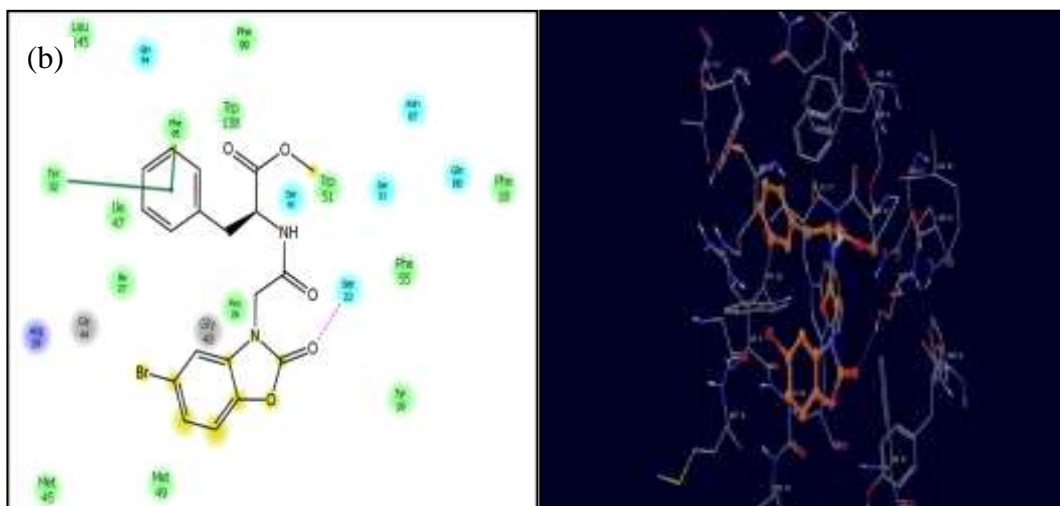
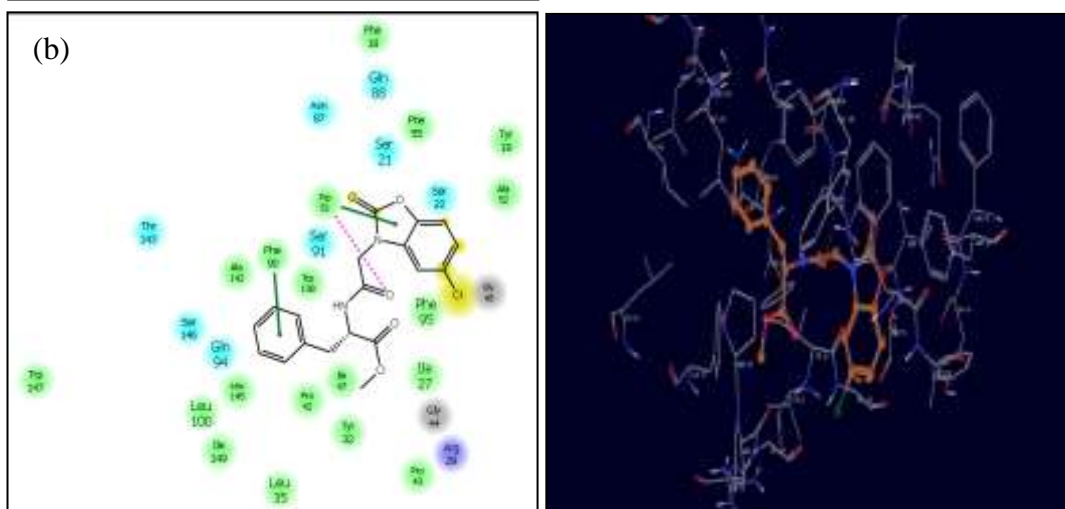
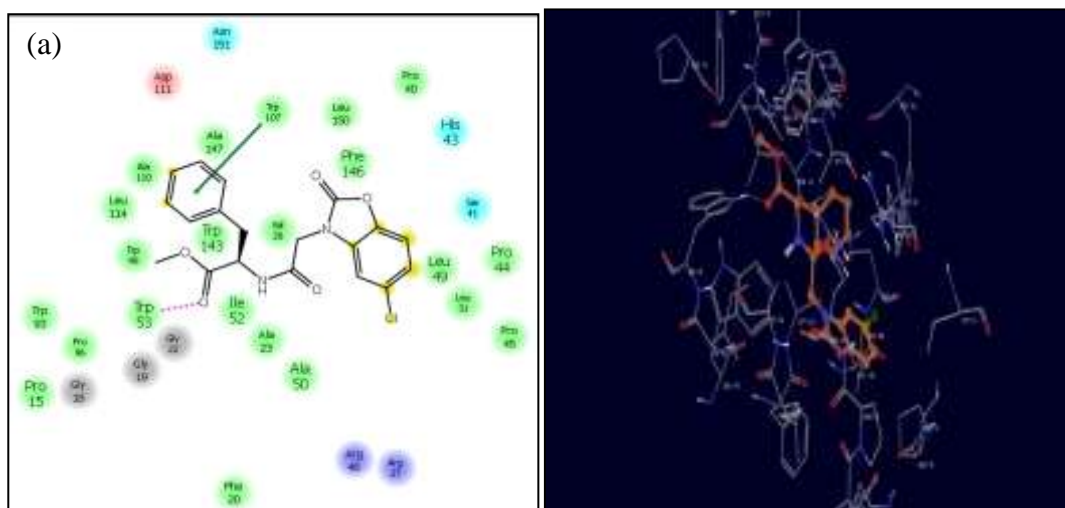


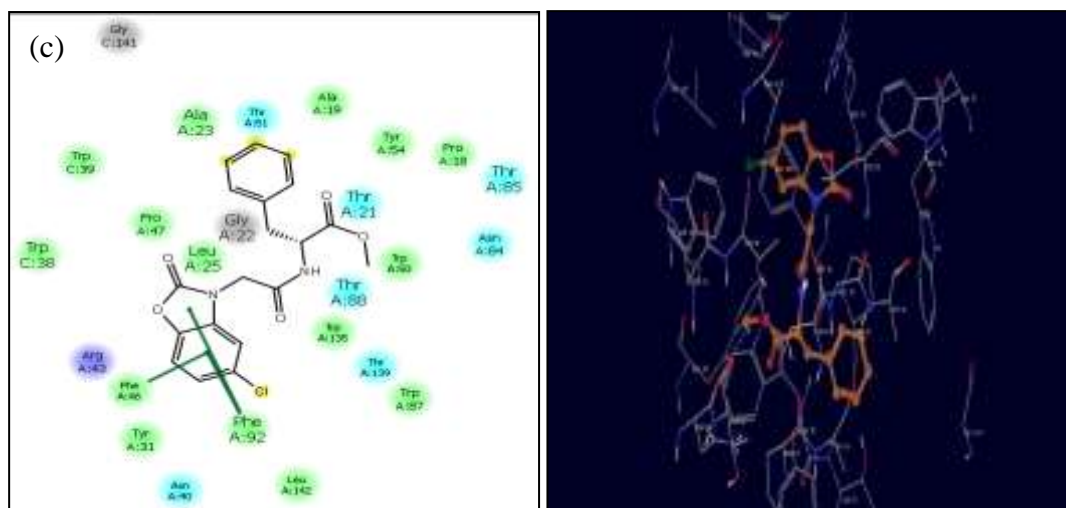
Fig. 3.11: 2D and 3D interaction diagrams of ABMO-Br with PDBs a) 4RYQ and b) 4UC1





(i)





(ii)

Fig. 3.12: 2D and 3D interaction diagrams of i) ABPO-Br and ii) ABPO-Cl with PDBs a) 2MGY, b) 4RYQ and c) 4UC1

The 2D and 3D interaction diagrams of methionine and phenylalanine analogues (ABMO and ABPO) are shown in Figs. 3.11 and 3.12, respectively showing π - π interactions and/or H bond interactions.

3.5 Conclusion

Designing of acetamidobenzoxazoline based TSPO ligand, Br/Cl-ABEOs (E=methyl esters of tryptophan, phenylalanine, and methionine) were carried out utilizing outcome of four featured pharmacophore AAAR. The database used for the pharmacophore was benzoxazoline based TSPO ligands with K_i values studied on kidney membrane. The designed molecules were close to the known TSPO ligands on the basis of predictive ADME analysis such as predicting their drug likeliness, bioavailability, plasma protein binding, metabolism, and toxicity. However, they were better in terms of logP values and binding affinity with serum than some of the known ligands such as FGIN-127 and PK11195 that could improve their diagnostic aspects. The docking studies were employed to assess the affinities of designed molecules

towards TSPO. In the docking study, the binding interactions and sites were assessed by molecular docking of six designed skeletons for their applicability towards TSPO targeting. Docking by the software Glide of Schrodinger reproduced the docked conformations of the ligand-protein complexes within 2 Å of RMSD of the X-ray structure. G_{score} s showed good affinities of the all the designed ligands for the protein binding pocket which were comparable for PDBs of different sources for the same ligand. Three different PDBs were taken for finding out more holistic results. These results predicted comparable affinities towards wild type TSPO for known as well as designed ligands. Additionally, the designed ligands may not be affected by intersubject variability as could be predicted on comparison with known acetamidobenzoxazolone based known and designed ligands. The Glide scores of these molecules were comparable to known TSPO ligands and interacting in the same binding pocket having H-bond and/or π - π interactions. These findings predict the potential of designed ligands for TSPO application. Although biological analysis will be essential for further assessment of the efficacy of the new molecules after synthesis, such screening may provide initial platform to explore novel potent molecules. After *in silico* validation, the Br/Cl-ABEO skeletons were found suitable which were further synthesized and characterized in succeeding chapter.

Chapter 4
Synthesis, characterization and
cytotoxicity studies

CHAPTER 4

SYNTHESIS, CHARACTERIZATION AND CYTOTOXICITY STUDIES

The previous chapter discussed the designing of acetamidobenzoxazolone based TSPO ligands through various *in silico* means such as pharmacophore modelling, ADME analysis and docking. In order to validate the virtually screened TSPO ligands, synthesis of these ligands were carried out. All the intermediates as well as final compounds were characterized through ¹H-NMR, ¹³C-NMR and mass spectroscopy. The synthetic procedures of all the designed ligands along with their characterization are mentioned in this chapter.

4.1 Synthesis

4.1.1 Procedure for synthesis of 2-(2-(5-bromo benzoxazolone)acetamido)-3-(1*H*-indol-3-yl)propanoate, ABTO-Br

2-(5-Bromo-benzoxazolone) acetic acid was synthesized as per scheme 1 by following the procedure reported in the literature with some modification (Fukaya *et al.*, 2013). To a solution of 2-(5-bromo-benzoxazolone) acetic acid (250 mg, 0.92 mmol) in DMF (5 ml), tryptophan methyl ester hydrochloride (351.2 mg, 1.38 mmol), HOBt (124.2 mg, 0.92 mmol) and EDCI (264.3 mg, 1.38 mmol) were added at room temperature and stirred for 7 h. Subsequently, water was added and the mixture was extracted using a toluene and ethyl acetate (1:1). Water and brine were used for washing of organic layer and subsequently anhydrous Na₂SO₄ was added for drying. After filtration, the solvent was removed in vacuo and purification of residue was carried out on silica gel column using CHCl₃/EtOAc (4:1 v/v) as eluent to give amide product as a white solid (ABTO-Br: yield 62%).

4.1.2 General procedure for synthesis of 5-chloro/bromo benzoxazol-2(3H)-one, ABO-Br/ Cl

The reaction was performed as per step a mentioned in scheme 2-4. To a solution of 4-chloro/bromo-2-aminophenol (34.83 mmol) in 150 ml THF, 1,1'-carbonyldiimidazole (CDI) (34.83 mmol) was mixed and refluxed with stirring for 2 h. Then the reaction mixture was cooled to rt and its quenching was performed by adding 2 M HCl solution. The extraction of product was done by using EtOAc which was washed with brine. Thereafter, anhydrous Na₂SO₄ was used for drying and filtered. Finally, in vacuo removal of solvent gave white solid as product.

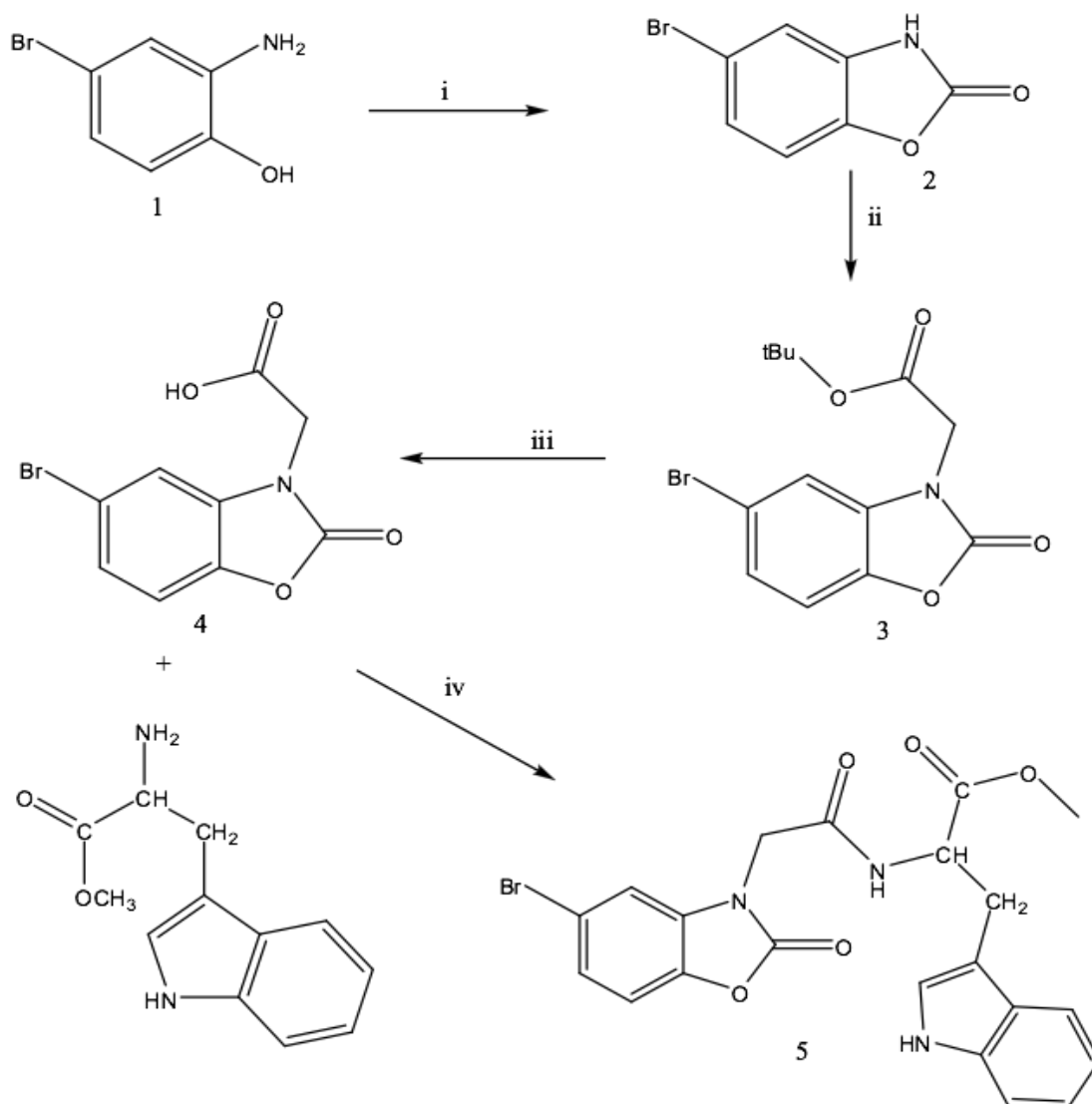
4.1.3 General procedure for chloroacetylation of methyl ester of amino acid

The reaction was performed as per step b mentioned in scheme 2-4. To a solution of methyl ester of amino acid (2.32 mmol) in deionized water (10 ml), triethyl amine (2.55 mmol) was added with stirring under nitrogen atmosphere on ice bath for 5 min. To the mixture, chloroacetyl chloride (2.55 mmol) in dichloromethane (10 ml) was added dropwise over 1 h and the reaction was carried out for 4 h. Thereafter, dichloromethane was used for the extraction of the product. The washing of dichloromethane layer was done twice by deionized water and brine solution. After washing, anhydrous Na₂SO₄ was used for drying the organic layer. Then in vacuo solvent removal gave the product and column chromatography using silica gel and CHCl₃ resulted in purified product.

4.1.4 General procedure for synthesis of Cl/Br-ABO-Amino Acid ester (ABEO-Br/Cl)

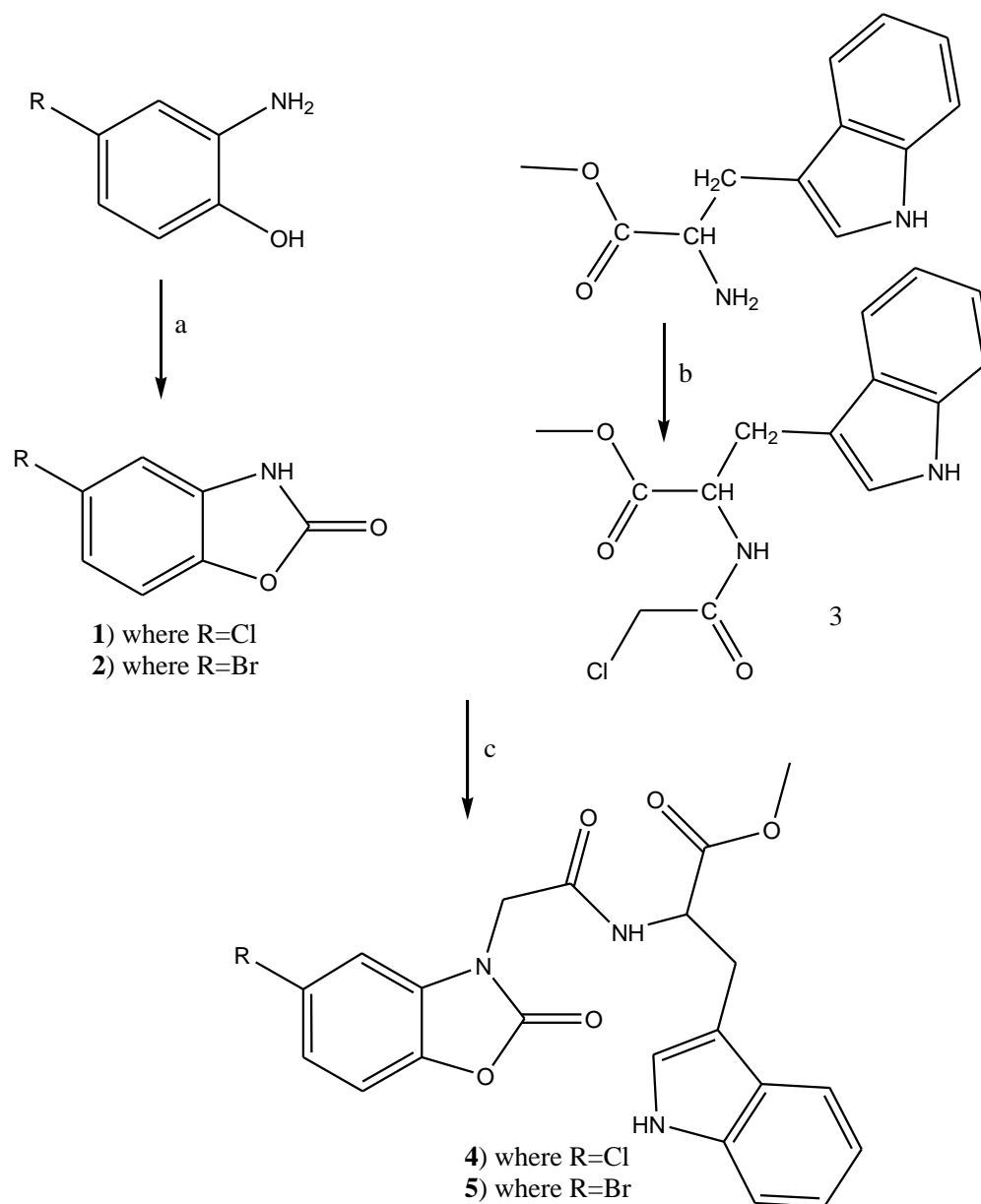
The reaction was performed as per step c mentioned in scheme 2-4. In 5 ml DMF, 5-chloro/bromo benzoxazol-2(3H)-one (1.48 mmol) and K₂CO₃ (2.22 mmol) were added. Chloroacetylated methyl ester of amino acid (1.48 mmol) was added to this solution with cooling on ice bath and then stirring was continued for 3 h in the

temperature range of 60-70°C. Thereafter, water was added after cooling the mixture to rt. Mixture of toluene and ethyl acetate in 1:1 ratio was used as extraction solvent. Washing of organic layer was done by water and brine solutions and then dried by anhydrous sodium sulphate. In vacuo solvent removal gave a solid which was further purified by column chromatography using silica gel and CHCl₃/EtOAc (4:1, v/v).



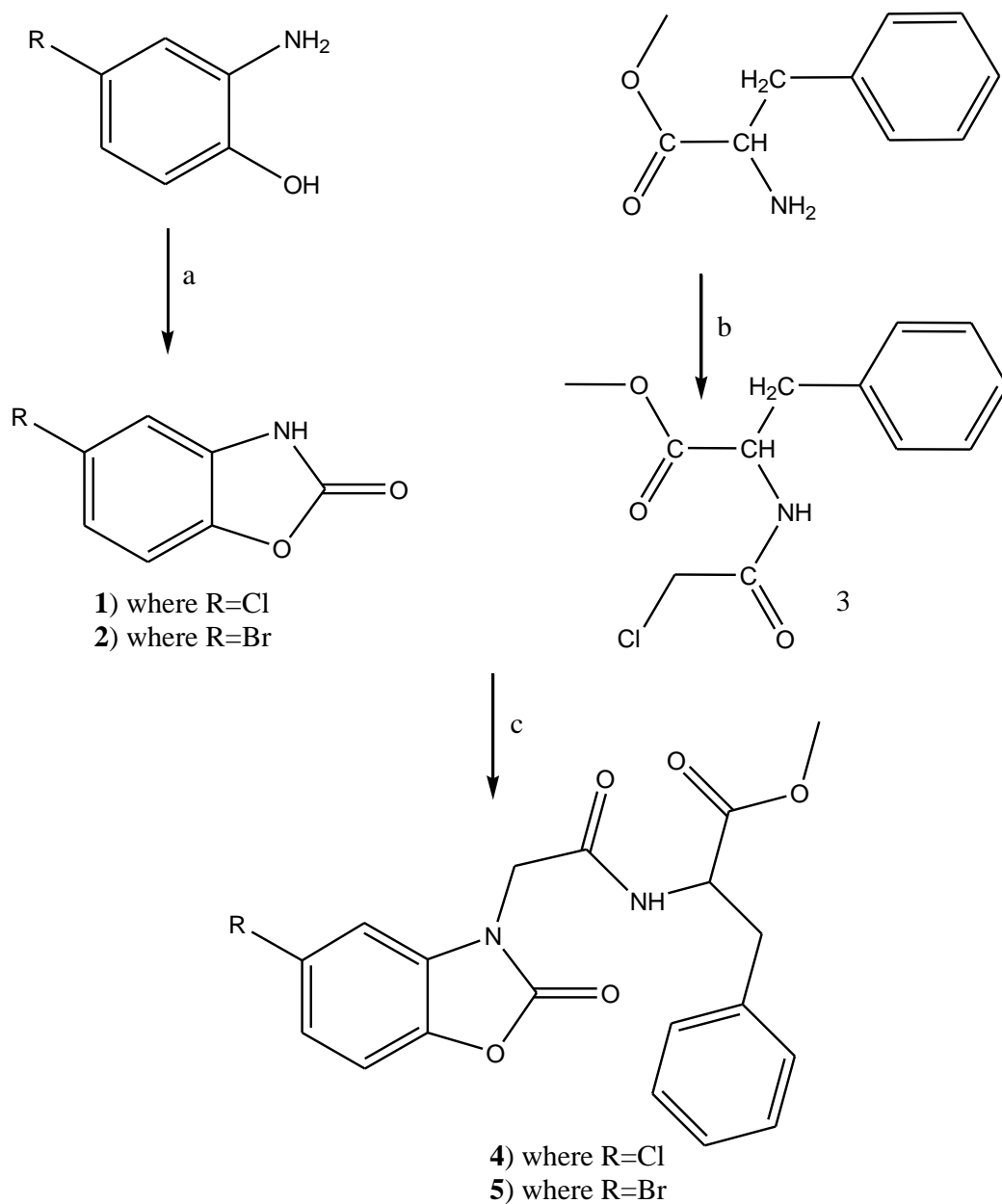
Scheme 1: Synthesis of 2-(2-(5-bromo benzoxazolone)acetamido)-3-(1H-indol-3-yl) propanoate (ABTO-Br)

Reagents and conditions: i) CDI, THF, rt; ii) Tert-Butyl bromoacetate, K₂CO₃, DMF, 70°C; iii) HCl, dioxane, AcOH, 50°C; iv) Tryptophan methyl ester hydrochloride, EDCI, HOBt, DMF, rt.



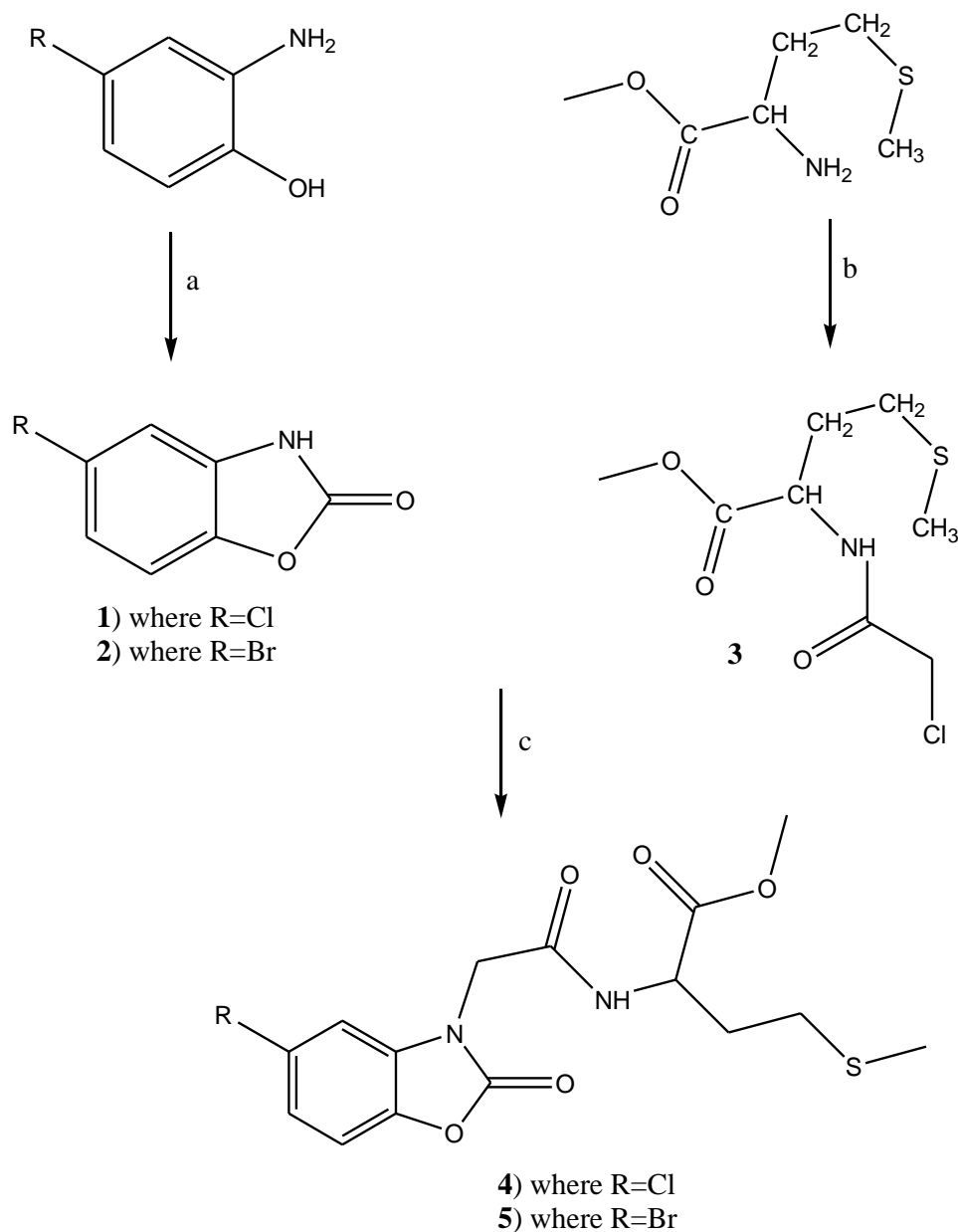
Scheme 2: Synthesis of 2-(2-(5-bromo/chlorobenzoxazolone)acetamido)-3-(1H-indol-3-yl) propanoate (ABTO-Br/Cl)

Reagents and conditions: a) CDI, THF, Reflux 2 h; b) Chloroacetyl chloride, Et₃N, H₂O/DCM, 0°C-rt; c) K₂CO₃, DMF, 60°-70°C, 3h.



Scheme 3: Synthesis of methyl 2-(2-(5-bromo/chloro-2-oxobenzoxazol-3(2H)-yl)acetamido)-3-phenylpropanoate (ABPO-Br/Cl)

Reagents and conditions: a) CDI, THF, Reflux 2 h; b) Chloroacetyl chloride, Et₃N, H₂O/DCM, 0°C-rt; c) K₂CO₃, DMF, 60°-70°C, 3h.



Scheme 4: Synthesis of 2-[2-(5-bromo/chloro-2-oxo-benzoxazol-3-yl)-acetylamino]-4-methylsulfanyl-butyrlic acid methyl ester (ABMO-Cl/Br)

Reagents and conditions: a) CDI, THF, reflux, 2h; b) Chloroacetyl chloride, Et₃N, H₂O/DCM, 0°C-rt; c) K₂CO₃, DMF, 60°-70°C, 3h.

4.2 Result and discussion

In the first approach, 2-(5-bromo-benzoxazolone)acetic acid, the precursor of compound ABTO-Br was synthesized from 4-bromo-2-amino phenol by the procedure reported in the literature with some modifications (Fukaya *et al.*, 2013). In the last step, the ligand 2-(2-(5-bromo benzoxazolone)acetamido)-3-(1*H*-indol-3-yl)propanoate was synthesized through amidation reaction of 5-bromo-benzoxazolone acetic acid and tryptophan methyl ester hydrochloride in the presence of HOBt and EDCI. Overall synthetic procedure is mentioned in scheme 1. The yield of the final product was 62% and was purified using column chromatography and preparative HPLC. The retention time of final product ABTO-Br was found to be 8.75 min. The chemical purity of the compound was determined using analytical HPLC and purity was found to be >97%. All the eight aromatic protons of benzoxazolone and indole moieties were observed in the region 6-8 ppm. ¹³C-NMR reflected appropriate peaks as per its formula. Three C=O peaks were observed at 172.3, 166.2 and 154.1 ppm which correspond to ester C=O, amide C=O and benzoxazolone C=O, respectively. Mass spectrum run in the negative mode has peak at 470.2 [M-H]⁺, which was in accordance with the proposed structural formula.

In order to optimize the synthesis, an alternative procedure has been tried which reduced the number of steps and increased the yield. The final ligand was synthesized by the procedure mentioned in scheme 2 in three steps with modification in earlier used procedure having four steps for ABTO-Br. The synthetic procedure involved

synthesis of methyl-2-(2-chloroacetamido)-3-(1*H*-indol-3-yl)propanoate (T-Cl) and 5-chloro benzoxazol-2(3*H*)-one (ABO-Cl), separately which were combined in the final step. The precursor molecule 5-chloro benzoxazolone was prepared by cyclization reaction of 4-chloro-2-amino phenol in presence of 1,1'-carbonyldiimidazole (CDI). Simultaneously, chloroacetylation was performed on L-tryptophan methyl ester. Thereafter, both the above mentioned products were combined through alkylation reaction in presence of K_2CO_3 in DMF. The synthesized ABTO-Cl had good yield (70%) which was purified using column chromatography and characterized by spectroscopic methods. The synthesis of final product was confirmed by $m/z=426.3$ $[M-H^+]$ peak present in mass spectroscopic data. The synthetic scheme 2 is better than scheme 1 in terms of yield, cost and duration of overall synthesis.

Encouraged by outcome and ease of alternative synthetic procedure in developing ABTO-Br/Cl, we directed our efforts towards development of ABPO-Br/Cl and ABMO-Br/Cl using scheme 2 having three steps.

The ABPO-Br/Cl were synthesized in three steps as per scheme 3. This scheme is similar to scheme 2 where phenylalanine methyl ester is used in place of tryptophan methyl ester. The compounds were purified using column chromatography and preparative HPLC. The chemical purities of the compounds were determined using analytical HPLC and purities were found to be >97%. All the eight aromatic protons of benzoxazolone and benzene moieties were observed in the region 6-8 ppm. ^{13}C -NMR reflected appropriate peaks as per their formulas. The C=O of benzoxazolone,

amide and ester were observed in the region 155-169 of ^{13}C -NMR of both the analogues reflecting the syntheses of ABPO-Cl/Br. The mass spectra also confirmed the syntheses with the presence of $[\text{M}-\text{H}^+]$ peaks of ABPO-Cl and ABPO-Br at 387.1 and 432.9, respectively.

Similarly, ABMO analogues (ABMO-Br/Cl) were synthesized using methionine methyl ester as per scheme 4. NMR and Mass spectroscopic techniques were used for the analysis of synthesized compounds. In ^{13}C -NMR, the presence of C=O of benzoxazolone peak around 154 in 5-bromo/chloro benzoxazol-2(3H)-one reflected their cyclization. In addition to this peak, presence of all the requisite peaks in aromatic region, ester and amide peaks in the range of 168-169 confirmed successful syntheses of the final compounds ABMO-Br/Cl.

4.3 Characterization

4.3.1 Characterization of 5-chloro benzoxazol-2(3H)-one (ABO-Cl)

MS (ESI) m/z : 167.8 $[\text{M}-\text{H}^+]$, Calculated m/z : 168.0 $[\text{M}-\text{H}^+]$ (Fig. 4.1)

^1H -NMR (DMSO, 600 MHz): δ (ppm) 7.1-7.4 (m, 3H) (Fig. 4.2)

^{13}C -NMR (DMSO, 150 MHz): δ (ppm) 110.3, 111.3, 122.0, 128.2, 132.2, 142.6, 154.7 (Fig. 4.3)

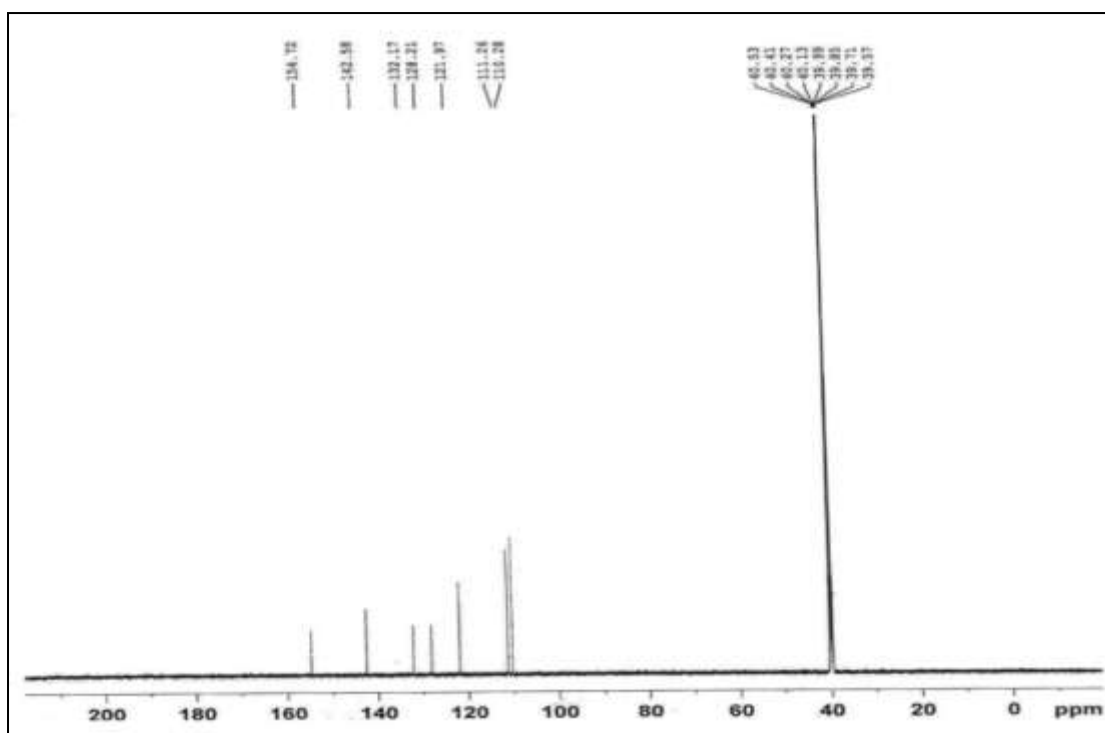


Fig. 4.3: ^{13}C -NMR spectrum of ABO-Cl

4.3.2 Characterization of 5-bromo benzoxazol-2(3H)-one (ABO-Br)

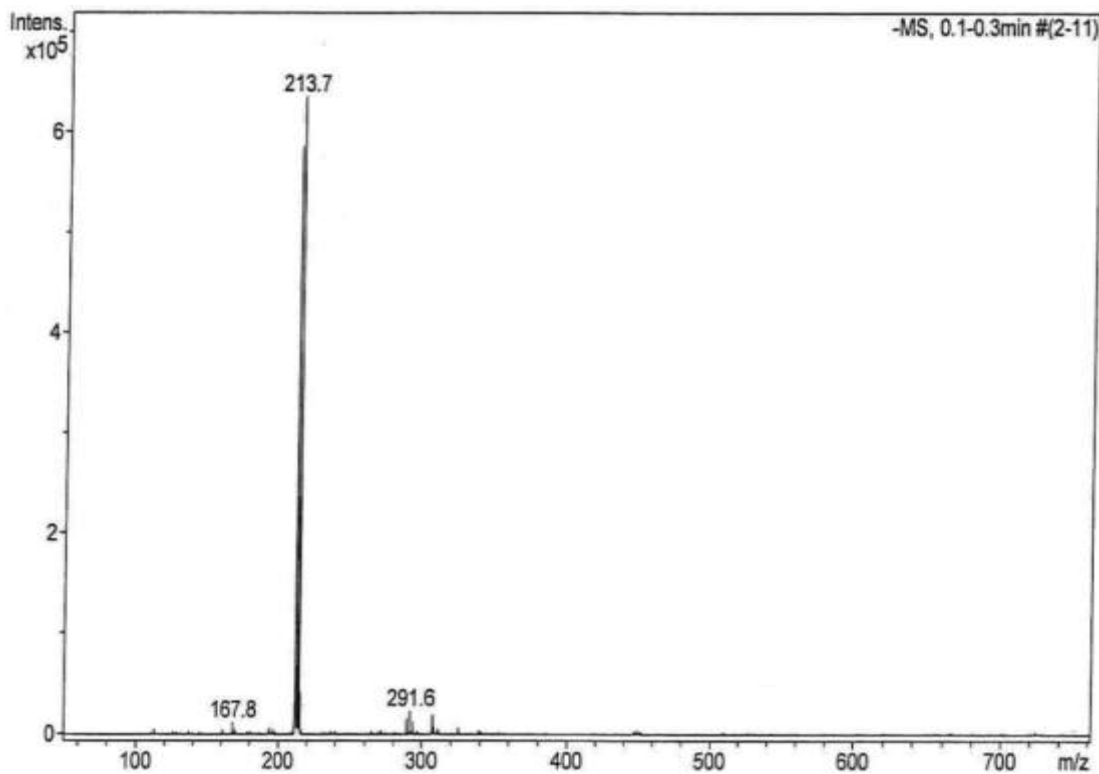


Fig. 4.4: Mass spectrum of ABO-Br

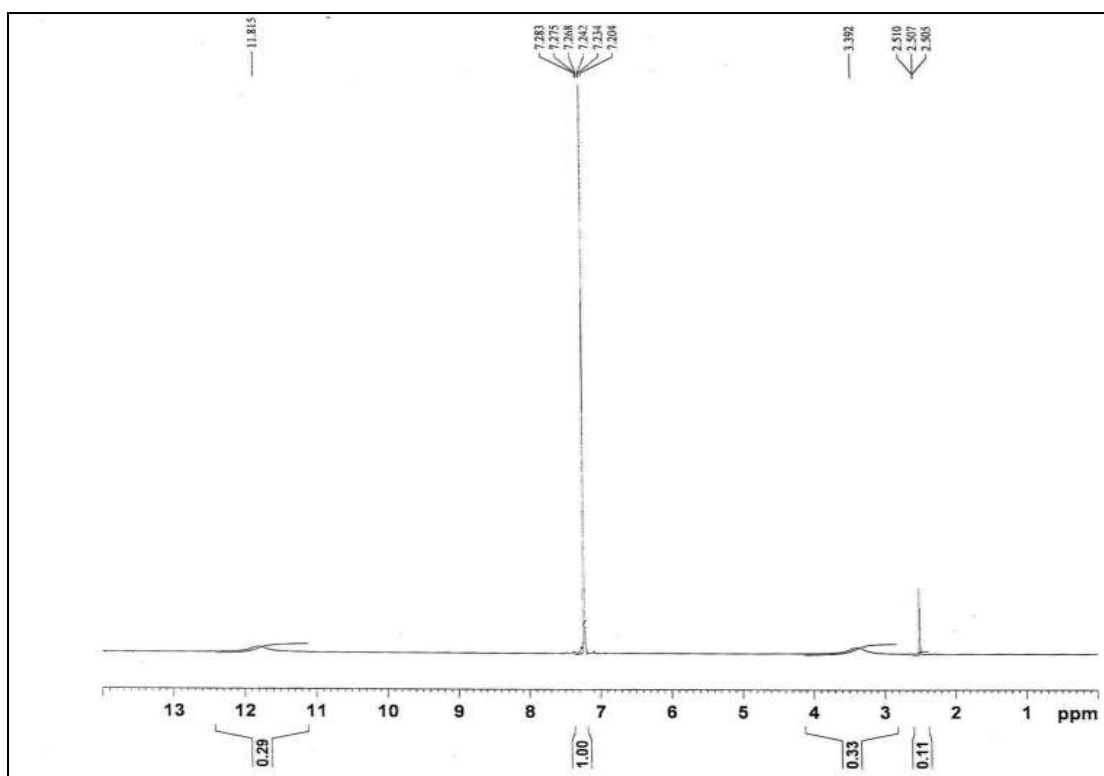


Fig. 4.5: ¹H-NMR spectrum of ABO-Br

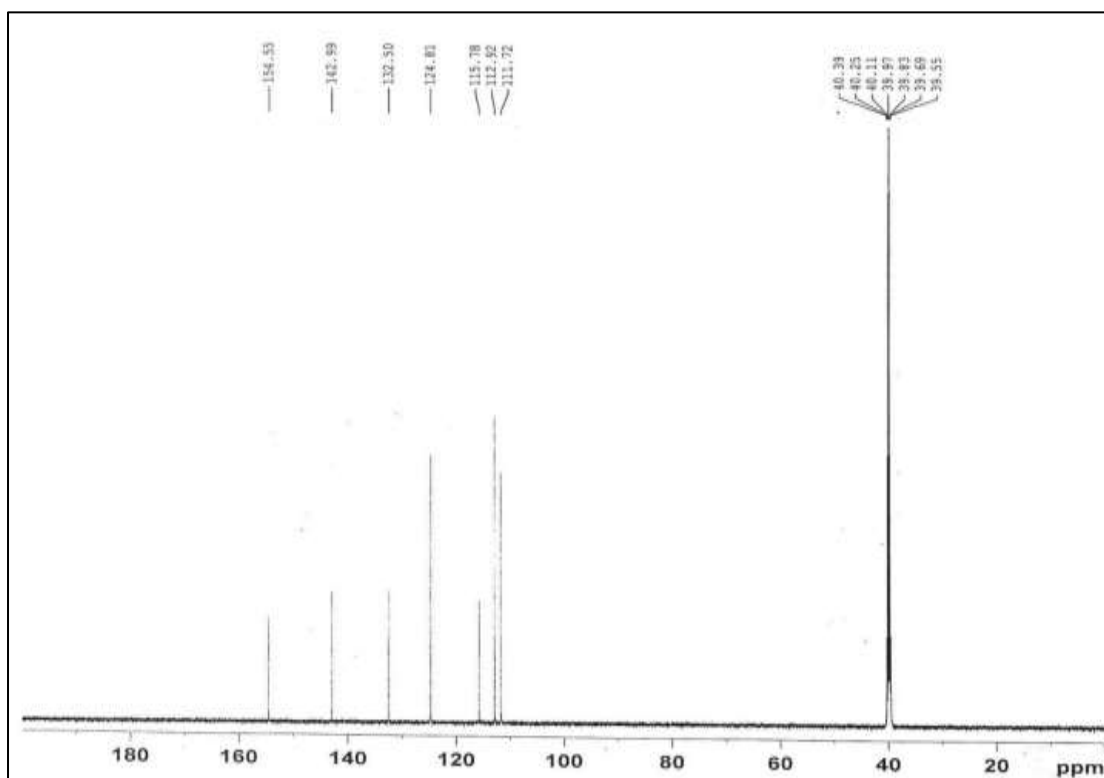


Fig. 4.6: ¹³C-NMR spectrum of ABO-Br

MS (ESI) m/z: 211.7 [M-H⁺], Calculated m/z: 211.9 [M-H⁺] (Fig. 4.4)

¹H-NMR (DMSO, 600 MHz): 7.20-7.28 (m, 3H) (Fig. 4.5)

¹³C-NMR (DMSO, 150 MHz): 111.7, 112.9, 115.8, 124.8, 132.5, 143.0, 154.6 (C=O)
(Fig. 4.6)

4.3.3 Characterization of methyl 2-(2-chloroacetamido)-3-(1*H*-indol-3-yl)propanoate (T-Cl)

MS (ESI) m/z: 293.1 [M-H⁺], calculated m/z: 293.1 [M-H⁺] (Fig. 4.7)

¹H-NMR (CDCl₃, 600 MHz): δ(ppm) 3.3-3.4 (d, 2H), 3.7 (s, 3H), 4.0 (s, 2H), 4.9-5.0 (m, 1H), 7.0-7.6 (m, 5H), 8.5 (br s, 1H) (Fig. 4.8)

¹³C-NMR (CDCl₃, 150 MHz): δ(ppm) 27.5, 42.5, 52.6, 53.3, 109.3-136.3 (8 peaks), 166.0, 171.8 (Fig. 4.9)

HPLC: T3 column, 4.6 x 250 mm; MeCN/H₂O, 6/4-8/2 (v/v); flow rate: 0.8 ml/min;

λ_{uv}= 254 nm; t_R= 6.645 min (Fig. 4.10)

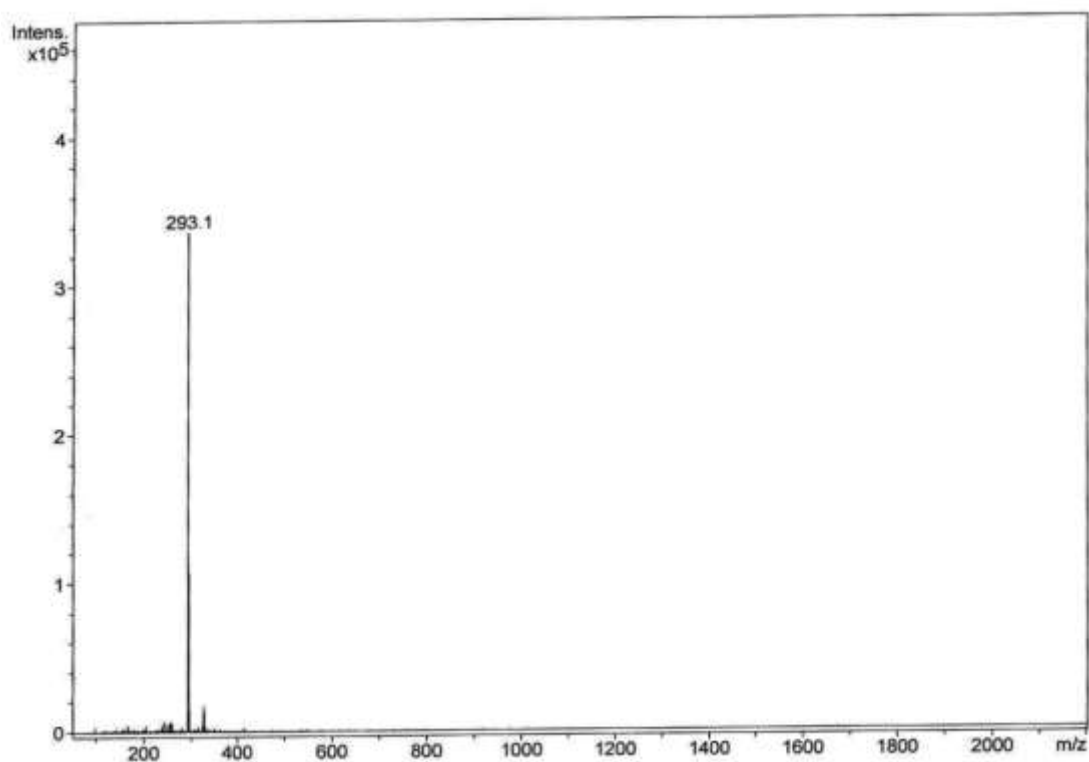


Fig. 4.7: Mass spectrum of T-Cl

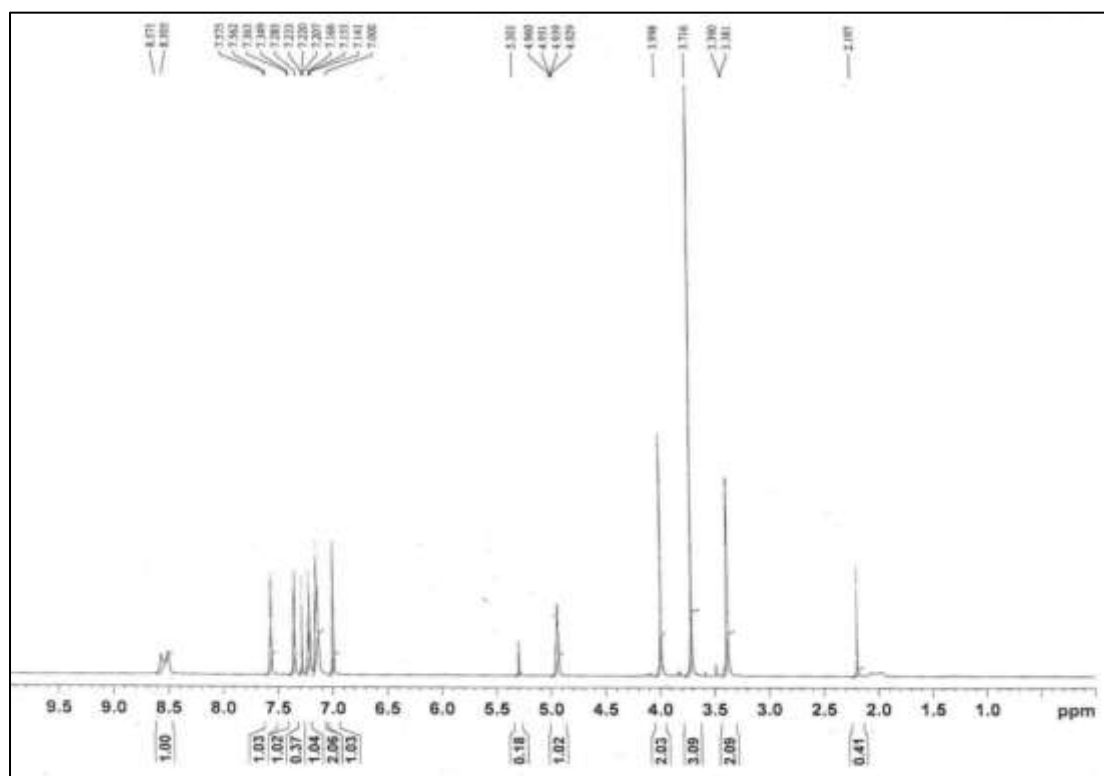


Fig. 4.8: $^1\text{H-NMR}$ spectrum of T-Cl

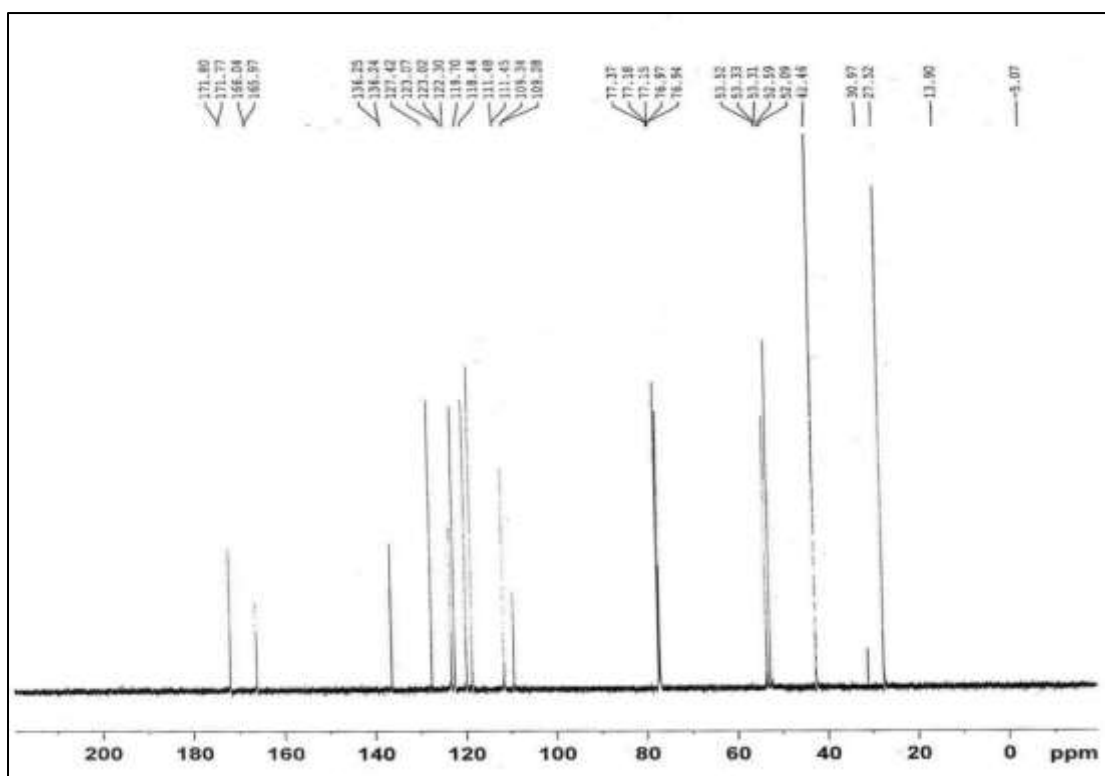


Fig. 4.9: ^{13}C -NMR spectrum of T-CI

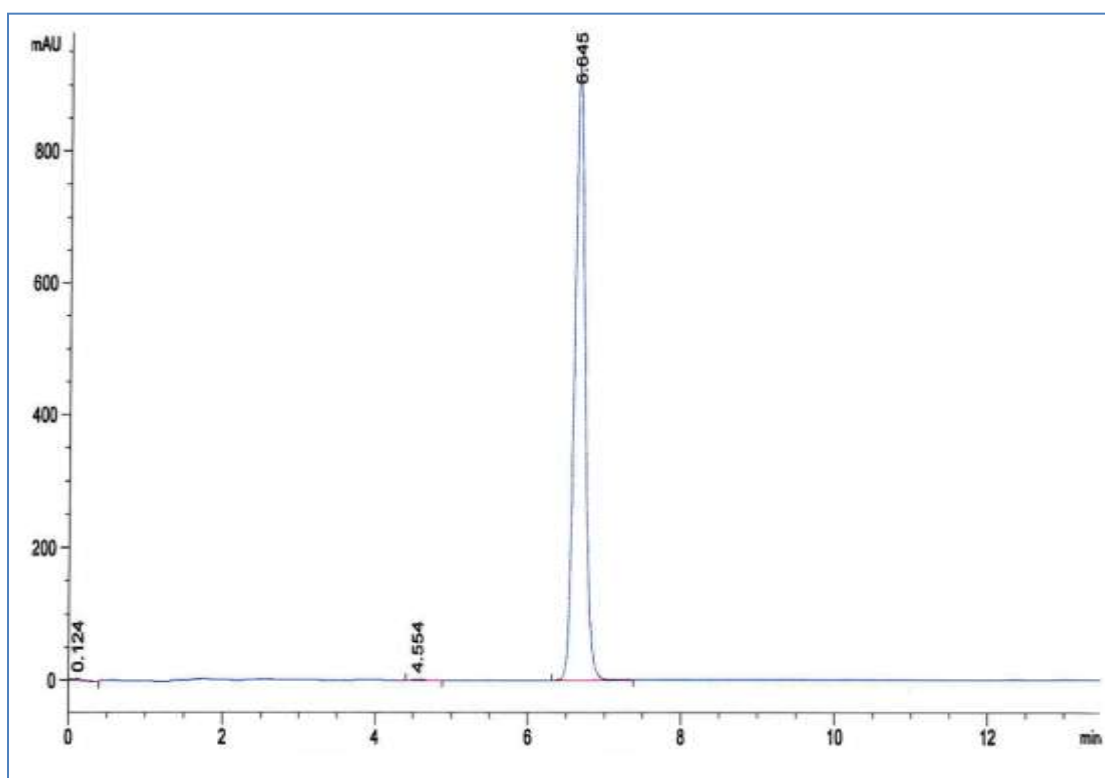


Fig. 4.10: HPLC profile of T-CI

4.3.4 Characterization of methyl 2-(2-chloroacetamido)-3-phenylpropanoate (P-Cl)

MS (ESI) m/z: 254.0 [M-H⁺], calculated m/z: 254.1 [M-H⁺] (Fig. 4.11)

¹H-NMR (CDCl₃, 600 MHz): 3.11-3.20 (m, 2 H), 3.74 (s, 3H), 3.98-4.04 (m, 2H), 4.86-4.90 (m, 1H), 7.12-7.33 (m, 5H)

¹³C-NMR (CDCl₃, 150 MHz): 37.8, 42.4, 52.5, 53.4, 127.3, 128.7, 129.2, 135.4, 165.6, 171.3 (Fig. 4.12)

HPLC: T3 column, 4.6 x 250 mm; MeCN/H₂O, 6/4-8/2 (v/v); flow rate: 0.8 ml/min; λ_{uv}= 254 nm; t_R= 8.855 min (Fig. 4.13)

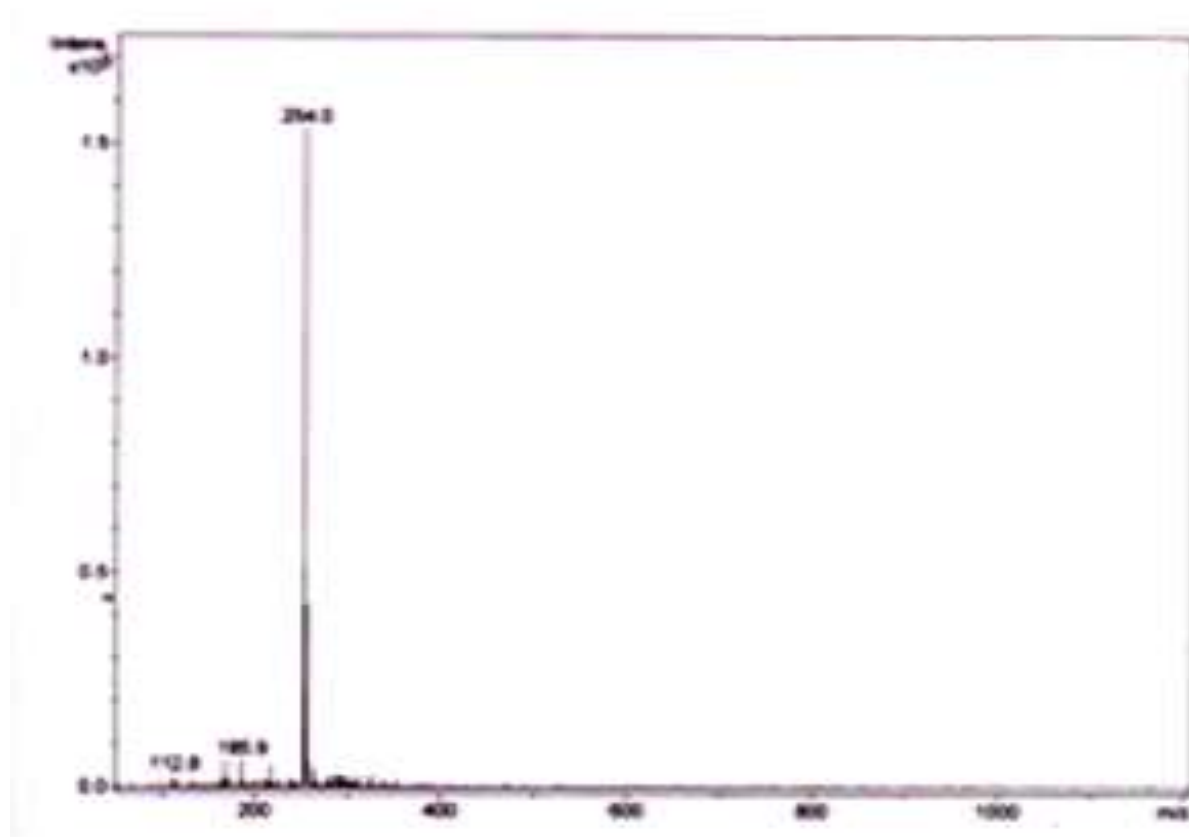


Fig. 4.11: Mass spectrum of P-Cl

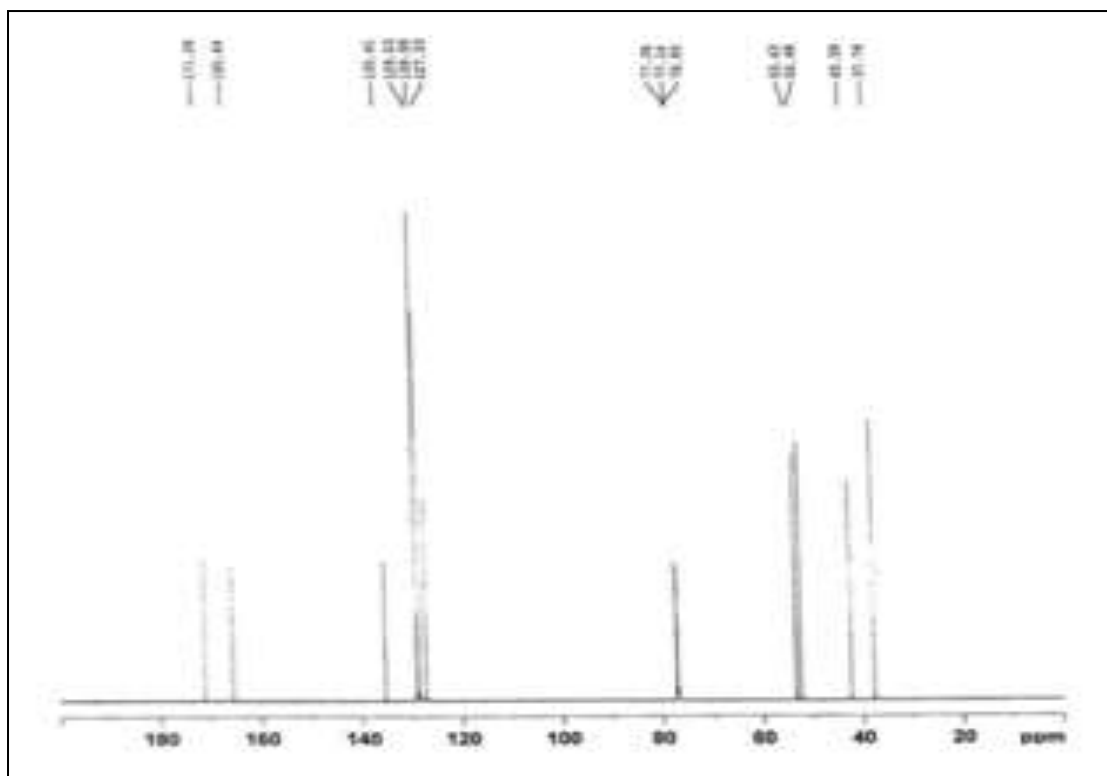


Fig. 4.12: ¹³C-NMR spectrum of P-Cl

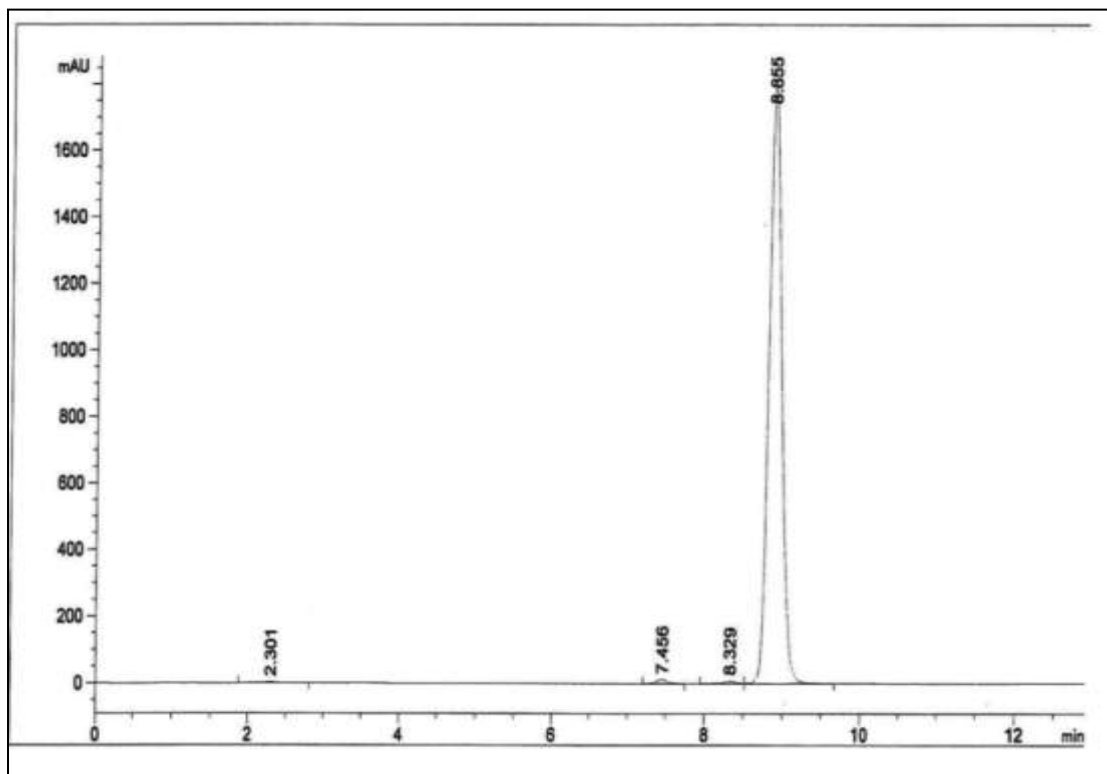


Fig. 4.13: HPLC profile of P-Cl

4.3.5 Characterization of 2-(2-chloro-acetyl-amino)-4-methylsulfanyl-butyrac acid methyl ester (M-Cl)

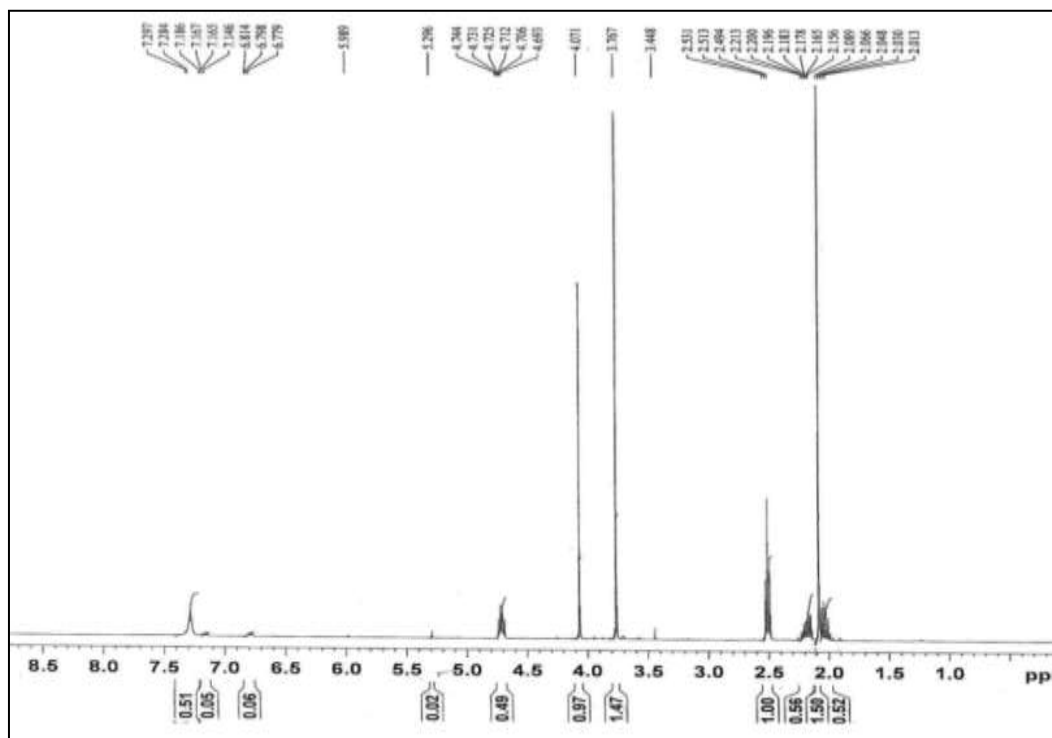


Fig. 4.14: ¹H-NMR spectrum of M-Cl

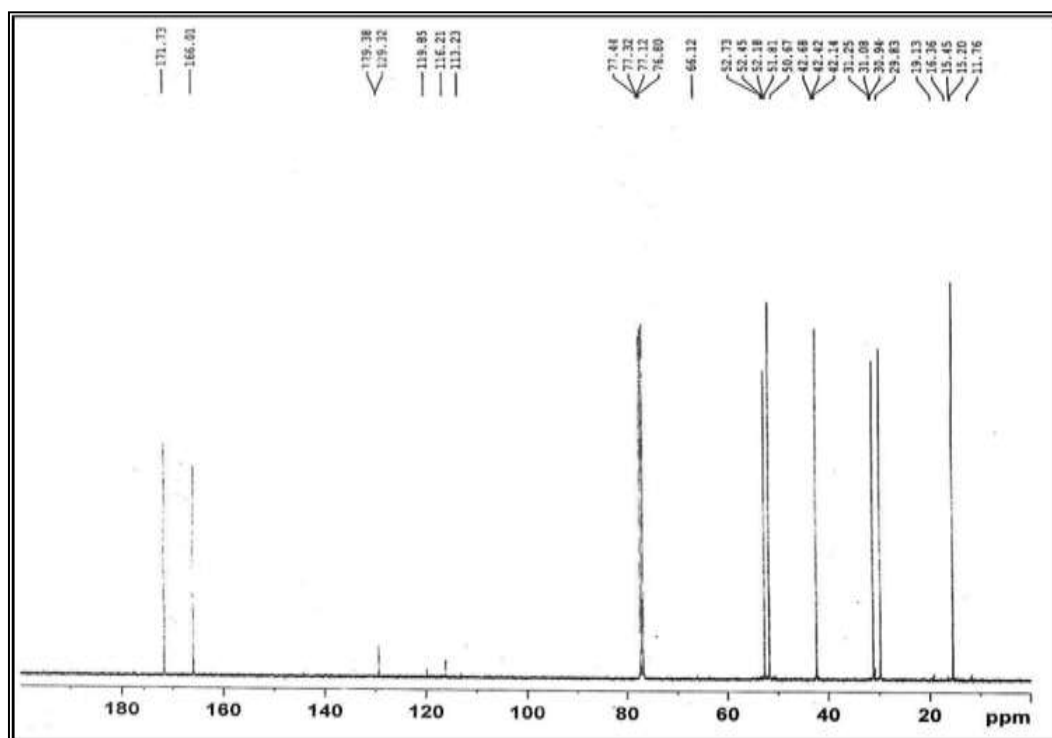


Fig. 4.15: ¹³C-NMR spectrum of M-Cl

¹H-NMR (400 MHz, CDCl₃): 2.01-2.07 (m, 1H), 2.09 (s, 3H), 2.15-2.22 (m, 1H), 2.49-2.54 (t, 2H), 3.76 (s, 3H), 4.07 (s, 2H), 4.69-4.75 (m, 1H), 7.29 (s, 1H) (Fig. 4.14)

¹³C-NMR (100 MHz, CDCl₃): 15.4, 29.8, 31.0, 42.4, 50.7, 51.8, 166.0, 171.7 (Fig. 4.15)

4.3.6 Characterization of 2-(2-(5-bromo benzoxazolone)acetamido)-3-(1*H*-indol-3-yl) propanoate (ABTO-Br)

MS (ESI) m/z: 470.2 [M-H⁺], calculated: 470.0 [M-H⁺] (Fig. 4.16)

¹H-NMR (DMSO, 400 MHz): δ (ppm) 3.1-3.2 (m, 2H), 3.6 (s, 3H), 4.4-4.6 (m, 3H), 6.9-7.5 (m, 8H) (Fig. 4.17)

¹³C-NMR (DMSO, 100 MHz): δ (ppm) 28.7, 44.4, 52.4, 53.9, 111.0-141.5 (14 C), 154.2, 166.3, 172.3 (Fig. 4.18)

HPLC: T3 column, 4.6 x 250 mm; MeCN/H₂O, 6/4-8/2 (v/v); flow rate: 0.8 ml/min;

λ_{uv} = 254 nm; t_R = 8.751 min (Fig. 4.19)

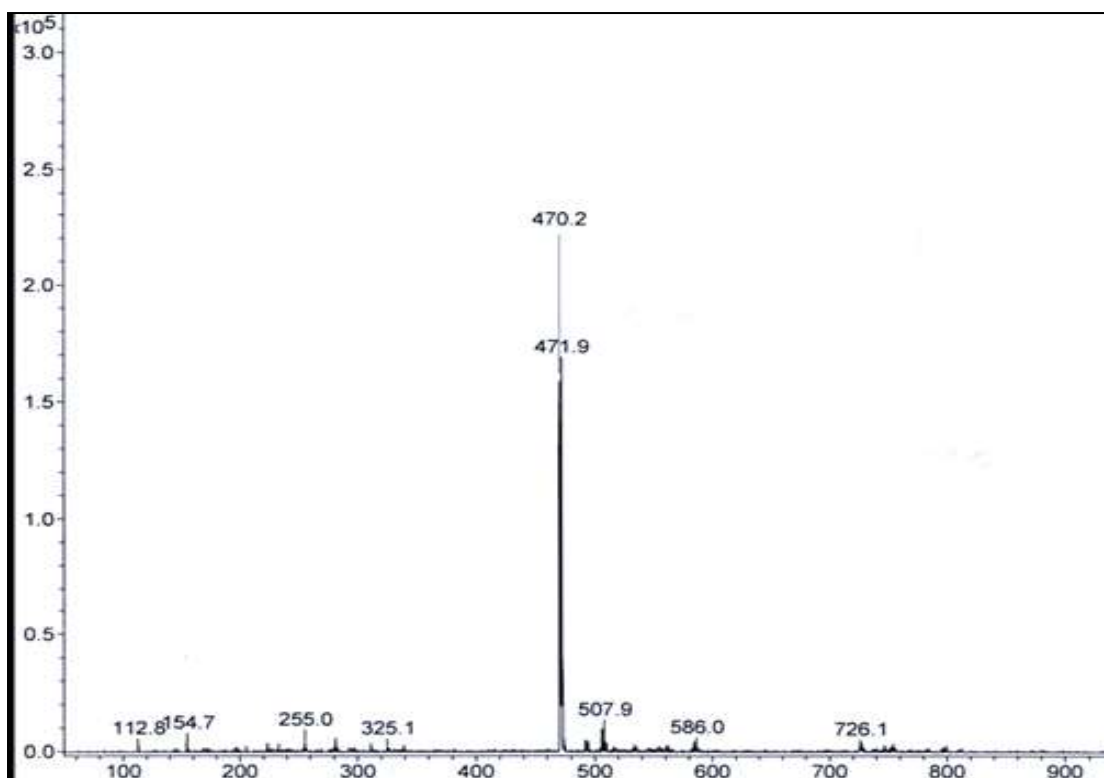


Fig. 4.16: Mass spectrum of ABTO-Br

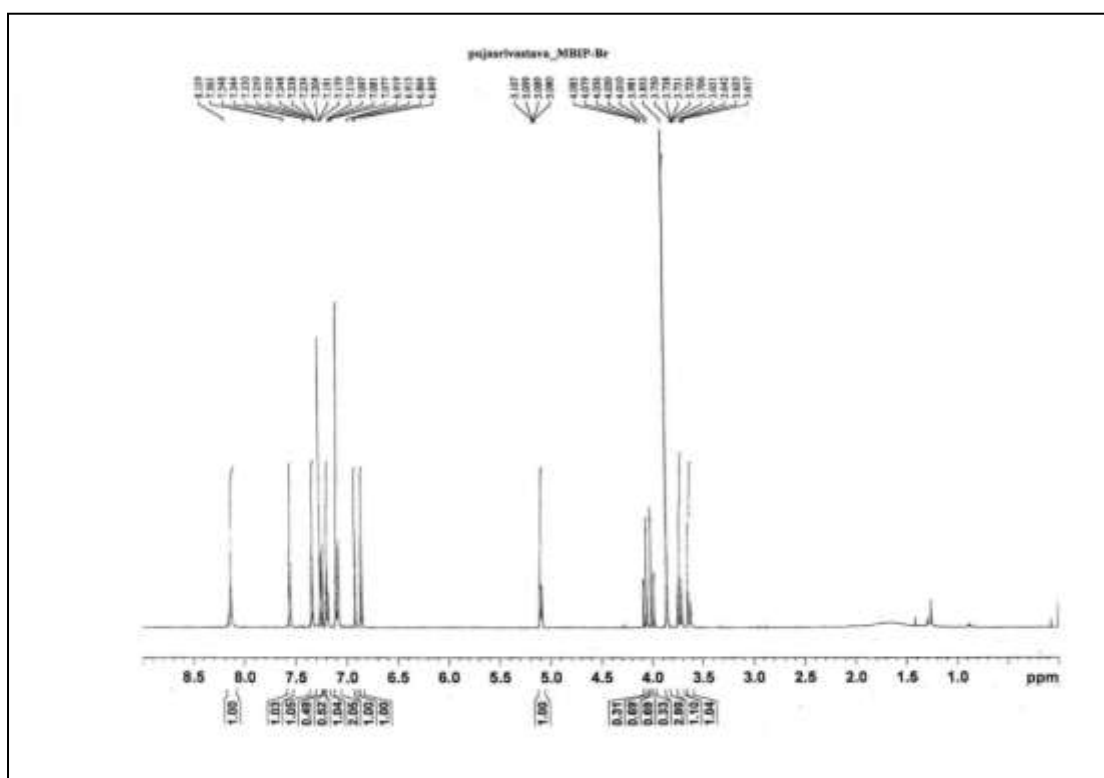


Fig. 4.17: ¹H-NMR spectrum of ABTO-Br

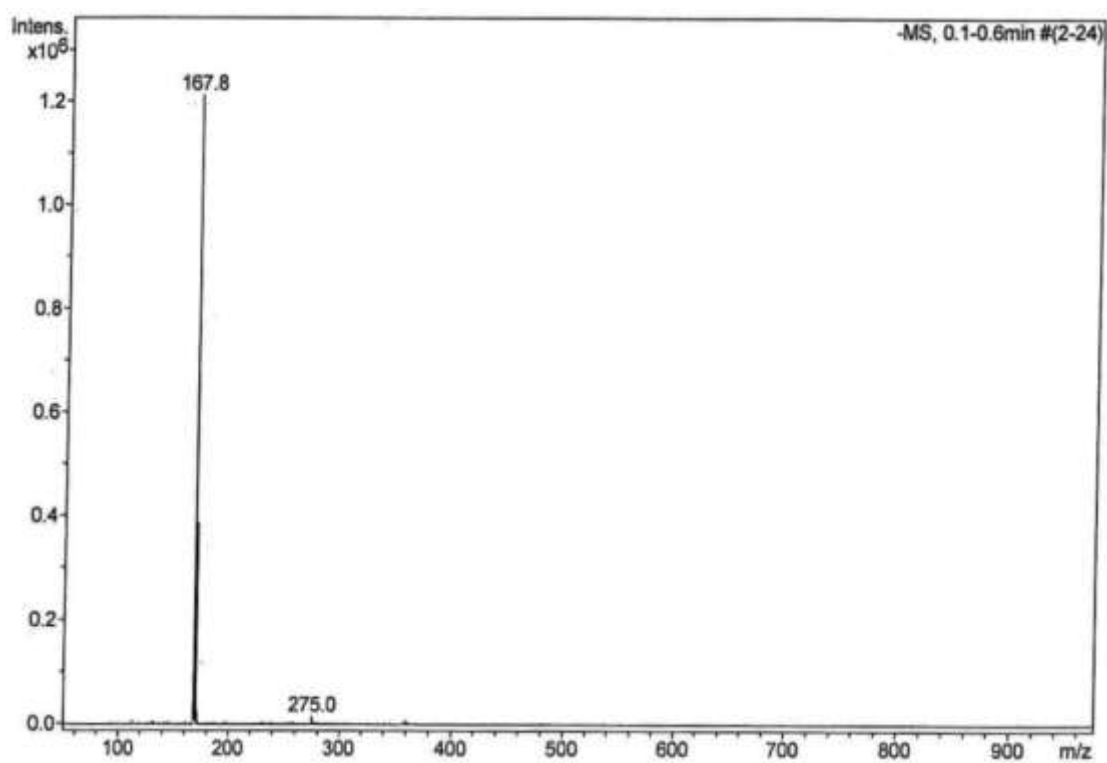


Fig. 4.1: Mass spectrum of ABO-Cl

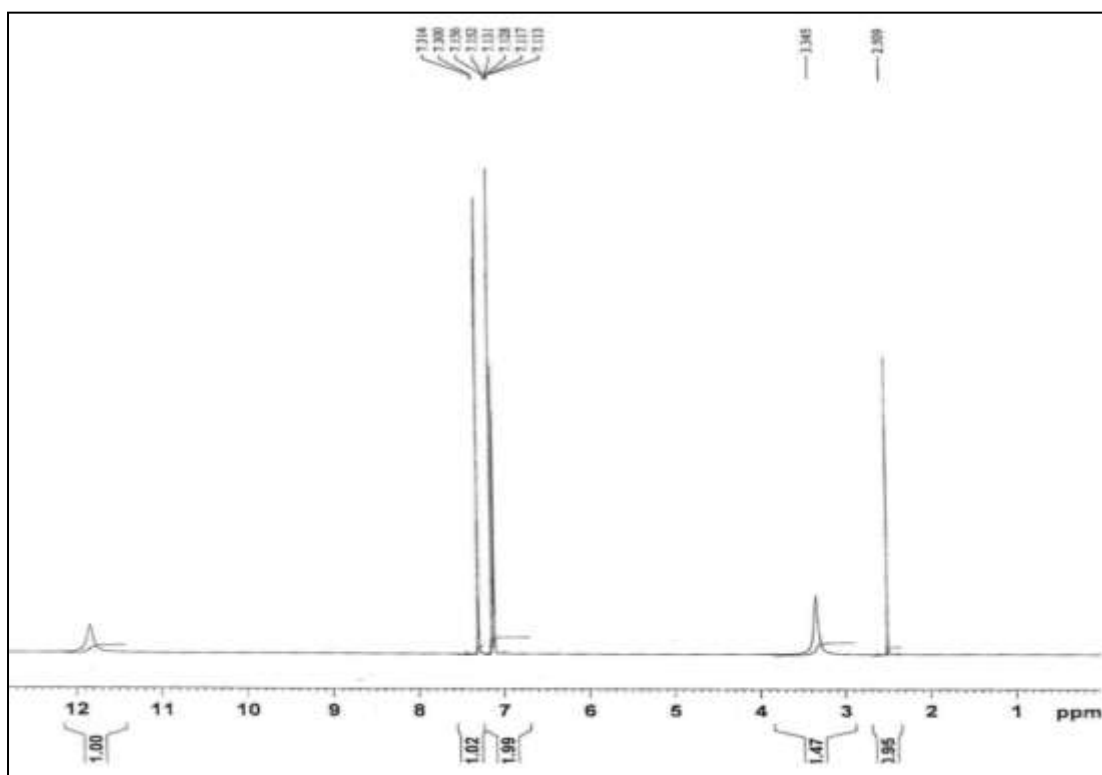


Fig. 4.2: $^1\text{H-NMR}$ spectrum of ABO-Cl

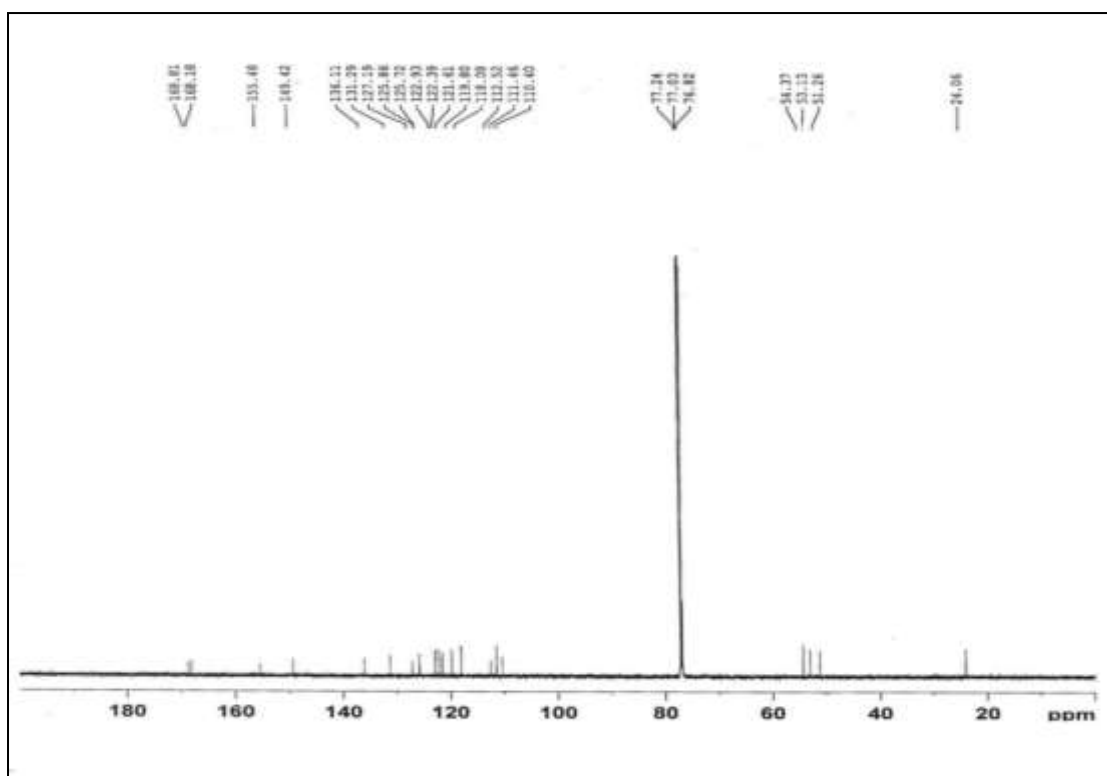


Fig. 4.18: ^{13}C -NMR spectrum of ABTO-Br

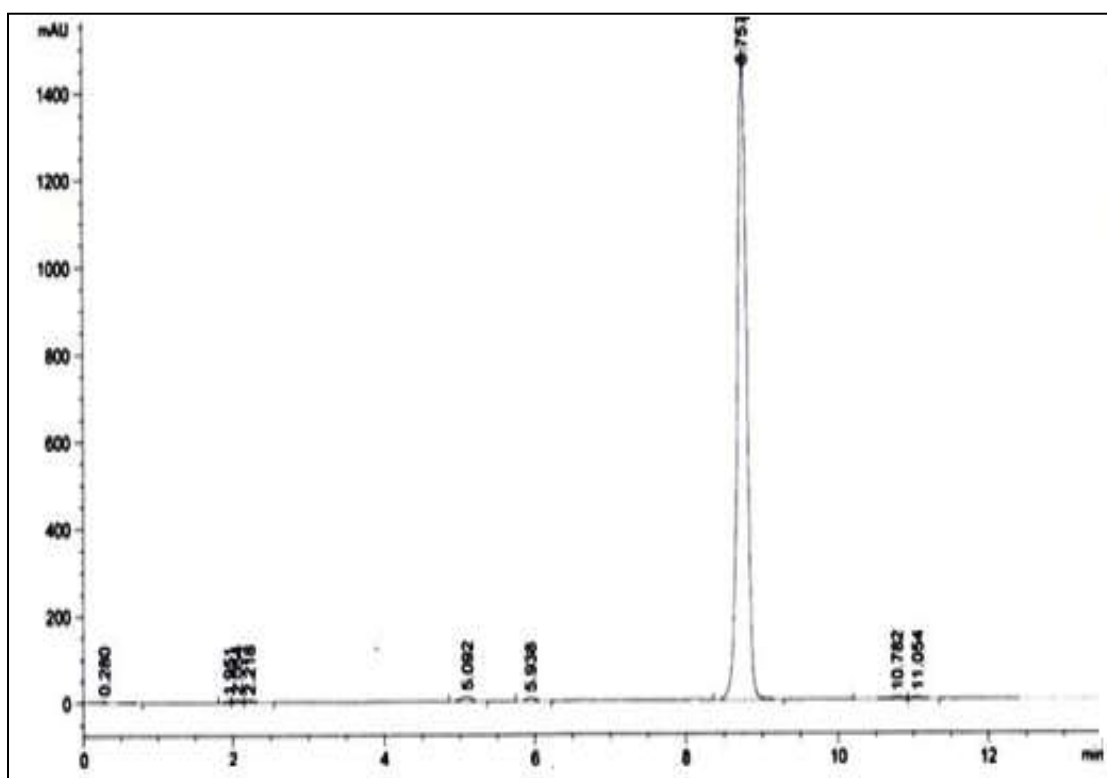


Fig. 4.19: HPLC profile of ABTO-Br

4.3.7 Characterization of 2-(2-(5-bromo benzoxazolone)acetamido)-3-(1*H*-indol-3-yl)propanoate (ABTO-Cl)

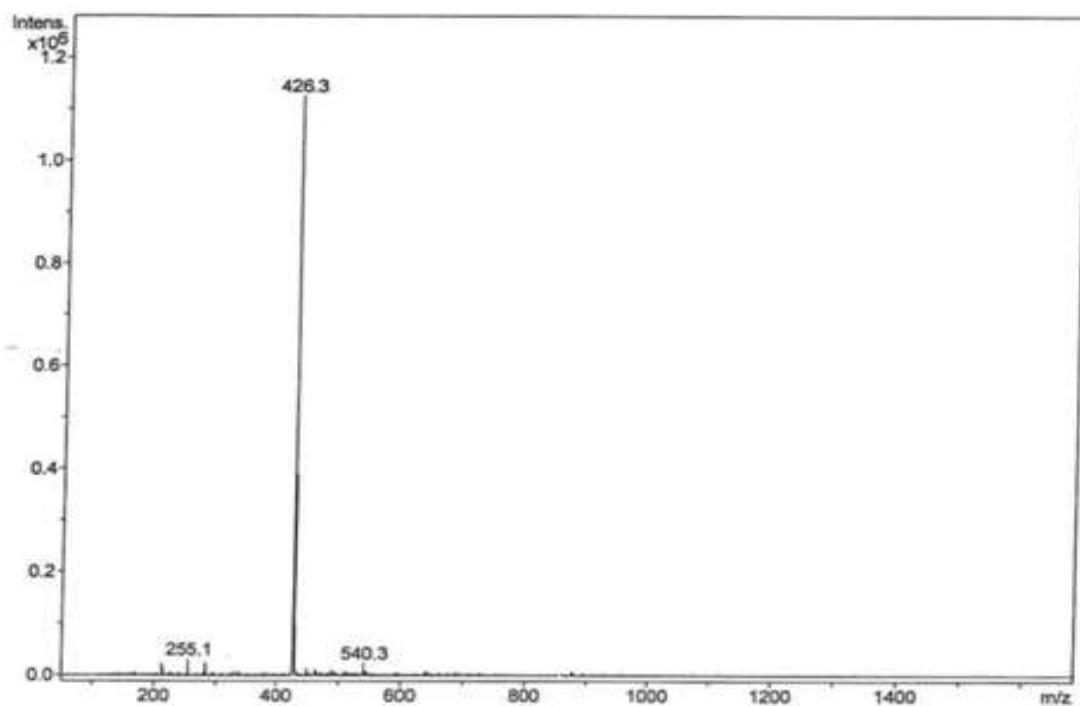


Fig. 4.20: Mass spectrum of ABTO-Cl

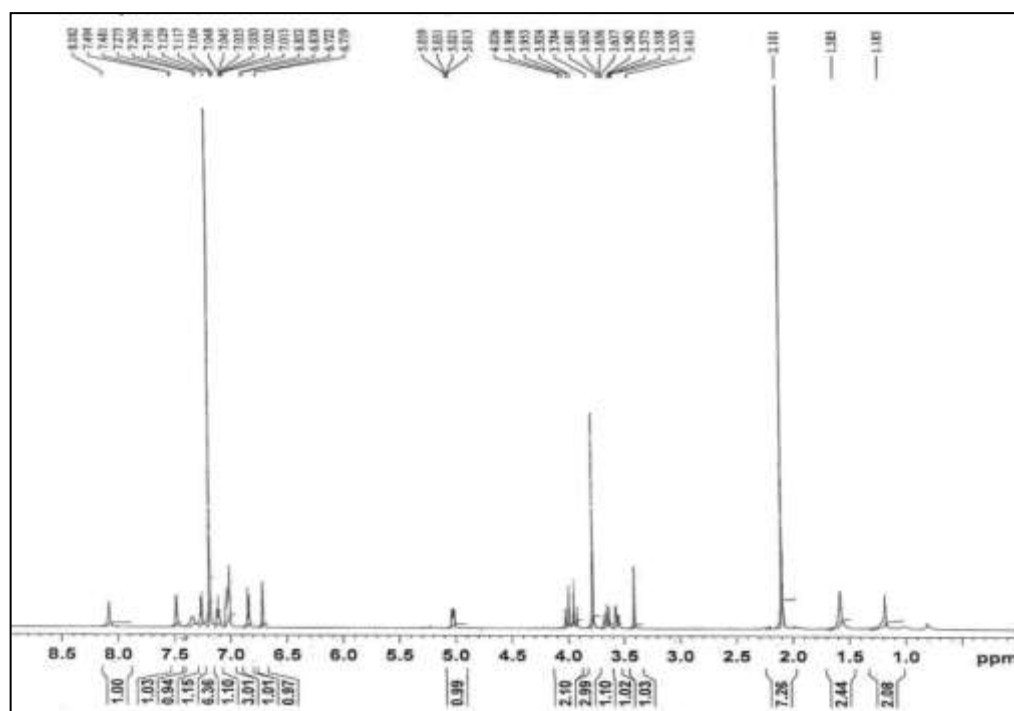


Fig. 4.21: ¹H-NMR spectrum of ABTO-Cl

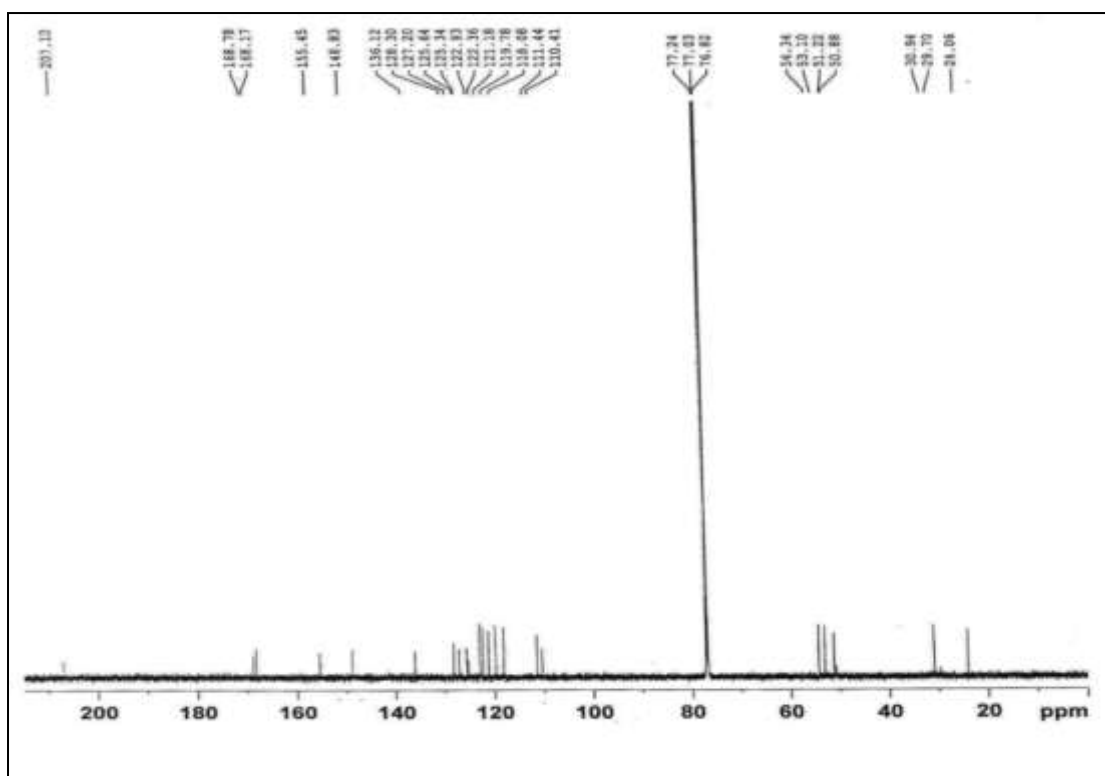


Fig. 4.22: ^{13}C -NMR spectrum of ABTO-Cl

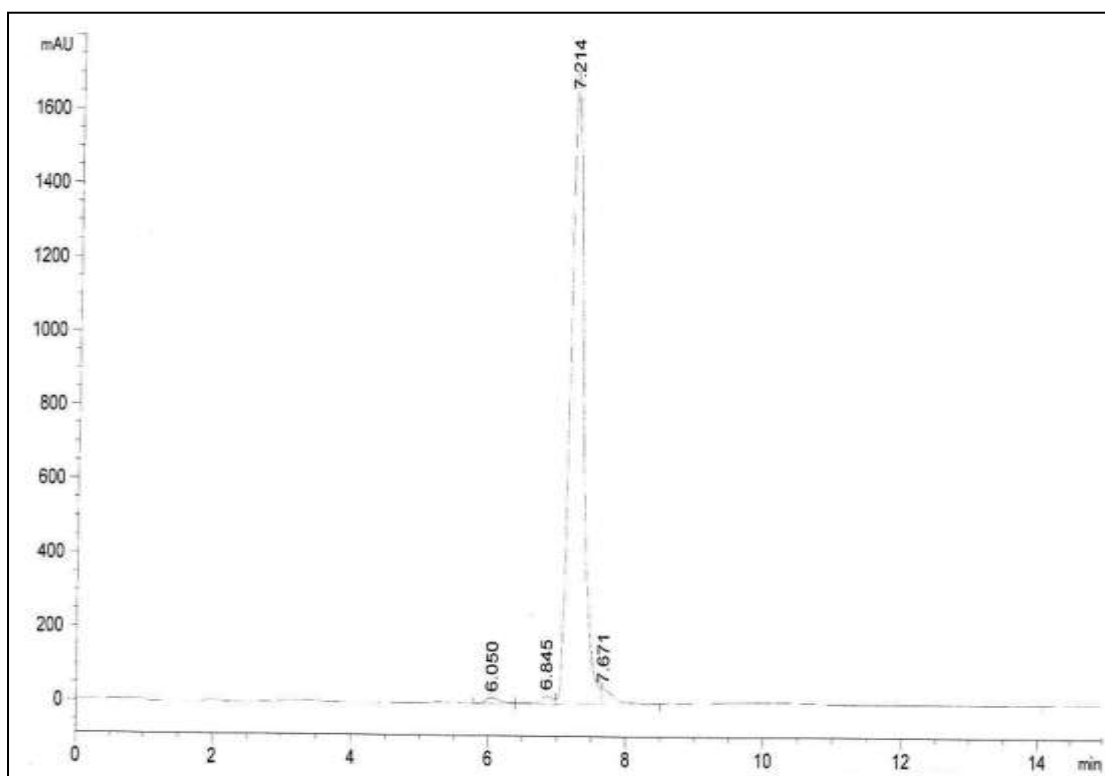


Fig. 4.23: HPLC profile of ABTO-Cl

MS (ESI) m/z : 426.3 [M-H⁺], Calculated m/z : 426.1 [M-H⁺] (Fig. 4.20)

¹H-NMR (CDCl₃, 600 MHz): δ (ppm) 3.5-3.7 (m, 2H), 3.8 (s, 3H), 3.9-4.0 (m, 2H), 5.0-5.1 (m, 1H), 6.7-7.5 (m, 8H), 8.1 (br s, 1H) (Fig. 4.21)

¹³C-NMR (CDCl₃, 150 MHz): 24.1, 51.2, 53.1, 54.3, 110.4-148.8 (14 peaks), 155.5, 168.2, 168.8 (Fig. 4.22)

HPLC: T3 column, 4.6 x 250 mm; MeCN/H₂O, 6/4-8/2 (v/v); flow rate: 0.8 ml/min; λ_{uv} = 254 nm; t_R = 7.214 min (Fig. 4.23)

4.3.8 Characterization of methyl 2-(2-(5-chloro-2-oxobenzoxazol-3(2H)-yl)acetamido)-3-phenylpropanoate (ABPO-Cl)

MS (ESI) m/z : 387.1 [M-H⁺], Calculated m/z : 387.1 [M-H⁺] (Fig. 4.24)

¹H-NMR (CDCl₃, 600 MHz): 3.50-3.60 (m, 2H), 3.86 (s, 3H), 4.19-4.27 (m, 2H), 5.07-5.10 (m, 1H), 6.96-7.33 (m, 8H) (Fig. 4.25)

¹³C-NMR (CDCl₃, 150 MHz): 34.0, 51.2, 53.2, 54.4, 121.3-148.8 (10 peaks), 155.3 (C=O), 168.1, 168.6 (Fig. 4.26)

HPLC: T3 column, 4.6 x 250 mm; MeCN/H₂O, 6/4-8/2 (v/v); flow rate: 0.8 ml/min; λ_{uv} = 254 nm; t_R = 8.970 min (Fig. 4.27)

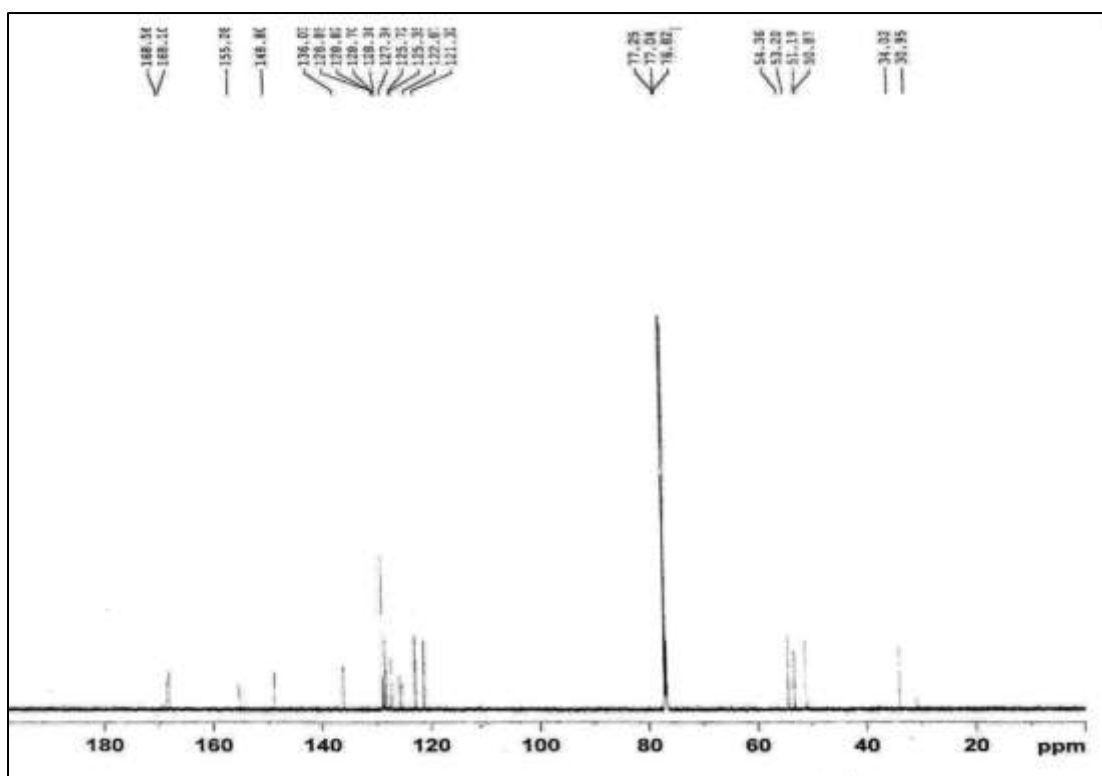


Fig. 4.26: ¹³C-NMR spectrum of ABPO-Cl

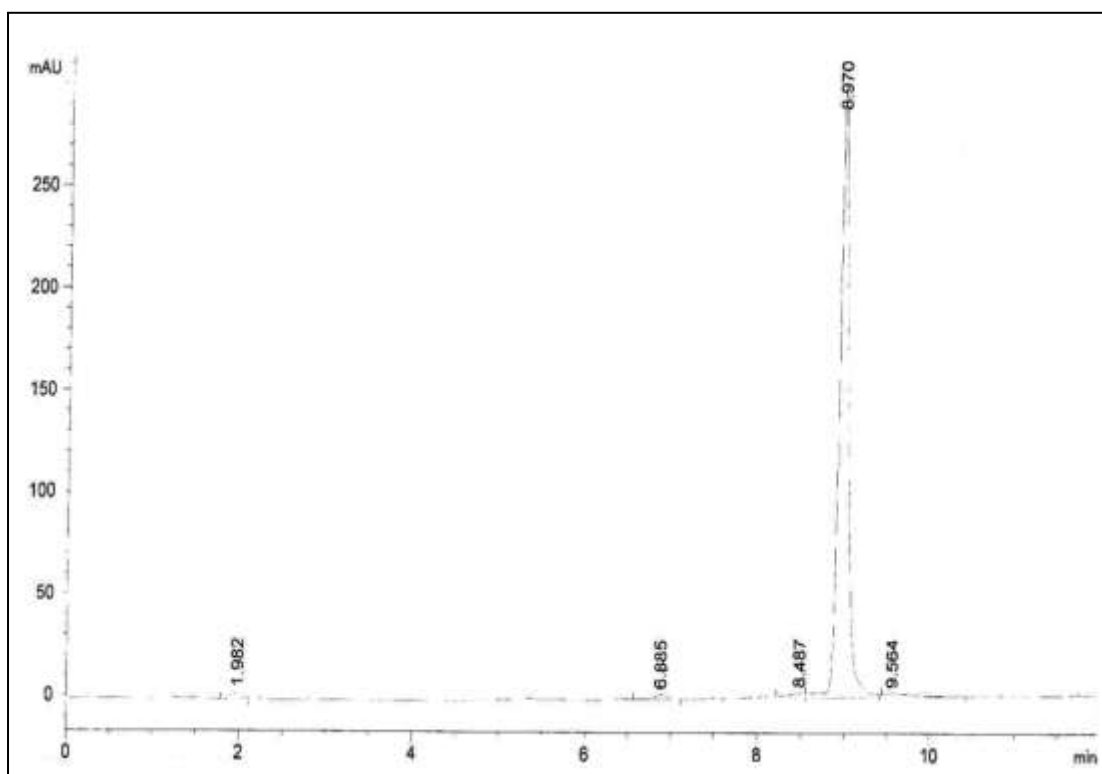


Fig. 4.27: HPLC profile of ABPO-Cl

4.3.9 Characterization of methyl 2-(2-(5-bromo-2-oxobenzoxazol-3(2H)-yl)acetamido)-3-phenylpropanoate (ABPO-Br)

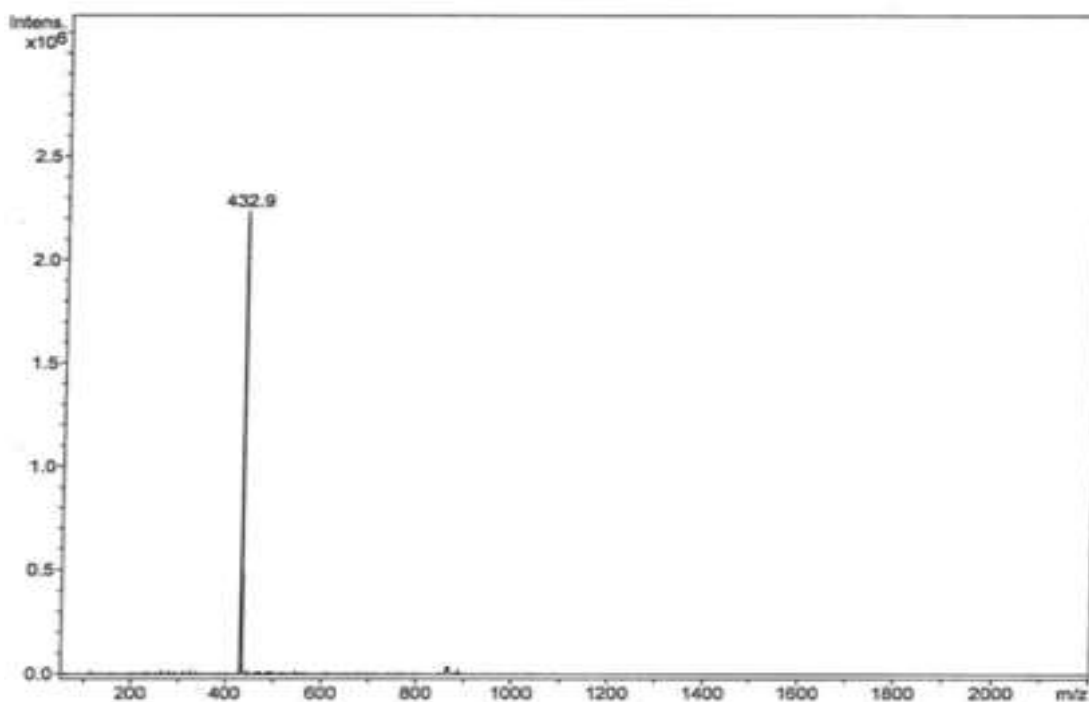


Fig. 4.28: Mass spectrum of ABPO-Br

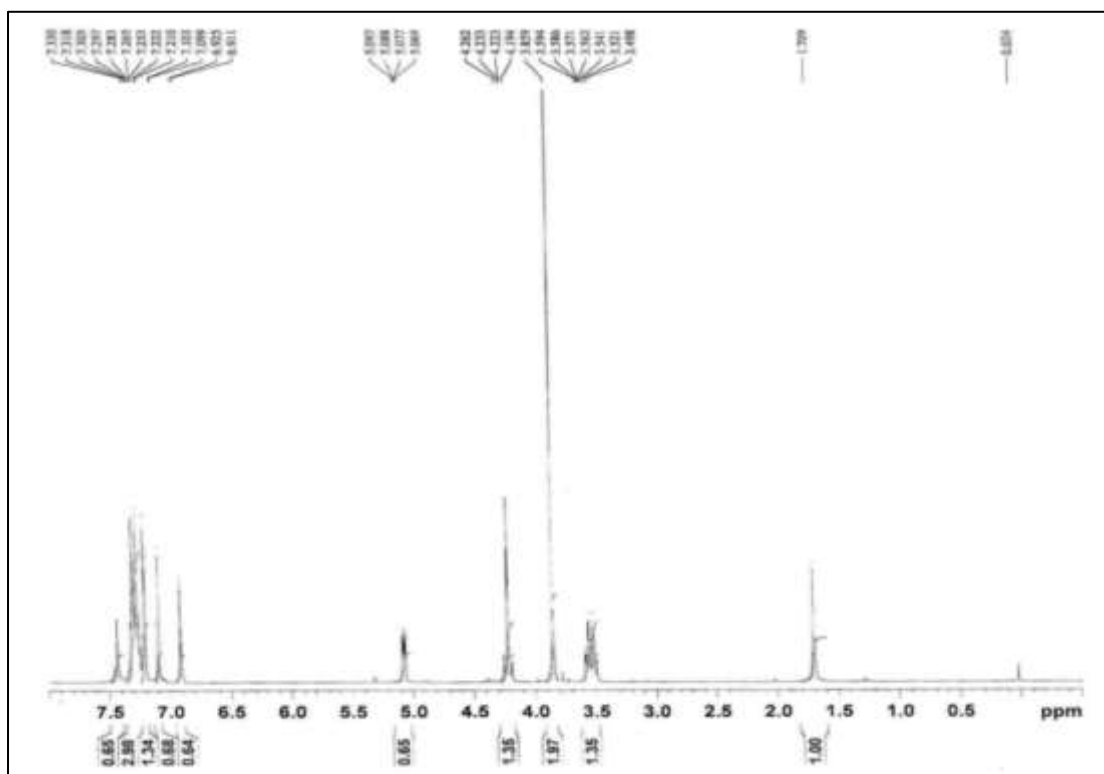


Fig. 4.29: ¹H-NMR spectrum of ABPO-Br

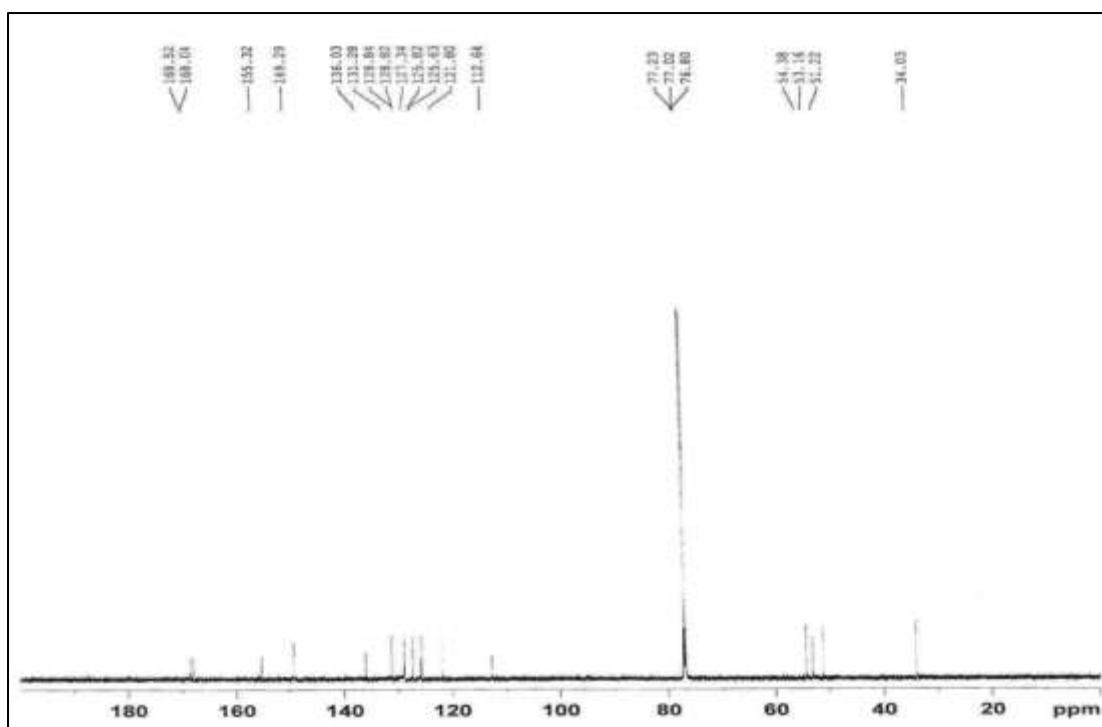


Fig. 4.30: ^{13}C -NMR spectrum of ABPO-Br

MS (ESI) m/z : 431.3 $[\text{M}-\text{H}^+]$, Calculated m/z : 431.0 $[\text{M}-\text{H}^+]$ (Fig. 4.28)

^1H -NMR (CDCl_3 , 600 MHz): 3.49-3.60 (m, 2H), 3.86 (s, 3H), 4.19-4.27 (m, 2H), 5.06-5.10 (m, 1H), 6.91-7.33 (m, 8H) (Fig. 4.29)

^{13}C - NMR (CDCl_3 , 150 MHz): 34.0, 51.2, 53.2, 54.4, 112.6-149.3 (10 peaks), 155.3 (C=O), 168.0, 168.5 (Fig. 4.30)

4.3.10 Characterization of 2-[2-(5-chloro-2-oxo-benzoxazol-3-yl)-acetylamino]-4-methylsulfanyl-butyrac acid methyl ester (ABMO-Cl)

MS (ESI) m/z : 371.0 $[\text{M}-\text{H}^+]$, Calculated m/z : 371.05 $[\text{M}-\text{H}^+]$ (Fig. 4.31)

^1H -NMR (600 MHz, CDCl_3): 2.11 (s, 3H), 2.49-2.65 (m, 4H), 3.80 (s, 3H), 4.43 (s, 2H), 4.99-5.03 (t, 1H), 6.93-6.95 (m, 1H), 7.14-7.16 (m, 2H) (Fig. 4.32)

^{13}C -NMR (150 MHz, CDCl_3): 15.4, 27.1, 30.9, 51.6, 52.3, 53.2, 120.7, 124.0, 125.1, 125.6, 128.6, 149.2, 155.6, 168.8, 169.0 (Fig. 4.33)

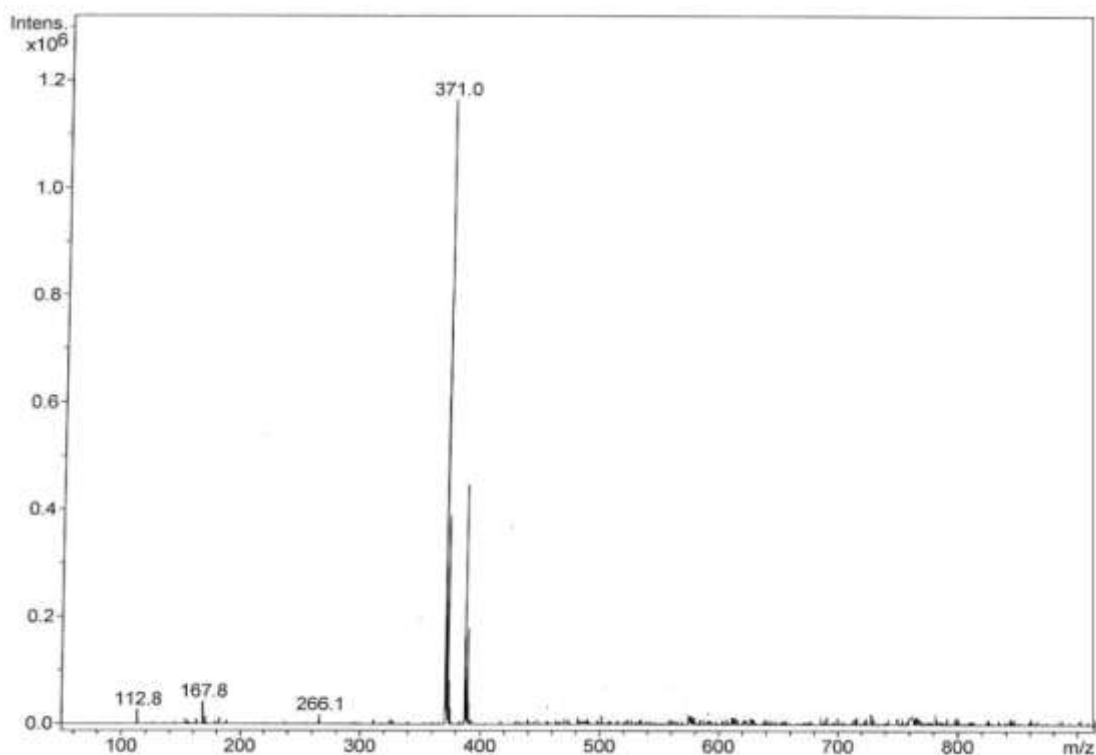


Fig. 4.31: Mass spectrum of ABMO-Cl

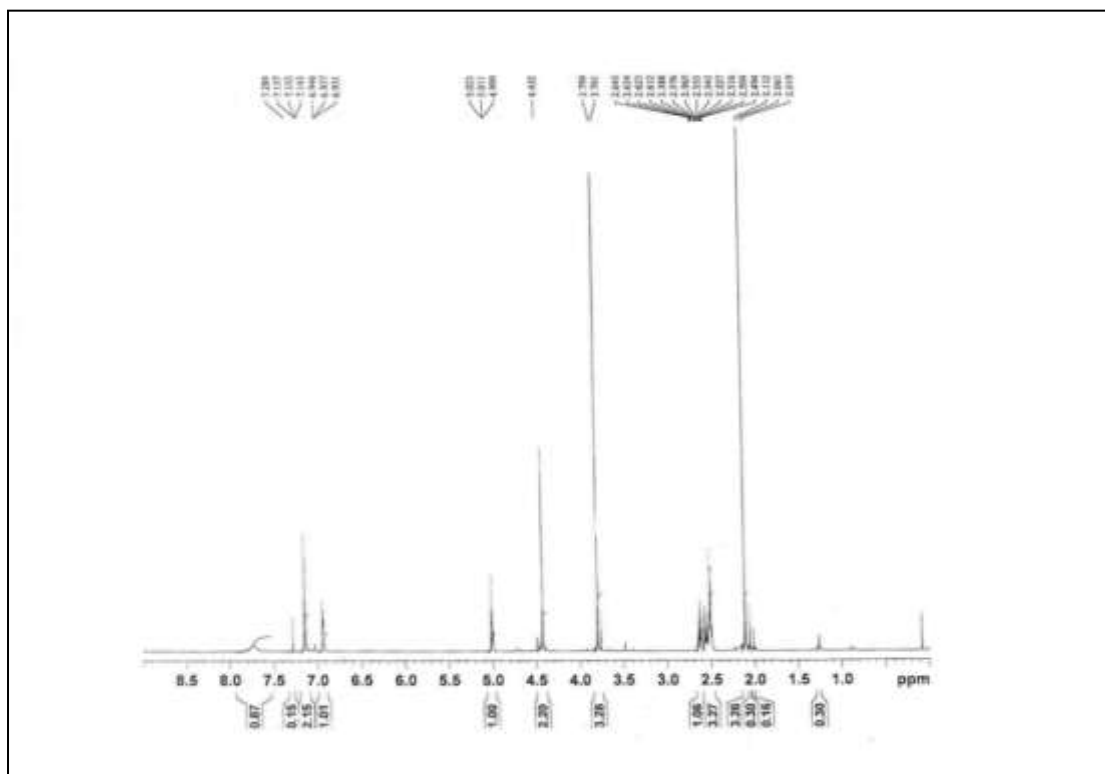


Fig. 4.32: $^1\text{H-NMR}$ spectrum of ABMO-Cl

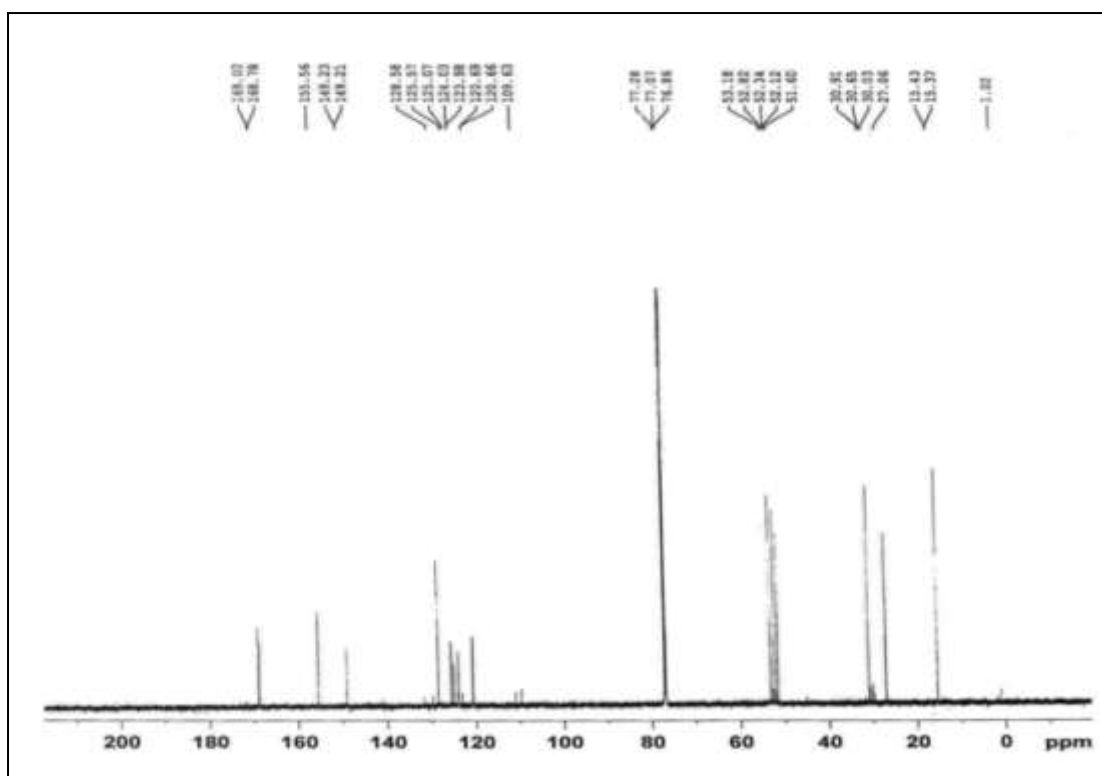


Fig. 4.33: ^{13}C -NMR spectrum of ABMO-Cl

4.3.11 Characterization of 2-[2-(5-bromo-2-oxo-benzoxazol-3-yl)-acetylamino]-4-methylsulfanyl-butyrac acid methyl ester (ABMO-Br)

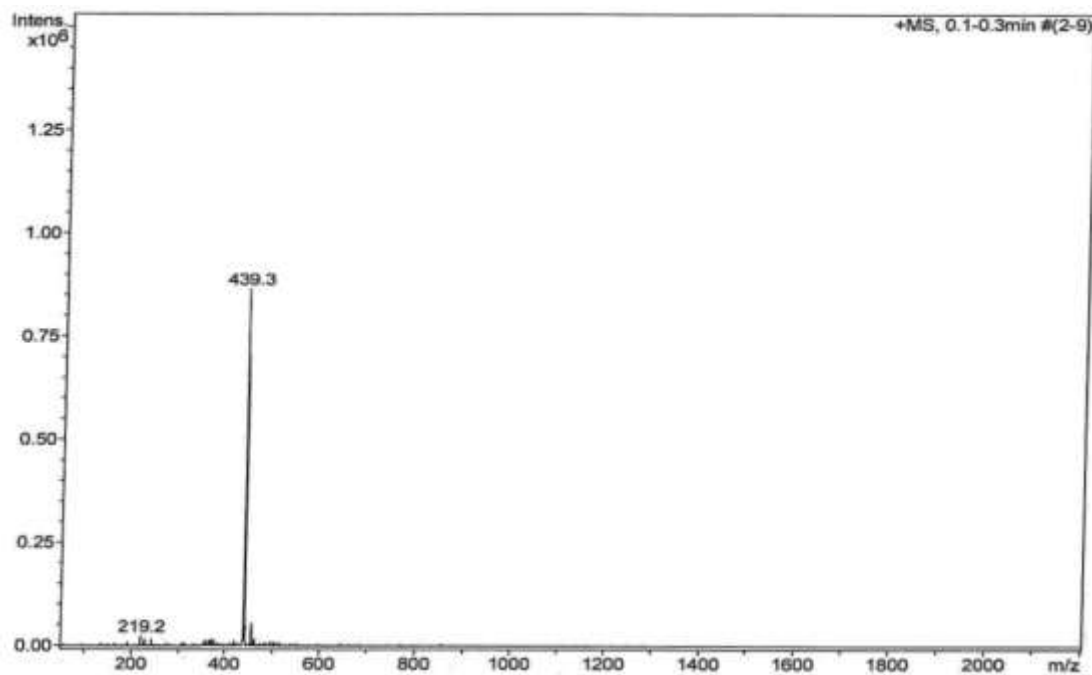


Fig. 4.34: Mass spectrum of ABMO-Br

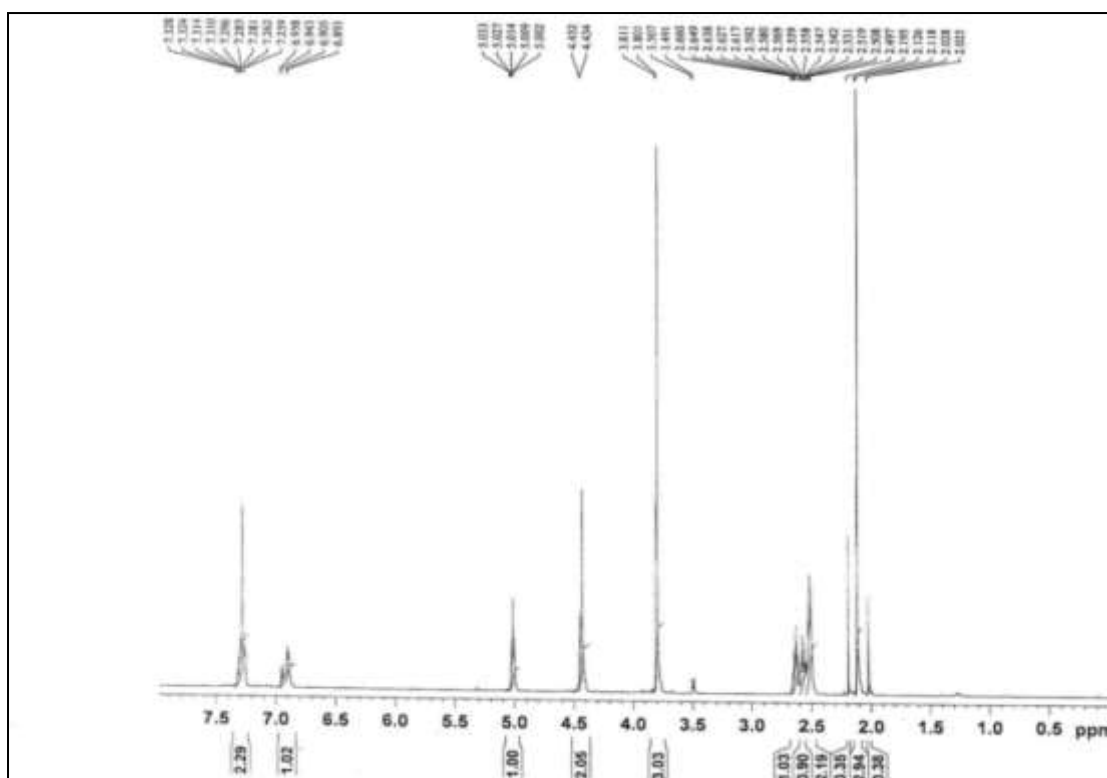


Fig. 4.35: ¹H-NMR spectra of ABMO-Br

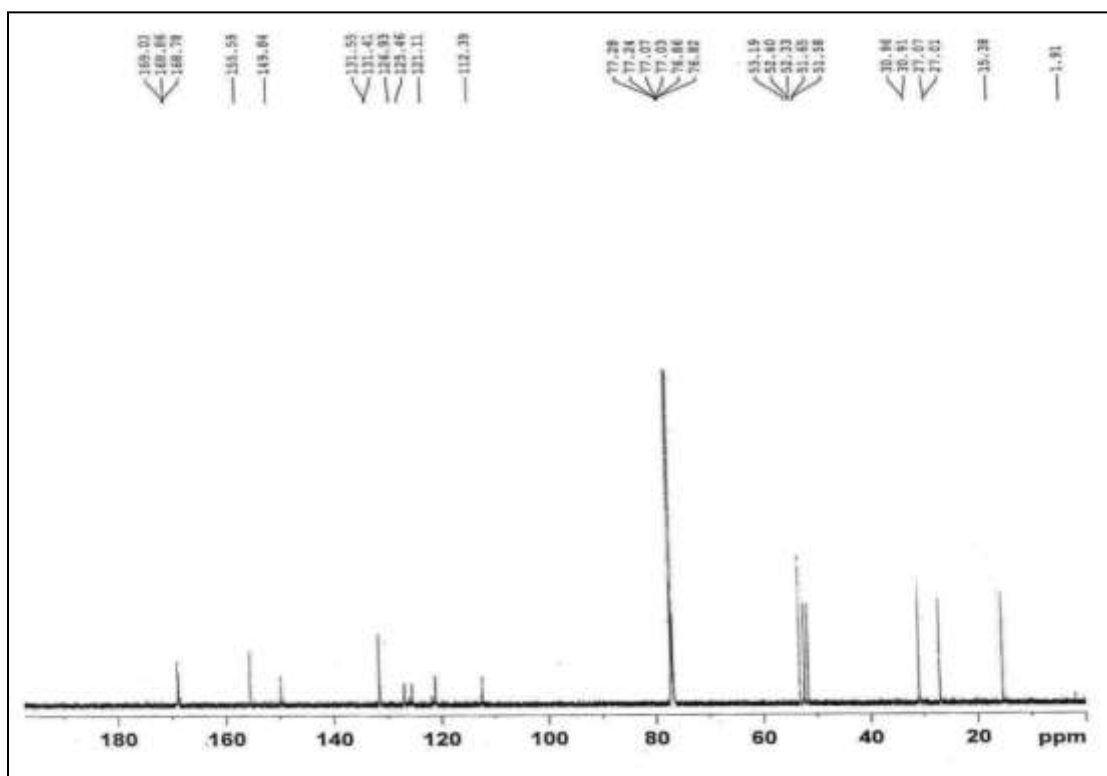


Fig. 4.36: ¹³C-NMR spectrum of ABMO-Br

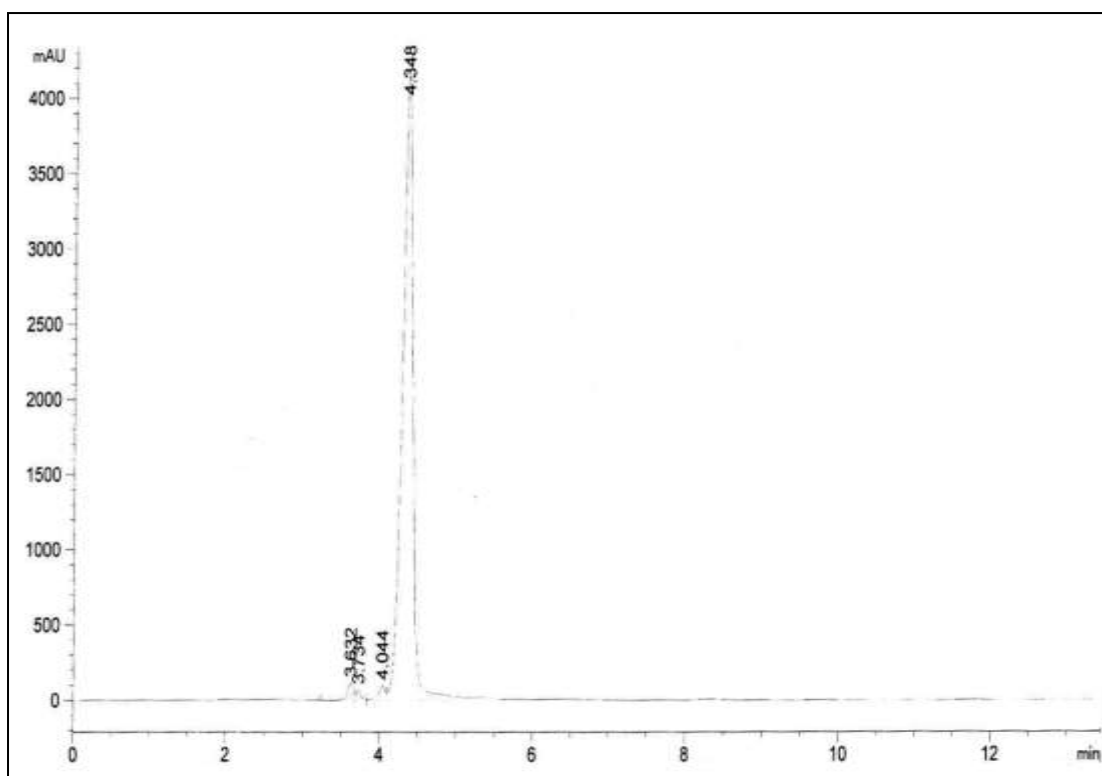


Fig. 4.37: HPLC profile of ABMO-Br

MS (ESI) m/z : 439.3 $[M+Na^+]$, Calculated m/z : 439.0 $[M+Na^+]$ (Fig. 4.34)

1H -NMR ($CDCl_3$, 600 MHz): 2.03 (s, 3H), 2.49-2.66 (m, 4H), 3.80 (s, 3H), 4.43 (s, 2H), 5.00-5.04 (t, 1H), 6.89-6.96 (m, 1H), 7.25-7.33 (m, 2H) (Fig. 4.35)

^{13}C -NMR ($CDCl_3$, 150 MHz): 15.4, 27.1, 30.9, 51.7, 52.3, 53.2, 112.4, 121.1, 125.5, 126.9, 131.6, 149.8, 155.6, 168.9, 169.0 (Fig. 4.36)

HPLC: T3 column, 4.6 x 250 mm; MeCN/ H_2O , 6/4-8/2 (v/v); flow rate: 0.8 ml/min;

λ_{uv} = 254 nm; t_R = 4.348 min (Fig. 4.37)

4.4 *In vitro* toxicity evaluation

The extent of toxicity was quantified using MTT assay. RAW 264.7 cell line has been chosen for the study because it demonstrated increase in TSPO level 24 h post

stimulation with LPS (Shao *et al.*, 2013). All the analogues of ABEO-Br/Cl demonstrated significant viability upto 10 μ M concentration.

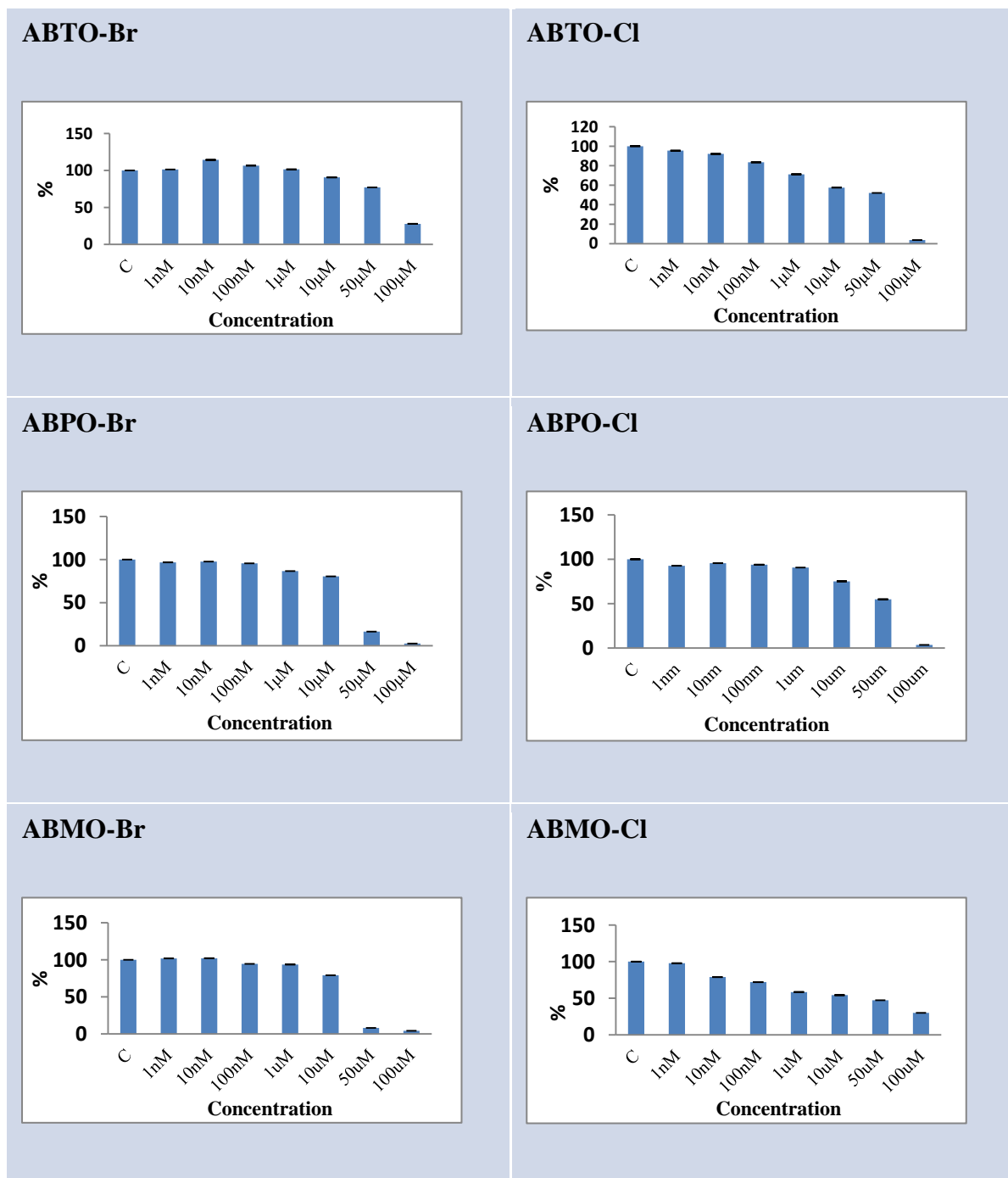


Fig. 4.38: Effect of ABEO-Br/Cl analogues on cell viability in RAW 264.7 cell line

4.5 Conclusion

The designed acetamidobenzoxazolone based analogues using amino acid esters have been synthesized. Initially four-stepped reaction was successfully tried for synthesizing the trptophan methyl ester analogue. In process of optimization, three steps reaction was tried. This demonstrated improvement in terms of yield, time and cost due to the parallel approach followed as compared to linear synthetic protocol in initial approach. All the intermediates as well as final compounds were characterized. For characterization purpose, mass spectroscopy, $^1\text{H-NMR}$, $^{13}\text{C-NMR}$ and HPLC were used. The evaluation of toxicities showed their potential for application under *in vivo* condition.

Chapter 5
Radiosynthesis and biological evaluation
of $^{99m}\text{Tc-ABEO-Br/Cl}$

CHAPTER 5

RADIOSYNTHESIS AND BIOLOGICAL EVALUATION OF ^{99m}Tc -ABEO-Br/Cl

The previous chapter contains the synthesis and characterization of the molecules designed as TSPO ligands through *in silico* means. In order to validate the results of the virtual screening, the synthesized ligands were complexed with radionuclide ^{99m}Tc and studied for specificity towards TSPO using *in vitro*, *ex vivo* and *in vivo* means. This part of the chapter contains radiosynthesis and biological evaluation of ^{99m}Tc -ABTO-Br/Cl. Uptake and specificity were demonstrated on human lung tumor cell line A549. Balb/c mice were used for biodistribution studies (*ex vivo* as well as *in vivo*). New Zealand rabbits were utilized for biodistribution (*in vivo*) as well as blood kinetic studies. In order to prove specificity of radioligands towards TSPO, lung tumor xenograft model (Nude mice) and lung inflammation models (Balb/c mice), known to have increased TSPO concentration, were used. Blocking studies were performed with known TSPO ligand PK11195 to demonstrate specificity in cell line, normal and modelled mice.

5.1.1 Radiosynthesis and stability studies of radiocomplexes

The ABTO-Br/Cl analogues were radiolabelled with ^{99m}Tc and were studied for their stabilities in saline as well as in serum as per procedures mentioned in chapter 2. After radiosynthesis, biological evaluation was performed through tracer technique.

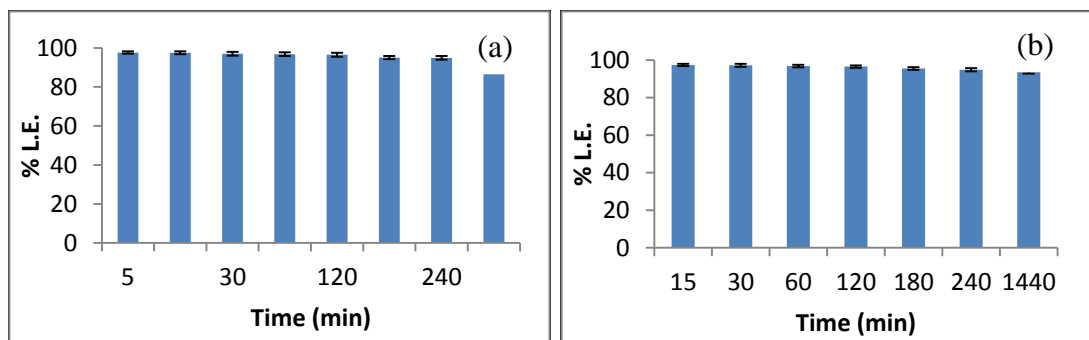


Fig. 5.1.1: Labelling efficiency (%LE) of a) ABTO-Br and b) ABTO-Cl with ^{99m}Tc NaTcO_4 at pH 7 was used for labelling. 0.1 cm segment of ITLC were used after developing it in acetone and PAW (pyridine, acetic acid and water in 3:5:1.5 ratio) solvents for count measurement.

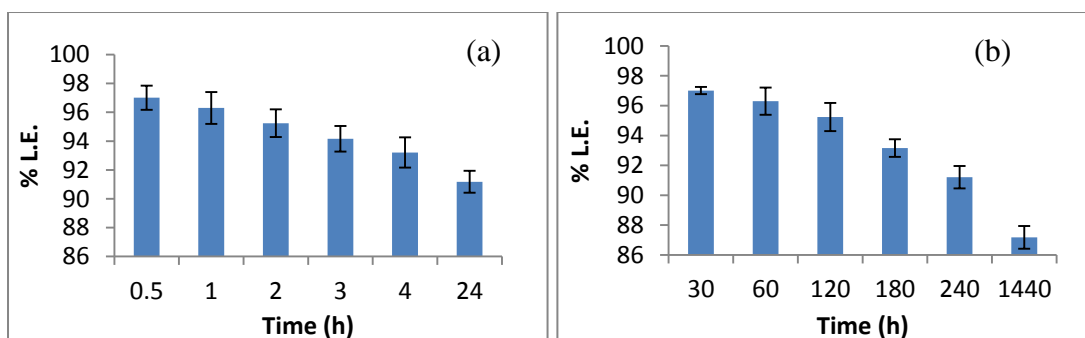


Fig. 5.1.2: Serum stability studies in terms of labelling efficiency (%LE) of a) ^{99m}Tc -ABTO-Br and b) ^{99m}Tc -ABTO-Cl over 24 h. Studies were performed in fresh human serum from healthy volunteers at physiological conditions i.e. 37°C .

The purified compounds ABTO-Br and ABTO-Cl were radiolabelled with $>96\%$ radiochemical yields. The stability of both the radiolabelled compounds were observed to be $>94\%$ in saline after 24 h reflecting that radiocomplexes were stable (Fig. 5.1.1).

Serum stability studies under *in vitro* condition clearly demonstrated the stabilities of radiocomplexes, ^{99m}Tc -ABTO-Br and ^{99m}Tc -ABTO-Cl, with no significant transchelation to proteins present in serum such as albumin which were 93% and

91% intact after 4 h (Fig. 5.1.2). Stability studies demonstrated stability of the complexes required to find application as SPECT agents for both the ligands.

5.1.2 In vitro studies

5.1.2.1 Cell uptake of ^{99m}Tc -radioligand in A549 human lung tumor cells

The human lung carcinoma cells (A549) were used to evaluate specificity of $^{99m}\text{Tc-ABTO-Br/Cl}$ towards TSPO through *in vitro* assay. The results of *in vitro* uptake of the radiocomplexes are shown in Fig. 5.1.3. They demonstrated that the uptake were dependent on time and increased till last time point of study i.e. 60 min for both bromo and chloro analogues. PK11195 was used for blocking studies. The blocking agent was incubated for 1 h before adding radiolabelled compound. The maximum reduction was 43.6% and 41.1% for bromo and chloro analogues, respectively. Increase in the uptake of blocked cells with time implied that the cells were not fully blocked still it gave preliminary idea about the specificity aspect of $^{99m}\text{Tc-ABTO-Br/Cl}$ towards TSPO.

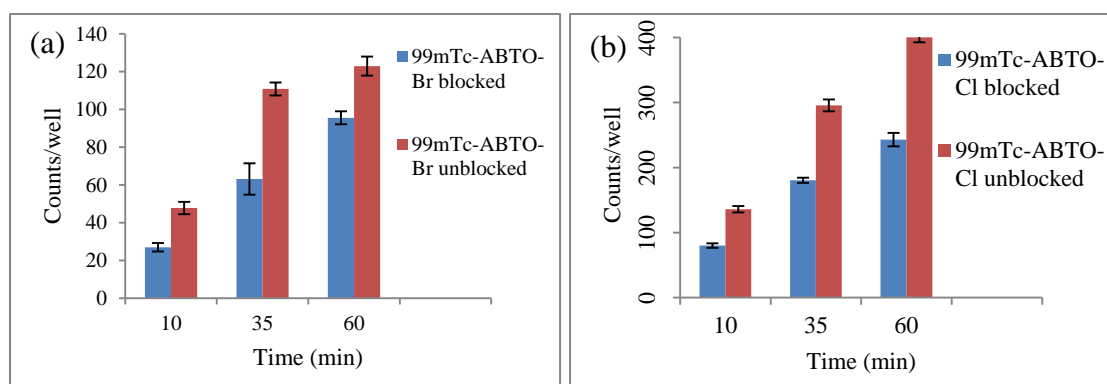


Fig. 5.1.3: Uptake kinetics of a) $^{99m}\text{Tc-ABTO-Br}$ and b) $^{99m}\text{Tc-ABTO-Cl}$ in A549 cells in the presence (blue) and absence (red) of PK11195
Data are expressed as counts per well (mean with S.D. n=3)

5.1.3 Ex vivo studies

5.1.3.1 Blood kinetic studies in New Zealand rabbits

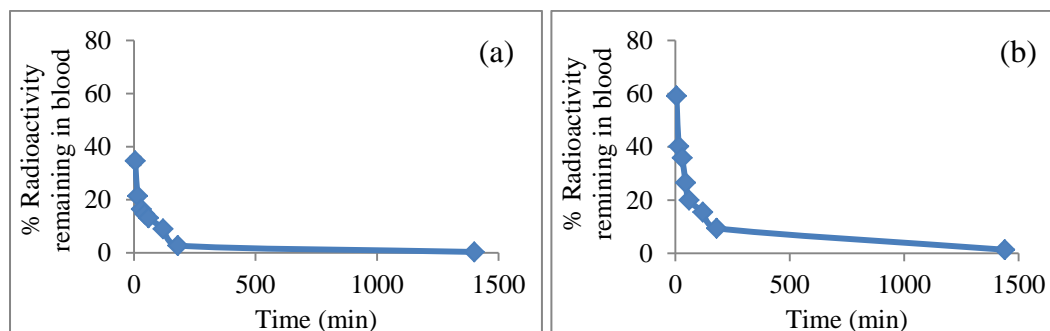


Fig. 5.1.4: Time activity curves showing blood clearance of a) $^{99m}\text{Tc-ABTO-Br}$ and b) $^{99m}\text{Tc-ABTO-Cl}$ postinjection in New Zealand rabbits

The blood clearance was studied on normal rabbits as per procedure mentioned in chapter 2. The blood samples were withdrawn from the ear vein at different time points till 24 h. The radioactivities of the blood samples were measured in the gamma counter to calculate the persistence of activity in the circulation. Both the tryptophan methyl ester analogues demonstrated a rapid radioactivity clearance from blood circulation. $^{99m}\text{Tc-ABTO-Br}$ and $^{99m}\text{Tc-ABTO-Cl}$ activity clearance were >62% and >66% in 1 h; and >92% and >84% in 3 h. This reflected the fast release kinetics as desired for diagnostic application (Fig. 5.1.4).

5.1.3.2 Biodistribution studies in Balb/c mice

Ex vivo biodistribution of radiocomplex was carried out to get an idea about its reach to the organs of interest i.e. TSPO rich organs and its excretion from the body. The distribution in different organs is represented as percentage of injected dose per organ at different time points. Fig. 5.1.5 showed the distribution patterns of both radioactive compounds at different time points post injection into the mice (n=3). One compound at a time has been discussed in detail. Firstly, $^{99m}\text{Tc-ABTO-Br}$ was considered. At 5

min, peak value of radioactivity was recorded in all the organs. Highest %ID/g was observed in liver i.e. 28.87 followed by kidneys, spleen and lungs which were 11.19, 10.25, and 5.20, respectively. 15 min onwards spleen contained highest radioactivity after liver i.e. 6.88, 5.18, 4.97, 3.42, and 1.72%ID/g at 15 min, 30 min, 60 min, 120 min, and 1440 min, respectively. Lungs and kidneys also had significant amount of radioactivity present till 30 min i.e. 3.15 and 3.50%ID/g, respectively. Thereafter, there was a sharp decrease in radioactivity in lungs with 25.0% to 5.5% of uptake at 5 min from 60 min to 1440 min. Similar trend but steepest fall was observed in kidneys i.e. 20% of the uptake at 5 min in 60 min and subsequent reduction to 8% in 1440 min. The biodistribution pattern demonstrated that the radioactivity was mainly localized in TSPO-expressing organs such as lungs, liver, spleen, and kidneys. The good uptake of radioactivity in requisite organs proved them as a TPSO targeting ligand.

In brain, small uptake of 0.06%ID/g at 5 min was observed which reduced to 0.01% at the last time point of observation. The small uptake in brain could be attributed to moderate concentration of TSPO in the healthy brain. Maximum radioactivity quantity in liver showed that the clearance of the radioligand was through hepatobiliary route.

$^{99m}\text{Tc-ABTO-Cl}$, chloro analogue of $^{99m}\text{Tc-ABTO-Br}$, had also been evaluated for the uptake in requisite organs and relative uptake through biodistribution studies as shown in fig. 5.1.5b.

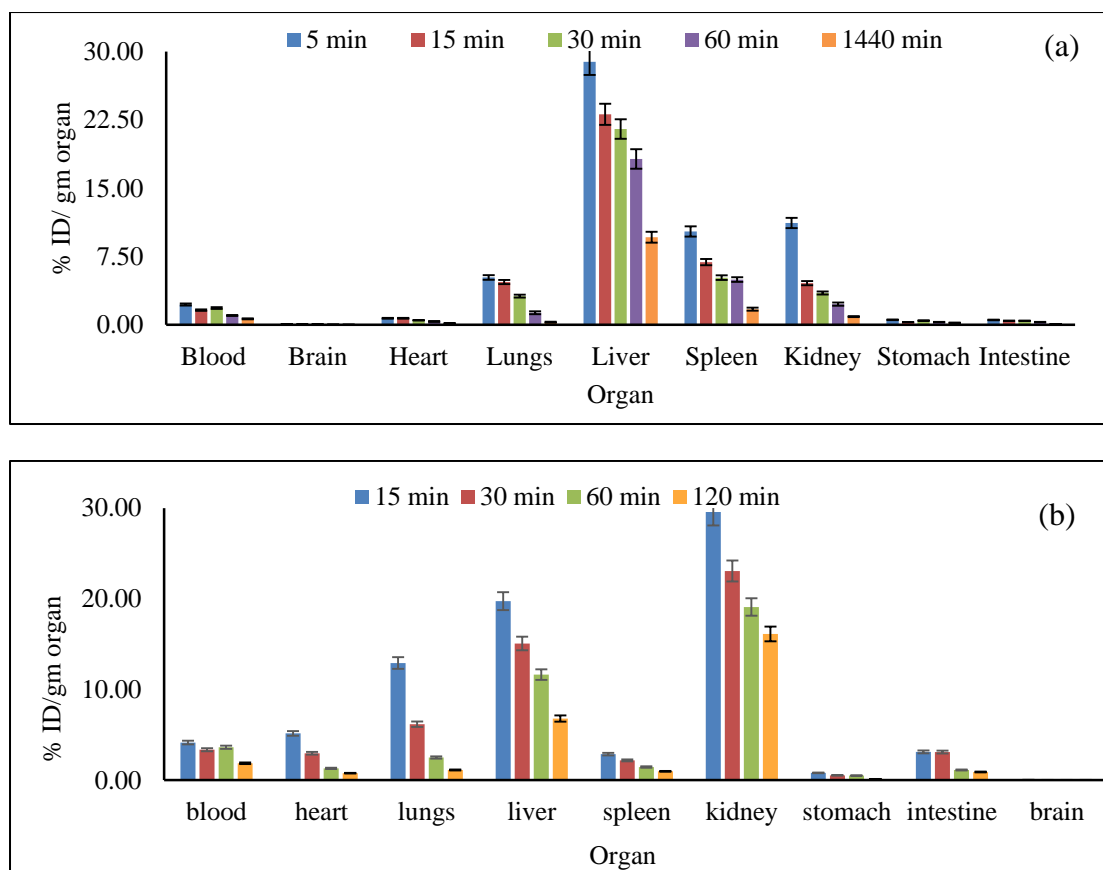


Fig. 5.1.5: Biodistribution patterns of a) $^{99m}\text{Tc-ABTO-Br}$ and b) $^{99m}\text{Tc-ABTO-Cl}$ in normal Balb/c mice

Mice (n=3) received 100 μCi of $^{99m}\text{Tc-ABTO}$ analogues by tail vein injection. Radioactivity uptake in different organs were measured by gamma counting and expressed as %ID/g, Mean \pm standard deviation

After 15 min, there were high uptake of radioactivity into organs having TSPO sites, such as kidneys (29.57%ID/g), heart (5.16%ID/g), spleen (2.87%ID/g), and lungs (12.91%ID/g). The uptake in lungs and heart were approx 2.75 and 7 fold as compared to $^{99m}\text{Tc-ABTO-Br}$ uptake at 15 min showing better distribution pattern for TSPO targeting (Fig. 5.1.5) which, in turn, would result in better SPECT ligand. Uptake of $^{99m}\text{Tc-ABTO-Cl}$ in liver was relatively lower than that of $^{99m}\text{Tc-ABTO-Br}$ (19.74 vs 23.12%ID/g). Rate of reductions were high in heart and lungs which reduced to 14.7% (5.16%ID/g to 0.76%ID/g) and 8.9% (12.91%ID/g to 1.12%ID/g), respectively between 15-120 min. Over same period kidneys, liver, spleen and blood

uptake were reduced to 54.5%, 34.0%, 33.8% and 45.0%, respectively. The amount of radiotracer in the blood and brain decreased with time. Uptake in kidneys and liver reflected that the excretion occurred through renal and hepatobiliary tract as expected for a compound with moderate lipophilicity.

5.1.3.3 Biodistribution studies of $^{99m}\text{Tc-ABTO-Br}$ in lung inflamed model of Balb/c mice

Ex vivo biodistribution studies concluded that $^{99m}\text{Tc-ABTO}$ analogues seemed to be suitable for lung imaging applications. Both the analogues were studied in mice model prepared by applying methods mentioned in chapter 2.

Firstly, blocking study was performed in lung inflammation model of Balb/c mice. Lung inflammation model was prepared through intranasal administration of Lipopolysaccharide. The saturation aspect of TSPO binding site by $^{99m}\text{Tc-ABTO-Br}$ has been studied by blocking with PK11195 on lung inflamed mice model. Three different concentrations of known TSPO ligand (PK11195) 2.5 mg/kg, 5 mg/kg, and 10 mg/kg were injected 10 min prior to $^{99m}\text{Tc-ABTO-Br}$ injection. PK11195 was dissolved in 100 μl (DMSO and saline) which was injected intravenously. All the experiments were performed in triplicate set (n=3). *In vivo* images were taken at 40 min post intravenous injection of radioligands.

$^{99m}\text{Tc-ABTO-Br}$ showed uptake in all the organs rich in TSPO. TSPO-rich peripheral organs showed blocking which was not concentration dependent for all (Fig 5.1.6). Blocking studies on TSPO ligands are complex as peripheral organs serve as a sink for radiotracers and although blocking/displacement drugs can reduce uptake, the

varied TSPO density in these organs will see different reduction in the different peripheral organs as their receptor density will vary.

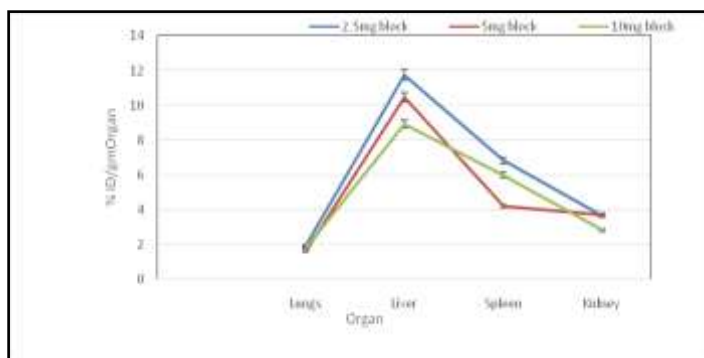


Fig. 5.1.6: $^{99m}\text{Tc-ABTO-Br}$ *ex vivo* biodistribution in lungs, liver, spleen and kidneys of lung inflamed mice at 40 min post i.v. injection with 10 min preadministration of 2.5/5/10 mg/kg PK11195 as blocking agent

5.1.4 *In vivo* studies

To find out the distribution under *in vivo* state, SPECT imaging was performed post injection of radiolabelled $^{99m}\text{Tc-ABTO-Br/Cl}$ ligands in normal mice and rabbits. For specificity, blocking studies were performed using a known TSPO ligand PK11195 in normal and modelled mice.

5.1.4.1 Biodistribution and blocking studies of $^{99m}\text{Tc-ABTO-Br/Cl}$ in normal Balb/c mice

The distribution under *in vivo* conditions in Balb/c mice for both the $^{99m}\text{Tc-ABTO}$ analogues were mainly localized in TSPO rich organs in unblocked as well as in blocked conditions.

The percentage blocking observed for $^{99m}\text{Tc-ABTO-Br}$ and $^{99m}\text{Tc-ABTO-Cl}$ were 30.9% and 31.9% in main organs on preadministration of PK11195 (Fig. 5.1.7a, Fig. 5.1.7b).

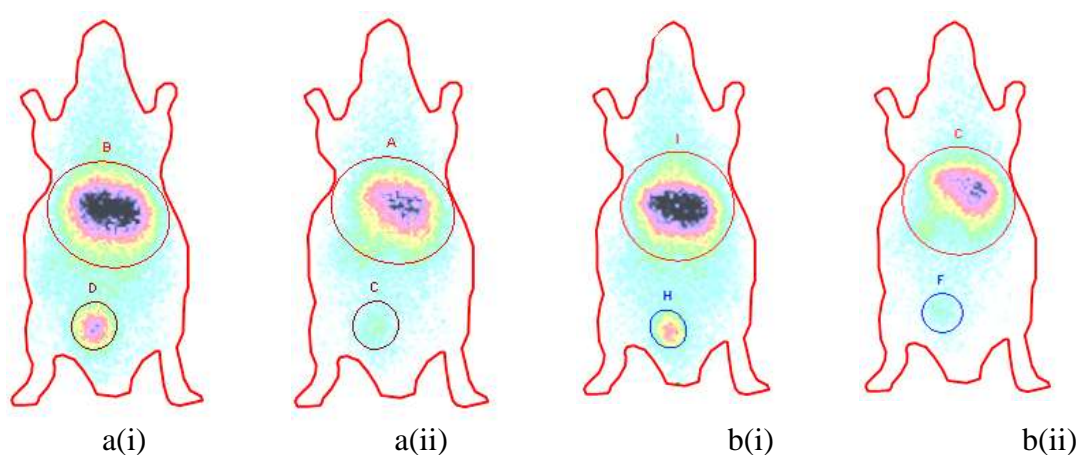
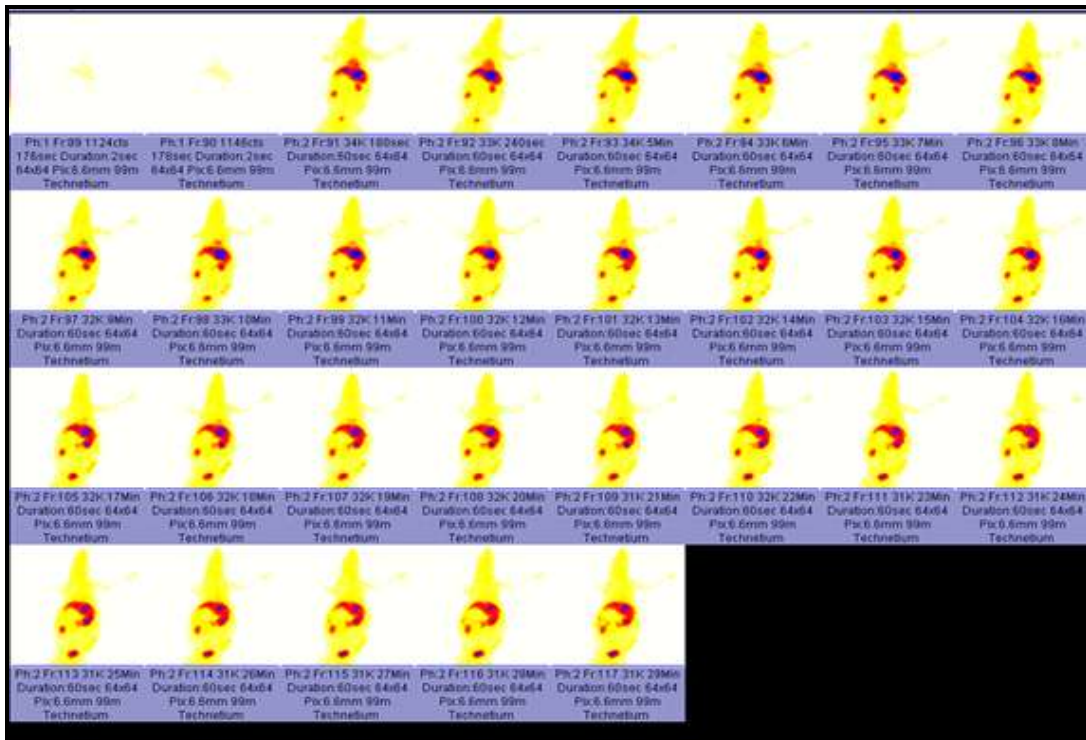


Fig. 5.1.7: *In vivo* SPECT images of $^{99m}\text{Tc-ABTO-Cl}$ a(i) without and a(ii) with PK11195 preadministration and $^{99m}\text{Tc-ABTO-Br}$ b(i) without and b(ii) with PK11195 preadministration at 40 min post injection of radioligand

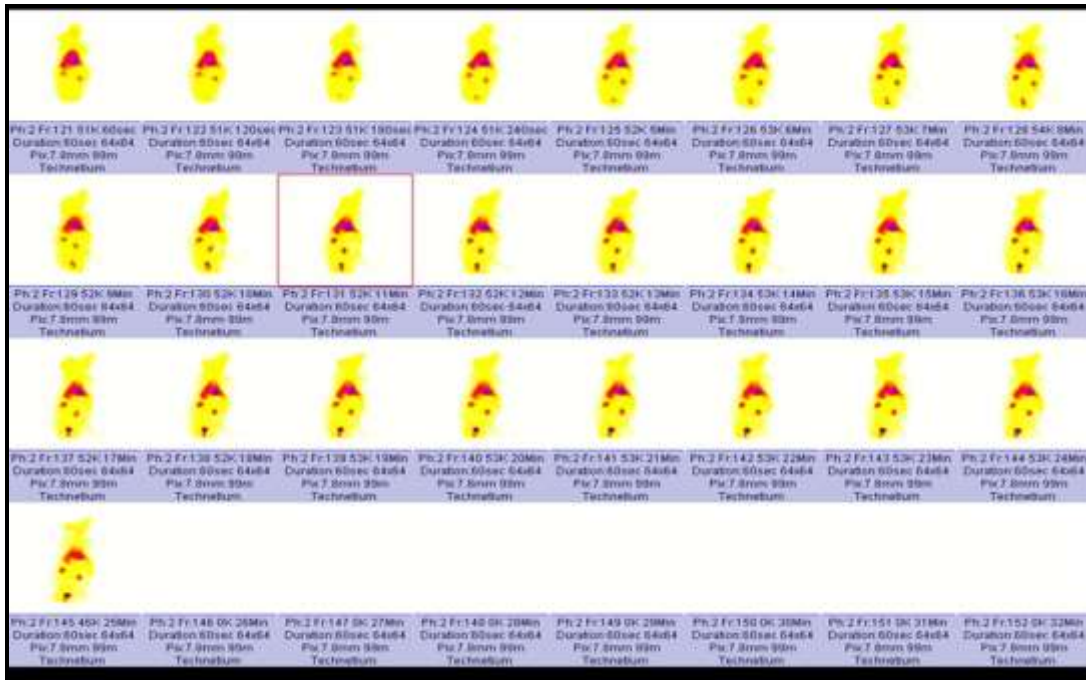
These data proved the selectivity and specificity of the compounds towards TSPO. It warrants further investigation on other mice models with increased TSPO concentration.

5.1.4.2 Biodistribution studies of $^{99m}\text{Tc-ABTO-Br/Cl}$ in New Zealand rabbits

In order to have better clarity about uptake pattern, New Zealand rabbits were used for *in vivo* imaging. SPECT studies of both the analogues of $^{99m}\text{Tc-ABTO}$ were carried out in New Zealand rabbits by intravenous injection of 300 μCi in 200 μl of radiolabelled complex through ear vein. The acquisition was performed dynamically for 30 min post injection. The biodistribution patterns shown in the images were similar to *ex vivo* biodistribution observed for both the radioligands. Also uptake in brains were observed at initial time points which reduced significantly within 15 min. Uptake in spleen was visible in $^{99m}\text{Tc-ABTO-Br}$ but not in $^{99m}\text{Tc-ABTO-Cl}$ which was also reflected in *ex vivo* biodistribution of mice (Fig. 5.1.8).



a)



b)

Fig. 5.1.8: *In vivo* biodistribution of a) $^{99m}\text{Tc-ABTO-Br}$ and b) $^{99m}\text{Tc-ABTO-Cl}$ in New Zealand rabbits (Dynamic studies for 30 min)

5.1.4.3 Biodistribution and blocking studies of $^{99m}\text{Tc-ABTO-Cl}$ in lung inflamed model of Balb/c mice

Further, $^{99m}\text{Tc-ABTO-Cl}$ was studied for its specificity towards TSPO on inflammation model of Balb/c mice. For this study, inflammation model was prepared through intratracheal injection of lipopolysaccharide in Balb/c mice. Two different concentrations, 5 mg/kg and 10 mg/kg, of PK11195 were taken for blocking.

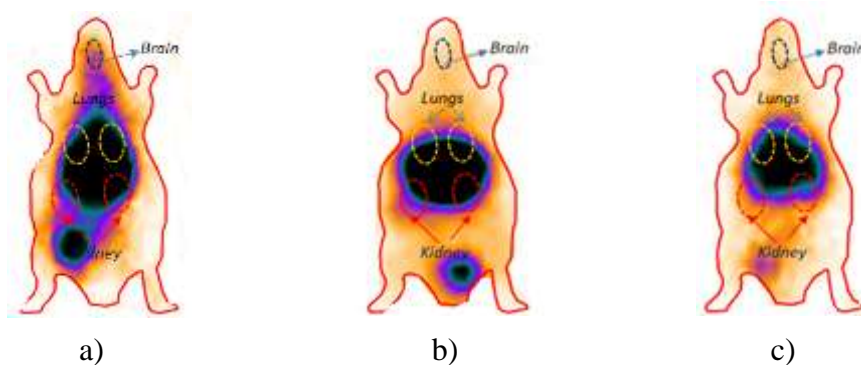


Fig. 5.1.9: *In vivo* SPECT images showing activity distribution of $^{99m}\text{Tc-ABTO-Cl}$ in inflamed mice a) without and b), c) with blocking at 40 min post i.v. injection with 10 min preadministration of 5/10 mg/kg PK11195 as blocking agent in lung inflammation model of Balb/c mice

To prove the over expression of TSPO protein in lung model, the uptake of modelled mice were compared with uptake in normal mice, specifically in the lungs region. The uptake in the lungs region increased in the modelled mice. The uptake in modelled mice in the upper area was 26.4% of the total uptake which was much higher than the uptake in normal mice in the same area i. e. 8.0% which was comparable to the *ex vivo* data of biodistribution in that area majorly comprising of uptake in heart and lungs. The blockings observed were 28.1% and 77.6% for blocked mice with blocking concentrations of PK11195 as 5 mg/kg and 10 mg/kg, respectively which can be seen in the whole-body SPECT images taken 40 min post injection of $^{99m}\text{Tc-ABTO-Cl}$ (Fig. 5.1.9, Fig. 5.1.10).

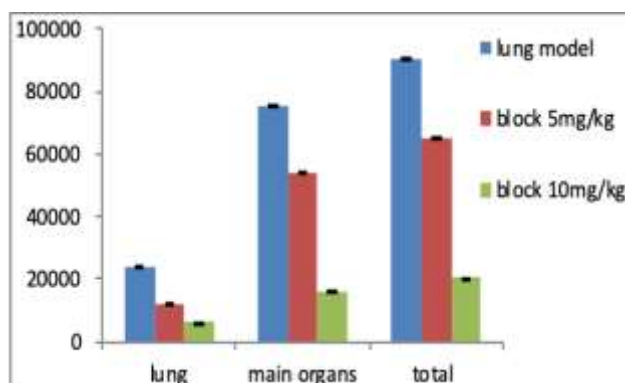


Fig. 5.1.10: $^{99m}\text{Tc-ABTO-Cl}$ *in vivo* biodistribution in lungs, main organs (lungs, liver, heart, kidneys and spleen) and total body uptake at 40 min post i.v. injection with 10 min preadministration of 5/10 mg/kg PK11195 as blocking agent in lung inflammation model of Balb/c mice

Similar findings of previous ligands used in nuclear medicine by other researchers were reported. Literature reported ^{99m}Tc -labelled 2-quinoline carboxamide ligands showed only significant effect in uptake of lungs but not in remaining tissues on preadministration of PK11195 (Cappelli *et al.*, 2008). PET TSPO ligands [^{18}F]-DPA-714 (Vicidomini *et al.*, 2015) and [^{18}F]-VC701 (Di Grigoli *et al.*, 2015) showed blockings in the range of 46%-72% and 37%-88%, respectively.

As per these findings, these ligands have the potential to specifically target TSPO with $^{99m}\text{Tc-ABTO-Cl}$ being better than $^{99m}\text{Tc-ABTO-Br}$ in terms of *in vivo* uptake of the compound in tissues expressing TSPO. Further, the introduction of the chloro group in place of bromo in ligand showed improved pharmacokinetic properties which, in turn, could improve the image resolution in mice using the SPECT modality. These data clearly indicated that ABTO-Cl should be considered as a viable SPECT ligand for further investigation in pathological conditions expressing TSPO.

5.1.4.4 Biodistribution and blocking studies of $^{99m}\text{Tc-ABTO-Br}$ in lung tumor xenograft model of nude mice

The other model studied for TSPO targeting was human lung tumor xenograft model. The A549 human lung cell line was used for the model generation. The blocking agents were PK11195 and benzoxazolone acetic acid, a MBMP precursor.

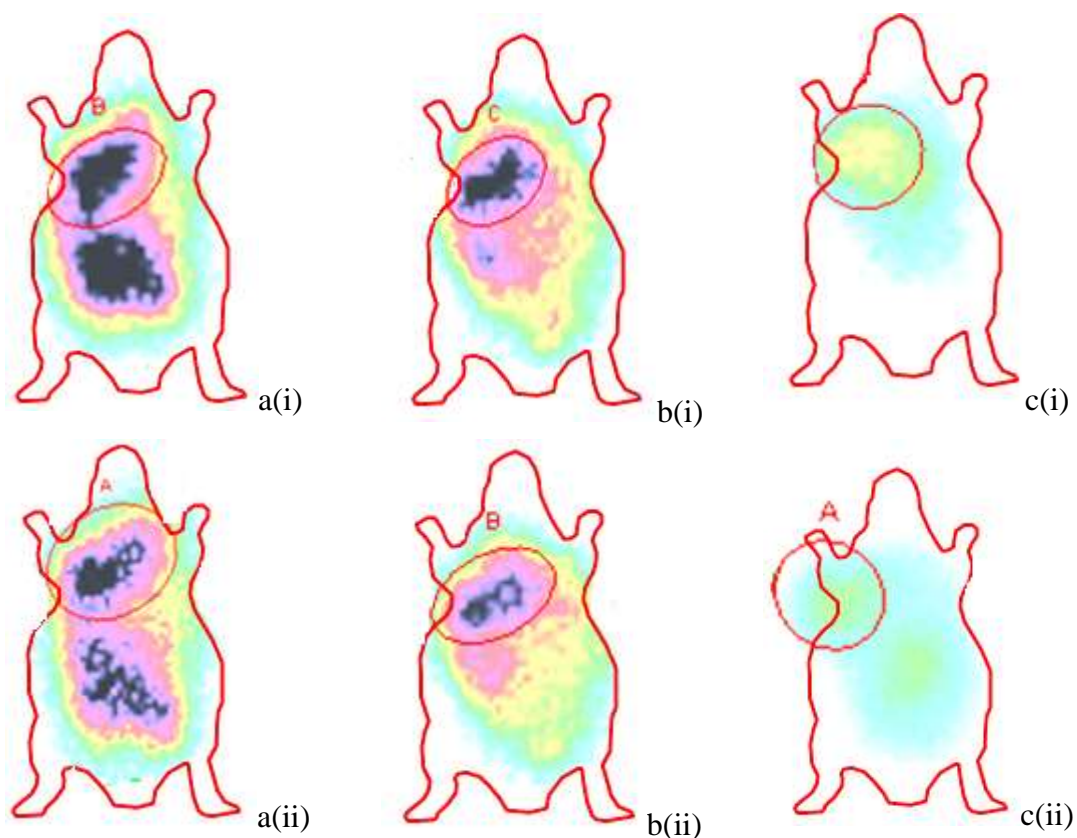


Fig. 5.1.11: Localization of $^{99m}\text{Tc-ABTO-Br}$ in lung tumor xenograft models in a) unblocked b) blocked with PK11195 and c) blocked with MBMP precursor at i) 1h and ii) 3 h

PK11195 is a well known TSPO agent and MBMB is TSPO ligand having same skeleton as lead skeleton for ABO analogues. The concentration used for both the blocking agents were 5 mg/kg.

The localization of $^{99m}\text{Tc-ABPO-Br}$ was more in tumor area than in any other organ. This would result in better diagnosis through good contrast. Out of all the uptake, percentage localizations of $^{99m}\text{Tc-ABTO-Br}$ in tumor at 1 h were 67.0%, 39.8% and 51.3% for unblocked, PK11195 blocked and benzoxazolone acetic acid blocked mice, respectively.

When PK11195 and benzoxazolone acetic acid were used as blocking agents and were injected 10 min prior to injection of radioligand, the blockings observed in tumor were 42.0% and 53.2%, respectively at 1 h post injection (Fig. 5.1.11).

5.1.5 Conclusion

The goal of the study was to evaluate $^{99m}\text{Tc-ABTO}$ based system for TSPO targeting. Two analogues of this skeleton, $^{99m}\text{Tc-ABTO-Br}$ and $^{99m}\text{Tc-ABTO-Cl}$, were prepared with more than 91% stability for 4 h. Both the radioligands were studied in normal Balb/c mice and New Zealand rabbits. Some models were also chosen for validation of specificity such as lung inflammation model in Balb/c for both the analogues and tumor xenograft model in nude mice for $^{99m}\text{Tc-ABTO-Br}$. All the studies performed on mice were also studied for blocking using PK11195, a known TSPO ligand. Uptake in TSPO rich organs in normal mice and rabbits along with increased uptake in inflamed/tumor models of mice with significant blocking demonstrated these compounds as TSPO ligands for SPECT. $^{99m}\text{Tc-ABTO-Cl}$, on comparison with $^{99m}\text{Tc-ABTO-Br}$, was found to have improved %ID uptake in peripheral organs and better release rate. High uptake at early time point and fast kinetics suggest that $^{99m}\text{Tc-ABTO-Br/Cl}$ may have potential as SPECT ligands for evaluation of TSPO-over expression. Further studies with other TSPO ligands on unregulated TSPO systems would be required to establish them as SPECT ligands for TSPO.

This part of the chapter contains the radiolabelling of ABPO-Br/Cl analogues, their stabilities both in saline as well as in serum and validation for selectivity and specificity towards TSPO through *ex vivo/in vivo* studies on New Zealand rabbits and Balb/c mice.

5.2.1 Radiosynthesis and stability studies of radiocomplexes

The synthesized acetamidobenzoxazolone based phenylalanine methyl ester derivatives were complexed with ^{99m}Tc for biological evaluation through tracer technique. The radiolabelling was performed as per the procedure mentioned in chapter 2. Complexation of the synthesized ligands with ^{99m}Tc gave 95.4% and 94.1% intactness of $^{99m}\text{Tc-ABPO-Br}$ and $^{99m}\text{Tc-ABPO-Cl}$, respectively, over 24 h (Fig. 5.2.1).

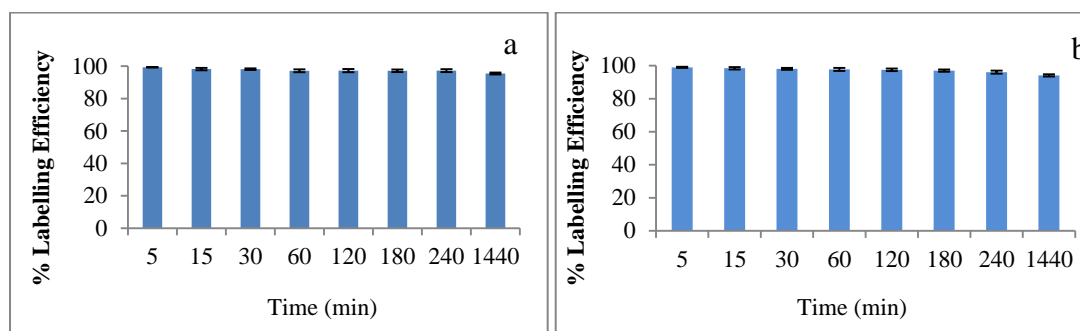


Fig. 5.2.1: Labelling efficiency (%LE) of a) ABPO-Br and b) ABPO-Cl with ^{99m}Tc NaTcO₄ at pH 7 was used for labelling. 0.1 cm segment of ITLC were used after developing it in acetone and PAW (pyridine, acetic acid and water in 3:5:1.5 ratio) solvents for count measurement.

Serum stability under *in vitro* condition clearly demonstrated the stability of radio complexes, $^{99m}\text{Tc-ABPO-Br}$ and $^{99m}\text{Tc-ABPO-Cl}$, with no significant transchelation to proteins present in serum such as albumin which were 92.4% and 91.4% intact after 24 h (Fig. 5.2.2). Stability studies demonstrated stability of the complexes required to find application as SPECT agents.

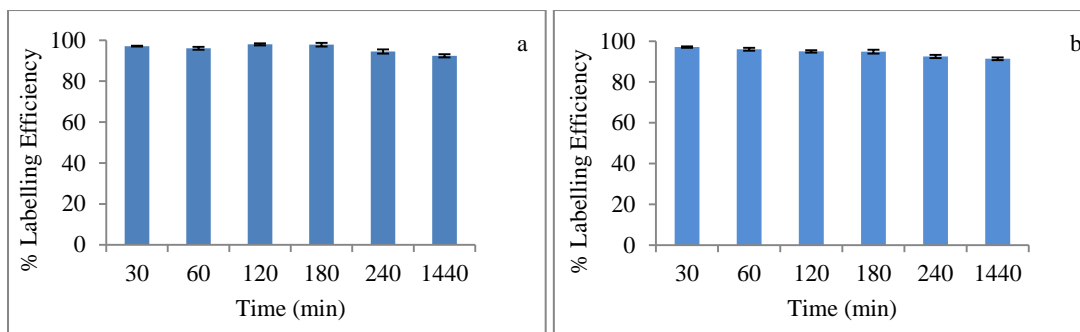


Fig. 5.2.2: Serum stability studies in terms of labelling efficiency (%LE) of a) $^{99m}\text{Tc-ABPO-Br}$ and b) $^{99m}\text{Tc-ABPO-Cl}$ over 24 h

Studies were performed in fresh human serum from healthy volunteers at physiological conditions i.e. 37°C

5.2.2 Ex vivo studies

5.2.2.1 Blood kinetic studies in New Zealand rabbits

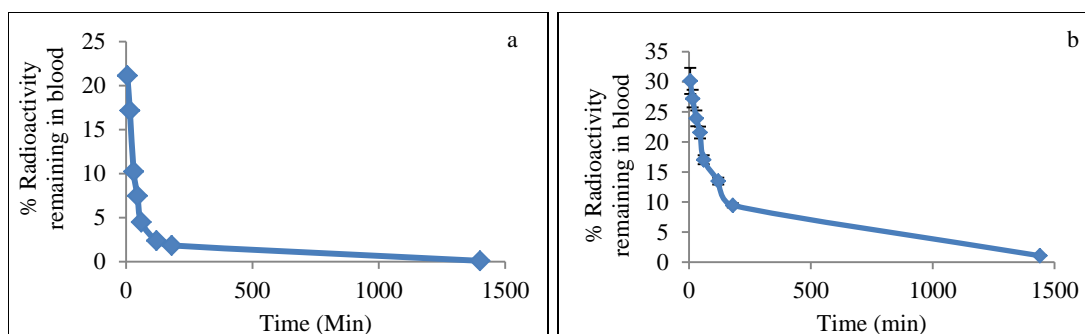


Fig. 5.2.3: Time-activity curves showing blood clearance of a) $^{99m}\text{Tc-ABTO-Br}$ and b) $^{99m}\text{Tc-ABTO-Cl}$ postinjection in New Zealand rabbits

The blood clearance was studied as per procedure mentioned in chapter 2 on normal New Zealand rabbits. Approximately, 74% and 55% of the activities of $^{99m}\text{Tc-ABPO-Br}$ and $^{99m}\text{Tc-ABPO-Cl}$ were cleared within 1 h and more than 92% and 69% activity clearance were observed in 4 h. This reflected the fast release kinetics as desired for diagnostic application. The release kinetic was faster for bromo analogue than for chloro analogue of $^{99m}\text{Tc-ABPO}$ (Fig. 5.2.3).

5.2.2.2 Biodistribution studies in Balb/c mice

Biodistribution of $^{99m}\text{Tc-ABPO-Br/Cl}$ were carried out as per the procedure mentioned in chapter 2 in order to have an idea about the reach of radioligands in body and their excretory pathways.

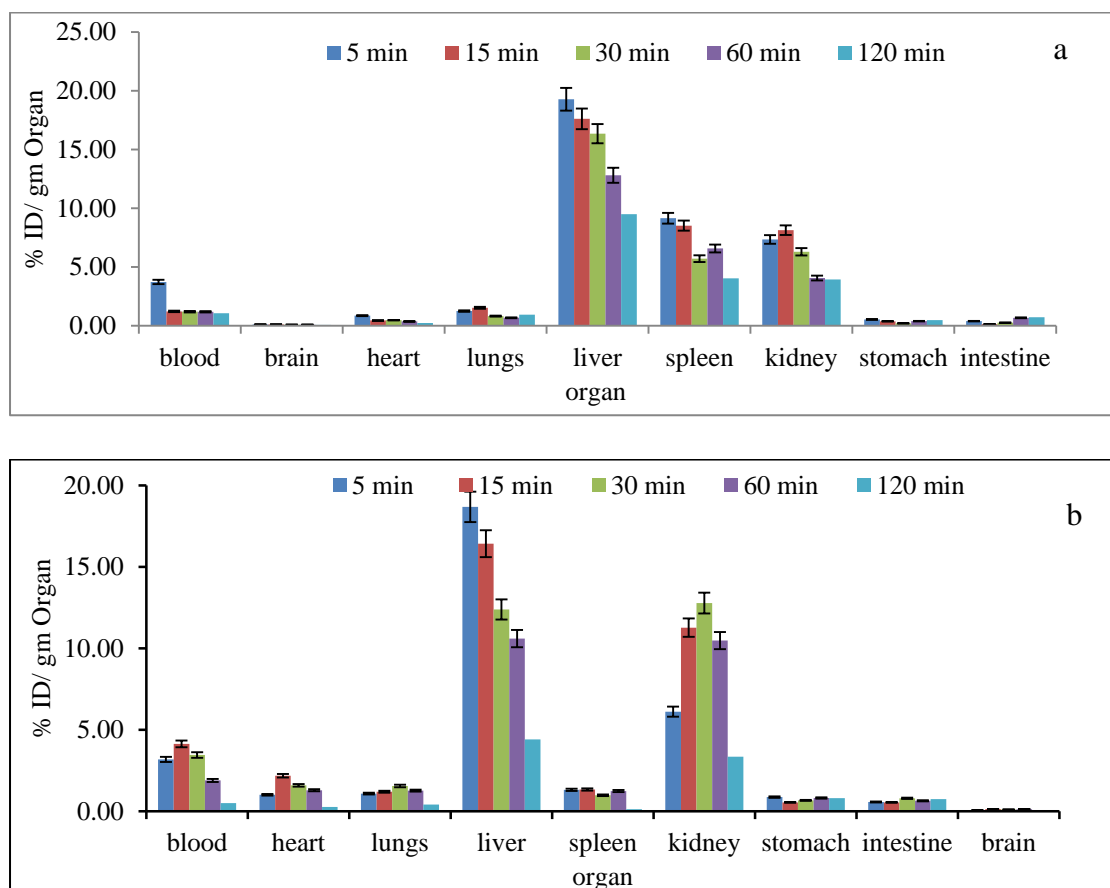


Fig. 5.2.4: Biodistribution patterns of a) $^{99m}\text{Tc-ABPO-Br}$ and b) $^{99m}\text{Tc-ABPO-Cl}$ in normal Balb/c mice

Mice (n=3) received 100 μCi of $^{99m}\text{Tc-ABPO}$ by tail vein injection. Radioactivity uptakes in different organs were measured by gamma counting and expressed as %ID/g, Mean \pm standard deviation

Firstly, bromo analogue, $^{99m}\text{Tc-ABPO-Br}$, was discussed for its biodistribution pattern (Fig. 5.2.4a). The uptake was observed in all TSPO rich organs with highest uptake in liver. The uptake in liver at 5 min was 19.28%ID/g which gradually decreased to 9.50%ID/g in 120 min. The second highest uptake was in spleen which was more than

uptake in kidney at all time points. In spleen, there were 9.16, 8.53, 5.71, 6.58, and 4.04%ID/g uptake at 5 min, 15 min, 30 min, 60 min, and 120 min, respectively. In kidneys, these values were 7.35, 8.14, 6.30, 4.07, and 3.95%ID/g. In this case, highest uptake was at 15 min, thereafter, gradually decreased till last time point of observation. In lungs and heart, the uptakes at 5 min were 1.25 and 0.87%ID/g, respectively. In lungs, increase was observed upto 1.53%ID/g in 15 min then decrease was shown till 0.94%ID/g in 120 min. However, in heart radioactivity gradually decreased with time to 0.24%ID/g till 120 min. In stomach and intestine, there were relatively low uptakes. In stomach the uptake reduced from 0.54%ID/g to 0.21%ID/g in 5-30 min and then increased upto 0.48%ID/g at 120 min. In intestine this value showed dip at 15 min (0.14%ID/g) and then increased till 120 min with 0.72%ID/g. The uptake in blood was slightly higher at initial point of observation which reduced drastically by 15 min to 1.22%ID/g and further demonstrated reducing trend till 120 min with 1.07 %ID/g at that time point. The uptake in brain was 0.11 %ID/g and it stayed till this level upto 15 min which further reduced to 0.09%ID/g in 60 min.

As per biodistribution patterns of both the radioligands, the radioactivity was primarily found in TSPO-rich organs such as lungs, liver, kidneys, and spleen demonstrating selectivity of the radioligands towards TSPO. The release kinetics was the highest for blood. In lungs, spleen and kidneys, the reduction was upto 49%, 44%, and 54% of the uptake at 5 min. However, this percentage reduction was relatively low in brain with 64% for same time span.

On comparing chloro analogue with bromo analogue of $^{99m}\text{Tc-ABPO}$, it was found that release kinetics of bromo analogue was much higher than chloro analogue for all

the TSPO rich organs as well as for blood as can be seen in the Fig. 5.2.4. For lungs, the highest uptake for both analogues were around 1.5%ID/g but at different time points i.e. 15 min and 30 min for $^{99m}\text{Tc-ABPO-Cl}$ and $^{99m}\text{Tc-ABPO-Br}$, respectively. The uptake in spleen and heart were 7 times higher at 5 min and 4.8 times higher at 15 min for $^{99m}\text{Tc-ABPO-Cl}$ than for $^{99m}\text{Tc-ABPO-Br}$. At 15 min, the uptake of $^{99m}\text{Tc-ABPO-Cl}$ was 1.8 times higher in heart than in lungs. This data was 0.29 times for $^{99m}\text{Tc-ABPO-Br}$. In brain, the uptake was higher for $^{99m}\text{Tc-ABPO-Br}$ i.e. 0.13%ID/g as compared to $^{99m}\text{Tc-ABPO-Cl}$ i.e. 0.11% (Fig. 5.2.4b).

Table 5.2.1: Ratio of uptake at 120 min with respect to highest uptake

Organs	$^{99m}\text{Tc-ABPO-Br}$	$^{99m}\text{Tc-ABPO-Cl}$
Blood	0.12	0.29
Brain	0.07	0.64
Heart	0.12	0.28
Lungs	0.27	0.61
Liver	0.24	0.49
Spleen	0.09	0.44
Kidneys	0.26	0.49

For $^{99m}\text{Tc-ABPO-Br}$, the fastest release kinetic was for spleen which was reduced to 9% of highest uptake at 120 min. Next to the fastest release rate were for blood and heart with ~12% of the highest uptake and ~23-26% for liver, lungs and kidneys. The uptake in stomach and intestine were <1%ID/g. In brain, the highest uptake were observed to be 0.06, 0.13, 0.10, 0.12, and 0.09%ID/g at 5, 15, 30, 60 and 120 min, respectively. It showed good uptake, reasonable window for study and fast release thereafter (Table 5.2.1).

5.2.3 *In vivo* studies

To find out the distribution under *in vivo* state, SPECT imaging was performed post injection of $^{99m}\text{Tc-ABPO}$ ligands in mice and rabbits. For specificity, blocking studies were performed in normal mice using a known TSPO ligand PK11195.

5.2.3.1 Biodistribution and blocking studies of $^{99m}\text{Tc-ABTO-Br/Cl}$ in normal Balb/c mice

The ^{99m}Tc labelled phenylalanine analogues of ABO were found to be localized in the TSPO rich organs. The selectivity and specificity of these radioligands were further studied with *in vivo* SPECT imaging with and without blocking using PK11195.

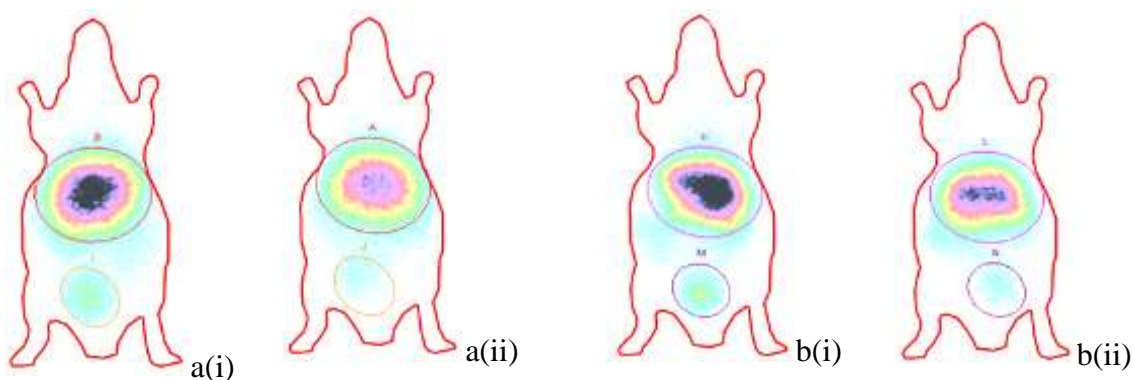


Fig. 5.2.5: *In vivo* SPECT images of $^{99m}\text{Tc-ABPO-Br}$ without a(i) and with a(ii) PK11195 preadministration and $^{99m}\text{Tc-ABPO-Cl}$ without b(i) and with b(ii) PK11195 preadministration at 40 min post injection of radioligand
Blockage was done with PK11195 (10 mg/kg), administered 10 min before radioligand injection

The percentage blocking observed for $^{99m}\text{Tc-ABPO-Br}$ and $^{99m}\text{Tc-ABPO-Cl}$ were 27.3% and 22.2% in main organs on preadministration of PK11195 10 min prior to radioligand administration (Fig. 5.2.5).

5.2.3.2 Biodistribution studies of $^{99m}\text{Tc-ABPO-Br/Cl}$ in New Zealand rabbits

Fig. 5.2.6: *In vivo* biodistribution of $^{99m}\text{Tc-ABPO-Br}$ in New Zealand rabbit (Dynamic image for 30 min)

In order to get better idea of uptake in organs, relatively bigger animal than mice i.e. New Zealand rabbit was chosen. During dynamic study after intravenous injection of $^{99m}\text{Tc-ABPO-Br}$, frames of 10 sec were captured. In these images, slight uptake in lungs, spleen and brain were seen. As the duration of image capture was 10 sec therefore, organs with relatively low uptake were not clearly visualized. Small uptake at later time points could be due to the fast release kinetics of $^{99m}\text{Tc-ABPO-Br}$ as demonstrated in kinetic data of blood in rabbit and all the organs in Balb/c mice (Fig. 5.2.6).



Fig. 5.2.7: *In vivo* biodistribution of ^{99m}Tc -ABPO-Cl in New Zealand rabbit (Dynamic image for 30 min)

In dynamic image of ^{99m}Tc -ABPO-Cl, 1 min frames were taken after 4 min which were sufficient to capture enough radioactivity signals to provide clear images of biodistribution pattern. The uptake in lungs, liver, heart, kidneys, spleen and brain were clearly seen. All these organs are TSPO rich. Uptake in brain was minimal at early time point of 5 min which was washed out significantly in 20 min. The uptake in brain was minimal as expected as brain contains minimal TSPO concentration in healthy condition but uptake though minimal proved that the radioligand was capable of crossing the blood brain barrier. This could be useful in studying diseased/inflamed condition of brain. Uptake in lungs was clearly

reflected at 5 min which seemed to be majorly out by 30 min. Spleen started visualizing by 5 min and uptake was increased until last time point. Uptake of $^{99m}\text{Tc-ABPO-Cl}$ at early time points in all the TSPO rich organs and then fast release in few of the organs such as lungs and brain demonstrated it as a potential candidate for SPECT modality (Fig. 5.2.7).

On comparing dynamic studies of both the analogues of $^{99m}\text{Tc-ABPO}$ on rabbits, it was found that both the radioligands were specific for TSPO but bromo analogue was having faster release kinetics than chloro analogue. Similar result has been demonstrated in case of *ex vivo/ in vivo* studies on mice and blood kinetics on rabbits.

5.2.4 Conclusion

In this chapter $^{99m}\text{Tc-ABPO-Br/Cl}$ radioligands were synthesized through radiochemistry. Both the radioligands were stable in saline as well as in serum over 24 h. They showed selectivity and specificity towards TSPO under *in vivo* studies on normal Balb/c mice with and without blocking using PK11195. Further, validation of uptake in desired organs were performed on New Zealand rabbits. The *in vivo* distribution patterns in rabbits demonstrated uptake majorly in TSPO rich organs. Release kinetics of both the analogues in blood and other organs in mice as well as in rabbits were studied. There was fast release of both the radioligands as desired by radioligands for diagnostic application. The release kinetics of bromo was faster than chloro as seen in all the *in vivo* and *ex vivo*

studies. Further studies in model reflecting increased concentration of TSPO in localized organ and with other known TSPO ligands as blocking agent would be required to establish them as SPECT ligands for TSPO.

This part of the chapter contains the radiolabelling of ABMO-Br/Cl analogues, their stabilities in saline and serum along with selectivity and specificity towards TSPO through *ex vivo/in vivo* studies on Balb/c mice and New Zealand rabbits.

5.3.1 Radiosynthesis and stability studies of radiocomplexes

The synthesized acetamidobenzoxazolone based methionine methyl ester derivatives were complexed with ^{99m}Tc for biological evaluation through tracer technique. The radiolabelling was performed as per the procedure mentioned in chapter 2.

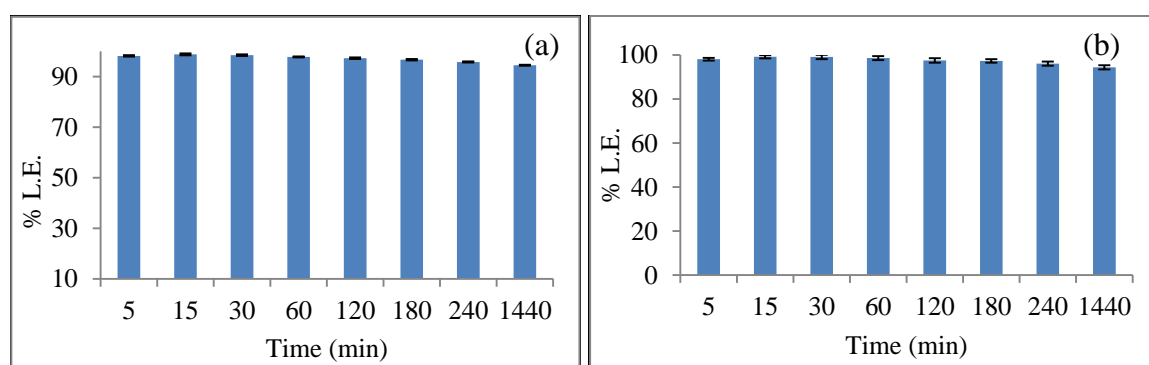


Fig. 5.3.1: Labelling efficiency (%LE) of a) ABMO-Br and b) ABMO-Cl with ^{99m}Tc
 NaTcO_4 at pH 7 was used for labelling. 0.1 cm segment of ITLC were used after developing it in acetone and PAW (pyridine, acetic acid and water in 3:5:1.5 ratio) solvents for count measurement.

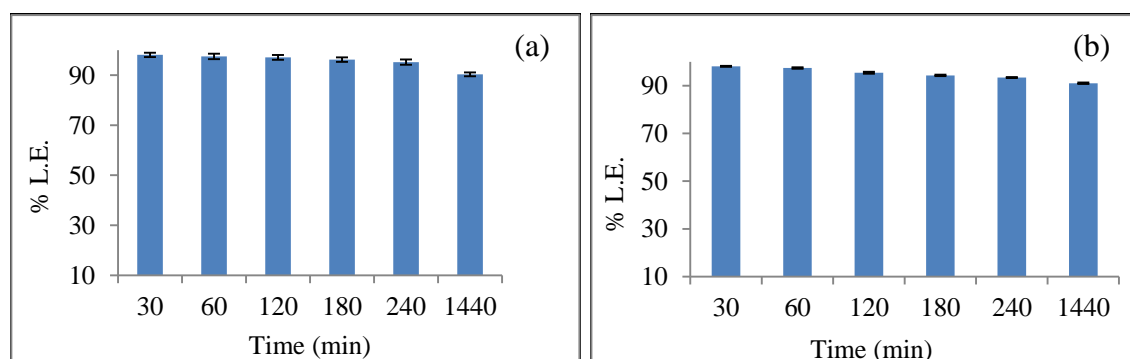


Fig. 5.3.2: Serum stability studies in terms of labelling efficiency (%LE) of a) ^{99m}Tc -ABMO-Br and b) ^{99m}Tc -ABMO-Cl over 24 h
 Studies were performed in fresh human serum from healthy volunteers at physiological conditions i.e. 37°C

The synthesized complexes of ^{99m}Tc were 94.5% and 93.4% stable for ABMO-Br and ABMO-Cl, respectively, at 24 h (Fig.5.3.1).

Serum stability under *in vitro* condition clearly demonstrated the stability of radiocomplexes, $^{99m}\text{Tc-ABMO-Br}$ and $^{99m}\text{Tc-ABMO-Cl}$, with no significant transchelation to proteins present in serum such as albumin which were 91.0% and 90.3% intact after 24 h (Fig. 5.3.2).

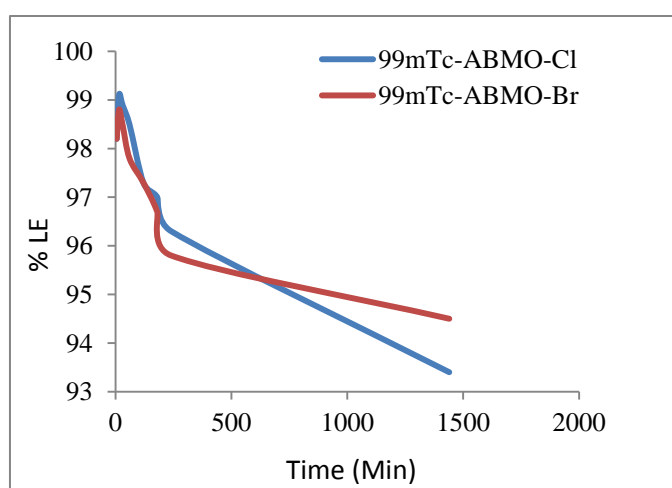


Fig. 5.3.3: Comparative stability of $^{99m}\text{Tc-ABMO-Br}$ and $^{99m}\text{Tc-ABMO-Cl}$ in saline

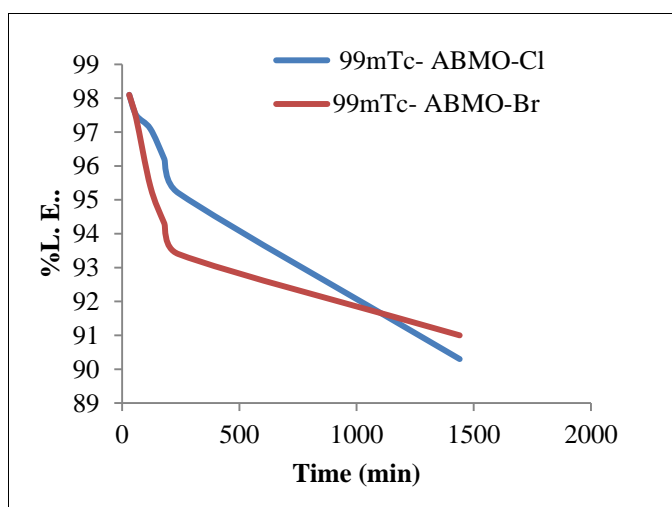


Fig. 5.3.4: Comparative stability of $^{99m}\text{Tc-ABMO-Br}$ and $^{99m}\text{Tc-ABMO-Cl}$ in human serum

On comparing both the analogues of ^{99m}Tc -ABMO, it was found that the chloro analogue was marginally stable in saline as well as in serum till 4 h. ^{99m}Tc -ABMO-Br had relatively better intactness at 24 h. However, stability studies demonstrated stability of the complexes required to find application as SPECT agent for both the ligands (Fig. 5.3.3, Fig.5.3.4).

5.3.2 *Ex vivo* studies

5.3.2.1 Blood kinetic studies in New Zealand rabbits

The blood clearance was studied on normal rabbits as per the protocol mentioned in the chapter 2. The ^{99m}Tc -labelled methionine amino acid ester conjugates demonstrated a rapid radioactivity clearance from blood circulation. Approximately 78% of ^{99m}Tc -ABMO-Br and 82% of ^{99m}Tc -ABMO-Cl were cleared within 1 h and more than 87% and 91% clearance of ^{99m}Tc -ABMO-Br and ^{99m}Tc -ABMO-Cl, respectively were observed in 4 h. Overall both the analogues reflected the fast release kinetics with chloro being faster than bromo analogue. The fast release kinetics is desirable for diagnostic application.

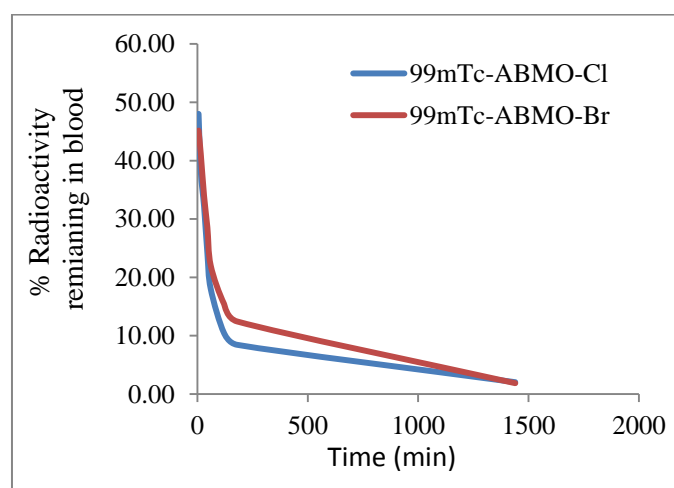


Fig. 5.3.5: Time activity curves showing blood clearance of ^{99m}Tc -ABMO-Br and ^{99m}Tc -ABMO-Cl postinjection in New Zealand rabbits

5.3.2.2 Biodistribution studies in Balb/c mice

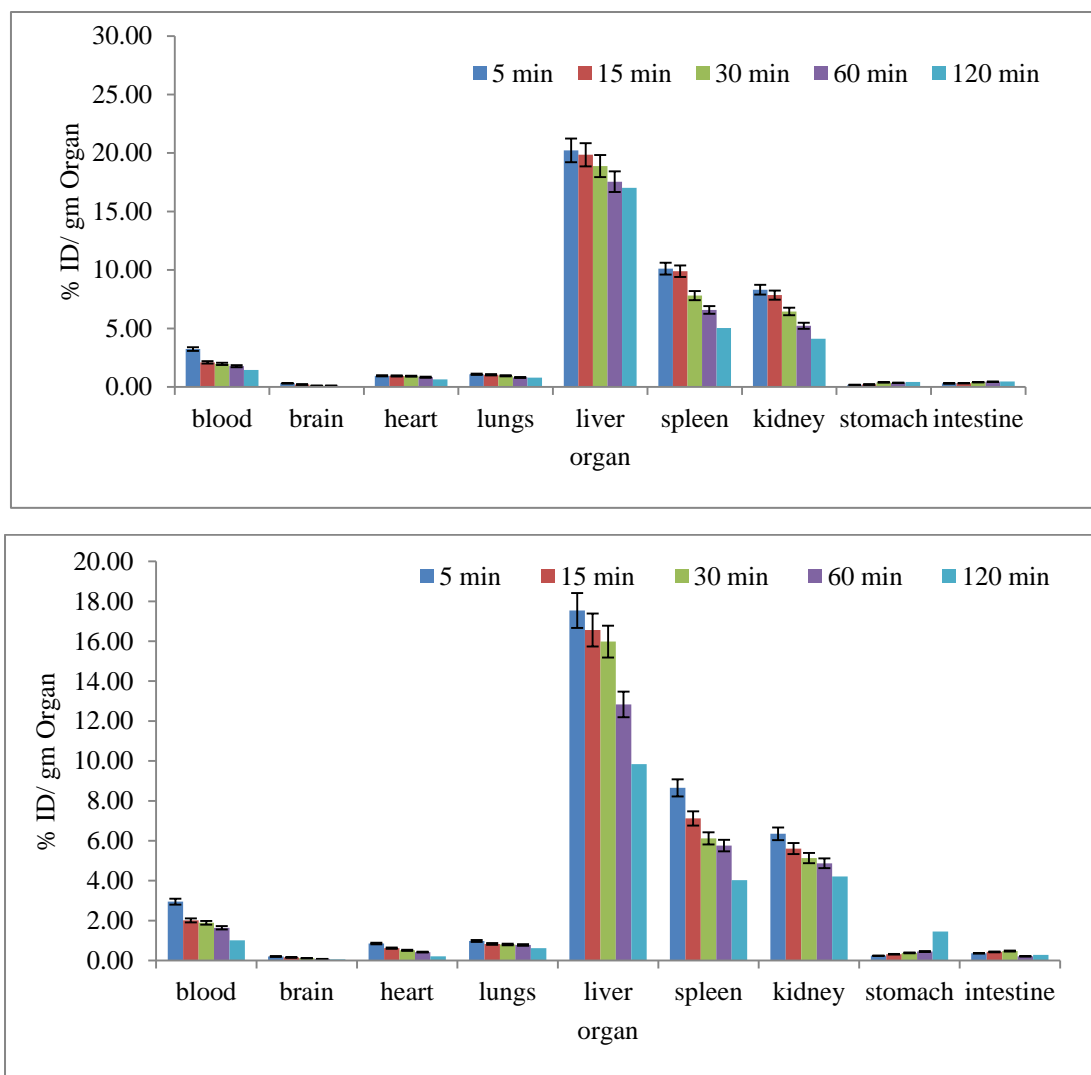


Fig. 5.3.6: Biodistribution patterns of a) $^{99m}\text{Tc-ABMO-Br}$ and b) $^{99m}\text{Tc-ABMO-Cl}$ in normal Balb/c mice

Mice (n=3) received 100 μCi of $^{99m}\text{Tc-ABMO}$ by tail vein injection. Radioactivity uptake in different organs were measured by gamma counting and expressed as %ID/g, Mean \pm standard deviation

Ex vivo biodistribution of $^{99m}\text{Tc-ABMO-Cl}$ demonstrated that its highest uptakes for all the organs were observed at 5 min. Major uptake was there in liver with 17.54%ID/g that reduced to 9.84%ID/g at 120 min. The second highest uptake was demonstrated in spleen with 8.65%ID/g at 5 min that reduced to around 47% of 5 min uptake at 120 min. The uptake in kidneys was around 1/3rd the uptake of liver till 60

min thereafter its release was slower. There were negligible uptake in stomach and intestine. In blood, initial uptake was 2.95%ID/g at 5 min which reduced to 1/3rd by 120 min. Overall, radioligand in lungs and kidneys reduced to 63% and 66% of the uptake at 5 min by 120 min. Liver showed faster release with similar value as 56%. Blood, brain and heart demonstrated relatively faster release with values at 120 min being 34%, 30%, and 25%, respectively of the value at 5 min. The uptake in brain was 0.20%ID/g at 5 min with significant value till 30 min.

The last radiocomplex studied for biodistribution was $^{99m}\text{Tc-ABMO-Cl}$. The radiocomplex had the highest uptake in liver, spleen and kidneys with 20.23, 10.12, and 8.31%ID/g, respectively at 5 min and reduced to 74%, 59%, and 50% of the values by 120 min. In stomach and intestine, the uptake were less than 0.47%ID/g at any time point of the study. The release rates in heart as well as in lungs were slow with initial values at 5 min being 0.95 and 1.08%ID/g, respectively that demonstrated reduction by 32% and 26%, respectively only in 120 min. However this reduction was significant for brain i.e. 84%. In blood, the uptake of 3.24%ID/g was observed at 5 min and reduced by 55% at 120 min with 1.45%ID/g.

On comparison of bromo and chloro analogues of $^{99m}\text{Tc-ABMO}$, it was found that release kinetics of $^{99m}\text{Tc-ABMO-Cl}$ was faster than that of $^{99m}\text{Tc-ABMO-Br}$ for heart (25% vs 68%), lungs (63% vs 74%), liver (56% vs 84%), and blood (34% vs 44%) but comparable for spleen (47% vs 50%) and slower for brain (30% vs 16%) and kidneys (66% vs 50%) for the percentage uptake at 120 min with respect to the highest uptake observed in the organs. The blood kinetic studies on rabbits also demonstrated faster release of chloro analogue as compared to bromo analogue.

5.3.3 *In vivo* studies

5.3.3.1 Biodistribution and blocking studies of $^{99m}\text{Tc-ABMO-Br/Cl}$ in normal

Balb/c mice

To find out the distribution under *in vivo* state, SPECT imaging was performed post injection of radiolabelled $^{99m}\text{Tc-ABMO}$ ligands in normal mice. For specificity, blocking was demonstrated using a known TSPO ligand PK11195. Qualitatively it was observed that $^{99m}\text{Tc-ABMO-Cl}$ demonstrated faster wash out from lungs and heart than $^{99m}\text{Tc-ABMO-Br}$. $^{99m}\text{Tc-ABMO-Br}$ showed better blocking than $^{99m}\text{Tc-ABMO-Cl}$. (Fig. 5.3.7)

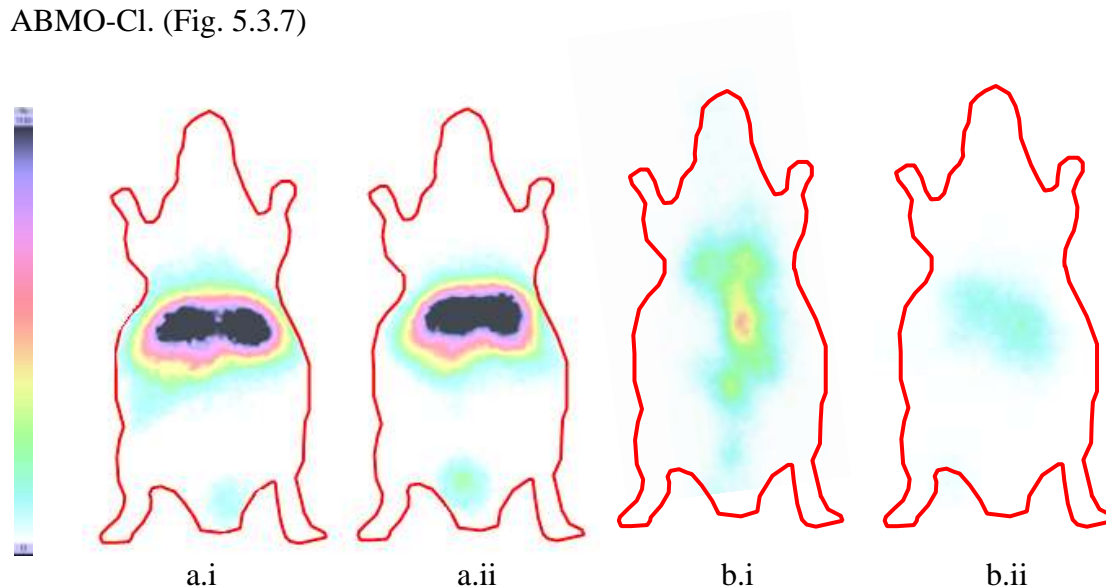


Fig. 5.3.7: *In vivo* SPECT images of $^{99m}\text{Tc-ABMO-Br}$ without (a.i) and with (a.ii) PK11195 preadministration and $^{99m}\text{Tc-ABMO-Cl}$ without (b.i) and with (b.ii) PK11195 preadministration at 40 min post injection of radioligand

5.3.3.2 Biodistribution studies of $^{99m}\text{Tc-ABMO-Br/Cl}$ in New Zealand rabbits

In order to get better idea of uptake in organs, relatively bigger animal than mice i.e. New Zealand rabbit was chosen. Dynamic images of both the analogues of $^{99m}\text{Tc-ABMO}$ were captured for 30 min post injection in three phases: 2 sec frame (30), 15 sec frame (8) and 60 sec frame (27). The uptake in lungs and heart were seen at initial

time points which reduced with time. Initially radioactivity in bladder was minimal which increased gradually over 30 min. Kidneys and liver were seen clearly. In brain, significant uptake was observed for $^{99m}\text{Tc-ABMO-Br}$ which reduced with time. In a nut shell, it was observed that the uptake was majorly observed in all the TSPO rich organs such as lungs, heart and brain at initial time point which eventually decreased with time. In excretory organs uptake were initially lower which increased with time till the last time point of observation (Fig. 5.3.8).

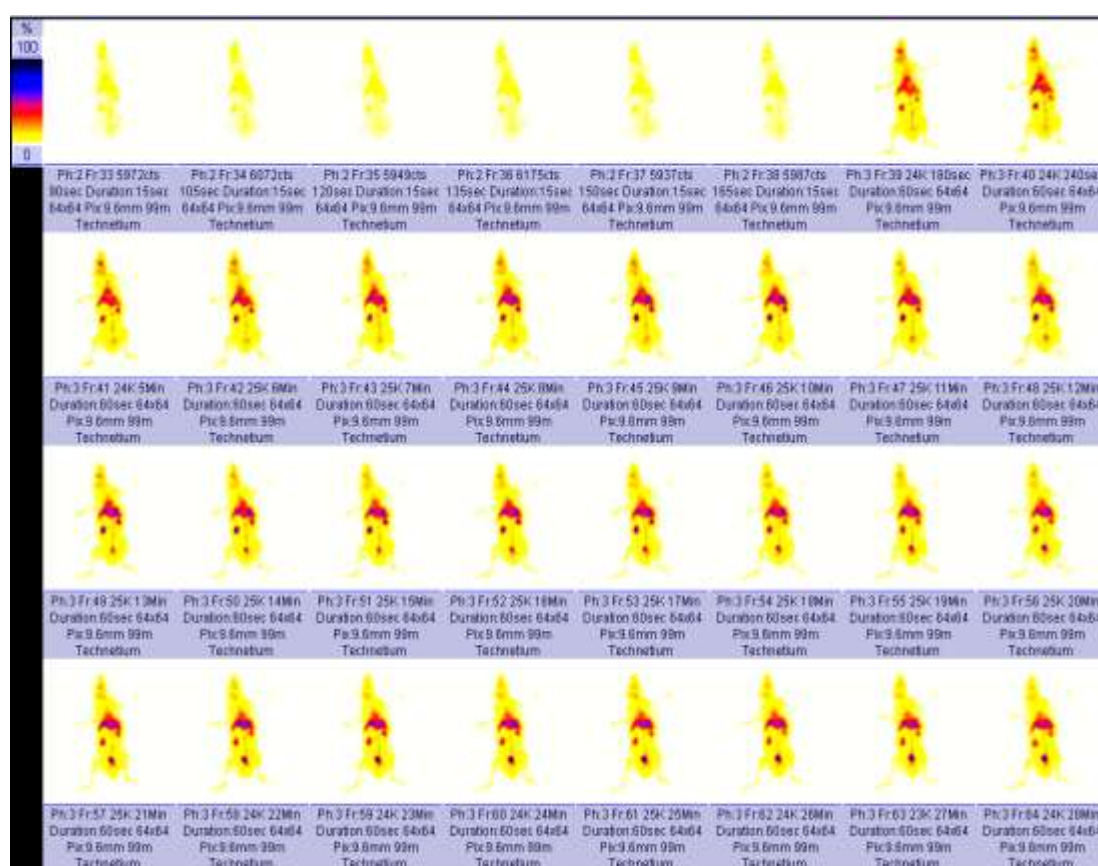




Fig. 5.3.8: *In vivo* biodistribution of a) ^{99m}Tc -ABMO-Br and b) ^{99m}Tc -ABMO-Cl in New Zealand rabbits (Dynamic studies for 30 min)

5.3.4 Conclusion

In this chapter, analogues of methionine derivatives of acetamidobenzoxazolone were analysed for SPECT application. The selectivity and specificity of the radioligands towards TSPO were analysed through tracer technique. ^{99m}Tc -labelled ABMO analogues were stable over 24 h in saline as well as in serum. Biodistribution represented uptake in TSPO rich organs under *in vivo* condition on New Zealand rabbits and in *ex vivo* studies carried out on Balb/c mice. The specificity of both the analogues of ABMO were demonstrated through blocking studies using PK11195 as blocking agent. The release kinetics of both the analogues were found to be fast in blood and other organs in mice as well as in rabbits as desired by radioligands for diagnostic application. These studies proved potential of the ^{99m}Tc -ABMO-Br/Cl for SPECT application to target TSPO.

In this part of the chapter comparative analysis of all the amino acid ester analogues of acetamidobenzoxazolone (ABEO, E=trptophan methyl ester, phenylalanine methyl ester and methionine methyl ester) were performed with respect to stability of radiocomplexes with ^{99m}Tc , their uptake and kinetics in different organs.

5.4.1 Comparative analysis of stability of radiocomplexes

These TSPO ligands need complexation with radionuclide for nuclear medicine application. The stability plays an important role. All the six analogues of ABO demonstrated complexation with ^{99m}Tc in the range of 93-95.5% over 24 h in saline (Fig. 5.4.1).

Serum stability studies under *in vitro* condition clearly demonstrated the stability of radiocomplexes, with no significant transchelation to proteins present in serum such as albumin which were 87%-92.4% intact after 24 h (Fig. 5.4.1). Stability studies demonstrated stability of the complexes required to find application as SPECT agents for all six the ligands.

Table 5.4.1: Stability in saline and serum at 24 h

TSPO ligand	Stability in saline (%)	Stability in serum (%)
^{99m}Tc -ABTO-Br	93.4	91.2
^{99m}Tc -ABTO-Cl	93.7	87.2
^{99m}Tc -ABPO-Br	94.1	91.3
^{99m}Tc -ABPO-Cl	95.4	92.4
^{99m}Tc -ABMO-Br	94.5	91.6
^{99m}Tc -ABMO-Cl	94.5	91.6

5.4.2 *Ex vivo* blood kinetic studies in New Zealand rabbits

There is requirement of fast release kinetics of the radioligand to get better contrast in TSPO organs. All the amino acid ester conjugates demonstrated a rapid radioactivity clearance from blood circulation. Approximately >80% of the activity clearance within 1 h and > 90% clearance in 4 h were observed. The fast release kinetics is desirable for diagnostic application. The fastest release kinetics was observed for $^{99m}\text{Tc-ABPO-Cl}$.

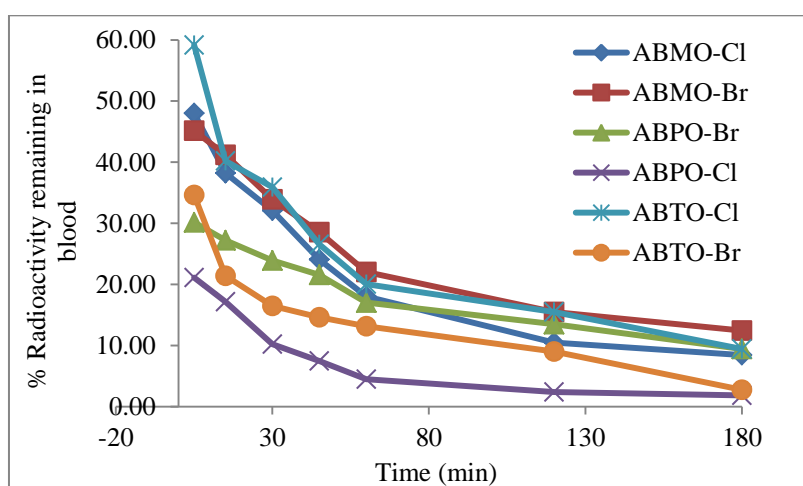


Fig. 5.4.1: Time-activity curves showing blood clearance of $^{99m}\text{Tc-ABEO-Br/Cl}$ analogues in New Zealand rabbits

5.4.3 *Ex vivo* biodistribution studies in Balb/c mice

On comparing biodistribution patterns of different analogues it was observed that all the analogues were showing uptake in TSPO rich organs only with varied uptake in different organs. This variation in uptake pattern could be utilized for diagnostic application for specific organ.

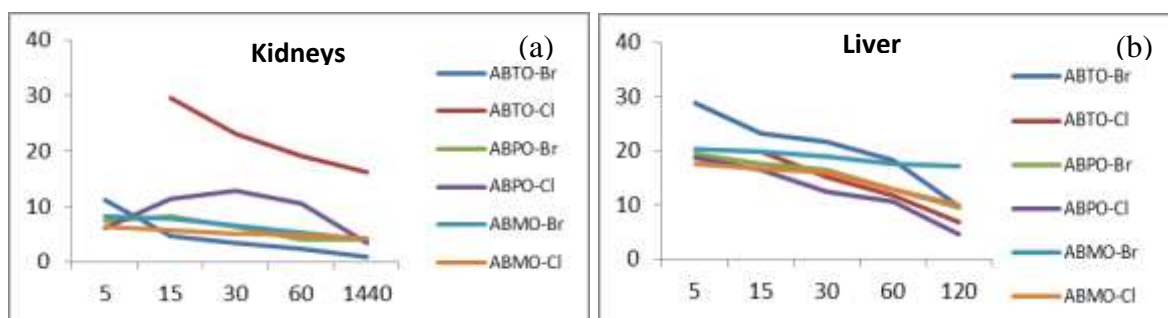


Fig. 5.4.2: Biodistribution (%ID/g, Mean) data of ^{99m}Tc -ABEO-Br/Cl for a) Kidneys and b) Liver

Kidneys and liver are excretory organs and out of all the designed ligands excretion of ^{99m}Tc -ABTO-Cl was highest through kidneys and excretion of ^{99m}Tc -ABTO-Br was highest through liver. ^{99m}Tc -labelled compounds showed preference for liver. In these cases except for ^{99m}Tc -ABTO-Br, all other analogues had excretion less than 20%ID/g through liver. Though %ID/g for ^{99m}Tc -ABTO-Br was the highest i.e. $\sim 30\%$ ID/g at 5 min, its release kinetics was relatively faster bringing the limit lower than 20%ID/g in 60 min which was further reduced to $<10\%$ in 2 h. Even the release kinetics of ^{99m}Tc -ABTO-Cl was high in liver (Fig. 5.4.2).

For brain application, methionine analogues seemed to have preference over phenylalanine and tryptophan analogues of ABO. Out of two analogues of ^{99m}Tc -ABMO, bromo analogue demonstrated higher uptake than chloro. In case of ^{99m}Tc -ABMO-Br, not only the release kinetics of liver was highest till 30 min but the uptake value was also highest till that time (Fig. 5.4.3a).

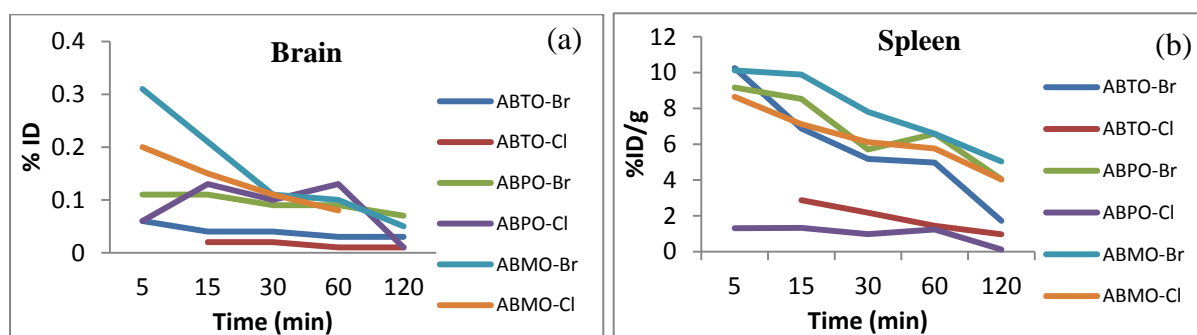


Fig. 5.4.3: Biodistribution (%ID/g, Mean) data of ^{99m}Tc -ABEO-Br/Cl for a) Brain and b) Spleen

For spleen, both the analogues of $^{99m}\text{Tc-ABMO}$ and bromo analogues of $^{99m}\text{Tc-ABPO}$ and $^{99m}\text{Tc-ABTO}$ showed better uptake and more or less similar release kinetics (Fig. 5.4.3b).

In case of heart, the highest uptake was considered for $^{99m}\text{Tc-ABTO-Cl}$ with fastest release kinetics. The second best molecule could be $^{99m}\text{Tc-ABPO-Cl}$ which was better than $^{99m}\text{Tc-ABTO-Cl}$ for 60 min study (Fig. 5.4.4a).

Both the tryptophan analogues were found suitable for lung application with chloro analogue being better with the fastest release kinetics (Fig. 5.4.4b).

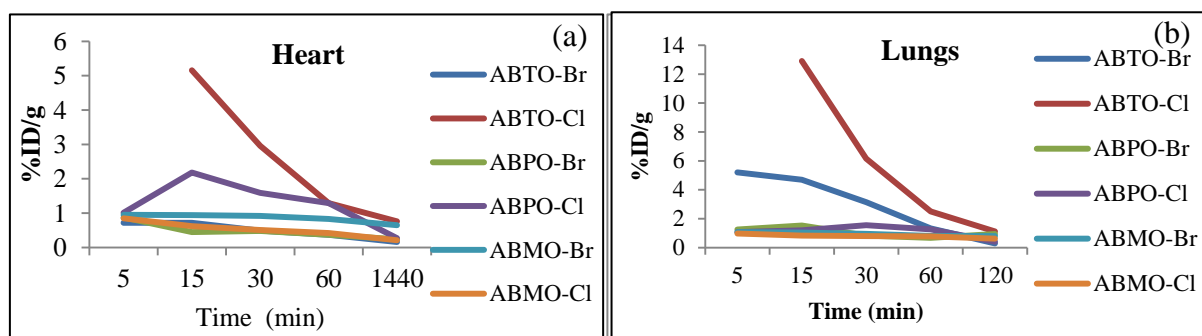


Fig. 5.4.4: Biodistribution (%ID/g, Mean) data of $^{99m}\text{Tc-ABEO-Br/Cl}$ for a) Heart and b) Lungs

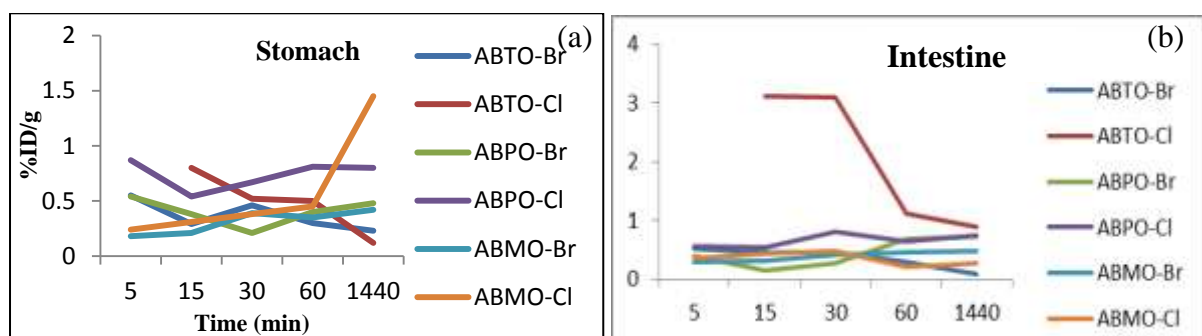


Fig. 5.4.5: Biodistribution (%ID/g, Mean) data of $^{99m}\text{Tc-ABEO-Br/Cl}$ for a) Stomach and b) Intestine

The uptake of these analogues were much low in case of stomach and intestine which were $< 1\% \text{ID/g}$ for all the ligands except for $^{99m}\text{Tc-ABTO-Cl}$ which showed less than

3%ID/g for initial time points (Fig. 5.4.5a). For TSPO ligands uptake in intestine and stomach must be minimal which are there in all the ^{99m}Tc -ABEO-Br/Cl ligands under consideration (Fig. 5.4.5b).

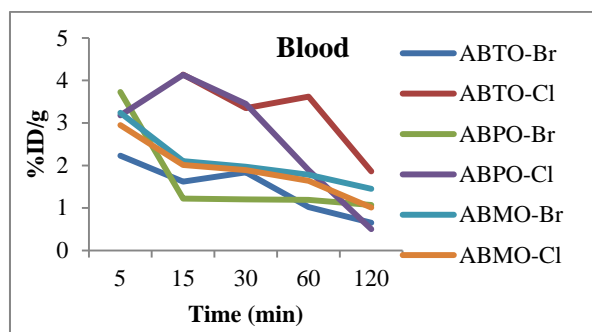


Fig. 5.4.6: Biodistribution (%ID/g, Mean) data of ^{99m}Tc -ABEO-Br/Cl for Blood

Uptake in blood was an important phenomenon for diagnostic application which was related to better contrast image. ^{99m}Tc -ABTO-Br seemed to have least present in blood (Fig. 5.4.6).

Further, designed radioligands were compared with the SPECT ligands reported in literature. ^{99m}Tc -ABTO-Cl uptake was found higher than ^{99m}Tc -labelled 2-quinolinecarboxamide in heart (2.96%ID/g vs negligible uptake) and lungs (6.16%ID/g vs 1.19 %ID/g) and comparable in spleen (2.18%ID/g vs 2.07%ID/g) at 30 min as reported in CD-1 mice (Cappelli *et al.*, 2008). Uptake of [^{123}I]-CLINME (Mattner *et al.*, 2015), an iodine based SPECT ligand, in heart, lungs, and spleen of SD rat were 3.53%ID/g, 3.53%ID/g, 2.65%ID/g at 15 min. This was also lower/comparable with ^{99m}Tc - ABTO-Cl in respective organs. The liver uptake was lower for ^{99m}Tc -ABTO-Cl in comparison with ^{99m}Tc -labelled 2-quinolinecarboxamide and ^{99m}Tc -ABTO-Br. This accounted for better image visualization (target organ to liver ratio) for ^{99m}Tc - ABTO-Cl.

Comparison of release rates among SPECT agents between 30-60 min for ^{99m}Tc -ABTO-Cl, [^{123}I]-CLINME, ^{99m}Tc -labelled 2-quinolinecarboxamide and ^{99m}Tc -ABTO-Br reflected better release rates of ^{99m}Tc -ABTO-Cl in lungs, liver, heart and spleen. Further, it was also compared with PET and SPECT ligands of ABO category. The release kinetic rates between 15-60 min for ^{18}F -FEBMP, ^{11}C -MBMP, ^{18}F -2-(5-(6-Fluoropyridin-3-yl)-2-oxobenzo[d]oxazol-3(2H)-yl)-N-methyl-N-phenylacetamide and ^{99m}Tc -ABTO-Cl were 0.175%ID/g/min, 0.150%ID/g/min, 0.070%ID/g/min and 0.085%ID/g/min in heart, this ratio became more comparable as 0.382%ID/g/min, 0.375%ID/g/min, 0.155%ID/g/min and 0.231%ID/g/min in lungs. In liver and kidneys, release kinetic rates were faster in ^{99m}Tc -ABTO-Cl which were found interesting for further evaluation. These evaluations demonstrated release rates of ^{99m}Tc -ABTO-Cl from different organs were comparable to known TSPO ligands, therefore it can be further evaluated for TSPO targeting.

5.4.4 *In vivo* images of radiocomplexes in New Zealand rabbits

In vivo imaging of all the radiocomplexes were performed in rabbits from 3 min to 24 h. As the images taken at 24 h showed negligible uptake, only one representative image is presented. All the images are at 0-100 scale, but for better representation, one representative image is shown with 0-100 & 0-50 scales both.

	3 min	30 min	1 h	2 h	3 h	4 h
^{99m}Tc - ABTO-Br						
^{99m}Tc - ABTO-Cl						
^{99m}Tc - ABMO-Br						
^{99m}Tc - ABMO-Cl						

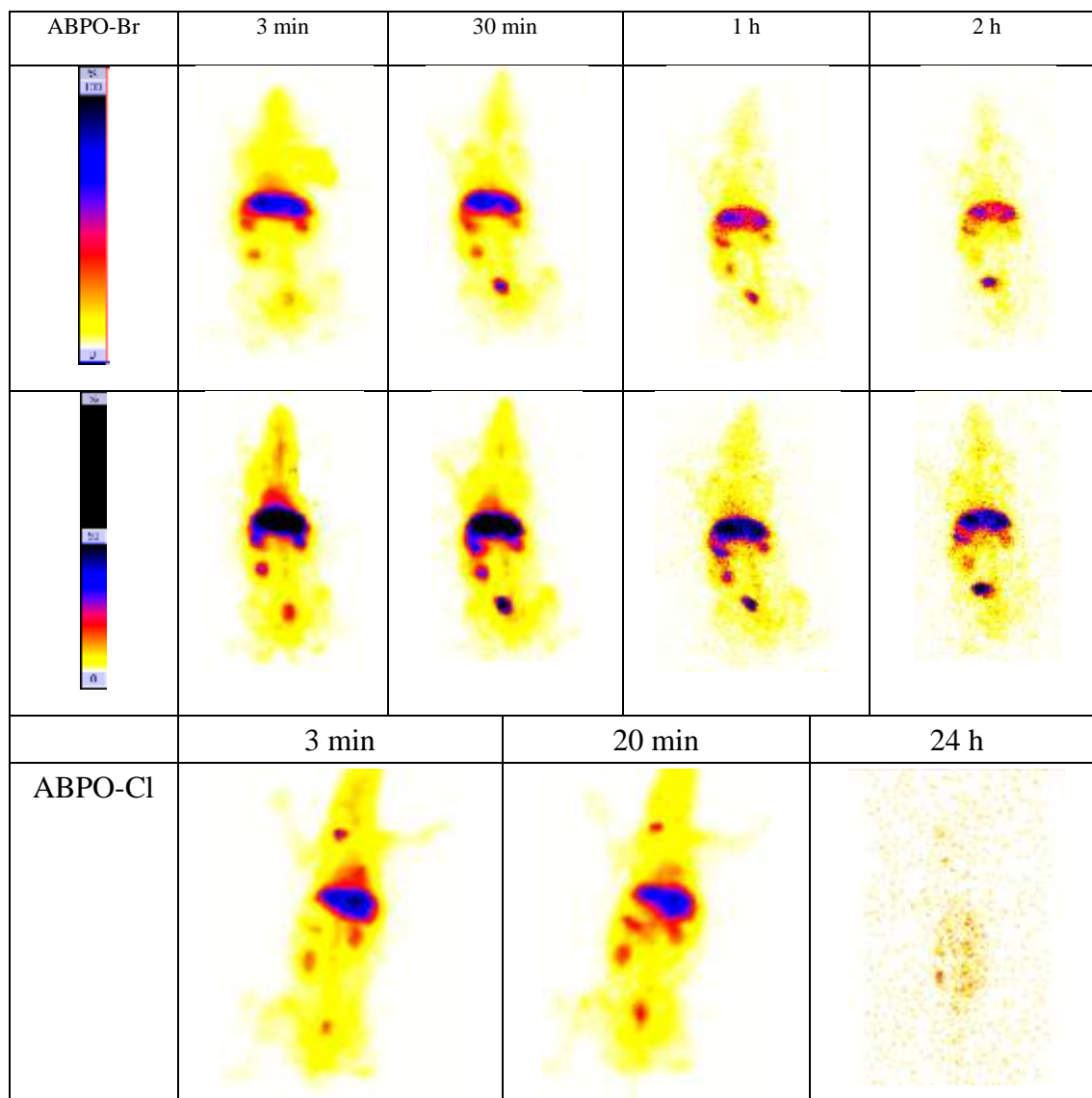


Fig. 5.4.7: *In vivo* images of $^{99m}\text{Tc-ABEO-Br/Cl}$ in New Zealand rabbits

Overall, all the ligands can be used for TSPO targeting in terms of release kinetics, uptake in intestine, stomach and blood. However, keeping uptake in specific organs in account, different analogues seems to applicable for different organs such as $^{99m}\text{Tc-ABTO-Cl}$ and $^{99m}\text{Tc-ABTO-Br}$ for lungs; $^{99m}\text{Tc-ABTO-Cl}$ and $^{99m}\text{Tc-ABPO-Cl}$ for heart; $^{99m}\text{Tc-ABMO}$ and $^{99m}\text{Tc-ABPO}$ analogues for spleen; and $^{99m}\text{Tc-ABMO}$ analogues for brain.

5.4.5 Conclusion

This chapter analyzed different ligands of TSPO for their applicability in different organs. Also stability of radiocomplexes with ^{99m}Tc in saline and serum as well as release kinetics were compared. In a nut shell, it can be explained that tryptophan analogues demonstrated preference for lungs, chloro analogues for heart, phenylalanine for spleen and methionine analogues for brain. Further studies with other TSPO ligands on unregulated TSPO systems would be required to establish them as SPECT ligands for TSPO.

Chapter 6
Summary, discussion and future
perspective

CHAPTER 6

SUMMARY, DISCUSSION AND FUTURE PERSPECTIVE

Studies on TSPO demonstrated it as biomarker for inflammation and tumor. This encouraged researchers to develop ligands for TSPO. Few of them were explored for PET application. The current work has focused the development of SPECT agent taking lead from third generation TSPO ligand. The acetamidabenzoxazolone was chosen as the lead moiety for development of TSPO ligands for SPECT application. The choice of the lead molecule was made due to its demonstration as TSPO ligand for PET application with no intersubject variability effect of single nucleotide polymorphism A147T by our group and other researchers world-wide. The pharmacophore modelling demonstrated AAAR as desirable hypothesis for TSPO affinity designed on the basis of acetamidobenzoxazolone based TSPO ligands reported in literature. The amino acid esters were chosen for introducing pharmacophoric features. The selection of three amino acid esters (tryptophan methyl ester, phenylalanine methyl ester and methionine methyl esters) were as per the required features of aromaticity/hydrophobicity and chelating arms for holding the metal ions for complexation. Both chloro and bromo analogues were chosen to introduce at 5th position of benzoxazolone for the better affinity pattern as per literature. The eight designed molecules were validated through in silico ligand-metal interaction. The chosen PDBs of TSPO were wild type (4RYQ and 2MGY) and mutant (4UC1). These interactions through docking validated the designed molecules as potential TSPO ligands as their G-scores were comparable to known TSPO ligands. The facile synthetic protocol were used for the producing the six designed ligands

involving reactions such as cyclization, acetylation and alkylation. Bromo and chloro groups at 5th position were introduced by taking the respective analogues as starting material. ¹H NMR, ¹³C NMR, Mass, and HPLC were used for characterization and purification. The synthesized molecules were further radiocomplexed with ^{99m}Tc for SPECT application. All the six radiocomplexes demonstrated good stability in saline as well as in serum over 24 h. The validation of molecules as TSPO ligands were performed through tracer technique. *Ex vivo* (biodistribution), *in vivo* (SPECT imaging) studies represented TSPO selectivity for all the six ligands. *Ex vivo* on Balb/c mice and *in vivo* studies on New Zealand rabbits and Balb/c mice were performed with all the six radioligands demonstrating uptake mainly in organs rich in TSPO such as lungs, liver, heart, kidneys and spleen. Images taken in rabbits reflected blood brain barrier crossing ability for all the radioligands as small amount of uptake were there at initial time points of the study. Blocking studies on Balb/c mice using PK11195 as blocking agent proved the specificity of radioligands towards TSPO as uptake were significantly reduced with blocking. Uptake patterns and blocking studies of ^{99m}Tc-ABTO analogues on A549 human lung cell and lung inflammation models also proved TSPO specificity of these compounds. In addition to this, tumor model used for ^{99m}Tc-ABTO-Br demonstrated increased uptake in tumor and significant reduction in uptake in tumor in presence of PK11195.

These results have made significant progress towards development of acetamidabenzoxazolone based TSPO radioligands using ^{99m}Tc as SPECT imaging agents. Till date no ^{99m}Tc based TSPO agent is in clinics for SPECT application. ^{99m}Tc ($t_{1/2}$ =6.03 h, 140 keV) is better than ¹²³I ($t_{1/2}$ =13.08 h, 159 KeV) in terms of cost and wide availability as there is a need of cyclotron for production of ¹²³I requiring

specific infrastructure which could be overcome by the use of generator produced ^{99m}Tc . The cost of production of these synthetic TSPO ligands and easy chemistry makes them potential candidates for further exploration as imaging agents. Though few models have been used for validation, other TSPO expressing pathological conditions can also be used for validation and quantification. These skeletons can also be modified not only for other metal-based PET and SPECT agents but also for few covalent bond formations for PET application using $^{11}\text{C}/^{18}\text{F}$. The skeleton has the potential to further conversion to PET ligands also.

References

REFERENCES

- Aalto, S., Brück, A., Laine, M., Någren, K., & Rinne, J. O. (2005). Frontal and temporal dopamine release during working memory and attention tasks in healthy humans: a positron emission tomography study using the high-affinity dopamine D₂ receptor ligand [¹¹C] FLB 457. *Journal of Neuroscience*, 25(10), 2471-2477.
- Abbott, N. J. (2004). Prediction of blood–brain barrier permeation in drug discovery from in vivo, in vitro and in silico models. *Drug Discovery Today: Technologies*, 1(4), 407-416.
- Airas, L., Dickens, A. M., Elo, P., Marjamäki, P., Johansson, J., Eskola, O., Jones, P.A., Trigg, W., Solin, O., Solin, M. H., Anthony, D. C., & Rinne, J. (2015). In vivo Positron Emission Tomography imaging demonstrates diminished microglial activation after fingolimod treatment in an animal model of multiple sclerosis. *Journal of Nuclear Medicine*, 56(2), 305-310.
- Ametamey, S. M., Bruehlmeier, M., Kneifel, S., Kokic, M., Honer, M., Arigoni, M., Buck, A., Samnick, S., Quack, G., & Schubiger, P. A. (2002). PET studies of ¹⁸F-memantine in healthy volunteers. *Nuclear Medicine and Biology*, 29(2), 227-231.
- Ametamey, S. M., Kessler, L. J., Honer, M., Wyss, M. T., Buck, A., Hintermann, S., Auberson, Y. P., Gasparini, F., & Schubiger, P. A. (2006). Radiosynthesis and preclinical evaluation of ¹¹C-ABP688 as a probe for imaging the metabotropic glutamate receptor subtype 5. *Journal of Nuclear Medicine*, 47(4), 698-705.
- Ametamey, S. M., Treyer, V., Streffer, J., Wyss, M. T., Schmidt, M., Blagoev, M., Hintermann, S., Auberson, Y., Gasparini, F., Fischer, U. C., & Buck, A. (2007). Human PET studies of metabotropic glutamate receptor subtype 5 with ¹¹C-ABP688. *Journal of Nuclear Medicine*, 48(2), 247-252.
- Anholt, R. R., Pedersen, P. L., De Souza, E. B., & Snyder, S. H. (1986). The peripheral-type benzodiazepine receptor. Localization to the mitochondrial outer membrane. *Journal of Biological Chemistry*, 261(2), 576-583.

- Antkiewicz-Michaluk, L., Guidotti, A., & Krueger, K. E. (1988). Molecular characterization and mitochondrial density of a recognition site for peripheral-type benzodiazepine ligands. *Molecular Pharmacology*, *34*(3), 272-278.
- Anzini, M., Cappelli, A., Vomero, S., Seeber, M., Menziani, M. C., Langer, T., Hagen, B., Manzoni, C., & Bourguignon, J. J. (2001). Mapping and fitting the peripheral benzodiazepine receptor binding site by carboxamide derivatives. Comparison of different approaches to quantitative ligand-receptor interaction modeling. *Journal of Medicinal Chemistry*, *44*(8), 1134-1150.
- Azulay, H., Striem, E., & Amedi, A. (2009). Negative BOLD in sensory cortices during verbal memory: a component in generating internal representations. *Brain Topography*, *21*(3-4), 221-231.
- Beer, A. J., Haubner, R., Goebel, M., Luderschmidt, S., Spilker, M. E., Wester, H. J., Weber W. A., & Schwaiger, M. (2005). Biodistribution and pharmacokinetics of the $\alpha_v\beta_3$ -selective tracer ^{18}F -galacto-RGD in cancer patients. *Journal of Nuclear Medicine*, *46*(8), 1333-1341.
- Beer, A. J., Haubner, R., Sarbia, M., Goebel, M., Luderschmidt, S., Grosu, A. L., Schnell, O., Niemeyer, M., Kessler, H., Wester, H. J., Weber, W. A., & Schwaiger, M. (2006). Positron emission tomography using [^{18}F] Galacto-RGD identifies the level of integrin $\alpha_v\beta_3$ expression in man. *Clinical Cancer Research*, *12*(13), 3942-3949.
- Benamer, H. T. S., Patterson, J., Grosset, D. G., Booij, J., De Bruin, K., Van Royen, E., Speelman, J. D., Horstink, M. H. I. M., Sips, H. J. W. A., Dierckx, R. A., Versijpt, J., Decoo, D., Van Der Linden, C., Hadley, D. M., Doder, M., Lees, A. J., Costa, D. C., Gacinovic, S., Oertel, W. H., Pogarell, O., Hoeffken, H., Joseph, K., Tatsch, K., Schwarz, J., & Ries, V. (2000). Accurate differentiation of Parkinsonism and essential tremor using visual assessment of [^{123}I]-FP-CIT SPECT imaging: The [^{123}I]-FP-CIT study group. *Movement Disorders: Official Journal of the Movement Disorder Society*, *15*(3), 503-510.
- Bernassau, J. M., Reversat, J. L., Ferrara, P., Caput, D., & Lefur, G. (1993). A 3D model of the peripheral benzodiazepine receptor and its implication in intra mitochondrial cholesterol transport. *Journal of Molecular Graphics*, *11*(4), 236-244.

- Beurdeley-Thomas, A., Miccoli, L., Oudard, S., Dutrillaux, B., & Poupon, M. F. (2000). The peripheral benzodiazepine receptors: a review. *Journal of Neuro-Oncology*, *46*(1), 45-56.
- Bhargavi, M., Sivan, S. K., & Potlapally, S. R. (2017). Identification of novel anti cancer agents by applying *in silico* methods for inhibition of TSPO protein. *Computational Biology and Chemistry*, *68*, 43-55.
- Biver, F., Wikler, D., Lotstra, F., Damhaut, P., Goldman, S., & Mendlewicz, J. (1997). Serotonin 5-HT₂ receptor imaging in major depression: focal changes in orbito-insular cortex. *The British Journal of Psychiatry*, *171*(5), 444-448.
- Blin, J., Denis, A., Yamaguchi, T., Crouzel, C., MacKenzie, E. T., & Baron, J. C. (1991). PET studies of [¹⁸F] methyl-MK-801, a potential NMDA receptor complex radioligand. *Neuroscience Letters*, *121*(1-2), 183-186.
- Blin, J., Sette, G., Fiorelli, M., Bletry, O., Elghozi, J. L., Crouzel, C., & Baron, J. C. (1990). A method for the In Vivo Investigation of the Serotonergic 5-HT₂ Receptors in the Human Cerebral Cortex Using Positron Emission Tomography and ¹⁸F-Labeled Setoperone. *Journal of Neurochemistry*, *54*(5), 1744-1754.
- Bollineni, V. R., Kramer, G. M., Jansma, E. P., Liu, Y., & Oyen, W. J. G. (2016). A systematic review on [¹⁸F] FLT-PET uptake as a measure of treatment response in cancer patients. *European Journal of Cancer*, *55*, 81-97.
- Breier, A., Su, T. P., Saunders, R., Carson, R. E., Kolachana, B. S., De Bartolomeis, A., Weinberger, D. R., Weisenfeld, N., Malhotra, A. K., Eckelman, W. C., & Pickar, D. (1997). Schizophrenia is associated with elevated amphetamine-induced synaptic dopamine concentrations: evidence from a novel positron emission tomography method. *Proceedings of the National Academy of Sciences*, *94*(6), 2569-2574.
- Bribes, E., Carrière, D., Goubet, C., Galiègue, S., Casellas, P., & Joëlle, S. L. (2004). Immunohistochemical assessment of the peripheral benzodiazepine receptor in human tissues. *Journal of Histochemistry & Cytochemistry*, *52*(1), 19-28.

- Brogssitter, C., Zöphel, K., & Kotzerke, J. (2013). ^{18}F -Choline, ^{11}C -choline and ^{11}C -acetate PET/CT: comparative analysis for imaging prostate cancer patients. *European Journal of Nuclear Medicine and Molecular Imaging*, 40(1), 18-27.
- Brown, R. C., Degenhardt, B., Kotoula, M., & Papadopoulous, V. (2000). Location-dependent role of the human glioma cell peripheral-type benzodiazepine receptor in proliferation and steroid biosynthesis. *Cancer Letters*, 156(2), 125-132.
- Buck, J. R., McKinley, E. T., Hight, M. R., Fu, A., Tang, D., Smith, R. A., Tantawy, M. N., Peterson, T. E., Colvin, D., Ansari, M. S., Baldwin, R. M., Zhao, P., Guleryuz, S., & Manning, H. C. (2011). Quantitative, preclinical PET of translocator protein expression in glioma using ^{18}F -N-fluoroacetyl-N-(2,5-dimethoxybenzyl)-2-phenoxyaniline. *Journal of Nuclear Medicine*, 52(1), 107-114.
- Campiani, G., Nacci, V., Fiorini, I., De Filippis, M. P., Garofalo, A., Ciani, S. M., Greco, G., Novellino, E., Williams, D. C., Zisterer, D. M., Woods, M. J., Mihai, C., Manzoni, C., & Mennini, T. (1996). Synthesis, biological activity, and SARs of pyrrolobenzoxazepine derivatives, a new class of specific "peripheral-type" benzodiazepine receptor ligands. *Journal of Medicinal Chemistry*, 39(18), 3435-3450.
- Canat, X., Carayon, P., Bouaboula, M., Cahard, D., Shire, D., Roque, C., Le, F.G., & Casellas, P. (1993). Distribution profile and properties of peripheral-type benzodiazepine receptors on human hemopoietic cells, *Life Sci.* 52, 107-118.
- Cappelli, A., Anzini, M., Vomero, S., De Benedetti, P. G., Menziani, M. C., Giorgi, G., & Manzoni, C. (1997). Mapping the peripheral benzodiazepine receptor binding site by conformationally restrained derivatives of 1-(2-chlorophenyl)-N-methyl-N-(1-methylpropyl)-3-isoquinolinecarboxamide (PK11195). *Journal of Medicinal Chemistry*, 40(18), 2910-2921.
- Cappelli, A., Mancini, A., Sudati, F., Valenti, S., Anzini, M., Belloli, S., Moresco, A., Matarrese, M., Vaghi, M., Fabro, A., Fazio, F., & Vomero, S. (2008). Synthesis and biological characterization of novel 2-quinolinecarboxamide ligands of the peripheral benzodiazepine receptors bearing technetium-99m or rhenium. *Bioconjugate Chemistry*, 19(6), 1143-1153.

- Carson, R. E., Lang, L., Watabe, H., Der, M. G., Adams, H. R., Jagoda, E., Herscovitch, P., & Eckelman, W. C. (2000). PET evaluation of [¹⁸F] FCWAY, an analogue of the 5-HT_{1A} receptor antagonist, WAY-100635. *Nuclear Medicine and Biology*, 27(5), 493-497.
- Casellas, P., Galiegue, S., & Basile, A. S. (2002). Peripheral benzodiazepine receptors and mitochondrial function. *Neurochemistry International*, 40(6), 475-486.
- Castellano, S., Taliani, S., Viviano, M., Milite, C., Da Pozzo, E., Costa, B., Barresi, E., Bruno, A., Cosconatli, S., Marinelli, L., Greco, G., Novellino, E., Sbardella, G., Settimo, F. D., & Martini, C. (2014). Structure–activity relationship refinement and further assessment of 4-phenylquinazoline-2-carboxamide translocator protein ligands as antiproliferative agents in human glioblastoma tumors. *Journal of Medicinal Chemistry*, 57(6), 2413-2428.
- Chang, Y. J., McCabe, R. T., Rennert, H., Budarf, M. L., Sayegh, R., Emanuel, B. S., Skolnick, P., & Strauss III, J. F. (1992). The human "peripheral-type" benzodiazepine receptor: regional mapping of the gene and characterization of the receptor expressed from cDNA. *DNA and Cell Biology*, 11(6), 471-480.
- Chaput, L., & Mouawad, L. (2017). Efficient conformational sampling and weak scoring in docking programs? Strategy of the wisdom of crowds. *Journal of Cheminformatics*, 9(1), 37.
- Chiamulera, C., Epping-Jordan, M. P., Zocchi, A., Marcon, C., Cottiny, C., Tacconi, S., Corsi, M., Orzi, F., & Conquet, F. (2001). Reinforcing and locomotor stimulant effects of cocaine are absent in mGluR₅ null mutant mice. *Nature Neuroscience*, 4(9), 873.
- Choi, J. Y., Iacobazzi, R. M., Perrone, M., Margiotta, N., Cutrignelli, A., Jung, J. H., Park, D. D., Moon, B. S., Denora, N., Kim, S. E., & Lee, B. C. (2016). Synthesis and Evaluation of Tricarbonyl ^{99m}Tc-Labeled 2-(4-Chloro) phenyl-imidazo [1, 2-a] pyridine analogues as Novel SPECT Imaging Radiotracer for TSPO-Rich Cancer. *International Journal of Molecular Sciences*, 17(7), 1085.
- Cinone, N., Hölftje, H. D., & Carotti, A. (2000). Development of a unique 3D interaction model of endogenous and synthetic peripheral benzodiazepine receptor ligands. *Journal of Computer-Aided Molecular Design*, 14(8), 753-768.

- Colasanti, A., Guo, Q., Muhlert, N., Giannetti, P., Onega, M., Newbould, R. D., Ciccarelli, O., Rison, S., Thomas, C., Nicholas, R., Muraro, P. A., Malik, O., Owen, D. R., Piccini, P., Gunn, R. N., Rabiner, E. A., & Matthews, P. M. (2014). In vivo assessment of brain white matter inflammation in multiple sclerosis with ^{18}F -PBR111 PET. *Journal of Nuclear Medicine*, *55*(7), 1112-1118.
- Cruciani, G., Carosati, E., Wade, R. C., & Baroni, M. (2007). Characterization of protein-binding sites and ligands using molecular interaction fields. *Comprehensive Med. Chem.*, II 2006, 4, 237-253.
- Corsi, L., Geminiani, E., Avallone, R., & Baraldi, M. (2005). Nuclear location-dependent role of peripheral benzodiazepine receptor (PBR) in hepatic tumoral cell lines proliferation. *Life Sciences*, *76*(22), 2523-2533.
- De Benedetti, P. G., Cocchi, M., Menziani, M. C., & Fanelli, F. (1994). Theoretical quantitative size and shape activity and selectivity analyses of 5-HT_{1A} serotonin and α 1-adrenergic receptor ligands. *Journal of Molecular Structure: THEOCHEM*, *305*, 101-110.
- de Jong, H. W. A. M., Rijzewijk, L. J., Lubberink, M., van der Meer, R. W., Lamb, H. J., Smit, J. W., Diamant, M., & Lammertsma, A. A. (2009). Kinetic models for analysing myocardial [^{11}C] palmitate data. *European Journal of Nuclear Medicine and Molecular Imaging*, *36*(6), 966-978.
- De Leon-Rodriguez, L. M., Lubag, A. J. M., Malloy, C. R., Martinez, G. V., Gillies, R. J., & Sherry, A. D. (2009). Responsive MRI agents for sensing metabolism in vivo. *Accounts of Chemical Research*, *42*(7), 948-957.
- de Vries, E. F., Dierckx, R. A., & Klein, H. C. (2006). Nuclear imaging of inflammation in neurologic and psychiatric disorders. *Current Clinical Pharmacology*, *1*(3), 229-242.
- Dewey, S. L., Macgregor, R. R., Brodie, J. D., Bendriem, B., King, P. T., Volkow, N. D., Schlyer, D. J., Fowler, J. S., Wolf, A. P., Gatley, S. J., & Hitzemann, R. (1990). Mapping muscarinic receptors in human and baboon brain using [^{11}C -methyl]-benztropine. *Synapse*, *5*(3), 213-223.

- Dewey, S. L., Smith, G. S., Logan, J., Brodie, J. D., Fowler, J. S., & Wolf, A. P. (1993). Striatal binding of the PET ligand ^{11}C -raclopride is altered by drugs that modify synaptic dopamine levels. *Synapse*, *13*(4), 350-356.
- Di Grigoli, G., Monterisi, C., Belloli, S., Masiello, V., Politi, L. S., Valenti, S., Paolino, M., Anzini, M., Matarrese, M., Cappelli, A., & Moresco, R. M. (2015). Radiosynthesis and preliminary biological evaluation of [^{18}F] VC701, a radioligand for translocator protein. *Molecular Imaging*, *14*(6), 7290-2015.
- Ding, Y. S., Fowler, J. S., Logan, J., Wang, G. J., Telang, F., Garza, V., Biegon, A., Pareto, D., Rooney, W., Shea, C., Alexoff, D., Volkow, N. D., & Vocci, F. (2004). 6- ^{18}F Fluoro-A-85380, a new PET tracer for the nicotinic acetylcholine receptor: Studies in the human brain and in vivo demonstration of specific binding in white matter. *Synapse*, *53*(3), 184-189.
- Dixit, M., Shi, J., Wei, L., Afari, G., & Bhattacharyya, S. (2013). Synthesis of clinical-grade [^{18}F]-fluoroestradiol as a surrogate PET biomarker for the evaluation of estrogen receptor-targeting therapeutic drug. *International Journal of Molecular Imaging*, 2013, Article ID 278607, 10 pages.
- Drevets, W. C., Frank, E., Price, J. C., Kupfer, D. J., Greer, P. J., & Mathis, C. (2000). Serotonin type-1A receptor imaging in depression. *Nuclear Medicine and Biology*, *27*(5), 499-507.
- Dubroff, J. G., & Newberg, A. (2008, September). Neuroimaging of traumatic brain injury. In *Seminars in Neurology* (Vol. 28, No. 04, pp. 548-557), Thieme Medical Publishers.
- Dupont, A. C., Largeau, B., Santiago Ribeiro, M. J., Guilloteau, D., Tronel, C., & Arlicot, N. (2017). Translocator protein-18 kDa (TSPO) positron emission tomography (PET) imaging and its clinical impact in neurodegenerative diseases. *International Journal of Molecular Sciences*, *18*(4), 785.
- Eckelman, W. C., Kilbourn, M. R., & Mathis, C. A. (2006). Discussion of targeting proteins in vivo: in vitro guidelines. *Nuclear Medicine and Biology*, *33*(4), 449-451.
- Farde, L., Hall, H., Ehrin, E., & Sedvall, G. (1986). Quantitative analysis of D_2 dopamine receptor binding in the living human brain by PET. *Science*, *231*(4735), 258-261.

- Farde, L., Halldin, C., Stone-Elander, S., & Sedvall, G. (1987). PET analysis of human dopamine receptor subtypes using ^{11}C -SCH23390 and ^{11}C -raclopride. *Psychopharmacology*, 92(3), 278-284.
- Farde, L., Ito, H., Swahn, C. G., Pike, V. W., & Halldin, C. (1998). Quantitative analyses of carbonyl-carbon-11-WAY-100635 binding to central 5-hydroxytryptamine-1A receptors in man. *The Journal of Nuclear Medicine*, 39(11), 1965-1971.
- Faulkner, W. M. (1996). Basic principles of MRI. *Outsource Inc.*
- Ferrero, P., Santi, M. R., Conti-Tronconi, B., Costa, E., & Guidotti, A. (1986). Study of an octadecaneuropeptide derived from diazepam binding inhibitor (DBI): biological activity and presence in rat brain. *Proceedings of the National Academy of Sciences*, 83(3), 827-831.
- Fink, G. R. (2004). Functional MR imaging: from the BOLD effect to higher motor cognition. In *Supplements to Clinical Neurophysiology* (Vol. 57, pp. 458-468). Elsevier.
- Frackowiak, R., Lenzi, G. L., Jones, T., & Heather, J. D. (1980). Quantitative measurement of regional cerebral blood flow and oxygen metabolism in man using ^{15}O and positron emission tomography: theory, procedure, and normal values. *Journal of Computer Assisted Tomography*, 4(6), 727-736.
- Francken, G. A., Waxman, A. D., Potter, R., & King, R. (1998). The effect of inertial changes on particle size distribution in nebulizers systems: The impact on clinical aerosol studies. *Clinical Nuclear Medicine*, 23(7), 490.
- Frankle, W. G., Lombardo, I., New, A. S., Goodman, M., Talbot, P. S., Huang, Y., Hwang, D. R., Slifstein, M., Curry, S., Abi-Dargham, A., Laruelle, M., & Siever, L. J. (2005). Brain serotonin transporter distribution in subjects with impulsive aggressivity: a positron emission study with [^{11}C] McN 5652. *American Journal of Psychiatry*, 162(5), 915-923.
- Froklage, F. E., Syvänen, S., Hendrikse, N. H., Huisman, M. C., Molthoff, C. F., Tagawa, Y., Reijneveld, J. C., Heimans, J. J., Lammertsma, A. A., Eriksson, J., de Lange, E. C., & Voskuyl, R. A. (2012). [^{11}C] Flumazenil brain uptake is influenced by the blood-brain barrier efflux transporter P-glycoprotein. *EJNMMI Research*, 2(1), 12.

- Fröman, N. (1996). Marie and Pierre Curie and the discovery of polonium and radium. *Lecture at the Royal Swedish Academy of Sciences, Stockholm*, 28.
- Fukaya, T., Kodo, T., Ishiyama, T., Kakuyama, H., Nishikawa, H., Baba, S., & Masumoto, S. (2012). Design, synthesis and structure–activity relationships of novel benzoxazolone derivatives as 18kDa translocator protein (TSPO) ligands. *Bioorganic & Medicinal Chemistry*, 20(18), 5568-5582.
- Fukaya, T., Kodo, T., Ishiyama, T., Nishikawa, H., Baba, S., & Masumoto, S. (2013). Design, synthesis and structure–activity relationship of novel tricyclic benzimidazolone derivatives as potent 18kDa translocator protein (TSPO) ligands. *Bioorganic & Medicinal Chemistry*, 21(5), 1257-1267.
- Gallezot, J. D., Bottlaender, M., Grégoire, M. C., Roumenov, D., Deverre, J. R., Coulon, C., Ottaviani, M., Dollè, F., Syrota, A., & Valette, H. (2005). In vivo imaging of human cerebral nicotinic acetylcholine receptors with 2-¹⁸F-fluoro-A-85380 and PET. *Journal of Nuclear Medicine*, 46(2), 240-247.
- Garnier, M., Dimchev, A. B., Boujrad, N., Price, J. M., Musto, N. A., & Papadopoulos, V. (1994). In vitro reconstitution of a functional peripheral-type benzodiazepine receptor from mouse Leydig tumor cells. *Molecular Pharmacology*, 45(2), 201-211.
- Gavish, M., Bachman, I., Shoukrun, R., Katz, Y., Veenman, L., Weisinger, G., & Weizman, A. (1999). Enigma of the peripheral benzodiazepine receptor. *Pharmacological Reviews*, 51(4), 629-650.
- Gong, H., Kovar, J. L., Cheung, L., Rosenthal, E. L., & Olive, D. M. (2014). A comparative study of affibody, panitumumab, and EGF for near-infrared fluorescence imaging of EGFR-and EGFRvIII-expressing tumors. *Cancer Biology & Therapy*, 15(2), 185-193.
- Goodman, M. M., Kilts, C. D., Keil, R., Shi, B., Martarello, L., Xing, D., Votaw J., Ely, T. D., Lambert, P., Owens, M. J., & Camp, V. M. (2000). ¹⁸F-labeled FECNT: a selective radioligand for PET imaging of brain dopamine transporters. *Nuclear Medicine and Biology*, 27(1), 1-12.
- Goswami, D., Goyal, S., Jamal, S., Jain, R., Wahi, D., & Grover, A. (2017). QSAR modeling and combinatorial library generation of 4-phenylquinazoline-2-carboxamide derivatives as antiproliferative agents in human Glioblastoma tumors. *Computational Biology and Chemistry*, 69, 147-152.

- Grassi, I., Nanni, C., Allegri, V., Morigi, J. J., Montini, G. C., Castellucci, P., & Fanti, S. (2012). The clinical use of PET with ^{11}C -acetate. *American Journal of Nuclear Medicine and Molecular Imaging*, 2(1), 33.
- Greco, G., Novellino, E., Fiorini, I., Nacci, V., Campiani, G., Ciani, S. M., Antonio, G., Bernasconi, P., & Mennini, T. (1994). A comparative molecular field analysis model for 6-arylpyrrolo [2, 1-d][1, 5] benzothiazepines binding selectively to the mitochondrial benzodiazepine receptor. *Journal of Medicinal Chemistry*, 37(24), 4100-4108.
- Guidotti, A., Forchetti, C. M., Corda, M. G., Konkol, D., Bennett, C. D., & Costa, E. (1983). Isolation, characterization, and purification to homogeneity of an endogenous polypeptide with agonistic action on benzodiazepine receptors. *Proceedings of the National Academy of Sciences*, 80(11), 3531-3535.
- Guo, Q., Colasanti, A., Owen, D. R., Onega, M., Kamalakaran, A., Bennacef, I., Matthews, P. M., Rabiner, E. A., Turkheimer, F. E., & Gunn, R. N. (2013). Quantification of the specific translocator protein signal of ^{18}F -PBR111 in healthy humans: a genetic polymorphism effect on in vivo binding. *Journal of Nuclear Medicine*, 54(11), 1915-1923.
- Guo, Y., Kalathur, R. C., Liu, Q., Kloss, B., Bruni, R., Ginter, C., Kloppmann, E., Rost, B., & Hendrickson, W. A. (2015). Structure and activity of tryptophan-rich TSPO proteins. *Science*, 347(6221), 551-555.
- Halgren, T. A., Murphy, R. B., Friesner, R. A., Beard, H. S., Frye, L. L., Pollard, W. T., & Banks, J. L. (2004). Glide: a new approach for rapid, accurate docking and scoring. 2. Enrichment factors in database screening. *Journal of Medicinal Chemistry*, 47(7), 1750-1759.
- Halldin, C., Foged, C., Chou, Y. H., & Karlsson, P. (1998). Carbon-11-NNC 112: a radioligand for PET examination of striatal and neocortical D_1 -dopamine receptors. *The Journal of Nuclear Medicine*, 39(12), 2061-2068
- Halldin, C., Gulyas, B., Langer, O., & Farde, L. (2001). Brain radioligands-state of the art and new trends. *The Quarterly Journal of Nuclear Medicine and Molecular Imaging*, 45(2), 139-152.

- Hamill, T. G., Krause, S., Ryan, C., Bonnefous, C., Govek, S., Seiders, T. J., Cosford, N. D. P., Roppe, J., Kamenecka, T., Patel, S., Gibson, R. E., Sanabria, S., Riffel, K., Eng, W., King, C., Yang, X., Green, M. D., O'Malley, S. S., Hargreaves, R., & Burns, H. D. (2005). Synthesis, characterization, and first successful monkey imaging studies of metabotropic glutamate receptor subtype 5 (mGluR₅) PET radiotracers. *Synapse*, 56(4), 205-216.
- Hardwick, M., Fertikh, D., Culty, M., Li, H., Vidic, B., & Papadopoulos, V. (1999). Peripheral-type benzodiazepine receptor (PBR) in human breast cancer: correlation of breast cancer cell aggressive phenotype with PBR expression, nuclear localization, and PBR-mediated cell proliferation and nuclear transport of cholesterol. *Cancer Research*, 59(4), 831-842.
- Hartvig, P., Valtysson, J., Lindner, K. J., Kristensen, J., Karlsten, R., Gustafsson, L. L., Persson, J., Svensson, J. O., Oye, I., Antoni, G. & Westerberg, G. (1995). Central nervous system effects of subdissociative doses of (S)-ketamine are related to plasma and brain concentrations measured with positron emission tomography in healthy volunteers. *Clinical Pharmacology & Therapeutics*, 58(2), 165-173.
- Hatty, C. R., & Banati, R. B. (2015). Protein-ligand and membrane-ligand interactions in pharmacology: the case of the translocator protein (TSPO). *Pharmacological Research*, 100, 58-63.
- Herzog, B. A., Husmann, L., Valenta, I., Gaemperli, O., Siegrist, P. T., Tay, F. M., Burkhard, N., Wyss, C. A., & Kaufmann, P. A. (2009). Long-term prognostic value of ¹³N-ammonia myocardial perfusion positron emission tomography: added value of coronary flow reserve. *Journal of the American College of Cardiology*, 54(2), 150-156.
- Hevesy, G. (1939). Application of isotopes in biology. *Journal of the Chemical Society*, 1213-1223.
- Hirvonen, J., Aalto, S., Lumme, V., Någren, K., Kajander, J., Vilkmann, H., Hagelberg, N., Oikonen, V., & Hietala, J. (2003). Measurement of striatal and thalamic dopamine D₂ receptor binding with ¹¹C-raclopride. *Nuclear Medicine Communications*, 24(12), 1207-1214.

- Hodgson, R. J., O'connor, P., & Moots, R. (2007). MRI of rheumatoid arthritis—image quantitation for the assessment of disease activity, progression and response to therapy. *Rheumatology*, *47*(1), 13-21.
- Horti, A. G., Chefer, S. I., Mukhin, A. G., Koren, A. O., Gündisch, D., Links, J. M., Kurian, V., Dannals, R. F., & London, E. D. (2000). 6-[¹⁸F] fluoro-A-85380, a novel radioligand for in vivo imaging of central nicotinic acetylcholine receptors. *Life Sciences*, *67*(4), 463-469.
- Houle, S., Ginovart, N., Hussey, D., Meyer, J. H., & Wilson, A. A. (2000). Imaging the serotonin transporter with positron emission tomography: initial human studies with [¹¹C] DAPP and [¹¹C] DASB. *European Journal of Nuclear Medicine*, *27*(11), 1719-1722.
- Huang, W. S., Lin, S. Z., Lin, J. C., Wey, S. P., Ting, G., & Liu, R. S. (2001). Evaluation of early-stage Parkinson's disease with ^{99m}Tc-TRODAT-1 imaging. *Journal of Nuclear Medicine*, *42*(9), 1303-1308.
- Ichimiya, T., Suhara, T., Sudo, Y., Okubo, Y., Nakayama, K., Nankai, M., Inoue, M., Yasuno, F., Takano, A., Maeda, J., & Shibuya, H. (2002). Serotonin transporter binding in patients with mood disorders: a PET study with [¹¹C](+) McN5652. *Biological Psychiatry*, *51*(9), 715-722.
- Iida, H., Takahashi, A., Tamura, Y., Ono, Y., & Lammertsma, A. A. (1995). Myocardial blood flow: comparison of oxygen-15-water bolus injection, slow infusion and oxygen-15-carbon dioxide slow inhalation. *Journal of Nuclear Medicine: Official Publication, Society of Nuclear Medicine*, *36*(1), 78-85.
- Ishiwata, K., Kawamura, K., Wang, W. F., Furumoto, S., Kubota, K., Pascali, C., Bogni, A., & Iwata, R. (2004). Evaluation of O-[¹¹C] methyl-L-tyrosine and O-[¹⁸F] fluoromethyl-L-tyrosine as tumor imaging tracers by PET. *Nuclear Medicine and Biology*, *31*(2), 191-198.
- Ito, H., Nyberg, S., Halldin, C., Lundkvist, C., & Farde, L. (1998). PET imaging of central 5-HT (2A) receptors with carbon-11-MDL 100,907. *The Journal of Nuclear Medicine*, *39*(1), 208-214.
- Iyo, M., Namba, H., Fukushi, K., Shinotoh, H., Nagatsuka, S., Suhara, T., Sudo, Y., Suzuki, K., & Irie, T. (1997). Measurement of acetylcholinesterase by positron emission tomography in the brains of healthy controls and patients with Alzheimer's disease. *The Lancet*, *349*(9068), 1805-1809.

- Jaber, M., Robinson, S. W., Missale, C., & Caron, M. G. (1996). Dopamine receptors and brain function. *Neuropharmacology*, *35*(11), 1503-1519.
- James, M. L., & Gambhir, S. S. (2012). A molecular imaging primer: modalities, imaging agents, and applications. *Physiological Reviews*, *92*(2), 897-965.
- Jaremko, Ł., Jaremko, M., Giller, K., Becker, S., & Zweckstetter, M. (2014). Structure of the mitochondrial translocator protein in complex with a diagnostic ligand. *Science*, *343*(6177), 1363-1366.
- Jaremko, M., Jaremko, Ł., Jaipuria, G., Becker, S., & Zweckstetter, M. (2015). Structure of the mammalian TSPO/PBR protein. *Biochemical Society Transactions*, *43*(4), 566-571.
- Jarkas, N., Votaw, J. R., Voll, R. J., Williams, L., Camp, V. M., Owens, M. J., Purselle, D. C., Bremner, J. D., Kilts, C. D., Nemeroff, C. B., & Goodman, M. M. (2005). Carbon-11 HOMADAM: a novel PET radiotracer for imaging serotonin transporters. *Nuclear Medicine and Biology*, *32*(3), 211-224.
- Kadir, A., Almkvist, O., Wall, A., Långström, B., & Nordberg, A. (2006). PET imaging of cortical ¹¹C-nicotine binding correlates with the cognitive function of attention in Alzheimer's disease. *Psychopharmacology*, *188*(4), 509-520.
- Kaufmann, P. A., Gnecci-Ruscone, T., Yap, J. T., Rimoldi, O., & Camici, P. G. (1999). Assessment of the reproducibility of baseline and hyperemic myocardial blood flow measurements with ¹⁵O-labeled water and PET. *The Journal of Nuclear Medicine*, *40*(11), 1848-1856.
- Kendziorra, K., Meyer, P., Wolf, H., Barthel, H., Hesse, S., Seese, A., Sorge, D., Patt, M., Becker, G., Schildan, A., Gertz, H. H., Sabri, O. (2006). Cerebral nicotinic acetylcholine receptors in patients with Alzheimer's disease assessed with 2-[¹⁸F] F-A85380 PET—correlations to dementia severity. *Neuroimage*, *31*, T39.
- Khalil, M. M., Tremoleda, J. L., Bayomy, T. B., & Gsell, W. (2011). Molecular SPECT imaging: an overview. *International Journal of Molecular Imaging*, *2011*, Article ID 796025, 15 pages.

- Koren, A. O., Horti, A. G., Mukhin, A. G., Gündisch, D., Kimes, A. S., Dannals, R. F., & London, E. D. (1998). 2-, 5-, and 6-Halo-3-(2 (S)-azetidinylmethoxy) pyridines: synthesis, affinity for nicotinic acetylcholine receptors, and molecular modeling. *Journal of Medicinal Chemistry*, *41*(19), 3690-3698.
- Kuge, Y., Sato, M., Zhao, S., Takei, T., Nakada, K., Seki, K. I., Strauss, H. W., Blankenberg, F. G., Tait, J. F., & Tamaki, N. (2004). Feasibility of ^{99m}Tc-annexin V for repetitive detection of apoptotic tumor response to chemotherapy: an experimental study using a rat tumor model. *Journal of Nuclear Medicine*, *45*(2), 309-312.
- Laakso, A., Bergman, J., Haaparanta, M., Vilkmann, H., Solin, O., & Hietala, J. (1998). [¹⁸F] CFT ([¹⁸F] WIN 35,428), a radioligand to study the dopamine transporter with PET: characterization in human subjects. *Synapse*, *28*(3), 244-250.
- Lacapere, J. J., Delavoie, F., Li, H., Péranski, G., Maccario, J., Papadopoulos, V., & Vidic, B. (2001). Structural and functional study of reconstituted peripheral benzodiazepine receptor. *Biochemical and Biophysical Research Communications*, *284*(2), 536-541.
- Lacapere, J. J., & Papadopoulos, V. (2003). Peripheral-type benzodiazepine receptor: structure and function of a cholesterol-binding protein in steroid and bile acid biosynthesis. *Steroids*, *68*(7-8), 569-585.
- Lartey, F. M., Ahn, G. O., Shen, B., Cord, K. T., Smith, T., Chua, J. Y., Rosenblum, S., Liu, H., James, M. L., Chernikova, S., Lee, S. W., Pisani, L. J., Tirouvanziam, R., Chen, J. W., Palmer, T. D., Chin, F. T., Guzman, R., Graves, E. E., & Loo, B. W. (2014). PET imaging of stroke-induced neuroinflammation in mice using [¹⁸F] PBR06. *Molecular Imaging and Biology*, *16*(1), 109-117.
- Lavisse, S., Guillermier, M., Hérard, A. S., Petit, F., Delahaye, M., Van Camp, N., Haim, L. B., Lebon, V., Remy, P., Dolle, F., Delzescaux, T., Bonvento, G., Hantraye, P., & Escartin, C. (2012). Reactive astrocytes overexpress TSPO and are detected by TSPO positron emission tomography imaging. *Journal of Neuroscience*, *32*(32), 10809-10818.

- Lewis, J. S., Laforest, R., Dehdashti, F., Grigsby, P. W., Welch, M. J., & Siegel, B. A. (2008). An imaging comparison of ^{64}Cu -ATSM and ^{60}Cu -ATSM in cancer of the uterine cervix. *Journal of Nuclear Medicine*, *49*(7), 1177-1182.
- Li, F., Liu, J., Zheng, Y., Garavito, R. M., & Ferguson-Miller, S. (2015). Crystal structures of translocator protein (TSPO) and mutant mimic of a human polymorphism. *Science*, *347*(6221), 555-558.
- Li, H., Degenhardt, B., Tobin, D., Yao, Z. X., Tasken, K., & Papadopoulos, V. (2001). Identification, localization, and function in steroidogenesis of PAP7: a peripheral-type benzodiazepine receptor-and PKA ($\text{RI}\alpha$)-associated protein. *Molecular Endocrinology*, *15*(12), 2211-2228.
- Lin, Y., Chen, Z. Y., Yang, F., Zhang, J. S., Wang, Y. X., Liu, J. B., Liao, J. Y., Liao, Y. Y., Zhou, Q. L., Li, B. C., & Liang, H. Y. (2015). Application of molecular imaging technologies in antitumor drug development and therapy. *Current Pharmaceutical Design*, *21*(16), 2136-2146.
- Liu, S., & Edwards, D. S. (1999). $^{99\text{m}}\text{Tc}$ -labeled small peptides as diagnostic radiopharmaceuticals. *Chemical Reviews*, *99*(9), 2235-2268.
- Lundberg, J., Odano, I., Olsson, H., Halldin, C., & Farde, L. (2005). Quantification of ^{11}C -MADAM binding to the serotonin transporter in the human brain. *Journal of Nuclear Medicine*, *46*(9), 1505-1515.
- Mallo, R. D., Salem, L., Lalani, T., & Flum, D. R. (2005). Computed tomography diagnosis of ischemia and complete obstruction in small bowel obstruction: a systematic review. *Journal of Gastrointestinal Surgery*, *9*(5), 690-694.
- Marshall, G. R., Barry, C. D., Bosshard, H. E., Dammkoehler, R. A., & Dunn, D. A. (1979) The conformational parameter in drug design: the active analogue approach. Computer Assisted Drug Design. In *ACS Symposium Series*, *112*, 205-226
- Massoud, T. F., & Gambhir, S. S. (2003). Molecular imaging in living subjects: seeing fundamental biological processes in a new light. *Genes & Development*, *17*(5), 545-580.

- Mattner, F., Quinlivan, M., Greguric, I., Pham, T., Liu, X., Jackson, T., Berghofer, P., Fookes, C. J. R., Dikic, B., Gregoire, M. C., Dolle, F., & Katsifis, A. (2015). Radiosynthesis, in vivo biological evaluation, and imaging of brain lesions with [^{123}I]-CLINME, a new SPECT tracer for the translocator protein. *Disease Markers*, 2015, Article ID 729698, 11 pages.
- McEnery, M. W., Snowman, A. M., Trifiletti, R. R., & Snyder, S. H. (1992). Isolation of the mitochondrial benzodiazepine receptor: association with the voltage-dependent anion channel and the adenine nucleotide carrier. *Proceedings of the National Academy of Sciences*, 89(8), 3170-3174.
- Meador, K. J., Ray, P. G., Echauz, J. R., Loring, D. W., & Vachtsevanos, G. J. (2002). Gamma coherence and conscious perception. *Neurology*, 59(6), 847-854.
- Min, J. J., & Gambhir, S. S. (2008). Molecular imaging of PET reporter gene expression. In *Molecular Imaging II* (pp. 277-303). Springer, Berlin, Heidelberg.
- Miyamoto, T., Miyamoto, M., Suzuki, K., Nishibayashi, M., Iwanami, M., & Hirata, K. (2008). ^{123}I -MIBG cardiac scintigraphy provides clues to the underlying neurodegenerative disorder in idiopathic REM sleep behavior disorder. *Sleep*, 31(5), 717-723.
- Morais, G. R., Paulo, A., & Santos, I. (2012). Organometallic complexes for SPECT imaging and/or radionuclide therapy. *Organometallics*, 31(16), 5693-5714.
- Morin, D., Musman, J., Pons, S., Berdeaux, A., & Ghaleh, B. (2016). Mitochondrial translocator protein (TSPO): From physiology to cardioprotection. *Biochemical Pharmacology*, 105, 1-13.
- Morrish, P. K., Rakshi, J. S., Bailey, D. L., Sawle, G. V., & Brooks, D. J. (1998). Measuring the rate of progression and estimating the preclinical period of Parkinson's disease with [^{18}F] dopa PET. *Journal of Neurology, Neurosurgery & Psychiatry*, 64(3), 314-319.
- Mukherjee, J., Yang, Z. Y., Brown, T., Lew, R., Wernick, M., Ouyang, X., Yasillo, N., Chen, C. T., Mintzer, R., & Cooper, M. (1999). Preliminary assessment of extrastriatal dopamine D-2 receptor binding in the rodent and nonhuman primate brains using the high affinity radioligand, ^{18}F -fallypride. *Nuclear Medicine and Biology*, 26(5), 519-527.

- Mulholland, G. K., Kilbourn, M. R., Sherman, P., Carey, J. E., Frey, K. A., Koeppe, R. A., & Kuhl, D. E. (1995). Synthesis, in vivo biodistribution and dosimetry of [^{11}C] N-methylpiperidyl benzilate ([^{11}C] NMPB), a muscarinic acetylcholine receptor antagonist. *Nuclear Medicine and Biology*, 22(1), 13-17.
- Muzic Jr, R. F., Berridge, M. S., Friedland, R. P., Zhu, N., & Nelson, D. (1998). PET quantification of specific binding of carbon-11-nicotine in human brain. *The Journal of Nuclear Medicine*, 39(12), 2048-2054.
- Nikjoo, H., Uehara, S., & Emfietzoglou, D. (2012). *Interaction of Radiation with Matter* (pp.89-93). CRC Press.
- Nyback, H., Halldin, C., Åhlin, A., Curvall, M., & Eriksson, L. (1994). PET studies of the uptake of (S)-and (R)-[^{11}C] nicotine in the human brain: difficulties in visualizing specific receptor binding in vivo. *Psychopharmacology*, 115(1-2), 31-36.
- Nyberg, S., Nilsson, U., Okubo, Y., Halldin, C., & Farde, L. (1998). Implications of brain imaging for the management of schizophrenia. *International Clinical Psychopharmacology*, 13, S15-20.
- Oh, U., Fujita, M., Ikonomidou, V. N., Evangelou, I. E., Matsuura, E., Harberts, E., Ohayon, J., Pike, V. W., Zhang, Y., Zoghbi, S. S., & Innis, R. B. (2011). Translocator protein PET imaging for glial activation in multiple sclerosis. *Journal of Neuroimmune Pharmacology*, 6(3), 354-361.
- Ohnuma, T., Augood, S. J., Arai, H., McKenna, P. J., & Emson, P. C. (1998). Expression of the human excitatory amino acid transporter 2 and metabotropic glutamate receptors 3 and 5 in the prefrontal cortex from normal individuals and patients with schizophrenia. *Molecular Brain Research*, 56(1-2), 207-217.
- Okubo, T., Yoshikawa, R., Chaki, S., Okuyama, S., & Nakazato, A. (2004). Design, synthesis and structure–affinity relationships of aryloxyanilide derivatives as novel peripheral benzodiazepine receptor ligands. *Bioorganic & Medicinal Chemistry*, 12(2), 423-438.
- Olson, J. M., Ciliax, B. J., Mancini, W. R., & Young, A. B. (1988). Presence of peripheral-type benzodiazepine binding sites on human erythrocyte membranes. *European Journal of Pharmacology*, 152(1-2), 47-53.

- Orlova, A., Tolmachev, V., Pehrson, R., Lindborg, M., Tran, T., Sandström, M., Nilsson, F. Y., Wennborg, A., Abrahmsen, L., & Feldwisch, J. (2007). Synthetic affibody molecules: a novel class of affinity ligands for molecular imaging of HER2-expressing malignant tumors. *Cancer Research*, *67*(5), 2178-2186.
- Owen, D. R., Yeo, A. J., Gunn, R. N., Song, K., Wadsworth, G., Lewis, A., Rhodes, C., Pulford, D. J., Bennacef, I., Parker, C. A., StJean, P. L., Cardon, L. R., Mooser, V. E., Matthews, P. M., Rabiner, E. A., & Rubio, J. P. (2012). An 18-kDa translocator protein (TSPO) polymorphism explains differences in binding affinity of the PET radioligand PBR28. *Journal of Cerebral Blood Flow & Metabolism*, *32*(1), 1-5.
- Owen, D. R. J., Gunn, R. N., Rabiner, E. A., Bennacef, I., Fujita, M., Kreisl, W. C., Innis, R. B., Pike, V. W., Reynolds, R., Matthews, P. M., & Parker, C. A. (2011). Mixed-affinity binding in humans with 18-kDa translocator protein ligands. *Journal of Nuclear Medicine*, *52*(1), 24-32
- Padhani, A. R., & Husband, J. E. (2001). Dynamic contrast-enhanced MRI studies in oncology with an emphasis on quantification, validation and human studies. *Clinical Radiology*, *56*(8), 607-620.
- Pagadala, N. S., Syed, K., & Tuszynski, J. (2017). Software for molecular docking: a review. *Biophysical Reviews*, *9*(2), 91-102.
- Papadopoulos, V., Aghazadeh, Y., Fan, J., Campioli, E., Zirkin, B., & Midzak, A. (2015). Translocator protein-mediated pharmacology of cholesterol transport and steroidogenesis. *Molecular and Cellular Endocrinology*, *408*, 90-98.
- Papadopoulos, V., Amri, H., Boujrad, N., Cascio, C., Culty, M., Garnier, M., Hardwick, M., Li, H., Vidic, B., Brown, A. S., Reversa, J. L., Bernassau, J. M., & Drieu, K. (1997). Peripheral benzodiazepine receptor in cholesterol transport and steroidogenesis. *Steroids*, *62*(1), 21-28.
- Papadopoulos, V., Berkovich, A., Krueger, K. E., Costa, E., & Guidotti, A. (1991). Diazepam binding inhibitor and its processing products stimulate mitochondrial steroid biosynthesis via an interaction with mitochondrial benzodiazepine receptors. *Endocrinology*, *129*(3), 1481-1488.

- Parola, A. L., Stump, D. G., Pepperl, D. J., Krueger, K. E., Regan, J. W., & Laird, H. E. (1991). Cloning and expression of a pharmacologically unique bovine peripheral-type benzodiazepine receptor isoquinoline binding protein. *Journal of Biological Chemistry*, 266(21), 14082-14087.
- Passchier, J., van Waarde, A., Pieterman, R. M., Elsinga, P. H., Pruijm, J., Hendrikse, H. N., Willemsen, A. T. M., & Vaalburg, W. (2000). Quantitative imaging of 5-HT_{1A} receptor binding in healthy volunteers with [¹⁸F] p-MPPF. *Nuclear Medicine and Biology*, 27(5), 473-476.
- Petrev, V. M., Tishchenko, V. K., & Krasikova, R. N. (2016). ¹⁸F-FDG and Other Labeled Glucose Derivatives for Use in Radionuclide Diagnosis of Oncological Diseases. *Pharmaceutical Chemistry Journal*, 50(4), 209-220.
- Phelps, M. E. (2000). Positron emission tomography provides molecular imaging of biological processes. *Proceedings of the National Academy of Sciences*, 97(16), 9226-9233.
- Rabiner, E. A., Bhagwagar, Z., Gunn, R. N., Sargent, P. A., Bench, C. J., Cowen, P. J., & Grasby, P. M. (2001). Pindolol augmentation of selective serotonin reuptake inhibitors: PET evidence that the dose used in clinical trials is too low. *American Journal of Psychiatry*, 158(12), 2080-2082.
- Rabinovici, G. D., Furst, A. J., O'neil, J. P., Racine, C. A., Mormino, E. C., Baker, S. L., Chetty, S., Patel, P., Pagliaro, T. A., Klunk, W. E., Mathis, C. A., Rosen, H. J., Miller, B. L., Jagust, W. J., & Mathis, C. A. (2007). ¹¹C-PIB PET imaging in Alzheimer disease and frontotemporal lobar degeneration. *Neurology*, 68(15), 1205-1212.
- Rajendran, J. G., & Krohn, K. A. (2015, March). F-18 fluoromisonidazole for imaging tumor hypoxia: imaging the microenvironment for personalized cancer therapy. In *Seminars in Nuclear Medicine* (Vol. 45, No. 2, pp. 151-162). Elsevier.
- Ramos, C.D. (2015). ¹⁸F-fluoride PET/CT in clinical practice. *Radiologiabrasileira*, 48(4), VII-VIII.
- Reske, S. N., Blumstein, N. M., Neumaier, B., Gottfried, H. W., Finsterbusch, F., Kocot, D., Moller, P., Glatting, G., & Perner, S. (2006). Imaging prostate cancer with ¹¹C-choline PET/CT. *Journal of Nuclear Medicine*, 47(8), 1249-1254.

- Rouse, S. T., Marino, M. J., Bradley, S. R., Awad, H., Wittmann, M., & Conn, P. J. (2000). Distribution and roles of metabotropic glutamate receptors in the basal ganglia motor circuit: implications for treatment of Parkinson's disease and related disorders. *Pharmacology & Therapeutics*, 88(3), 427-435.
- Rowe, C. C., Ng, S., Ackermann, U., Gong, S. J., Pike, K., Savage, G., Cowie, T. F., Dickinson, K. L., Maruff, P., Darby, B., Smith, C., Woodward, M., Merory, J., Tochon-Danguy, H., O'Keefe, G., Klunk, W. E., Mathis, C. A., Price, J. C., Masters, C. L., & Villemagne, V. L. (2007). Imaging β -amyloid burden in aging and dementia. *Neurology*, 68(20), 1718-1725.
- Roy, K., De, A. U., & Sengupta, C. (2003). QSAR of peripheral benzodiazepine receptor ligand 2-phenylimidazo-[1, 2-a] pyridine derivatives with physico-chemical parameters. *Indian J Biochembiophys.*, 40(3), 203-208.
- Saha, G. B., & Saha, G. B. (2004). *Fundamentals of Nuclear Pharmacy* (Vol. 6, pp. 96-100). New York: Springer.
- Samanta, S., Panda, P., Alam, S. M., & Jha, T. (2007). Search for structural requirements of 2-Phenylimidazo [1, 2- α] pyridineacetamide analogues to improve affinity and selectivity towards central and/or peripheral benzodiazepine receptors. *Internet Electron J. Mol. Des*, 6, 183-199.
- Sandell, J., Halldin, C., Chou, Y. H., Swahn, C. G., Thorberg, S. O., & Farde, L. (2002). PET-examination and metabolite evaluation in monkey of [^{11}C] NAD-299, a radioligand for visualisation of the 5-HT_{1A} receptor. *Nuclear Medicine and Biology*, 29(1), 39-45.
- Seeman, P., & Van Tol, H. H. (1994). Dopamine receptor pharmacology. *Trends in Pharmacological Sciences*, 15(7), 264-270.
- Selleri, S., Bruni, F., Costagli, C., Costanzo, A., Guerrini, G., Ciciani, G., Costa, B., & Martini, C. (2001). 2-Arylpyrazolo [1, 5-a] pyrimidin-3-yl acetamides. New potent and selective peripheral benzodiazepine receptor ligands. *Bioorganic & Medicinal Chemistry*, 9(10), 2661-2671.
- Selleri, S., Gratteri, P., Costagli, C., Bonaccini, C., Costanzo, A., Melani, F., Guerrini, G., Ciciani, G., Costa, B., Spinetti, F., Martini, C., & Bruni, F. (2005). Insight into 2-phenylpyrazolo [1, 5-a] pyrimidin-3-yl acetamides as peripheral benzodiazepine receptor ligands: synthesis, biological evaluation and 3D-QSAR investigation. *Bioorganic & Medicinal Chemistry*, 13(16), 4821-4834.

- Shao, X., Wang, X., English, S. J., Desmond, T., Sherman, P. S., Quesada, C. A., & Piert, M. R. (2013). Imaging of carrageenan-induced local inflammation and adjuvant-induced systemic arthritis with [^{11}C] PBR28 PET. *Nuclear Medicine and Biology*, *40*(7), 906-911.
- Shiue, C. Y., Shiue, G. G., Cornish, K. G., & O'Rourke, M. F. (1995). PET study of the distribution of [^{11}C] fluoxetine in a monkey brain. *Nuclear Medicine and Biology*, *22*(5), 613-616.
- Shoghi-Jadid, K., Small, G. W., Agdeppa, E. D., Kepe, V., Ercoli, L. M., Siddarth, P., Read, S., Satyamurthy, N., Petric., A., Huang, S. C., & Barrio, J. R. (2002). Localization of neurofibrillary tangles and beta-amyloid plaques in the brains of living patients with Alzheimer disease. *The American Journal of Geriatric Psychiatry*, *10*(1), 24-35.
- Siegle, G. J., Thompson, W., Carter, C. S., Steinhauer, S. R., & Thase, M. E. (2007). Increased amygdala and decreased dorsolateral prefrontal BOLD responses in unipolar depression: related and independent features. *Biological Psychiatry*, *61*(2), 198-209.
- Siméon, F. G., Brown, A. K., Zoghbi, S. S., Patterson, V. M., Innis, R. B., & Pike, V. W. (2007). Synthesis and simple ^{18}F -labeling of 3-fluoro-5-(2-(2-(fluoromethyl)thiazol-4-yl) ethynyl) benzonitrile as a high affinity radioligand for imaging monkey brain metabotropic glutamate subtype-5 receptors with positron emission tomography. *Journal of Medicinal Chemistry*, *50*(14), 3256-3266.
- Singhal, T., Narayanan, T. K., Jain, V., Mukherjee, J., & Mantil, J. (2008). ^{11}C -1-methionine positron emission tomography in the clinical management of cerebral gliomas. *Molecular Imaging and Biology*, *10*(1), 1-18.
- Slobodyansky, E., Guidotti, A., Wambebe, C., Berkovich, A., & Costa, E. (1989). Isolation and Characterization of a Rat Brain Triakontatetrapeptide, a Post translational Product of Diazepam Binding Inhibitor: Specific Action at the Ro5-4864 Recognition Site. *Journal of Neurochemistry*, *53*(4), 1276-1284.
- Snyder, S. H., Verma, A. J. A. Y., & Trifiletti, R. R. (1987). The peripheral-type benzodiazepine receptor: a protein of mitochondrial outer membranes utilizing porphyrins as endogenous ligands. *The FASEB Journal*, *1*(4), 282-288.

- Sotgiu, M. L., Bellomi, P., & Biella, G. E. (2003). The mGluR₅ selective antagonist 6-methyl-2-(phenylethynyl)-pyridine reduces the spinal neuron pain-related activity in mononeuropathic rats. *Neuroscience Letters*, *342*(1-2), 85-88.
- Spooren, W. P., Vassout, A., Neijt, H. C., Kuhn, R., Gasparini, F., Roux, S., Porsolt, R. D., & Gentsch, C. (2000). Anxiolytic-like effects of the prototypical metabotropic glutamate receptor 5 antagonist 2-methyl-6-(phenylethynyl)pyridine in rodents. *Journal of Pharmacology and Experimental Therapeutics*, *295*(3), 1267-1275.
- Strasser, B., Sperner-Unterweger, B., Fuchs, D., & Gostner, J. M. (2016). Mechanisms of inflammation-associated depression: immune influences on tryptophan and phenylalanine metabolisms. In *Inflammation-Associated Depression: Evidence, Mechanisms and Implications* (pp. 95-115). Springer, Cham.
- Takahashi, K., Murakami, M., Miura, S., Iida, H., Kanno, I., & Uemura, K. (1999). Synthesis and autoradiographic localization of muscarinic cholinergic antagonist (+) N-[¹¹C] methyl-3-piperidyl benzilate as a potent radioligand for positron emission tomography. *Applied Radiation and Isotopes*, *50*(3), 521-525.
- Talbot, P. S., & Laruelle, M. (2002). The role of in vivo molecular imaging with PET and SPECT in the elucidation of psychiatric drug action and new drug development. *European Neuropsychopharmacology*, *12*(6), 503-511.
- Taliani, S., Pugliesi, I., & Da Settimo, F. (2011). Structural requirements to obtain highly potent and selective 18 kDa translocator protein (TSPO) ligands. *Current Topics in Medicinal Chemistry*, *11*(7), 860-886.
- Tang, D., Hight, M. R., McKinley, E. T., Fu, A., Buck, J. R., Smith, R. A., Tanawy, M. N., Peterson, T. E., Colvin, D., Ansari, M. S., Nickels, M., & Nickels, M. (2012). Quantitative preclinical imaging of TSPO expression in glioma using N, N-diethyl-2-(2-(4-(2-¹⁸F-fluoroethoxy) phenyl)-5, 7-dimethylpyrazolo [1, 5-a] pyrimidin-3-yl) acetamide. *Journal of Nuclear Medicine*, *53*(2), 287-294.
- Terasaki, T., Ohtsuki, S., Hori, S., Takanaga, H., Nakashima, E., & Hosoya, K. I. (2003). New approaches to in vitro models of blood-brain barrier drug transport. *Drug Discovery Today*, *8*(20), 944-954.

- Thorek, D. L., Chen, A. K., Czupryna, J., & Tsourkas, A. (2006). Superparamagnetic iron oxide nanoparticle probes for molecular imaging. *Annals of Biomedical Engineering*, 34(1), 23-38.
- Tiwari, A. K., Fujinaga, M., Yui, J., Yamasaki, T., Xie, L., Kumata, K., Mishra, A. K., Shimoda, Y., Hatori, A., Ji, B., Ogawa, M., Kawamura, K., Wang, F., & Zhang, M. R. (2014). Synthesis and evaluation of new ^{18}F -labelled acetamidobenzoxazolone-based radioligands for imaging of the translocator protein (18 kDa, TSPO) in the brain. *Organic & Biomolecular Chemistry*, 12(47), 9621-9630.
- Tiwari, A. K., Ji, B., Yui, J., Fujinaga, M., Yamasaki, T., Xie, L., Luo, R., Shimoda, Y., Kumata, K., Zhang, Y., Hatori, A., Maeda, J., Higuchi, M., Wang, F., & Zhang, M. R. (2015). [^{18}F] FEBMP: positron emission tomography imaging of TSPO in a model of neuroinflammation in rats, and in vitro autoradiograms of the human brain. *Theranostics*, 5(9), 961-969.
- Tiwari, A. K., Yui, J., Fujinaga, M., Kumata, K., Shimoda, Y., Yamasaki, T., Xie, L., Hatori, A., Maeda, J., Nengaki, N., & Zhang, M. R. (2014). Characterization of a novel acetamidobenzoxazolone-based PET ligand for translocator protein (18 kDa) imaging of neuroinflammation in the brain. *Journal of Neurochemistry*, 129(4), 712-720.
- Tiwari, A. K., Yui, J., Zhang, Y., Fujinaga, M., Yamasaki, T., Xie, L., Shimoda, Y., Kumata, K., Hatori, A., & Zhang, M. R. (2015). [^{18}F] FPBMP:—a potential new positron emission tomography radioligand for imaging of translocator protein (18 kDa) in peripheral organs of rats. *RSC Advances*, 5(123), 101447-101454.
- Trapani, G., Laquintana, V., Denora, N., Trapani, A., Lopodota, A., Latrofa, A., Franco, M., Serra, M., Pisu, M. G., Floris, I., Sanna, E., Biggio, G., & Liso, G. (2005). Structure-Activity Relationships and Effects on Neuroactive Steroid Synthesis in a Series of 2-Phenylimidazo [1, 2-a] pyridineacetamide Peripheral Benzodiazepine Receptors Ligands. *Journal of Medicinal Chemistry*, 48(1), 292-305.
- Tsukada, H., Takahashi, K., Miura, S., Nishiyama, S., Kakiuchi, T., Ohba, H., Sato, K., Hatazawa, J., & Okudera, T. (2001). Evaluation of novel PET ligands (+) N-[^{11}C] methyl-3-piperidyl benzilate ([^{11}C](+) 3-MPB) and its stereoisomer [^{11}C](-) 3-MPB for muscarinic cholinergic receptors in the conscious monkey brain: A PET study in comparison with [^{11}C] 4-MPB. *Synapse*, 39(2), 182-192.

- Tuccinardi, T., Taliani, S., Bellandi, M., Da Settimo, F., Da Pozzo, E., Martini, C., & Martinelli, A. (2009). A Virtual Screening Study of the 18 kDa Translocator Protein using Pharmacophore Models Combined with 3D-QSAR Studies. *Chem. Med. Chem.*, *4*(10), 1686-1694.
- Turkbey, B., Kobayashi, H., Ogawa, M., Bernardo, M., & Choyke, P. L. (2009). Imaging of tumor angiogenesis: functional or targeted? *American Journal of Roentgenology*, *193*(2), 304-313.
- Varrone, A., Mattsson, P., Forsberg, A., Takano, A., Nag, S., Gulyás, B., Borg, J., Boellaard, R., Tawil, N. A., Eriksson, M., Zimmermann, T., Mosgau, M. S., Thiele, A., Hoffmann, A., Lammertsma, A. A., & Halldin, C. (2013). In vivo imaging of the 18-kDa translocator protein (TSPO) with [¹⁸F] FEDAA1106 and PET does not show increased binding in Alzheimer's disease patients. *European Journal of Nuclear Medicine and Molecular Imaging*, *40*(6), 921-931.
- Veenman, L., Vainshtein, A., & Gavish, M. (2015). TSPO as a target for treatments of diseases, including neuropathological disorders. *Cell Death & Disease*, *6*(10), e1911.
- Verhoeff, N. P., Wilson, A. A., Takeshita, S., & Trop, L. (2004). In-Vivo Imaging of Alzheimer Disease β -Amyloid with [¹¹C] SB-13 PET. *The American Journal of Geriatric Psychiatry*, *12*(6), 584-595.
- Verhaeghe, J., Bertoglio, D., Kosten, L., Thomae, D., Verhoye, M., Van Der Linden, A., Wyffels, L., Stroobants, S., Wityak, J., Dominguez, C., Mrzljak, L., & Staelens, S. (2018). Noninvasive relative quantification of [¹¹C] ABP688 PET imaging in mice versus an input function measured over an arteriovenous shunt. *Frontiers in Neurology*, *9*, Article 516, 11 pages.
- Verma, A., & Snyder, S. H. (1989). Peripheral type benzodiazepine receptors. *Annual Review of Pharmacology and Toxicology*, *29*(1), 307-322.
- Vicidomini, C., Panico, M., Greco, A., Gargiulo, S., Coda, A. R. D., Zannetti, A., Gramanzini, M., Roviello, G. N., Quarantelli, M., Alfano, B., Tavitian, B., Dolle, F., Salvatore, M., Brunetti, A., & Pappata, S. (2015). In vivo imaging and characterization of [¹⁸F] DPA-714, a potential new TSPO ligand, in mouse brain and peripheral tissues using small-animal PET. *Nuclear Medicine and Biology*, *42*(3), 309-316.

- Vlychou, M., & Athanasou, N. A. (2008). Radiological and pathological diagnosis of paediatric bone tumours and tumour-like lesions. *Pathology*, *40*(2), 196-216.
- Wagner, H. N., Burns, H. D., Dannals, R. F., Wong, D. F., Langström, B., Duelfer, T Frost, J. J., Ravert H. T., Links, J. M., Rosenbloom, S. B., Lukas, S.E., Kramer, A. V., & Kuhar, M. (1984). Assessment of dopamine receptor densities in the human brain with carbon-11-labeled N-methylspiperone. *Annals of Neurology*, *15*(S1), 79-84.
- Walker, K., Reeve, A., Bowes, M., Winter, J., Wotherspoon, G., Davis, A., Gentry, A., Kesingland, A., Gasparini, F., Spooren, W., Stoehr, N., Pagano, A., Flor, P. J., Vranesic, I., Lingenhoehl, K., Johnson, E. C., Varney, M., Urban, L., Kuhn, R. (2001). mGlu5 receptors and nociceptive function II. mGlu₅ receptors functionally expressed on peripheral sensory neurones mediate inflammatory hyperalgesia. *Neuropharmacology*, *40*(1), 10-19.
- Wang, X. J., Lin, B. H., Yang, Z., Ouyang, T., Li, J. F., Xu, B., Zhang, Y., & Zhang, M. Y. (2006). Preliminary study on a new sentinel lymphoscintigraphy agent ^{99m}Tc-Rituximab for breast patient. *Chinese Journal of Oncology*, *28*(3), 200-203.
- Weissleder, R. (2006). Molecular imaging in cancer. *Science*, *312*(5777), 1168-1171.
- Weissleder, R., & Pittet, M. J. (2008). Imaging in the era of molecular oncology. *Nature*, *452*(7187), 580-589.
- Wernick, M. N., & Aarsvold, J. N. *Emission Tomography: The Fundamentals of PET and SPECT*. Orlando, FL: Academic, 2004.
- Williams, L. E. (2008). Anniversary paper: nuclear medicine: fifty years and still counting. *Medical Physics*, *35*(7 Part 1), 3020-3029.
- Willmann, J. K., Van Bruggen, N., Dinkelborg, L. M., & Gambhir, S. S. (2008). Molecular imaging in drug development. *Nature Reviews Drug Discovery*, *7*(7), 591-607.
- Woods, M. J., Zisterer, D. M., & Williams, D. C. (1996). Two cellular and subcellular locations for the peripheral-type benzodiazepine receptor in rat liver. *Biochemical Pharmacology*, *51*(10), 1283-1292.

- Xia, W., Ray, W. J., Ostaszewski, B. L., Rahmati, T., Kimberly, W. T., Wolfe, M. S., Zhang, J., Goate, A. M., & Selkoe, D. J. (2000). Presenilin complexes with the C-terminal fragments of amyloid precursor protein at the sites of amyloid β -protein generation. *Proceedings of the National Academy of Sciences*, 97(16), 9299-9304.
- Xie, L., Yamasaki, T., Ichimaru, N., Yui, J., Kawamura, K., Kumata, K., Hatori, A., Nonomura, N., Zhang, M. R., Li, X. K., & Takahara, S. (2012). [^{11}C] DAC-PET for Noninvasively Monitoring Neuroinflammation and Immunosuppressive Therapy Efficacy in Rat Experimental Autoimmune Encephalomyelitis Model. *Journal of Neuroimmune Pharmacology*, 7(1), 231-242.
- Yui, J., Maeda, J., Kumata, K., Kawamura, K., Yanamoto, K., Hatori, A., Yamasaki, T., Nengaki, N., Higuchi, M., & Zhang, M. R. (2010). ^{18}F -FEAC and ^{18}F -FEDAC: PET of the monkey brain and imaging of translocator protein (18 kDa) in the infarcted rat brain. *Journal of Nuclear Medicine*, 51(8), 1301-1309.
- Zhang, S., Merritt, M., Woessner, D. E., Lenkinski, R. E., & Sherry, A. D. (2003). PARACEST agents: modulating MRI contrast via water proton exchange. *Accounts of Chemical Research*, 36(10), 783-790.
- Zheng, J., Klinz, S. G., De Souza, R., Fitzgerald, J., & Jaffray, D. A. (2015). Longitudinal tumor hypoxia imaging with [^{18}F] FAZA-PET provides early prediction of nanoliposomal irinotecan (nal-IRI) treatment activity. *EJNMMI research*, 5(1), 57.
- Ziemus, B., Baumann, O., Luerding, R., Schlosser, R., Schuierer, G., Bogdahn, U., & Greenlee, M. W. (2007). Impaired working-memory after cerebellar infarcts paralleled by changes in BOLD signal of a cortico-cerebellar circuit. *Neuropsychologia*, 45(9), 2016-2024.
- Zubieta, J. K., Koeppe, R. A., Frey, K. A., Kilbourn, M. R., Mangner, T. J., Foster, N. L., & Kuhl, D. E. (2001). Assessment of muscarinic receptor concentrations in aging and Alzheimer disease with [^{11}C] NMPB and PET. *Synapse*, 39(4), 275-287.

List of Publications/ Conferences

PUBLICATIONS

Publications from Thesis

1. **Srivastava, P.**, Kumari, N., Kakkar, D., Kaul, A., Kumar, P., & Tiwari, A. K. (2019). Comparative evaluation of ^{99m}Tc -MBIP-X/11[C]-MBMP for visualization of 18 kDa translocator protein. *New Journal of Chemistry*, 43, 11288-11295. (IF: 3.069)
2. **Srivastava, P.**, Kakkar, D., Kumar, P., & Tiwari, A. K. (2019). Modified benzoxazolone (ABO-AA) based single photon emission computed tomography (SPECT) probes for 18 kDa translocator protein. *Drug Development Research*, 2019, 1-9. (IF: 1.742)
3. **Srivastava, P.**, Kumar, P., & Tiwari A. K. (2019). Design, synthesis and in silico evaluation of methyl 2-(2-(5-bromo/chloro-2-oxobenzooxazol-3(2H)-yl)acetamido)-3-phenylpropanoate for TSPO targeting, *Radiochemistry*, Accepted.
4. **Srivastava, P.**, Kaul, A., Ojha, H., Kumar, P., & Tiwari, A. K. (2016). Design, synthesis and biological evaluation of methyl-2-(2-(5-bromo benzoxazolone) acetamido)-3-(1H-indol-3-yl) propanoate: TSPO ligand for SPECT. *RSC Advances*, 6(115), 114491-114499. (IF: 3.049)

Other publications

5. Kumari, N., Chadha, N., **Srivastava, P.**, Mishra, L. C., Bhagat, S., Mishra, A. K., & Tiwari, A. K. (2017). Modified benzoxazolone derivative as 18-kDa TSPO ligand. *Chemical Biology & Drug Design*, 90(4), 511-519. (IF= 2.256)

Conferences Abstract

1. **Srivastava, P.**, Tiwari, A. K., Kaul, A., & Mehra, L. Evaluation of acetamidobenzoxazolone derivatized biomarkers for assessing translocator protein in brain and peripheral organs, 50th Annual Conference of the Society of Nuclear Medicine, India (SNMICON2018), 22-25 Nov, 2018, Chandigarh
2. Tiwari, A. K., **Srivastava, P.**, Kumar, P., Mishra, A. K. Modified third generation translocator protein-selective positron emission tomography radiotracer to access microglial activation in ischemic rat brain, 50th Annual Conference of the Society of Nuclear Medicine, India (SNMICON2018), 22-25 Nov, 2018, Chandigarh
3. **Srivastava, P.**, Faheem, M., Singh, V. K., Kumar, A., & Mittal, G. Synthesis of biocompatible hydrogel based on CMCNa salt-system crosslinked with EDTA and enhances the absorbing property by PEG, Recent approaches and innovations in Chemical Sciences (RAICS), Nov, 2018, Lucknow (Third Prize)
4. **Srivastava, P.**, Kaul, A., Faheem, M., Kumar, P., & Tiwari, A. K. Acetamidobenzoxazolone (ABO) based derivative for assessment of Translocator Protein (18 kDa) for brain injury/inflammation, 49th Annual Conference of the Society of Nuclear Medicine, India (SNMICON2017), 14-17 Dec, 2017, Delhi
5. Kumari, N., **Srivastava, P.**, Bhagat, S., & Tiwari, A. K. N₄ vehicle based acetamidobenzoxazolone derivative for imaging of Translocator Protein (18 kDa) during inflammatory condition, Indian J Nucl Med. 2015 Dec; 30 (Suppl 1): S29–S72, Lucknow



CrossMark
click for updates

Cite this: *RSC Adv.*, 2016, 6, 114491

Received 2nd August 2016
Accepted 22nd November 2016

DOI: 10.1039/c6ra19514h

www.rsc.org/advances

Design, synthesis and biological evaluation of methyl-2-(2-(5-bromo benzoxazolone)acetamido)-3-(1*H*-indol-3-yl)propanoate: TSPO ligand for SPECT†

Pooja Srivastava,^{*ab} Ankur Kaul,^a Himanshu Ojha,^a Pravir Kumar^b and Anjani K. Tiwari^{*a}

The translocator protein (TSPO, 18 kDa), a transmembrane mitochondrial protein, has been explored as an important biomarker by researchers because of its involvement in inflammation, immune modulation and cell proliferation. Recently, our group has explored a modified benzoxazolone derivative for diagnostic applications that has overcome few problems of first and second generation TSPO PET ligands. In this study, a new skeleton acetamidobenzoxazolone–indole, a conjugation of two TSPO pharmacophoric moieties benzoxazolone and indole, has been designed, synthesized and evaluated for TSPO targeting for SPECT. The methyl-2-(2-(5-bromo benzoxazolone)acetamido)-3-(1*H*-indol-3-yl)propanoate (MBIP) ligand was designed on the basis of pharmacophore modeling done on benzoxazolone based TSPO ligands which was then validated computationally for TSPO binding through docking studies (PDB ID: 4RYO, 4RYQ, and 4UC1) which showed a comparable Glide G_{score} as compared to known ligands like PK11195, PBR28, and FGIN-127. MBIP was synthesized by amidation reaction of 2-(5-bromo-benzoxazolone)acetic acid with tryptophan methyl ester hydrochloride (yield 62%). The compound was synthesized and characterized using spectroscopic techniques like ¹H-NMR, ¹³C-NMR, and mass spectroscopy. Purification was carried out by column chromatography and analytical HPLC (purity > 97%). The purified compound was labelled with ^{99m}Tc (radiochemical yield > 96%). The radiolabelled compound showed >94% stability in solution and >91% stability in serum after 24 h indicating the stable nature of the radio complex. A biodistribution study on BALB/c mice showed uptake of ^{99m}Tc-MBIP in TSPO rich organs and appropriate pharmacokinetics of excretion and release for a SPECT agent. Further evaluation of the ^{99m}Tc-MBIP may prove it as a potential candidate for TSPO targeting using SPECT.

1. Introduction

Inflammation is linked to the preliminary stage of many complications of diseases associated with lung inflammatory diseases, chronic obstructive pulmonary disease, acute liver damage, immune response to heart, brain injury, neurodegenerative diseases, psychiatric disorders and cancer.^{1–8} Peripheral benzodiazepine receptor (PBR), renamed as translocator protein (TSPO, 18 kDa),⁹ has been found to be an important biomarker for inflammation in the TSPO enriched organs. Recent investigations of TSPO in various biological processes and its importance in certain pathological situations due to altered concentration has led to development of various ligands for diagnostic purposes.^{10–14}

Various radionuclides have been tried for diagnostic applications by targeting TSPO such as ¹¹C and ¹⁸F for positron emission tomography (PET),^{15–21} ¹²³I and ^{99m}Tc for single photon emission computed tomography (SPECT).^{22–27} Other nuclides such as Eu³⁺ and Gd³⁺ have also been tried for optical and magnetic resonance imaging (MRI), respectively.^{28,29} Different classes of TSPO ligands, for example, isoquinoline carboxamides, indoleacetamides, pyrazolopyrimidines, imidazolepyridines, benzodiazepines and benzoxazolone analogs have been developed.^{30,31} Till date no ligand has been found ideal for human application throughout the globe. Few first generation ligands, such as PK11195 showed poor specificity and poor signal-to-noise ratio. Although second generation ligands, such as PBR28, DAA1106, DPA713, and PBR111 demonstrated improved signal-to-noise ratio but suffered from inter subject variability. This inter subject variability was attributed to rs6971 polymorphism in TSPO gene which results into single amino acid substitution *i.e.* Ala147Thr.³² This amino acid substitution constitute three classes in terms of binding affinity: high affinity binder (HAB) having alanine at 147, low affinity binder (LAB) having threonine at 147 and mixed affinity binder (MAB) having alanine and threonine both. Low-binding affinity TSPO is present in 30% of Caucasians and 25% of Africans.²⁰

^aDivision of Cyclotron and Radiopharmaceutical Sciences, Institute of Nuclear Medicine and Allied Sciences, Brig. S. K. Mazumdar Road, Delhi-110054, India. E-mail: pshree_14@yahoo.co.in; anjani7797@rediffmail.com; Fax: +91-11-23919509; Tel: +91-11-23905362; +91-11-23905387

^bMolecular Neuroscience and Functional Genomics Laboratory, Department of Biotechnology, Delhi Technological University, Delhi 110042, India

† Electronic supplementary information (ESI) available. See DOI: 10.1039/c6ra19514h

^{11}C and ^{18}F labeling have their own limitations as they require on site cyclotron to produce the radioisotopes. $^{99\text{m}}\text{Tc}$, an ideal single photon of 140 keV emitting radionuclide with half life of 6 h, has lesser radiation burden as compared to PET radionuclide and is generated through $^{99}\text{Mo}/^{99\text{m}}\text{Tc}$ generator. Although number of TSPO ligands have been synthesized but few of them have been modified for diagnostic purposes using metals for example $^{99\text{m}}\text{Tc}$, ^{188}Re , Gd^{3+} and Eu^{3+} etc.^{24–29} As these metal based ligands have been used for receptor targeting, this aspect can be further explored for TSPO. Some modification on quinoline carboxamide²⁵ and imidazolepyridines^{24,26} have been reported with $^{99\text{m}}\text{Tc}$ for SPECT application which are the basis of TSPO ligands like analogues of PK11195 and CB86, respectively.

Recently, acetamidobenzoxazolone based skeleton, developed from first generation ligand RoS-4864 has been used by our group for the development of PET ligand [^{11}C]MBMP and [^{18}F]FEBMP with improved TSPO targeting properties over (R) [^{11}C]PK11195.^{18–21} MBMP/FEBMP skeleton has shown favourable biodistribution pattern, high *in vitro* and *in vivo* specific binding for TSPO and has overcome the problem of intersubject variability. In our previous studies human postmortem brains of HABs and LABs were used for *in vitro* autoradiographic studies of MBMP/FEBMP. The binding ratios of (R) [^{11}C]PK11195, [^{11}C]DAA1106, [^{11}C]AC-5216, and [^{11}C]PBR28, for HAB to that of LAB were approximately 0.45, 1.19, 4.60, and 11.1, respectively, showing excellent correlation with the K_i ratios of these ligands for LAB to that of HAB. The compound [^{18}F]FEBMP has shown binding ratio of LAB to that of HAB as 0.9. This study presents [^{18}F]FEBMP as a promising TSPO ligand and skeleton for new ligands with negligible effect of rs6971 polymorphism on binding towards TSPO.²⁰

Taking lead from this work, we have developed a new SPECT ligand using $^{99\text{m}}\text{Tc}$ for TSPO imaging. We have introduced a new skeleton acetamidobenzoxazolone indole propanoate as a TSPO ligand by conjugating acetamidobenzoxazolone moiety present in MBMP with indole moiety present in TSPO ligand, FGIN-127.³⁰ MBMP and FGIN-127 both display TSPO affinity in nanomolar range. The affinity of MBIP towards TSPO has been validated through docking studies using wild type as well as mutant PDBs of TSPO. Thereafter, newly designed potential TSPO ligand was synthesized through a simple and efficient four steps synthetic procedure which was characterized by NMR, mass and purified by HPLC. The purified compound was radiolabelled with $^{99\text{m}}\text{Tc}$ for biological evaluation. Stability of complex for *in vivo* application was evaluated in serum and biodistribution study was performed to evaluate its % uptake with time in TSPO enriched organs.

2. Materials and methods

2.1. Chemistry

2.1.1. Chemicals. All the chemicals and solvents were purchased from Sigma-Aldrich and Merck. $^{99\text{m}}\text{Tc}$ was procured from Regional Centre for Radiopharmaceuticals, Board of Radiation and Isotope Technology (BRIT), Department of Atomic Energy, India. Column chromatography was carried out using silica MN60 having mesh 60–120, thin layer

chromatography (TLC) on aluminium plates coated with silica gel 60 F₂₅₄ and instant thin layer chromatography silica gel (ITLC-SG) was used for identification of labeling, purity and R_f of radiocomplex.

2.1.2. Instrumentation. ^1H and ^{13}C NMR spectra were recorded on Bruker Avance II 400 MHz system at 400 MHz and 100 MHz, respectively. Mass spectroscopy was done on 6310 system of Agilent using ESI positive mode. γ -Scintigraphic studies were done on Hawkeye Camera and a γ -scintillation counter was used for counting radioactivity. High performance liquid chromatography (HPLC) was carried out on 1200 series of Agilent using analytical T3 Waters column (4.6 \times 250 mm) for analysis and C-18 column (21.2 \times 150 mm) for purification. SPECT images were taken on GE Triumph system.

2.1.3. Animal models. Animal protocols were approved by the Institutional Animal Ethics Committee (INM/DASQA/IAEC/09/015). BALB/c mice (22–28 g) were used for animal experiments.

2.1.4. Pharmacophore hypothesis generation. The pharmacophore hypothesis was developed by aligning pharmacophoric features of 51 TSPO ligands retrieved from the literature^{33,34} using PHASE, Schrödinger, Maestro LLC 9.1 software. Generation of conformers was carried out with the help of MacromodelConfGen using OPLS2005 force field with rapid torsional search. Geometric alignment of site points in the active molecules to the site points in the hypothesis was the basis of hypothesis score generation. Each active molecule conformer generates hypothesis. Scores of the compounds were determined by 3D-QSAR model developed from compounds by aligning on the hypothesis. PLS analysis was carried out to evaluate the pharmacophore hypothesis using atom-based PHASE QSAR models generation with a maximum of three PLS factors for each pharmacophore type. Best hypothesis was further used for designing the TSPO ligand.

2.1.5. Docking studies. To design modified TSPO ligand, docking studies for ligand–protein interaction were carried out with extra precision (XP) mode of GLIDE, Schrödinger, Maestro LLC 9.1 software. Structures of ligands were drawn using ChemBioDraw. We have chosen wild type (4RYO and 4RYQ) as well as mutant (4UC1) PDBs for docking studies from different sources such as BcTSPO and RstTSPO. The rs6971 polymorphism in human resulting in A147T single amino acid change is equivalent to A139T in RstTSPO. Ultra 10.0.LigPrep and protein preparation modules were used for ligands and protein preparation, respectively. Protein preparation module consists of a series of steps that perform preprocess, optimization and minimization of protein structure. Receptor grids generation were required for docking with ligands. OPLS2005 forcefield has been used for the receptor grid as well as ligand grid generation. Docking simulation was performed in implicit solvent.

The ligand strain energy is the difference between the energy of the ligand as it is in the complex and the energy of the extracted ligand, minimized, starting from the geometry in the refined complex. This local strain energy is used for comparison of different poses of the same ligand. Calculations to assess the strain were performed in implicit solvent.

2.1.6. Synthesis

2.1.6.1 Synthesis of 2-(2-(5-bromo benzoxazolone)acetamido)-3-(1H-indol-3-yl)propanoate, 5 (MBIP). 2-(5-Bromo-benzoxazolone)acetic acid was synthesized as per Scheme 1 by following the procedure reported in the literature.³³ To a solution of 2-(5-bromo-benzoxazolone)acetic acid (250 mg, 0.92 mmol) in DMF (5 ml), tryptophan methyl ester hydrochloride (351.2 mg, 1.38 mmol), HOBt (124.2 mg, 0.92 mmol) and EDCl (264.3 mg, 1.38 mmol) were added at room temperature and stirred for 7 h. Subsequently, water was added and the mixture was extracted using a toluene and ethyl acetate (1 : 1). Water and brine were used for washing of organic layer and subsequently anhydrous Na₂SO₄ was added for drying. After filtration, the solvent was removed *in vacuo* and purification of residue was carried out on silica gel column chromatography using CHCl₃/EtOAc (4 : 1 v/v) as eluent to give amide as a white solid (MBIP: yield 62%). Chemical purity > 97% by HPLC: T3 column, 4.6 × 250 mm; MeCN/H₂O, 6/4–8/2 (v/v); flow rate: 0.8 ml min⁻¹; λ_{uv} = 254 nm; t_R = 8.75 min.

¹H-NMR (DMSO, 400 MHz): δ (ppm) 3.10–3.16 (2H, m), 3.59 (3H), 4.47–4.53 (3H, s), 7.00–7.50 (8H, m), 8.85–8.87 (1H, d), 10.90 (1H, s).

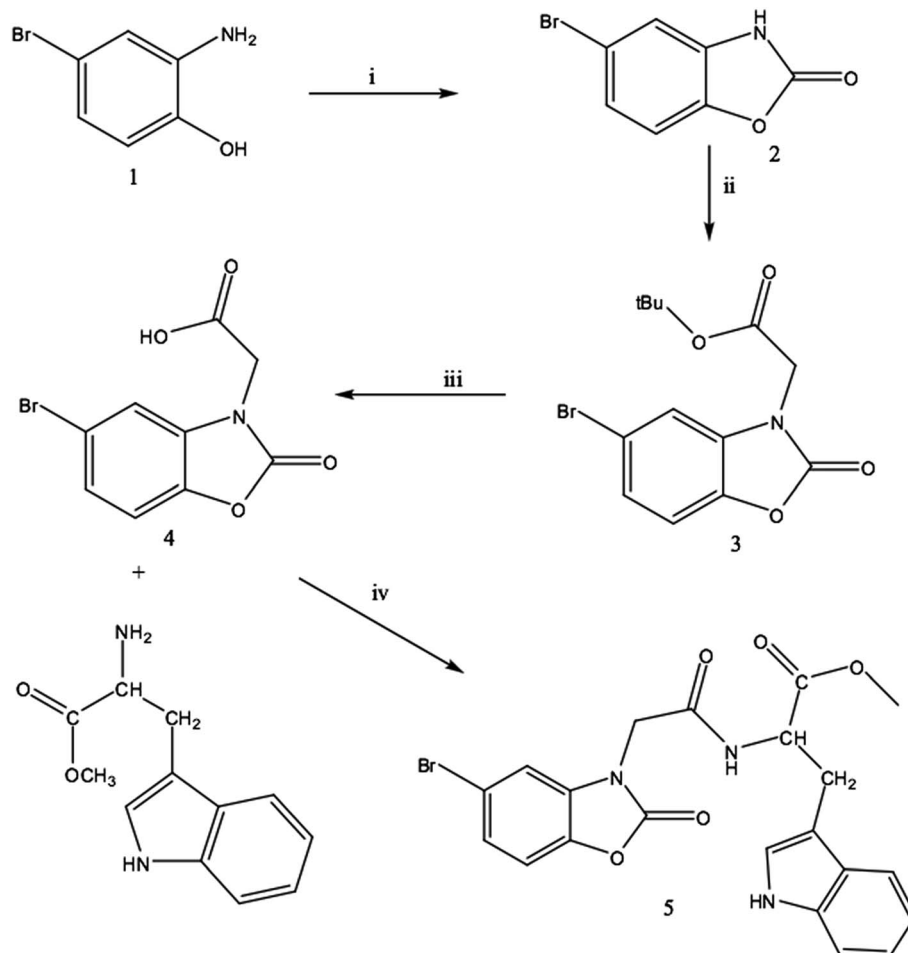
¹³C-NMR (DMSO, 100 MHz): δ (ppm) 28.72 (CH₂-CH), 44.41 (CH₃-O), 52.44 (NH-CH-C=O), 53.91 (N-CH-C=O), 111–

141.52 (14 carbon of aromatic rings), 154.15 (O-C=O-N), 166.28 (NH-C=O), 172.35 (O-C=O).

MS (ESI) *m/z*: 496.3 [M + Na]⁺; calculated mass 496.38 [M + Na]⁺.

2.1.6.2 Radiosynthesis. 200 μl solution of the compound (0.03 nM) was added in SnCl₂·2H₂O (1 × 10⁻² M) (purged nitrogen 10% acetic acid (1 ml)). Thereafter, 75 MBq, 100 μl saline solution of sodium pertechnetate (freshly eluted NaTcO₄) was added. The pH was adjusted to 7.0 by addition of 0.1 M NaHCO₃ solution to the reaction mixture and the contents were shaken manually. Vial was kept at room temperature for 20–30 min. ^{99m}Tc complex's labeling, chemical purity and R_f were determined by ITLC-SG strips by using developing solvents such as acetone and PAW (pyridine, acetic acid and water in 3 : 5 : 1.5 ratio) simultaneously. 0.1 cm segments of ITLC were taken for count measurement to find out the percentage of free and labeled ligand *i.e.* radiochemical purity.

2.1.7. In vitro serum stability assay. Blood was collected from healthy volunteers and was made to clot in a humidified incubator maintained at 5% carbon dioxide and 95% air at 37 °C for 1 h and was used to prepare serum. Centrifugation of sample at 400 rpm was followed by filtration through 0.22 μm syringe and filtrate was kept into sterile plastic culture tubes.



Scheme 1 Chemical synthesis. Reagents and conditions: (i) CDI, THF, rt; (ii) ^tbutylbromoacetate, K₂CO₃, DMF, 70 °C; (iii) HCl, dioxane, AcOH, 50 °C; (iv) tryptophan methyl ester hydrochloride, EDCl, HOBt, DMF, rt.

Incubation of the freshly prepared radiocomplex in fresh human serum was done at physiological conditions *i.e.* at 37 °C (concentration 100 nM ml⁻¹) and then it was analyzed by ITLC-SG to detect any dissociation of the complex at different time intervals. Percentage dissociation of the complex was determined by calculating percentage of free pertechnetate at a particular time by using saline and acetone as mobile phases. This represents percentage dissociation of the complex at that particular time point in serum.

2.1.8. Biodistribution studies. Tissue distribution studies were performed on BALB/c mice. All the guidelines of the Institutional Animal Ethics Committee were followed during animal handling and experimentation. Radiolabelled compound was injected in mice through tail vein (10 µCi). Mice were sacrificed at six time intervals (5 min, 15 min, 30 min, 60 min, 120 min, and 1440 min), blood was collected and different organs (brain, heart, lung, liver, spleen, kidney, stomach and intestine) were dissected for analysis. Radioactivity was measured in the gamma counter. Radioactivity injected in each mouse was found out by subtracting the activity left in tail from the activity injected. Radioactivity found in each organ was expressed as percentage administered dose per gram (% ID per g) of tissue. Blood volume was calculated as 7% of the total body weight. Decay correction was applied to radioactivity measurements.

2.1.9. Preparation of mice model. The inflammatory model was prepared as per previous literature.^{35–39} 10 weeks old male BALB/c mice of 22–25 g weight were taken to develop inflammation model. 40 µl of *E. coli* lipopolysaccharide (5 mg kg⁻¹) in PBS was administered intranasally in each mouse. Mice were housed under a 12 h dark–light cycle and were allowed free access of food pellets and water. After 24 h the mice were used for animal studies.

For *ex vivo* biodistribution blocking evaluation, three different concentration of TSPO ligand (PK11195) 2.5 mg kg⁻¹, 5 mg kg⁻¹, and 10 mg kg⁻¹ were injected 10 min prior to ^{99m}Tc-MBIP injection (100 µl of 1 mg kg⁻¹). All the experiments were performed in triplicate set (*n* = 3). During this study 5 mg kg⁻¹ blocking was found most appropriate that is why it was taken for *in vivo* imaging at 40 min post radioligand intravenous injection.

3. Result and discussion

MBIP, acetamidobenzoxazolone–indole based ligand designed on the basis of pharmacophore modeling and docking studies, has been synthesized as per Scheme 1 and radiolabelled with ^{99m}Tc for its evaluation as a diagnostic agent for TSPO targeting whose concentration is perturbed during inflammation in TSPO enriched organs. The stability of ^{99m}Tc complex, biodistribution and serum stability studies of the ligand were found appropriate for SPECT application.

Ligand based drug design makes use of the knowledge of other known ligands for same target. These ligands could provide information about minimum structural characteristics necessary for binding with biological target in terms of pharmacophoric model. This model/hypothesis could be useful in

designing new ligands. Pharmacophore model was developed with TSPO ligands having benzoxazolone to understand the key features responsible for affinity. *K_i* values taken for all the ligands were studied against TSPO of the kidney membrane.

As per our previous findings about acetamidobenzoxazolone pharmacophore based skeleton was found suitable for new TSPO ligand which is not affected by intersubject variability. Besides that Fukaya and others³³ have also confirmed that appropriate hydrophobic/acceptor groups attached with benzoxazolone and acetamide have potential to bind TSPO selectively in nM concentration.

Different pharmacophoric features like hydrogen bond donor (D), acceptor (A), hydrophobic group (H), and aromatic ring (R) were chosen to generate the hypothesis. The 51 TSPO ligands were divided into test set and training set with 13 and 38 ligands, respectively. Ligands of these sets were aligned with each other to find the pharmacophore and thereafter PLS analysis was performed. Hypothesis AAAR showed best result in terms of predictive ability and internal validation (Fig. 1) with *R*² = 0.95 and standard deviation in the range of 0.237 to 0.760. This hypothesis was further utilized for designing of new ligand.

Based on these concepts we have designed MBIP as TSPO ligand. A substituent on the benzoxazolone derivative specifically at C-5 position of phenyl ring plays an important role in TSPO binding. Substitution by halogen in place of aromatic ring system at this position provides sub-nanomolar binding affinity.³³ This is the rationale behind selecting Br for C-5 position for designing the benzoxazolone ring. This has also been mentioned in literature that compound suffered from poor solubility due to phenyl substituent at acetamida side. We have tried biocompatible amino acid analogue at this position

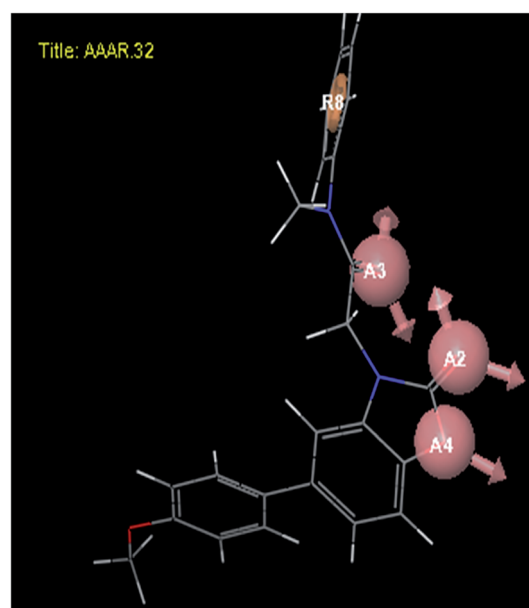


Fig. 1 Pharmacophore model AAAR used for designing TSPO ligand derived from the benzoxazolone derivatives. Pharmacophoric features with colour code: A–hydrogen bond acceptor (pink) and R–aromatic moiety (orange).

to solve solubility issue for better prospect of clinical application in future. The R contained in MBIP is also present in TSPO ligands-FGIN-127 which has nanomolar binding affinity for TSPO. Its limited *in vivo* use is due to its high lipophilicity. The designed ligand MBIP showed decreased computational log *P* (2.31) value as compared to FGIN-127 (computational log *P* = 6.94).³⁰

The intersubject variability issue for MBIP has been studied computationally by taking 2 wild type PDBs (4RYO and 4RYQ) and one mutant PDB (4UC1) representing required SNP for docking studies. MBIP has shown good interactive score (G_{score}) for wild type and mutant PDBs similar to PK11195 and FEBMP which are successful ligands against intersubject variability (ESI†). The validation of docking protocol was done before docking the compounds with PDB. The ligand present in co-crystallized PDB was removed and docked with binding site. The root mean square deviation between predicted and observed X-ray crystallographic conformers was found to be around 0.5 Å predicting the reproduction of binding mode of docked compound using this docking protocol.

After designing, the next step is validation for TSPO binding/affinity which was carried out through docking studies to gain better insight of its interaction with TSPO as compared to other known TSPO ligands. MBIP demonstrated comparable or better affinity with TSPO in terms of G_{score} (−10.448 for MBIP > −7.451 to −10.15 for other known ligands) (Table 1). Both the parent ligands FEBMP and FGIN-127 have G_{score} −10.151 and −9.319, respectively on docking with TSPO. The MBIP interaction with 4RYO has been reflected in their interactions shown in 2D and 3D interaction diagram (Fig. 2). Various interactions were observed in docking including pi–pi interaction with Phe90 and Phe95, hydrogen bonding with Gly44 and Ser22. Both the aromatic rings were participating in pi–pi interactions. One hydrogen bond was observed due to NH of indole moiety in the ligand. These interactions were different from interactions of MBMP and its fluoro analog with TSPO (Try27, Tyr28, Phe19 and Try99).¹⁹

Table 1 Glide G_{score} of MBIP and other known TSPO ligands on docking with TSPO (PDB ID: 4RYO). Docking was performed using extra precision mode of GLIDE, Schrödinger, Maestro LLC 9.1 software

Ligand	G_{Score}
MBIP	−10.448
DAA1106	−9.493
DIAZEPAM	−7.451
DPA713	−6.180
FEBMP	−10.151
FEDAA1106	−9.809
FGIN-127	−9.319
FPBMP	−9.633
PBR28	−9.658
PBR111	−7.475
PK11195	−9.881
RO5-4864	−9.034
SSR180575	−7.992
XBD173	−9.406

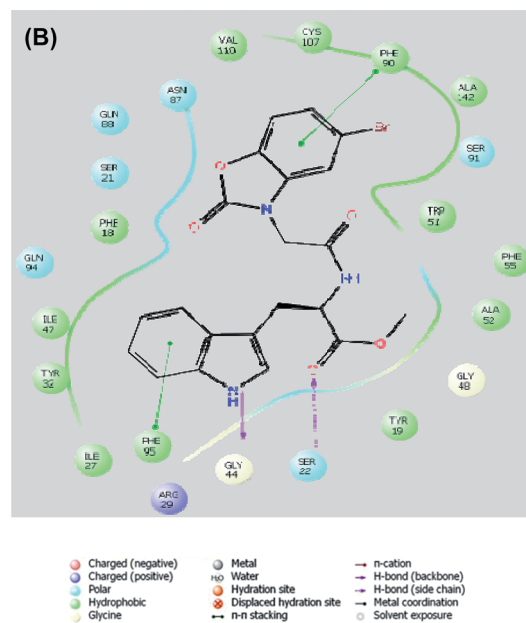


Fig. 2 3D (A) and 2D (B) interaction diagram of MBIP on docking with TSPO (PDB ID: 4RYO). Docking was performed using extra precision mode of GLIDE, Schrödinger, Maestro LLC 9.1 software. MBIP formed pi–pi interactions of aromatic rings with Phe90 and Phe95 and hydrogen bond interactions with Gly44 and Ser22.

BcTSPO-PK11195 model showed interaction between oxygen of carbonyl group of PK11195 with indole groups of Try51 and Try138, van der Waal interaction with Ser22, Tyr32, Pro42, Ile47, Phe55, Phe90, Ser91, Gln94, Cys107, Ala142 and Leu145. Few of the interaction of PK11195 as on Ser22 and Phe90 were similar to MBIP interactions with TSPO protein.⁴⁰ MBIP and FEBMP both the compounds have shown similar binding modes. The C=O of benzoxazolone forms H-bond with the Try51 in 4RYQ. This is in agreement with the interaction of PK11195 with

4RYQ. Few more interaction sites are common to MBIP in 4RYO and 4RYQ such as Ser22, Phe55, Phe90, Ser91, Gln94, Cys107, Ala142. Their glide G_{score} and their contribution from different sub interactions were found comparable (ESI†).

The precursor 2-(5-bromo-benzoxazolone)acetic acid of compound MBIP was synthesized in three steps starting from 4-bromo-2-amino phenol by the procedure reported in the literature.³³ In the last step, the ligand 2-(2-(5-bromo benzoxazolone)acetamido)-3-(1*H*-indol-3-yl)propanoate was synthesized through amidation reaction of 5-bromo-benzoxazolone acetic acid and tryptophan methyl ester hydrochloride in the presence of HOBt and EDCl. The yield of the final product was 62% and was purified using column chromatography and preparative HPLC. The retention time of final product MBIP was found to be 8.75 min. The chemical purity of the compound was determined using analytical HPLC and purity was found to be >97%. In the ¹H-NMR, two singlet NH peaks of same intensity were observed at 8.8 and 10.9 ppm which correspond to NH of amide and NH of indole, respectively. This indicates the successful synthesis of the proposed structure. All the eight aromatic protons of benzoxazolone and indole moieties were observed in the region 6–8 ppm. ¹³C-NMR reflected appropriate peaks as per its formula. Three C=O peaks were observed at 172.3, 166.2 and 154.1 ppm which correspond to ester C=O, amide C=O and

benzoxazolone C=O, respectively. MS run in the positive mode has peak at 496.3 [M + Na]⁺ which was in accordance with the proposed structural formula. After synthesis, biological evaluation was performed by tracer method using ^{99m}Tc. The radiolabelling study was carried out with the procedure reported in our previous work.⁴¹ Stability of the complex is one of the most important criteria for use of the ligand *in vivo* as it avoids metabolite formation and transchelation which changes the desired property for SPECT application. Complexation of the synthesized ligand with ^{99m}Tc gave sufficient stability over 24 h (Fig. 3). *In vitro* serum stability clearly indicates the stable nature of radio complex without any transchelation to serum protein like albumin which was observed to be >91% intact after 24 h (Fig. 4). Stability studies showed requisite stability of the complex to act as a SPECT agent.

Biodistribution using radiocomplex was carried out to have an idea whether the radioligand is reaching the organs of interest which are rich in TSPO and its excretion from the body. The distribution in different organs is represented as percentage of injected dose per organ at different time points. Table 2 showed the distribution of radioactive compound at six different time points post injection into the mice ($n = 3$). At 5 min, peak value of activity was recorded in all the organs. Highest % ID per g was observed in liver *i.e.* 28.87 followed by

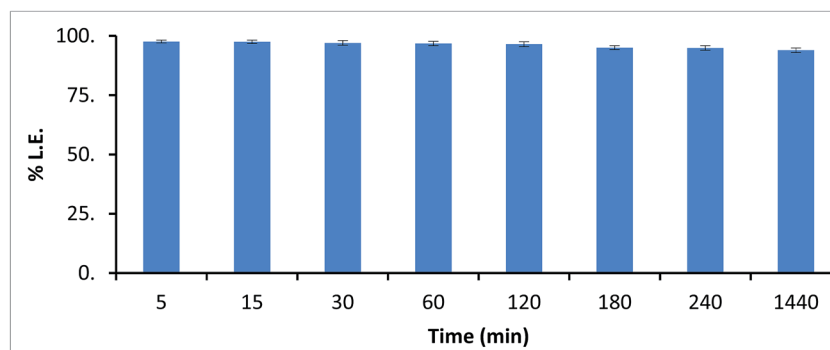


Fig. 3 Labeling efficiency (% LE) of MBIP with ^{99m}Tc. NaTcO₄ at pH 7 was used for labeling. 0.1 cm segment of ITLC were used after developing it in solvents acetone and PAW (pyridine, acetic acid and water in 3 : 5 : 1.5 ratio) for count measurement.

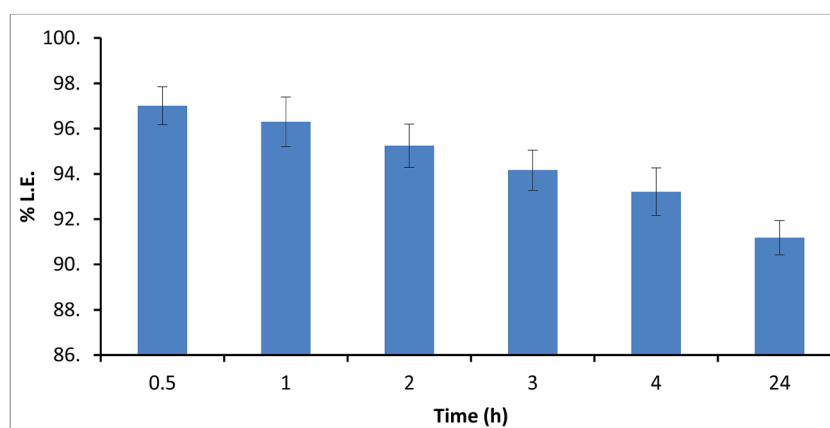


Fig. 4 Serum stability study in terms of labeling efficiency (% LE) of ^{99m}Tc-MBIP over 24 h. Studies were performed in fresh human serum from healthy volunteers at physiological conditions *i.e.* 37 °C.

Table 2 Biodistribution of ^{99m}Tc -MBIP in normal BALB/c mice. Mice ($n = 3$) received 10 μCi of ^{99m}Tc -MBIP by tail vein injection. Radioactivity uptake in different organs were measured by gamma counting and expressed as % ID per g, mean \pm standard deviation

Organ/tissue	5 min	15 min	30 min	60 min	120 min	1440 min
Blood	2.23 \pm 0.11	1.62 \pm 0.08	1.84 \pm 0.09	1.02 \pm 0.09	0.98 \pm 0.05	0.65 \pm 0.05
Brain	0.06 \pm 0.01	0.04 \pm 0.01	0.04 \pm 0.01	0.03 \pm 0.02	0.03 \pm 0.01	0.01 \pm 0.01
Heart	0.72 \pm 0.04	0.72 \pm 0.04	0.49 \pm 0.02	0.37 \pm 0.02	0.02 \pm 0.02	0.16 \pm 0.01
Lungs	5.20 \pm 0.26	4.70 \pm 0.23	3.15 \pm 0.16	1.33 \pm 0.16	0.94 \pm 0.07	0.29 \pm 0.05
Liver	28.87 \pm 1.44	23.12 \pm 1.16	21.50 \pm 1.07	18.21 \pm 1.07	12.07 \pm 0.91	9.62 \pm 0.60
Spleen	10.25 \pm 0.51	6.88 \pm 0.34	5.18 \pm 0.26	4.97 \pm 0.26	3.42 \pm 0.25	1.72 \pm 0.17
Kidney	11.19 \pm 0.56	4.57 \pm 0.23	3.50 \pm 0.17	2.27 \pm 0.17	1.09 \pm 0.11	0.90 \pm 0.05
Stomach	0.55 \pm 0.03	0.29 \pm 0.01	0.46 \pm 0.02	0.30 \pm 0.02	0.04 \pm 0.02	0.23 \pm 0.01
Intestine	0.53 \pm 0.03	0.45 \pm 0.02	0.45 \pm 0.02	0.30 \pm 0.02	0.02 \pm 0.02	0.08 \pm 0.01

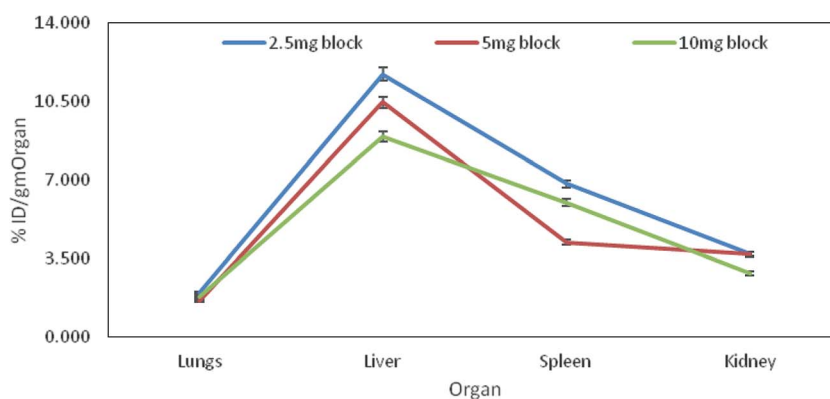


Fig. 5 ^{99m}Tc -MBIP ex vivo biodistribution in lung, liver, spleen and kidney at 40 min post i.v. injection with 10 min preadministration of 2.5/5/10 mg kg^{-1} PK11195 as blocking agent.

kidney, spleen and lung which were 11.19, 10.25, and 5.20, respectively. 15 min onwards spleen contained highest radioactivity after liver *i.e.* 6.88, 5.18, 4.97, 3.42, and 1.72% ID per g at 5 min, 15 min, 30 min, 60 min, 120 min, and 1440 min, respectively. Lung and kidney also have significant amount of radioligand present till 30 min *i.e.* 3.15 and 3.50% ID per g, respectively. Thereafter, radioactivity decreased sharply in lungs with 25% to 5.5% of uptake at 5 min from 60 min to 1440 min. Similar trend was observed in kidney *i.e.* 20% of the uptake at 5 min in 60 min and subsequent reduction to 8% in 1440 min. The biodistribution pattern revealed that the radioactivity is mainly localized in TSPO-expressing organs such as lung, liver, spleen, and kidney. The good uptake of radioactivity in requisite organs proves it as TSPO targeting ligand. In literature, highest uptake in liver, after intestine, has been reported for ^{99m}Tc labelled 2-quinoline carboxamide analogs.²⁵ ^{99m}Tc -MBIP demonstrated negligible uptake in intestine which is desirable for TSPO ligand.

In brain, small uptake of 0.06% ID per g at 5 min was observed which decreased to 0.01% at the last time point of observation. The small % ID in brain could be attributed to moderate expression of TSPO in the healthy brain. Maximum quantity of radioactivity in liver showed that the clearance of the radioligand is through hepatobiliary route.

The saturation aspect of TSPO binding site by ^{99m}Tc -MBIP has been studied by blocking with PK11195 on lung inflamed

mice model. ^{99m}Tc -MBIP showed uptake in all the TSPO enriched organs. Blocking percentage in lungs and other peripheral organs was found in the range of 23–60% as per ROI derived data (ESI†) which is similar to the findings of previous ligands used in nuclear medicine. Literature reported ^{99m}Tc -labelled 2-quinoline carboxamide ligands showed only significant effect in uptake of lung but not in remaining tissues on pre-administration of PK11195.²⁵ PET TSPO ligands [^{18}F]-DPA-714¹⁷ and [^{18}F]-VC701⁴² showed blocking in the range of 46–72% and 36–88%, respectively.

TSPO enriched peripheral organs have shown blocking but it was not concentration dependent for all (Fig. 5), which could be attributed to small sample size or staging of inflamed condition. Further studies with different animal models may clarify the saturation trend once blocked with cold reference like PK11195.

In summary, *in silico* studies on modified MBMP skeleton followed by facile synthesis and biological evaluation were carried out for TSPO target for SPECT application.

4. Conclusion

This work resulted in the synthesis of a new TSPO ligand 2-(2-(5-bromo benzoxazolone)acetamido)-3-(1*H*-indol-3-yl)propanoate (MBIP) for diagnostic application using SPECT. The ligand binding interaction with TSPO was calculated through MM

analysis and subsequently synthesized in four steps. MBIP formed a stable complexation with ^{99m}Tc which remained >91% stable at 24 h in serum alongwith favorable *ex vivo* bio-distribution in TSPO expressing organs. Stable nature of complex, high uptake at early time points in desired organs with fast kinetics proved MBIP as potential candidate for SPECT. Further studies are required to prove its efficiency as TSPO ligands for human clinical application.

Acknowledgements

We extend special thanks to Dr A. K. Mishra, Head, Division of Cyclotron and Radiopharmaceutical Science, INMAS, Delhi, for providing us the facility to carry out experiments. We thank Dr Anshoo Gautam, Scientist D, INMAS for her support to develop animal model. This work was supported by INMAS, Delhi under Task Project ST/15-16/INM-03. There is no conflict of interest among authors of this manuscript.

References

- R. Rupprecht, V. Papadopoulos, G. Rammes, T. C. Baghai, J. Fan, N. Akula, G. Groyer, D. Adams and M. Schumacher, *Nat. Rev. Drug Discovery*, 2010, **9**(12), 971–988.
- R. Jean, E. Bribe, L. Knabe, A. F. Petit, I. Vachier and A. Bourdin, *Rev. Mal. Respir.*, 2015, **32**(3), 320.
- H. A. Jones, P. S. Marino, B. H. Shakur and N. W. Morrell, *Eur. Respir. J.*, 2003, **21**, 567–573.
- L. Veenman and M. Gavish, *Pharmacol. Ther.*, 2006, **110**(3), 503–524.
- A. Hatori, J. Yui, L. Xie, T. Yamasaki, K. Kumata, M. Fujinaga, H. Wakizaka, M. Ogawa, N. Nengaki, K. Kawamura and M. R. Zhang, *PLoS One*, 2014, **9**(1), e86625.
- V. Papadopoulos and L. Lecanu, *Exp. Neurol.*, 2009, **219**, 53–57.
- V. M. Milenkovic, R. Rupprecht and C. H. Wetzel, *Mini-Rev. Med. Chem.*, 2015, **15**, 366–372.
- L. Veenman, A. Vainshtein and M. Gavish, *Cell Death Dis.*, 2015, **6**, e1911.
- V. Papadopoulos, M. Baraldi, T. R. Guilarte, T. B. Knudsen, J. J. Lacapère, P. Lindemann, M. D. Norenberg, D. Nutt, A. Weizman and M. R. Zhang, *Trends Pharmacol. Sci.*, 2006, **27**, 402–409.
- J. Fan, P. Lindemann, M. G. Feuilleoy and V. Papadopoulos, *Curr. Mol. Med.*, 2012, **12**, 369–386.
- R. Lin, A. Angelin, F. da Settimo, C. Martini, S. Taliani, S. Zhu and D. C. Wallace, *Aging Cell*, 2014, **13**, 507–518.
- J. H. Cho, J. H. Park, C. G. Chung, H. J. Shim, K. H. Jeon, S. W. Yu and S. B. Lee, *Biochem. Biophys. Res. Commun.*, 2015, **463**, 1–6.
- E. Levin, A. Premkumar, L. Veenman, W. Kugler, S. Leschiner, I. Spanier, G. Weisinger, M. Lakomek, A. Weizman and S. H. Snyder, *Biochemistry*, 2005, **44**, 9924–9935.
- G. Weisinger, E. Kelly-Hershkovitz, L. Veenman, I. Spanier, S. Leschiner and M. Gavish, *Biochemistry*, 2004, **43**, 12315–12321.
- W. C. Kreisl, M. Fujita, Y. Fujimura, N. Kimura, K. J. Jenko, P. Kannan, J. Hong, C. L. Morse, S. S. Zoghbi, R. L. Gladding, S. Jacobson, U. Oh, V. W. Pike and R. B. Innis, *NeuroImage*, 2010, **49**, 2924–2932.
- T. Yamasaki, K. Kumata, K. Yamamoto, A. Hatori, M. Takei, Y. Nakamura, S. Koike, K. Ando, K. Suzuki and M. R. Zhang, *Nucl. Med. Biol.*, 2009, **36**, 801–809.
- C. Vicidomini, M. Panico, A. Greco, S. Gargiulo, A. R. D. Coda, A. Zannetti, M. Graman zini, G. N. Roviello, M. Quarantelli, B. Alfano, B. Tavitian, F. Dolle, M. Salvatore, A. Bru netti and S. Pappata, *Nucl. Med. Biol.*, 2015, **42**, 309–316.
- A. K. Tiwari, J. Yui, M. Fujinaga, K. Kumata, Y. Shimoda, T. Yamasaki, L. Xie, A. Hatori, J. Maeda, N. Nengaki and M. R. Zhang, *J. Neurochem.*, 2014, **129**(4), 712–720.
- A. K. Tiwari, M. Fujinaga, J. Yui, T. Yamasaki, L. Xie, K. Kumata, A. K. Mishra, Y. Shimoda, A. Hatori, B. Ji, M. Ogawa, K. Kawamura, F. Wang and M. R. Zhang, *Org. Biomol. Chem.*, 2014, **12**(47), 9621–9630.
- A. K. Tiwari, B. Ji, M. Fujinaga, T. Yamasaki, L. Xie, R. Luo, Y. Shimoda, K. Kumata, Y. Zhang, A. Hatori, J. Maeda, M. Higuchi, F. Wang and M. R. Zhang, *Theranostics*, 2015, **5**(9), 961–969.
- A. K. Tiwari, J. Yui, Y. Zhang, M. Fujinaga, T. Yamasaki, L. Xie, Y. Shimoda, K. Kumata, A. Hatori and M. R. Zhang, *RSC Adv.*, 2015, **5**(123), 101447–101454.
- S. Tsartsalis, N. Dumas, B. B. Tournier, T. Pham, M. Moulin-Sallanon, M. C. Gregoire, Y. Charnay and P. Millet, *EJNMMI Res.*, 2015, **5**(9), 1–6.
- F. Mattner, M. Quinlivan, I. Greguric, T. Pham, X. Liu, T. Jackson, P. Berghofer, C. J. R. Fookes, B. Dikic, M. C. Gregoire, F. Dolle and A. Katsifi, *Dis. Markers*, 2015, 729698.
- S. Piccinonna, N. D. Enora, N. Margiotta, V. Laquintana, G. Trapani and G. Natile, *Z. Anorg. Allg. Chem.*, 2013, **639**(8–9), 1606–1612.
- A. Cappelli, A. Mancini, F. Sudati, S. Valenti, M. Anzini, S. Belloli, R. M. Moresco, M. Matarrese, M. Vaghi, A. Fabro, F. Fazio and S. Vomero, *Bioconjugate Chem.*, 2008, **19**(6), 1143–1153.
- S. Piccinonna, N. Marietta, N. Denora, R. M. Lacobazzi, C. Pacifico, G. Trapani and G. Natle, *Dalton Trans.*, 2013, **42**, 10112–10115.
- N. Denora, N. Margiotta, V. Laquintana, A. Lopodota, A. Cutrignelli, M. Losacco, M. Franco and G. Natile, *ACS Med. Chem. Lett.*, 2014, **5**, 685–689.
- E. Cerutti, *Magn. Reson. Chem.*, 2013, **51**(2), 116–122.
- H. C. Manning, T. Goebel, R. C. Thompson, R. R. Price, H. Lee and D. J. Bornhop, *Bioconjugate Chem.*, 2004, **15**, 1488–1495.
- M. L. James, S. Selleri and M. Kassiou, *Curr. Med. Chem.*, 2006, **13**, 1991–2001.
- F. Chauveau, H. Boutin, N. V. Camp, F. Dolle and B. Tavitian, *Eur. J. Nucl. Med. Mol. Imaging*, 2008, **35**, 2304–2319.
- D. R. Owen, R. N. Gunn, E. A. Rabiner, I. Bennacef, M. Fujita, W. C. Kreisl, R. B. Innis, V. W. Pike, R. Reynolds and P. M. Matthews, *J. Nucl. Med.*, 2011, **52**, 24–32.

- 33 T. Fukaya, T. Kodo, T. Ishiyama, H. Kakuyama, H. Nishikawa, S. Baba and S. Masumoto, *Bioorg. Med. Chem.*, 2012, **22**, 5568–5582.
- 34 T. Fukaya, T. Kodo, T. Ishiyama, H. Nishikawa, S. Baba and S. Masumoto, *Bioorg. Med. Chem.*, 2013, **21**, 1257–1267.
- 35 Y. S. Kim, J. W. Hwang, J. H. Jang, S. Son, I. B. Seo, J. H. Jeong, E. H. Kim, S. H. Moon, B. T. Jeon and P. J. Park, *Molecules*, 2016, **21**, 392.
- 36 M. Starkhammar, S. K. Georen, L. Swedin, S. E. Dahlen, M. Adner and L. O. Cardell, *PLoS One*, 2012, **7**(2), e32110.
- 37 S. Knapp, S. Florquin, D. T. Golenbock and T. V. poll, *J. Immunol.*, 2006, **176**, 3189–3195.
- 38 J. Lefort, L. Motreff and B. B. Vargaftig, *Am. J. Respir. Cell Mol. Biol.*, 2001, **24**, 345–351.
- 39 <http://www.biomodels.com/animal-models/pulmonary-disease/acute-lung-injurycopd/>.
- 40 Y. Guo, R. C. Kalathur, Q. Liu, B. Kloss, R. Bruni, C. Ginter, E. Kloppmann, B. Rost and W. A. Hendrickson, *Science*, 2015, **347**(6221), 551–555.
- 41 A. K. Tiwari, D. Sinha, A. Datta, D. Kakkar and A. K. Mishra, *Chem. Biol. Drug Des.*, 2011, **77**, 388–392.
- 42 G. D. Grigoli, C. Monterisi, S. Belloli, V. Masiello, L. S. Politi, S. Valenti, M. Paolino, M. Anzini, M. Matarrese, A. Cappelli and R. M. Moresco, *Mol. Imaging*, 2015, **14**, 1–9.

Design, synthesis and in silico evaluation of methyl 2-(2-(5-bromo/chloro-2-oxobenzooxazol-3(2H)-yl)acetamido)-3-phenylpropanoate for TSPO targeting

Pooja Srivastava^{1,2}, Pravir Kumar², Anjani K. Tiwari^{1,3}

¹Division of Cyclotron and Radiopharmaceutical Sciences, Institute of Nuclear Medicine and Allied Sciences, Brig. S. K. Mazumdar Road, Delhi-110054, India

²Molecular Neuroscience and Functional Genomic Laboratory, Department of Biotechnology, Delhi Technological University, Delhi 110042, India

³Department of Chemistry, School of Physical & Decision Sciences (SPDS), Babasaheb Bhimrao Ambedkar Central University, Vidya Vihar, Raebareli Road, Lucknow-226025, U.P., India

Address for correspondence:

1) Dr Anjani K Tiwari

Department of Chemistry, School of Physical & Decision Sciences (SPDS), Babasaheb Bhimrao Ambedkar Central University, Vidya Vihar, Raebareli Road, Lucknow-226025, U.P., India

& Division of Cyclotron and Radiopharmaceutical Sciences, Institute of Nuclear Medicine and Allied Sciences, Brig. S. K. Mazumdar Road, Delhi-110054, India

Email- anjanik2003@gmail.com

Ph no- +91-7503381343, fax no- +91-522-2440821

2-Pooja Srivastava

Division of Cyclotron and Radiopharmaceutical Sciences, Institute of Nuclear Medicine and Allied Sciences, Brig. S. K. Mazumdar Road, Delhi-110054, India

Email- pushree14@gmail.com

Ph no- +91-11-23905362, fax no- +91-11-23919509

Abstract

The high expression of the TSPO makes it an ideal target for imaging and therapy. The present study aims to optimize acetamidobenzoxazolone based TSPO ligands by modification in its structures which may overcome the limitations of two generation TSPO ligands such as non-specificity and polymorphism. Herein, we have selected three different TSPO PDBs 2MGY, 4RYQ and 4UC1 in native and mutated form. The acetamidobenzoxazolone modified with phenylalanine methyl ester (methyl 2-(2-(5-bromo/chloro-2-oxobenzooxazol-3(2*H*)-yl)acetamido)-3-phenylpropanoate, ABPO-Br, ABPO-Cl) through better/comparable dock scores than known TSPO ligands such as MBMP, FEBMP, FPBMP and PK11195 are identified as potential TSPO ligands. The ABPO-Cl and ABPO-Br were synthesized by using methyl ester of phenylalanine as moiety for incorporation of desired pharmacophoric feature. All the intermediates and final compounds were purified using column chromatography and analytical HPLC (purity > 97%). The purified compounds were characterized using spectroscopic techniques such as ¹H-NMR, ¹³C-NMR, and mass spectroscopy. Drug likeliness and comparative bioactivity analysis were performed using QikProp through prediction of various properties. Both the analogs follow all the five Lipinski rules and three Jorgensen's rules predicting its drug likeliness. Other important aspect related to TSPO ligands such as blood brain barrier penetration and better contrast have been predicted through lipophilicity (QPlog P=2.76 and 2.74 for ABPO-Br and ABPO-Cl, respectively) and serum binding (QPLogK_{hsa} = -0.18 and -0.25 for ABPO-Br and ABPO-Cl, respectively). Selectivity and distribution of these TSPO ligands were confirmed by ^{99m}Tc-ABPO-Br dynamic image in New Zealand rabbit. These results have shown that the ABPO analogs would have the potential to act as better ligand as compared to known acetamidobenzoxazolone derivatives and would be of interest as promising starting point for designing compounds for TSPO targeting.

Key Words: TSPO, Acetamidobenzoxazolone, phenylalanine methyl ester, ADME, docking, ABPO-Cl, ABPO-Br

Introduction

The translocator protein (18 kDa, TSPO), previously named as the peripheral benzodiazepine receptor (PBR), was identified as a diazepam's peripheral binding site in 1977.¹ This was distinguished from central benzodiazepine receptor on the basis of functional role, unique structure and cellular location. The TSPO has 169 amino acid protein arranged in five transmembrane domains.¹ It is primarily located on the outer membrane of mitochondria and also proposed to be located in non-mitochondrial site such as nuclear or microsomal in some cells.²⁻³

TSPO has been found as an important diagnostic and therapeutic target for inflammation and tumor.⁴⁻⁶ Since TSPO was identified by diazepam, benzodiazepines, and Ro5-4864, several classes of TSPO ligands with diverse structure including isoquinoline carboxamides, benzodiazepine, benzothiazepines, indole acetamide, phenoxyphenyl acetamide, imidazopyridine acetamides, and pyrazolopyrimidine acetamides have been developed.^{1,7-8}

The isoquinoline carboxamide based ligand PK11195 is currently considered as the state-of-the-art ligand for TSPO. Its most widely studied PET ligand ¹¹C(R) PK11195 ligand from first generation has limitation of high non-specific binding and low brain penetration resulting in low signal to background ratio. Some of the second generation TSPO ligands could overcome these limitations with relatively higher signal to noise ratio than PK11195 for improved imaging. Several radioligands of second generation TSPO ligands used in clinical human studies are [¹¹C]DAA1106, [¹⁸F]DPA714, and [¹¹C]PBR28 and [¹¹C]AC-5216.⁹⁻¹²

Although second generation TSPO ligands have few advantages over PK11195, there is a problem of intersubject variability due to single nucleotide polymorphism.¹³ A new skeleton acetamidobenzoxazolone (ABO)¹⁴⁻¹⁵, derived through opening and reorganizing RoS-4864, has been explored for PET application (MBMP, FEBMP and FPBMP) to overcome the problems of inter subject variability.¹⁶⁻²⁰ ABO has been modified to ABO-Amino Acid (ABO-AA) for SPECT application by conjugating it with methyl ester of tryptophan to maintain affinity and biocompatibility.²¹

This encouraged us to try conjugation of benzoxazolone with other amino acids. Moreover, in a recent study, preference for amino acid transport system LAT1 over other LATs, A and ASC in normal as well as tumor cells in the uptake of phenylalanine based radio tracers have been demonstrated through competitive uptake inhibition using inhibitors specific for system A, ASC and L.²² Therefore, phenylalanine can be better candidate for improving cell uptake.

Before synthesis, it is important to evaluate the molecule for drug likeliness and TSPO affinity *in silico*. The literature of drug discovery gives emphasis to combinatorial chemistry and the screening of compounds for its drugability involving ADME/toxicity as the screening of millions of compounds results into limited number of drug-like compounds. Therefore, it has been advocated that the drugability should be checked before screening for the receptor activity. In current scenario, there is a considerable increase in the application of computer aided drug design methods to predict potential drugs for the diagnosis/treatment of several diseases. *In silico* prediction of pharmacokinetic parameters like absorption, distribution, metabolism and excretion (ADME) studies have become increasingly important for early screening of potential drug candidates.²³

Around the beginning of 21st century, a simple thumb rule was reported by Lipinski et al. for *in silico* prediction of oral absorption of a compound through solubility and permeability. As per rule of five, $\approx 90\%$ of oral molecules clear three out of following four rules: $MW \leq 500$ Da, calculated LogP (cLogP) ≤ 5 and ≥ 0 , hydrogen bond acceptors (HBAs) ≤ 10 , and hydrogen bond donors (HBD) ≤ 5 .²⁴⁻²⁵ The bioavailability of molecules are predicted by using Jorgensen's rule of 3 (LogS_{wat} > -5.7 , Apparent Caco-2 permeability > 22 nm/s and number of primary metabolites < 7).²⁶⁻²⁷ Subsequently, few more *in silico* properties such as polar surface area (PSA $\leq 140 \text{ \AA}^2$), the number of rotatable bonds ($\leq 10-20$), have been added to expand the correlations with ADME parameters.²⁸

In silico approaches include docking, quantitative structure activity relationships, virtual ligand screening, pharmacophore modeling etc are other important tools in the discovery and optimization of novel molecules with enhanced affinity and specificity for the selected therapeutic targets.²⁹⁻³² Availability of different TSPO PDBs from wild type as well as mutants such as 2MGY, 4RYQ and 4UC1 have enabled TSPO affinity screening through the docking studies at design level.³³⁻³⁶

In this study, in continuation of our effort to develop effective TSPO ligand a new skeleton methyl-2-(2-(5-bromo/chloro-2-oxobenzoxazol-3(2*H*)-yl)acetamido)-3-phenylpropanoate has been designed by combining 5-bromo/chloro-benzoxazolone with phenylalanine methyl ester and evaluated for its ADME properties as well as its affinity for TSPO *in silico*. Conjugating TSPO pharmacophore (acetamidobenzoxazolone) with methyl phenylalanine could be promising strategy for drug design as it may improve efficacy. Thereafter, conjugation has

been carried out in three steps and characterized using NMR, Mass and HPLC for further application as TSPO ligand in animal model.

Materials and methods

Chemicals:

The chemicals and solvents used in the reactions were purchased from Sigma-Aldrich and Merck. The silica used for purification using column chromatography was MN60 having mesh 60–120 and aluminum plates coated with silica gel 60 F254 was used for thin layer chromatography (TLC) for monitoring the reaction.

Instrumentation:

Nuclear Magnetic Resonance Spectroscopy (^1H and ^{13}C NMR) were recorded on Bruker Avance III 600 MHz system) at 600 MHz and 150 MHz, respectively. Mass spectroscopy was performed on Agilent 6310 system using ESI. High performance liquid chromatography (HPLC) was carried out on 1200 series of Agilent using analytical T3 Waters column (4.6X250 mm) for analysis.

Gamma Camera Design

For scintigraphic images of $^{99\text{m}}\text{Tc}$ -labeled complexes in animal, a gamma camera (Symbia, T2, True point SPECT/CT Siemens, INMAS, DRDO, Delhi) equipped with dual head, low energy, high resolution and parallel-hole collimator was used which has an interface to a computer network system. For image acquisition, animal was fixed on a mechanical support for standardization of orientation and position.

Image Acquisition Parameters

Dorsal ear vein was used for injection in rabbit. Images were acquired at defined time point in case of static imaging. For dynamic imaging, acquisition was done for 30 mins immediately after injection. Anterior images for 30 min with 2 sec/frame for 2 min, 15 sec/frame for 2 min and 60 min/frame for 26 min were acquired. A 15% window centered on 140 KeV i.e. $^{99\text{m}}\text{Tc}$ peak with zoom factor 1 was used. The matrices used for dynamic imaging was 128 X 128.

Image analysis:

The computational data of scintigraphy were extracted and analyzed on a Pegasys workstation (ADAC laboratory). After image acquisition, region of interest (ROI) were drawn over organ of interest and the total field of view.

Ligand preparation:

The lead skeleton was taken from our previous work which proved its potential for TSPO targeting. Further new analogues were designed and drawn using chemdraw Ultra 10.0 and were checked for drug likeliness using Lipinski rule. These analogs and few known TSPO ligands in .mol format were used as input structures for processing in LigPrep, Schrödinger, Maestro LLC 9.1 software. A series of steps in the LigPrep process are as follows: conversions, corrections to the structures, generating variations on the structures, elimination of unwanted structures and finally the optimization the structures.

Protein Preparation:

Prior to docking, identification of the binding site in the target protein is important. This information is taken through the structures of the complexes of the TSPO proteins with its substrate PK11195. The PDB structure files of the proteins are imported and prepared through protein preparation wizard of the Schrodinger by applying the OPLS_2005 force field. The steps involved in the process of protein preparation are processing, optimization and minimization of proteins.

The validation of docking protocol was performed through docking back after removing the PK11195 from active site. For the current study PDB structures were taken from RCSB Protein Data Bank (PDB) and the PDBs used were 2MGY (wild type TSPO), 4RYQ (wild type TSPO, resolution 1.7 Å) and 4UC1 (Mutant TSPO, resolution 1.8 Å).

Docking:

Docking is a computational simulation process to predict the preferred orientation of protein-ligand interaction by forming a complex with high stability. Glide, Schrödinger, Maestro LLC 9.1 offers the speedy and accurate high throughput virtual screening of several compounds with extremely accurate binding mode predictions.

Both the newly designed analogs as well as few well known TSPO ligands were subjected to docking with the protein using Glide. The molecules were docked to the active site of TSPO. The molecules docked with negative G Score are suitable for further evaluation. Only the

TSPO ligands would have the accurate hydrophobic contact between ligand and protein resulting to favorable docking scores.

ADME Prediction:

ADME properties were calculated with the help of Qikprop of Schrodinger. It predicts both physicochemical descriptors and pharmacokinetic properties. QikProp provides ranges for all the descriptors and properties of 95% of known drugs for comparison purpose. It also evaluates the suitability of analogs on the basis of Lipinski's rule of five which predicts drug like pharmacokinetic profile for rational drug design. In the present study, QikProp derived physicochemical properties used for ADME analysis are molecular weight, number of hydrogen bond donors, number of hydrogen bond acceptors, partition coefficients, number of rotatable bonds and molecular volume etc which, in turn, predict the properties for assessing drug likeness, bioavailability, plasma protein binding, and metabolism. As the molecules are for brain application, we have considered following predictive properties

- a) QPlogP octanol/water
- b) QPlogS aqueous solubility
- c) QPlogS -Conformation independent aqueous solubility
- d) QPlog K_{hsa} Serum protein binding
- e) QPlogBB for blood brain
- f) No of primary metabolites
- g) Apparent Caco-2 permeability (nm/s)
- h) Apparent MDCK permeability (nm/sec)
- i) % Human oral absorption in GI
- j) Qualitative model for human oral absorption

Synthesis and characterization:

Synthesis of 5-Chloro benzoxazol-2(3H)-one (**1**)

To a solution of 5-chloro-2-aminophenol (500.0 mg, 2.96 mmol) in 150 ml THF, 1, 10-carbonyldiimidazole (576.0 mg, 3.55 mmol) was added. The mixture was refluxed with stirring for 2 h. The reaction mixture was quenched by adding 2 M HCl solution after cooling to room temperature. EtOAc was used for extraction which was washed with brine, dried over anhydrous sodium sulphate and filtered. Thereafter, solvent was removed in vacuo to get the product as white solid.

MS (ESI) m/z: 167.8 [M-H⁺], calculated m/z: 168.0 [M-H⁺]

¹H-NMR (DMSO, 600 MHz): 7.11-7.31(m, 3H)

^{13}C -NMR (DMSO, 150 MHz): 110.3, 111.3, 122.0, 128.2, 132.2, 142.6, 154.7

Synthesis of methyl 2-(2-chloroacetamido)-3-phenylpropanoate (**2**)

To a solution of L-phenylalanine methyl ester (500.0 mg, 2.32 mmol) in deionized water (10 ml), triethyl amine (360 μl , 2.52 mmol) was added with stirring under nitrogen atmosphere on ice bath for 5 minutes. To the mixture, chloroacetyl chloride (205 μl , 2.52 mmol) in dichloromethane (10 ml) was added drop wise over 1 h and the reaction was carried out for 4 h. Thereafter, the mixture was extracted with dichloromethane. The organic layer was washed twice by deionized water and brine solution. After washing, organic layer was dried over anhydrous sodium sulphate. After filtration, the solvent was removed in vacuo, checked by TLC using $\text{CHCl}_3/\text{MeOH}$ (9:1, v/v) as mobile phase and purified by silica gel column chromatography using 100% CHCl_3 as eluent.

MS (ESI) m/z: 254.0 $[\text{M}-\text{H}^+]$, calculated m/z: 254.1 $[\text{M}-\text{H}^+]$

^1H -NMR (CDCl_3 , 600 MHz): 3.11-3.20 (m, 2 H), 3.74 (s, 3H), 3.98-4.04 (m, 2H), 4.86-4.90 (m, 1H), 7.02-7.33 (m, 6H)

^{13}C -NMR (CDCl_3 , 150 MHz): 37.8, 42.4, 52.5, 53.4, 127.3, 128.7, 129.2, 135.4, 165.6, 171.3

Synthesis of methyl 2-(2-(5-chloro-2-oxobenzooxazol-3(2*H*)-yl)acetamido)-3-phenylpropanoate, **ABPO-Cl(3)**

To a solution of 5-Chloro benzoxazol-2(3*H*)-one (250.0 mg, 1.48 mmol) and K_2CO_3 (306.0 mg, 2.22 mmol) in DMF (5 ml), methyl 2-(2-chloroacetamido)-3-phenylpropanoate (415.2 mg, 1.63 mmol) was added with cooling on ice bath. The reaction mixture was stirred at 60-70 $^\circ\text{C}$ for 3 h. Thereafter, reaction mixture was cooled to room temperature before adding water. Mixture of toluene and ethyl acetate in 1:1 ratio was used as extraction solvent. Water and brine solutions were used for washing the organic layer and anhydrous sodium sulphate for drying. Solvent was removed in vacuo after filtration and was purified by silica gel column chromatography using $\text{CHCl}_3/\text{EtOAc}$ (4:1, v/v) as eluent.

MS (ESI) m/z: 387.1 $[\text{M}-\text{H}^+]$, Calculated m/z: 387.1 $[\text{M}-\text{H}^+]$

^1H -NMR (CDCl_3 , 600 MHz): 3.50-3.60 (m, 2H), 3.86 (s, 3H), 4.19-4.27 (m, 2H), 5.07-5.10 (m, 1H), 6.96-7.33 (m, 8H)

^{13}C -NMR (CDCl_3 , 150 MHz): 34.0, 51.2, 53.2, 54.4, 121.3-148.8 (10 peaks), 155.3, 168.1, 168.6

Synthesis of 5-Bromo benzoxazol-2(3*H*)-one (**4**)

To a solution of 4-bromo-2-aminophenol (500.0 mg, 2.66 mmol) in 150 ml THF, 1,10-carbonyldiimidazole (518.0 mg, 3.19 mmol) was added. The mixture was refluxed with stirring for 2 h. The reaction mixture was quenched by adding 2 M HCl solution after cooling to room temperature. EtOAc was used for extraction which was washed with brine, dried over anhydrous sodium sulphate and filtered. Thereafter, solvent was removed in vacuo to get the product as white solid.

MS (ESI) m/z: 211.7 [M-H⁺], Calculated m/z: 211.9 [M-H⁺]

¹H-NMR (DMSO, 600 MHz): 7.20-7.28 (m, 3H)

¹³C-NMR (DMSO, 150 MHz): 111.7, 112.9, 115.8, 124.8, 132.5, 143.0, 154.6

Synthesis of methyl 2-(2-(5-bromo-2-oxobenzooxazol-3(2*H*)-yl)acetamido)-3-phenylpropanoate, **ABPO-Br (5)**

To a solution of 5-bromo benzoxazol-2(3*H*)-one (250.0 mg, 1.17 mmol) and K₂CO₃ (242.2 mg, 1.76 mmol) in DMF (5 ml), methyl 2-(2-chloroacetamido)-3-phenylpropanoate (328.2 mg, 1.29 mmol) was added with cooling on ice bath. The reaction mixture was stirred at 60-70⁰C for 3 h. Thereafter, reaction mixture was cooled to room temperature before adding water. Mixture of toluene and ethyl acetate in 1:1 ratio was used as extraction solvent. Water and brine solutions were used for washing the organic layer and anhydrous sodium sulphate for drying. Solvent was removed in vacuo after filtration and was purified by silica gel column chromatography using CHCl₃/EtOAc (4:1, v/v) as eluent.

MS (ESI) m/z: 431.3 [M-H⁺], Calculated m/z: 431.0 [M-H⁺]

¹H-NMR (CDCl₃, 600 MHz): 3.49-3.60 (m, 2H), 3.86 (s, 3H), 4.19-4.27 (m, 2H), 5.06-5.10 (m, 1H), 6.91-7.33 (m, 8H)

¹³C-NMR (CDCl₃, 150 MHz): 34.0, 51.2, 53.2, 54.4, 112.6-149.3 (10 peaks), 155.3, 168.0, 168.5

Radio labeling protocol:

Radiolabeling was performed as per the method mentioned in literature³⁷⁻³⁸. 1 ml 1X10⁻² M SnCl₂.2H₂O was added to 200 µl 3 mM cold ligand solution. Then 2 mCi sodium pertechnetate in 100 µl saline was added. 0.1 M NaHCO₃ was used for pH adjustment to 7 and then content was manually shaken and kept at room temperature for 20 min. ITLC-SG strip as stationary phase and acetone and PAW (pyridine, acetic acid and water in 3:5:1.5 ratio) as mo-

bile phase were used to determine complexation with ^{99m}Tc and purity of the labeled compound. Count measurement was done by cutting ITLC into 0.1 cm segments.

Animal Studies:

Animals were supplied by experimental animal facility (EAF) of Institute of Nuclear Medicine and Allied Sciences (INMAS), Delhi. The animals were maintained as per the regulations of the Committee for the Purpose of Control and Supervision of Experiments on Animals (CPCSEA). All the animals were maintained on standard diet (Hindustan Lever Ltd., Mumbai, India) and water. They were kept in the animal house of the institute which was maintained at $22 \pm 2^\circ\text{C}$ and 50% humidity under a 12 h dark/light cycles.

Scintigraphy studies:

Scintigraphy studies of ^{99m}Tc -labeled complexes were carried out in New Zealand rabbit. 0.2 mCi of labeled complex was injected intravenously through the ear vein and images were acquired for 30 min post injection of radiocomplex.

Results and Discussion:

A new series of ligands acetamidobenzoxazolone-phenylalanine, ABPO, (methyl 2-(2-(5-bromo/chloro-2-oxobenzoxazol-3(2*H*)-yl)acetamido)-3-phenylpropanoate) have been designed, evaluated for drug likeliness on the basis of predictive ADME properties *in silico*, synthesized and assessed for their affinity towards TSPO through docking. ABPO comprises of benzoxazolone and phenylalanine methyl ester coupled with acetamide group. Two halogen analogues- chloro and bromo at 5th position of benzoxazolone have been prepared. The rationale of choosing chloro analog was presence of chloro group in several TSPO ligands and bromo analog can provide opportunity to further optimize property through substitution reaction. The predictive affinity towards TSPO and drug likeliness properties of ABPO skeleton was found appropriate for biomedical application in which TSPO are over expressed.

It is important to know the pharmacokinetic profile of any molecule to be used in vivo conditions which can be studied through ADME properties *in silico*. Often drugs fail to enter the market due to poor pharmacokinetic profile. Thus, it is imperative to design the compound

with easy transportability to desired site, proper interaction at desired site, not or minimally metabolize before its action and finally excrete after expected action. The incorporation of desired ADME properties at early stages of drug discovery using computer aided drug design methods reduces the chances of failure of compound at later stages. This has further advantage of low cost and less time required over wet screening.

As we are targeting the receptors/proteins which are found on outer mitochondrial surface of glial cells, our molecules should be able to reach glial cells of brain. This means their capability to crossing blood brain barrier is essential and their lipophilicity must be optimum as lipophilic substances are required to cross the BBB. During this process, transportation/binding pattern with human serum is also important for consideration.

The ligands ABPO-Cl/Br satisfy pharmacological properties of 95% available drugs available in Schrödinger database. The drug-likeness or capability for becoming a good drug candidate for clinical application was predicted by Lipinski rule of 5 which is normally used in CADD analysis. ABPO-Cl and ABPO-Br follow all the five rules of Lipinski reflecting its drug like properties. Additionally, hydrogen bond acceptors are well within the acceptable proposed limit of 10 for Lipinski rule. However, QPlogP, an important property for molecule to cross blood brain barrier, is followed by both the designed ligands which are 2.74 and 2.76 for bromo and chloro analogs, respectively. (Table 1)

Bioavailability prediction:

The computed parameters useful for predicting oral absorption are aqueous solubility, conformation independent aqueous solubility, % of human oral absorption in GI, qualitative model for human oral absorption, compliance of Jorgensen's rule of three.

Out of all known ligands taken for comparison purpose, only two are violating this rule for QPlogS > -5.7 (-7.4 for FGIN-127 and -6.22 for PBR111). For designed ligands, the solubilities with QPlogS -4.06 to -3.72 reflect better or comparable solubility than the known ligands.

The Caco-2 permeabilities for designed ligands are 248 and 477 and for known ligands between 2290-6015 all are much >25 nm/s, the limit of poor permeability as mentioned by software. The other parameter responsible for absorption, conformation independent QPlogS value for designed molecules (-4.62 to -5.54 for chloro and bromo analogs, respectively) are comparable to that of known ligand (-7.17 to -4.44). Reasonably good absorptions are also

reflected by % human oral absorption in GI which is >85 for proposed ligands and 100 for known. Even qualitative model for human oral absorption are predicting high oral absorption.

Molecular flexibility is related to number of rotatable bonds which is connected to bioavailability (increases with the decrease in number of rotors). Their numbers in designed molecule are 6 which is comparable to known TSPO ligands such as DAA1106, PBR06 and PBR28. However, some known ligands have either high (12 for FGIN-127) or low (0 for RoS-4864). There is requirement of optimum rotatable bonds to bind in the pocket of receptor for binding as there is loss of entropy on binding because of conformational restriction in case of flexible molecules. As the molecule is meant for diagnostic application, too low number of rotatable bonds may lead to stickiness to the target receptor. Therefore, designed ligands with 6 rotatable bonds as present in known ligands also seem to be reasonable for ligands for diagnostic purpose. (Table 1)

Prediction of blood-brain barrier (BBB) penetration:

In the current study, the molecule proposed have potential application for brain that makes it mandatory for them to cross the blood brain barrier. Too polar molecules may not be able to cross the BBB. To assess the access of drug to the brain, blood-brain partition co-efficient (QPlogB/B) is computed. The values for known TSPO ligands that are from first and second generation and designed ligands are in between -1.09 to 0.362. This range is permissible limit for crossing blood brain barrier. (Table 1)

Prediction of binding with plasma protein:

The degree of binding to the blood plasma proteins (like human serum albumin, glycoprotein, lipoproteins, alpha, beta and gamma globulins) affects the efficiency of a drug as it greatly reduces the drug quantity in circulation of blood which passes through traverse cell membranes or diffuses less efficiently. Therefore, the ability of all the designed ligands were predicted to act on human serum albumin through QPlogK_{hsa}. For known ligands considered this range is from 0.032 to 1.31. For PK11195, its value is quite high i.e. 0.65 resulting in its non-specific binding which leads to poor signal to noise ratio in case of radiolabeled PET ligands. Out of the ligands chosen for comparison purpose, DPA-713 and DAA1106 are better with values being 0.03 and 0.35 which reflects their improved signal to noise ratio. The designed skeletons ABPO-Br/Cl (-0.18 & -0.26) have moderate interaction which is well within limit (-1.5 to 1.5). (Table 1)

Molecular Volume

Another crucial factor for binding in the active site of receptor is molecular volume. The volume of ligand and that of active site should match for perfect interaction. To assess the structural compatibility of molecule at active site, molecular volume has been analyzed. For known ligands its range was observed to be 941 and 1502 for RoS4864 and FGIN-127. However, molecular volume for rest of the known ligands are in the range 1129-1307. Both the designed molecules fall in the range 1144-1172 in which most of the known ligands are lying. This predicts that proposed ligands have sufficient molecular volume for ligand-protein interaction. (Table 1)

Further the ligands were synthesized in three steps as per scheme 1 and scheme 2. The parallel synthesis of both the precursors 5-bromo/chloro benzoxazol-2(3*H*)-one and methyl 2-(2-chloroacetamido)-3-phenylpropanoate were carried out starting from commercially available 4-bromo/chloro-2-aminophenol and phenyl alanine methyl ester using cyclization reaction and chloro acetylation reaction as per procedures reported in the literature with some modification.^{14, 39} For cyclization reaction, CDI was used and for chloroacetylation reaction, chloroacetyl chloride with triethyl amine as base were taken. The final compounds ABPO-Br/Cl were synthesized through alkylation reaction of 5-bromo/chloro-benzoxazolone and methyl 2-(2-chloroacetamido)-3-phenylpropanoate in the presence of K₂CO₃ in DMF solvent. The compounds were purified using column chromatography and preparative HPLC. The chemical purity of the compound was determined using analytical HPLC and purity was found to be >97%. All the eight aromatic protons of benzoxazolone and benzene moieties were observed in the region 6-8 ppm. ¹³C-NMR reflected appropriate peaks as per its formula. The C=O of benzoxazolone, amide and ester were observed in the region 155-169 of ¹³C-NMR of both the analogs reflecting the synthesis of ABPO-Cl/Br. The mass spectroscopy also confirmed the synthesis with the presence of [M-H⁺] peaks of ABPO-Cl and ABPO-Br at 387.1 and 432.9, respectively.

The selection of phenylalanine based biocompatible ligand was on the basis of their preference for LAT1 over other LATs, A and ASC system in the uptake mechanism. Validation for TSPO binding/affinity which was carried out through docking studies to know about interaction with different amino acid residues of TSPO as compared to other known TSPO ligands. ABPO-Cl/Br demonstrated comparable or better affinity with TSPO in terms of G_{score}, when compared with known ligand like PK11195 and MBMP. Various interactions were observed in docking including pi-pi interaction and hydrogen bonding. Phenylalanine aromatic ring is

participating in pi-pi interactions while one hydrogen bond was observed due to NH of acetamidobenzoxalone moiety. (Fig. 1, 2)

Docking studies using mutated PDB 4UC1 (A139T) of RsTSPO, the ligands ABPO-Cl/Br showed similarity in interactions with FPBMP/FEBMP. G_{score} were also found comparable for FPBMP, FEBMP and MBMP. As FEBMP shows no intersubject variability, it can be predicted that the ABPO-Cl/Br could reflect the same. Further studies are required for its validation. (Fig. 2, 3)

The radiolabeling study was carried out with the procedure mentioned in literature with some modification. Complexation of the synthesized ligands with $^{99\text{m}}\text{Tc}$ gave 95.4% stability of $^{99\text{m}}\text{Tc-ABPO-Br}$ over 24 h. *In vitro* serum stability clearly indicates the stable nature of radio complexes without much transchelation to serum protein like albumin which was observed to be intact with 92.4% of $^{99\text{m}}\text{Tc-ABPO-Br}$.

Selectivity and distribution of these TSPO ligands were confirmed by tracer techniques in New Zealand rabbit (Dynamic image for 30 min). (Fig. 4.a) In brain, significant uptake was observed which reduced with time. In a nut shell it is observed that the uptake was majorly in all the TSPO rich organs at initial time point which eventually decreased with time. In excretory organs uptakes were initially lower which increased with time till the last time point of observation.

During dynamic studies after intravenous injection of $^{99\text{m}}\text{Tc-ABPO-Br}$, frames of 10 sec were captured. In these images, slight uptake in lungs, spleen and brain is seen. As the duration of image capture was 10 sec therefore, organs with relatively lower uptake were not clearly visualized. Small uptake at later time points was seen which may be due to fast release kinetics of $^{99\text{m}}\text{Tc-ABPO-Br}$. (Fig. 4.b)

In summary, *in silico* studies on modified MBMP skeleton i.e. ABPO for ADME properties and interaction with TSPO protein followed by facile synthesis were carried out for over expressed TSPO targeting.

Conclusion: The goal of the study was synthesis, characterization and *in silico* evaluation of acetamidobenzoxazolone-phenylalanine methyl ester, methyl 2-(2-(5-bromo-2-oxobenzooxazol-3(2*H*)-yl)acetamido)-3-phenylpropanoate for TSPO targeting. Binding affinity towards TSPO was assessed through ligand-protein docking method and ADME property through qikprop modules of Schrodinger software. Biodistribution of these ligands and

their selectivity towards TSPO were demonstrated under in vivo condition on New Zealand rabbit. Further pre-clinical animal studies are required to prove its efficiency as TSPO marker.

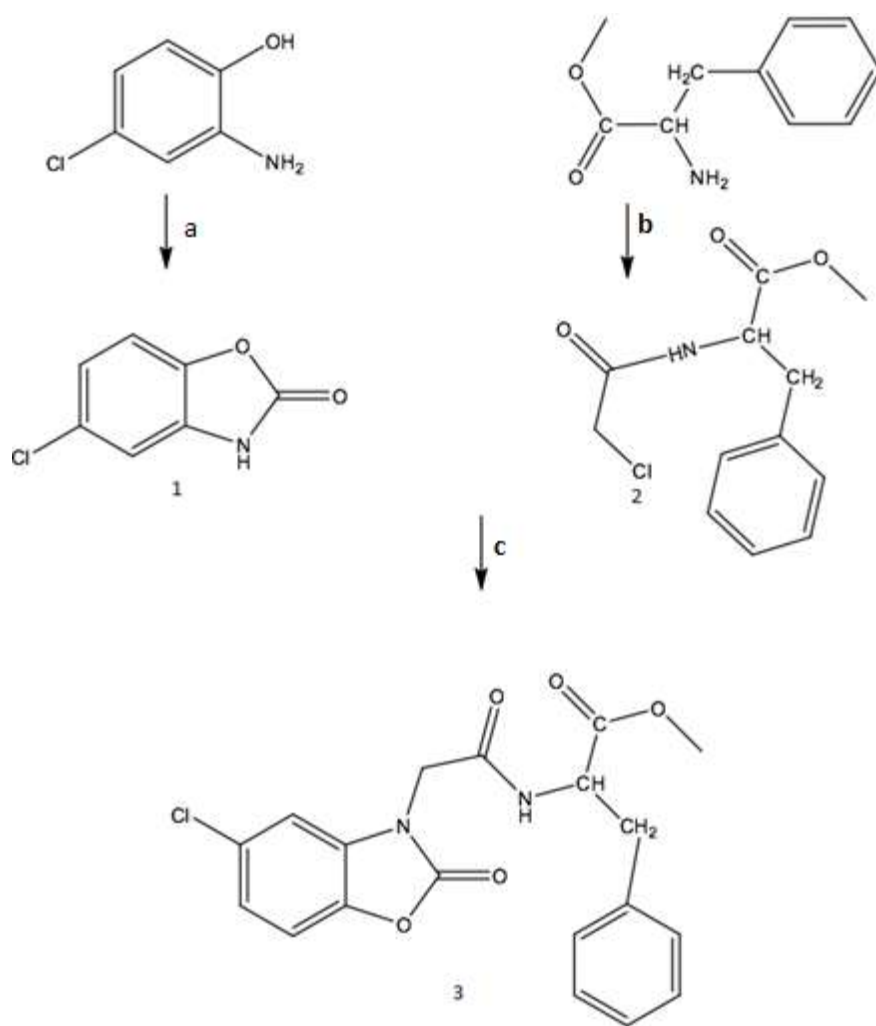
Acknowledgement:

We extend special thanks to Dr Tarun Sekhri, Director INMAS, Dr A. K. Mishra, Head, Division of Cyclotron and Radiopharmaceutical Science, INMAS, Delhi, and Dr Gaurav Mittal, Head CCM for providing us the facility to carry out experiments. I also thank Dr Himanshu Ojha, Scientist, Dr Sonia Gandhi, Scientist and Mr Sunil Pal, Technical Officer, Mr Harish Rawat, INMAS for their technical support. This work was supported by INMAS, Delhi under Task Project ST/15-16/INM-03. There is no conflict of interest among authors of this manuscript

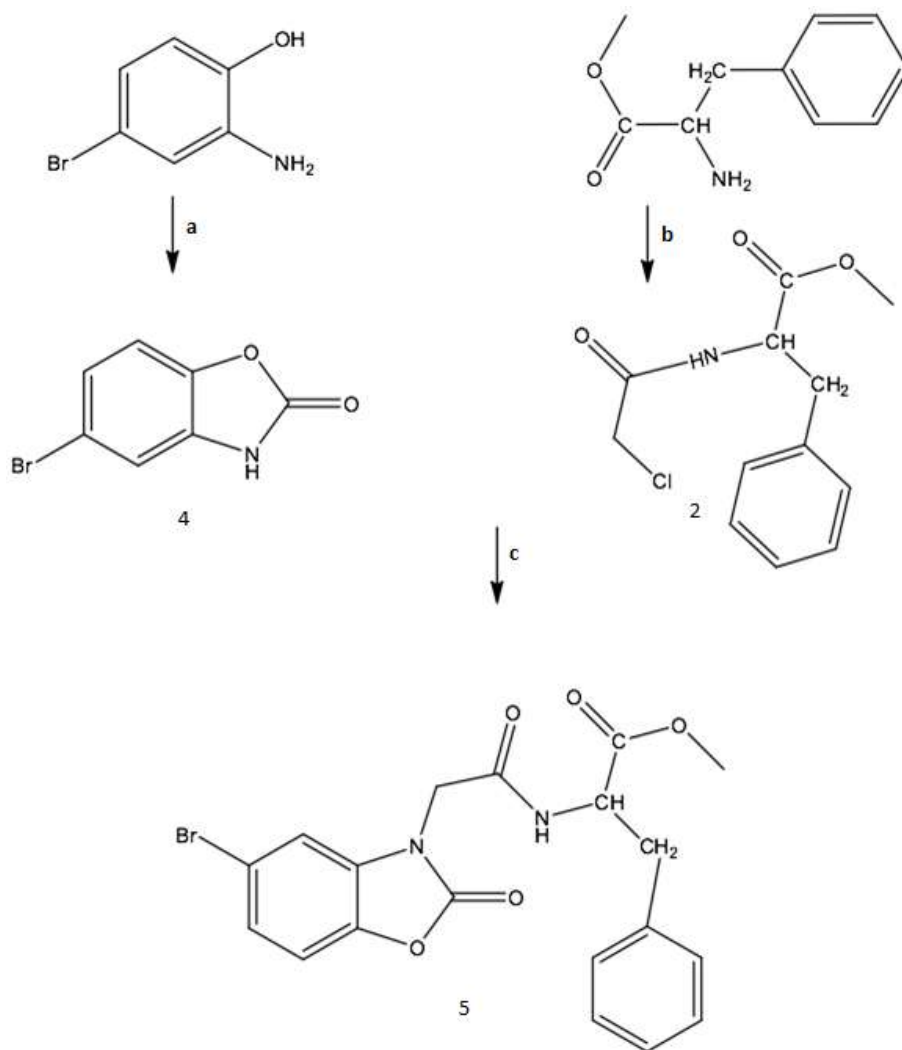
References:

- 1) V. Papadopoulos, M. Baraldi, T. R. Guilarte, T. B. Knudsen, J. J. Lacapère, P. Lindemann, M. D. Norenberg, D. Nutt, A. Weizman, M. R. Zhang and M. Gavish, *Trends Pharmacol. Sci.*, 27 (2006) 402–409.
- 2) F. Li, J. Liu, N. Liu, L. A. Kuhn, R. M. Garavito, and S. F. Miller, *Biochemistry* 55(2016)2821–2831.
- 3) F. Li, J. Liu, R. M. Garavito, S. F. Miller, *Pharmacol. Res.* 99(2015)404–409.
- 4) D. S. Albrecht, C. Granziera, J. M. Hooker, and M. L. Loggia, *ACS Chem. Neurosci.* 7(2016)470–483.
- 5) W. C. Kreisl, M. Fujita, Y. Fujimura, N. Kimura, K. J. Jenko, P. Kannan, J. Hong, C. L. Morse, S. S. Zoghbi, R. L. Gladding, S. Jacobson, U. Oh, V. W. Pike, R. B. Innis, *Neuroimage* 49 (2010) 2924–2932.
- 6) N. Denora, R. M. Iacobazzi, G. Natile, N. Margotta, *Coord. Chem. Rev.* 341(2017)1–18.
- 7) N. Denora, N. Margiotta, V. Laquintana, A. Lopodota, A. Cutrignelli, M. Losacco, M. Franco, and G. Natile, *ACS Med. Chem. Lett.* 5(2014)685–689.
- 8) C. Milite, E. Barresi, E. D. Pozzo, B. Costa, M. Viviano, A. Porta, A. Messere, G. Sbardella, F. D. Settimo, E. Novellino, S. Cosconati, S. Castellano, S. Taliani, and C. Martini, *J. Med. Chem.* (2017) DOI: 10.1021/acs.jmedchem.7b01031.
- 9) M. R. Zhang, T. Kida, J. Noguchi, K. Furutsuka, J. Maeda, T. Suhara and K. Suzuki, *Nucl. Med. Biol.* 30 (2003) 513–519.
- 10) M. L. James, R. R. Fulton, J. Vercoullie, D. J. Henderson, L. Garreau, S. Chalon, F. Dollé, S. Selleri, D. Guilloteau and M. Kassiou, *J. Nucl. Med.* 49 (2008) 814–822.
- 11) E. Briard, S. S. Zoghbi, M. Imaizumi, J. P. Gourley, H. U. Shetty, J. Hong, V. Cropley, M. Fujita, R. B. Innis and V. W. Pike, *J. Med. Chem.* 51 (2008) 17–30.
- 12) M. R. Zhang, K. Kumata, J. Maeda, K. Yanamoto, A. Hatori, M. Okada, M. Higuchi, S. Obayashi, T. Suhara and K. Suzuki, *J. Nucl. Med.* 48 (2007) 1853–1861.
- 13) D. R. Owen, A. J. Yeo, R. N. Gunn, *J. Cereb. Blood Flow Metab.* 32 (2012) 1–5.
- 14) T. Fukaya, T. Kodo, T. Ishiyama, H. Kakuyama, H. Nishikawa, S. Baba, S. Masumoto, *Bioorg. Med. Chem.* 22 (2012) 5568–5582.

- 15) Takayuki Fukaya, Takeo Ishiyama, Satoko Baba, and Shuji Matsumoto, *J. Med. Chem.* 56 (2013) 8191–8195.
- 16) A. K. Tiwari, J. Yui, M. Fujinaga, K. Kumata, Y. Shimoda, T. Yamasaki, L. Xie, A. Hatori, J. Maeda, N. Nengaki, M. R. Zhang, *J. Neurochem.* 129 (2014) 712–720.
- 17) A. K. Tiwari, M. Fujinaga, J. Yui, T. Yamasaki, L. Xie, K. Kumata, A. K. Mishra, Y. Shimoda, A. Hatori, B. Ji, M. Ogawa, K. Kawamura, F. Wang, M. R. Zhang, *Org. Biomol. Chem.* 12 (2014) 9621–9630.
- 18) A. K. Tiwari, B. Ji, M. Fujinaga, T. Yamasaki, L. Xie, R. Luo, Y. Shimoda, K. Kumata, Y. Zhang, A. Hatori, J. Maeda, M. Higuchi, F. Wang, M. R. Zhang, *Theranostics* 5 (2015) 961–969.
- 19) (a) A. K. Tiwari, J. Yui, Y. Zhang, M. Fujinaga, T. Yamasaki, L. Xie, Y. Shimoda, K. Kumata, A. Hatori, M. R. Zhang, *RSC Adv.* 123 (2015) 101447–101454.
- (b) N Kumari, N Chadha, P Srivastava, L C Mishra, S Bhagat, A K Mishra and A. K. Tiwari, *Chem Biol Drug Des.* 90(4), (2017) 511–519.
- 20) M. Fujinaga, R. Luo, K. Kumata, Y. Zhang, A. Hatori, T. Yamasaki, L. Xie, W. Mroi, Y. Kurihara, Ogawa, N. Nengaki, F. Wang, M. R. Zhang, *J. Med Chem.* 60 (2017) 4047–4061.
- 21) P. Srivastava, A. Kaul, H. Ojha, P. Kumar, A. K. Tiwari, *RSC Adv.* 6 (2016) 11449–114499.
- 22) H. Hanaoka, Y. Ohshima, Y. Suzuki, A. Yamaguchi, S. Watanabe, T. Uehara, S. Nagamori, Y. Kanai, N. S. Ishioka, Y. Tsushima, K. Endo, and Y. Arano, *J. Nucl. Med.*, 56 (2015) 791–797.
- 23) F. N. Kang, An in silico evaluation of the ADMET profile of the StreptomeDB database, *Springer Plus* 2 (2013) 353.
- 24) C. A. Lipinski, F. Lombardo, B. W. Dominy, P. J. Feeney, *Adv Drug Delivery Rev* 23 (1997) 3–25.
- 25) C.A. Lipinski, *J. Pharmacol. Toxicol. Methods* 44 (2000) 235–249.
- 26) W. L. Jorgensen, E. M. Duffy, *Adv Drug Deliv Rev.* 54 (2002) 355–366.
- 27) W. L. Jorgensen, E. M. Duffy, *Bioorg. Med. Chem. Lett.* 10 (2000) 1155–1158.
- 28) D. F. Veber, S. R. Johnson, H. Y. Cheng, B. R. Smith, K. W. Ward, K. D. Kopple, *J Med. Chem.* 45 (2002) 2615–2623.
- 29) J. J. Irwin and B. K. Shoichet, *J. Med. Chem.* 59 (2016) 4103–4120.
- 30) N. S. Pagadala, K. Syed, J. Tuszynski, *Biophys Rev* 9 (2017) 91–102.
- 31) L. Chaput, and L. Mouawad, *J. Cheminform.* 9 (2017) 37.
- 32) M. Bhargavi, S. K. Sivan, S. R. Potlapally, *Comp. Biol. Chem.* 68 (2017) 43–55.
- 33) L. Jaremko, M. Jaremko, K. Giller, S. Becker, M. Zweckstetter, *Science* 343 (2014) 1363–1366.
- 34) Y. Guo, R. C. Kalathur, Q. Liu, B. Kloss, R. Bruni, C. G. Inter, E. Kloppmann, B. C. Rost, W. A. Hendrickson, *Science* 347 (2015) 551–555.
- 35) F. Li, J. Liu, Y. Zheng, R. M. Garavito, S. F. Miller, *Science* 347 (2015) 555–558.
- 36) L. Jaremko, M. Jaremko, K. Giller, S. Becker, M. Zweckstetter, *Science* 343 (2014) 1363–1366.
- 37) Pooja Srivastava, A K Tiwari, N Chadha, K Chuttani, A K Mishra. *Eur J Med Chem*, 65 (2013) 12–20.
- 38) D Sinha, G Shukla, A K Tiwari, S Chaturvedi, K Chuttani, H Chandra, A K Mishra. *Chem Biol Drug Des.* 74 (2009) 159–64.
- 39) S. Singh, A. K. Tiwari, R. Varshney, R. Mathur, P. P. Hazari, B. Singh, and A. K. Mishra *RSC Adv.* 5 (2015) 41977–84.



Scheme 1: Synthesis of ABPO-Cl, reagents: a) CDI, THF, Reflux; b) Chloroacetyl chloride, Et_3N , $H_2O/DCM, 0^{\circ}C-rt$; c) K_2CO_3 , DMF, $60^{\circ}-70^{\circ}C$, 3h



Scheme 2: Synthesis of ABPO-Br, reagents: a) CDI, THF, Reflux; b) Chloroacetyl chloride, Et₃N, H₂O/DCM, 0°C-rt; c) K₂CO₃, DMF, 60⁰-70⁰C, 3h

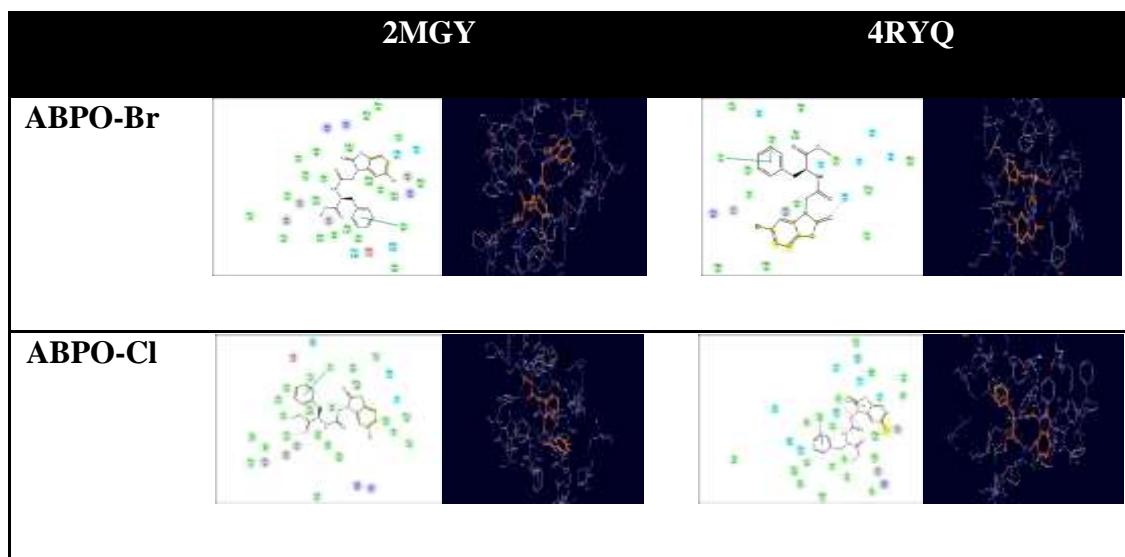


Fig 1: 2D and 3D interaction diagram of a) ABPO-Br and b) ABPO-Cl with wild type PDBs 2MGY and 4RYQ

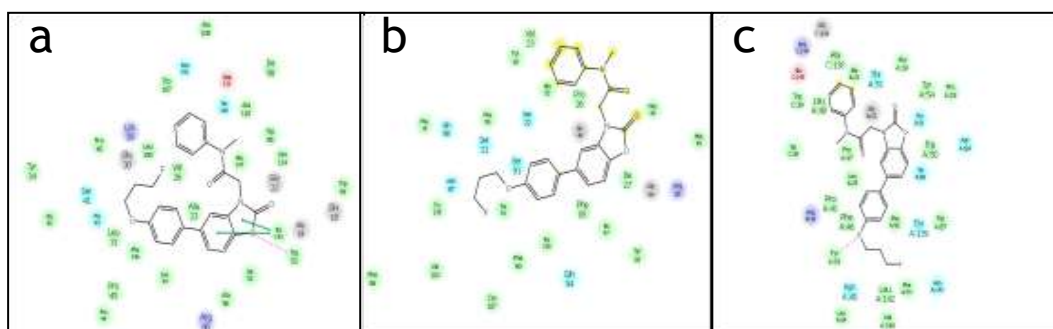


Fig 2: 2D interaction diagram of FEBMP, FPBMP with PDBs a) 2MGY, b) 4RYQ and c) 4UC1

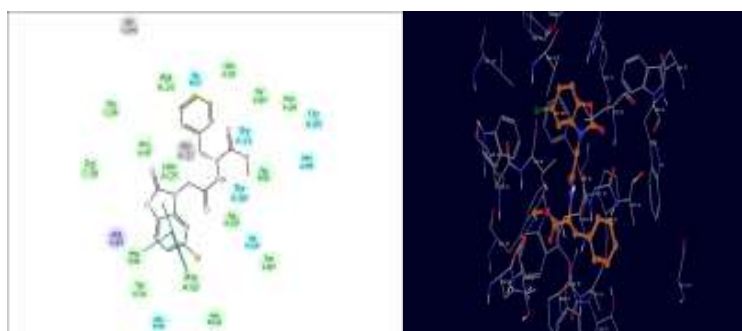
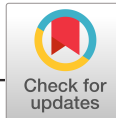


Fig 3: 2D and 3D interaction diagram of ABPO-Cl with mutant type PDBs 4UC1



Fig. 4: *In vivo* biodistribution of a) ^{99m}Tc -ABPO-Cl and b) ^{99m}Tc -ABPO-Br in New Zealand rabbit (Dynamic image)



Modified benzoxazolone (ABO-AA) based single photon emission computed tomography (SPECT) probes for 18 kDa translocator protein

Pooja Srivastava^{1,2} | Dipti Kakkar¹ | Pravir Kumar² | Anjani Kumar Tiwari^{1,3}

¹Division of Cyclotron and Radiopharmaceutical Sciences, Institute of Nuclear Medicine and Allied Sciences, Delhi, India

²Molecular Neuroscience and Functional Genomic Laboratory, Department of Biotechnology, Delhi Technological University, Delhi, India

³Department of Chemistry, School of Physical & Decision Sciences (SPDS), Babasaheb Bhimrao Ambedkar Central University, Lucknow, UP, India

Correspondence

Anjani K. Tiwari, Department of Chemistry, School of Physical & Decision Sciences (SPDS), Babasaheb Bhimrao Ambedkar Central University, Vidya Vihar, Raebareli Road, Lucknow 226025, UP, India & Division of Cyclotron and Radiopharmaceutical Sciences, Institute of Nuclear Medicine and Allied Sciences, Brig. S. K. Mazumdar Road, Delhi 110 054, India.
Email: anjanik2003@gmail.com

Pooja Srivastava, Division of Cyclotron and Radiopharmaceutical Sciences, Institute of Nuclear Medicine and Allied Sciences, Brig. S. K. Mazumdar Road, Delhi 110054, India.
Email: pushree14@gmail.com

Funding information

INMAS

Abstract

Acetamidobenzoxazolone (ABO) has been modified to ABO-AA, 2-(2-(5-bromo/chloro benzoxazolone)acetamide)-3-(1*H*-indol-3-yl)propionate to improve pharmacokinetics and lipophilicity ($\log p = 2.04$). The final compound was synthesized in better yield and in fewer steps than previously reported MBIP-Br (70% vs. 62%). Computational docking confirmed binding of MBIP-Cl with translocator protein (TSPO) as well as with mutant TSPO (-8.99 for PDB: 4RYQ and -9.30 for PDB: 4UC1, respectively). Ex-vivo bio-distribution and scintigraphy showed that ^{99m}Tc-MBIP-Cl is better than ^{99m}Tc-MBIP-Br in terms of uptake in TSPO-rich organs and release kinetics 0–120 min postinjection. At 15 min, uptake was 2.75-fold (12.91%ID/g vs. 4.69%ID/g) in lung and seven-fold (5.16% ID/g vs. 0.72%ID/g) in heart for ^{99m}Tc-MBIP-Cl compared to that of ^{99m}Tc-MBIP-Br which gives warrant to utilize this single photon emission computed tomography agent in higher animals.

KEYWORDS

acetamidobenzoxazolone, inflammation, SPECT, tryptophan methyl ester, TSPO

1 | INTRODUCTION

Translocator protein (TSPO) first described as peripheral benzodiazepine receptor (PBR) is a 18 kDa protein and initially identified in 1977 as peripheral binding site for the benzodiazepine. The name PBR described its high affinity binding to benzodiazepine in peripheral tissues (Chen & Guilarte, 2008; Fan, Lindemann, Feuilloley, & Papadopoulos, 2012; Milenkovic, Rupprecht, & Wetzel, 2015; Veenman, Vainshtein, & Gavish, 2015). It is an intracellular protein which forms a complex with voltage dependent anion channel (VCAD, 32 kDa) and adenine nucleotide translocator (ANT, 30 kDa) in mitochondria. There are few classical ligands available such as PK11195, RoS-4864, and FGIN-127 which are isoquinoline carboxamide, benzodiazepine and indole derivatives,

respectively. All three of them showed compatibility to tetrapyrrole protoporphyrin IX (PPIX) structure which is a well-known endogenous TSPO ligand (Best, Ghadery, Pavese, Tai, & Straffella, 2019; Veenman, Vainshtein, Yasin, Azrad, & Gavish, 2016). TSPO has been investigated as biomarker for inflammatory conditions of lung, liver, kidney, and brain, etc. Its role has also been studied in other disorders such as depression, anxiety, and neurodegenerative disorders (Hatori et al., 2014; Jean et al., 2015; Jones, Marino, Shakur, & Morrell, 2003; Kraus, Kadriu, Lanzenberger, Zarate, & Kasper, 2019; Lagarde, Sarazin, & Bottlaender, 2018; Veenman & Gavish, 2006; Vicidomini et al., 2015). Therefore, high affinity TSPO ligands can find application for noninvasive diagnosis of pathologically affected tissues. This led to the development of TSPO ligands as diagnostic ligands (Arlicot et al., 2012; Boutin

et al., 2007; Dolle, Luus, Reynolds, & Kassiou, 2009; Hatori et al., 2014; Kreisl et al., 2010; Trapani, Palazzo, de Candia, Lasorsa, & Trapani, 2013; Veenman et al., 2016).

^{11}C (R) PK11195 ligand is most widely studied PET TSPO ligand from first generation which has limitation of high lipophilicity and low in vivo specific binding. These limitations were overcome by second generation TSPO ligands for improved imaging. Some of the TSPO ligands used in clinical human studies are ^{18}F FEDAA, ^{11}C DAA, ^{11}C JPBR28, ^{18}F DPA714, and ^{11}C JAC-5216 (Arlicot et al., 2012; Boutin et al., 2007; Dolle et al., 2009; Hatori et al., 2014; Kreisl et al., 2010; Trapani et al., 2013; Veenman et al., 2016). These second-generation ligands have the problem of intersubject variability (Owen, Yeo, & Gunn, 2012). A new skeleton acetamidobenzoxazolone (ABO) which has been derived from RoS-4,864 by opening the diazepine ring and reorganizing it (Fukaya et al., 2012; Fukaya et al., 2013) to overcome the problems of intersubject variability and nonspecific binding (Tiwari, Yui, et al., 2015). In recent past, our group has explored this skeleton for diagnostic application using positron emission tomography (PET) with ^{11}C and ^{18}F radionuclides such as 2-[5-(4- ^{11}C Methoxyphenyl)-2-oxo-1,3-benzoxazol-3(2H)-yl]-N-methyl-N-phenylacetamide (^{11}C -MBMP), 2-[5-(4- ^{18}F fluoroethoxy/propoxyphenyl)-2-oxo-1,3-benzoxazol-3(2H)-yl]-N-methyl-N-phenylacetamide (^{18}F -FEBMP and ^{18}F -FPBMP) and using single photon emission computed tomography (SPECT) with $^{99\text{m}}\text{Tc}$ such as $^{99\text{m}}\text{Tc}$ -MBIP (Kumari et al., 2017; Srivastava, Kaul, Ojha, Kumar, & Tiwari, 2016; Tiwari, Fujinaga, et al., 2014; Tiwari, Yui, et al., 2014; Tiwari, Ji, et al., 2015).

Here we compare two ligands of similar category acetamidobenzoxazolone, $^{99\text{m}}\text{Tc}$ -MBIP-Br, and $^{99\text{m}}\text{Tc}$ -MBIP-Cl, in terms of ex vivo biodistribution and in vivo radioactivity uptake in TSPO enriched organs. The release kinetics of these tracers has been compared to see their retention in different organs under in vivo conditions. Besides that, computational ligand-protein interaction, synthetic yield and lipophilicity have also been compared to get more insight about the complete pharmacokinetics of ABO-AA skeleton for SPECT application.

2 | MATERIALS AND METHODS

2.1 | Instrumentation

Spectroscopic techniques used for the characterization were ^1H and ^{13}C NMR spectroscopy (Bruker Avance III 600 MHz system) at 600 MHz and 150 MHz, respectively, and mass spectroscopy (Agilent 6310 system) using ESI. HRMS was recorded on Agilent 6520 Q-TOF (ESI-HRMS) mass spectrometer having ESI source in positive mode. Radioligand related studies were performed on Siemens Symbia Camera for imaging and γ -scintillation counter for radioactivity counting. The lipophilicities of the compounds were calculated using the ChemDraw software.

2.2 | Animal models

Institutional Animal Ethics Committee (INM/DASQA/IAEC/09/015) approved protocols were used for studies. BALB/c mice (22–28 g,

10 weeks old, male) and New Zealand rabbit (2.3 kg, 1 year 5 months, male) were used for biodistribution studies and imaging.

Animals were supplied by experimental animal facility (EAF) of Institute of Nuclear Medicine and Allied Sciences (INMAS), Delhi. The animals were maintained as per the regulations of the Committee for the Purpose of Control and Supervision of Experiments on Animals (CPCSEA). All the animals were maintained on standard diet (Hindustan Lever Ltd., Mumbai, India) and water. They were kept in the animal house of the institute which was maintained at $22 \pm 2^\circ\text{C}$ and 50% humidity under a 12 hr dark/light cycles.

A lung inflammation model was prepared in balb/c mice by intratracheal delivery of lipopolysaccharide (LPS). For this, 6–8 weeks old balb/c (22–25 g, male) mice were anesthetized by isoflurane sedation. While anesthetized, an incision was made around the thoracic region in mice and 100 μL of 0.5 mg/mL of LPS solution was delivered intratracheally into the mice. After 24 hr, the mice were used for experimental purpose to validate the uptake of radioligand in inflamed lungs, overexpressing TSPO receptors. The blocking studies were performed in these models by preadministering 10 mg/kg unlabeled PK11195, 10 min prior to 100 μCi $^{99\text{m}}\text{Tc}$ -MBIP-Cl injection and was imaged 40 min postinjection of the radioligand. The lung model was assessed by tracer technique by comparing biodistribution of radio-complex in lung-modeled mice with and without blocking.

2.3 | In vitro cell uptake of $^{99\text{m}}\text{Tc}$ -MBIP-cl in A549 cells

Human lung carcinoma A549 cells were cultured as per protocol in literature (Dumoga et al., 2016). A549 cells were maintained in RPM1 medium supplemented with 10% (v/v) heat inactivated fetal bovine serum, 2 mM L-glutamine and 100 U mL^{-1} penicillin-streptomycin in a humidified incubator at 37°C in 5% CO_2 . The A549 cells (1×10^6 per well) were incubated with $^{99\text{m}}\text{Tc}$ -MBIP-Cl/Br (in 10% ethanol, 5% tween 20 and water) for 10, 30, 60, and 120 min, respectively. In an inhibition study for specificity, 300 mM solution of PK11195 was added to the cells prior to incubation and the cells were washed with PBS after 1 hr. Thereafter radiocomplex ($^{99\text{m}}\text{Tc}$ -MBIP-Cl/Br) was added and its cell uptake was studied at 10, 30, 60, and 120 min with the help of a gamma counter.

2.4 | Synthesis

2.4.1 | Synthesis of methyl 2-(2-chloroacetamido)-3-(1H-indol-3-yl)propanoate

To a solution of L-tryptophan methyl ester (500 mg, 2.32 mmol) and deionized water (10 mL), triethyl amine (355 μL , 2.55 mmol) was added with constant stirring under nitrogen atmosphere on ice bath for 5 min. To the mixture, chloroacetyl chloride (203 μL , 2.55 mmol) in dichloromethane (10 mL) was added drop wise over 1 hr and the reaction was carried out for 4 hr. Thereafter, the mixture was extracted with dichloromethane (3x). The organic layer was washed twice by deionized water and brine solution. After washing, the organic layer

was dried over anhydrous sodium sulfate. After filtration, the solvent was removed in vacuo, and purified by silica gel column chromatography using 100% CHCl₃ as eluent (Yield = 75%).

¹H-NMR (CDCl₃, 600 MHz): δ (ppm) 3.3–3.4 (d, 2H), 3.7 (s, 3H), 4.0 (s, 2H), 4.9–5.0 (m, 1H), 7.0–7.6 (m, 5H), 8.5 (br s, 1H)

¹³C-NMR (CDCl₃, 150 MHz): δ (ppm) 27.5, 42.5, 52.6, 53.3, 109.3–136.3 (8 peaks), 166.0, 171.8

MS (ESI) m/z: 293.1 [M–H⁺], calculated m/z: 293.1 [M–H⁺].

2.4.2 | Synthesis of 5-chloro benzoxazol-2(3H)-one

To a solution of 4-chloro-2-aminophenol (5 g, 34.83 mmol) in 150 mL THF, 1,1'-carbonyldiimidazole (5.65 g, 34.83 mmol) was added. The mixture was refluxed with stirring for 2 hr. The reaction mixture was quenched by adding 2 M HCl solution after cooling down to room temperature. EtOAc was used for extraction which was washed with brine, dried over anhydrous sodium sulfate and filtered. Thereafter, solvent was removed in vacuo to get the product as a white solid (yield = 91%).

¹H-NMR (DMSO, 600 MHz): δ (ppm) 7.1–7.4 (m, 3H)

¹³C-NMR (DMSO, 150 MHz): δ (ppm) 110.3, 111.3, 122.0, 128.2, 132.2, 142.6, 154.7

MS (ESI) m/z: 167.8 [M–H⁺], Calculated m/z: 168.0 [M–H⁺].

2.4.3 | Synthesis of 2-(2-(5-chloro benzoxazolone) acetamido)-3-(1H-indol-3-yl) propanoate (MBIP-Cl)

To a solution of 5-chloro benzoxazol-2(3H)-one (250 mg, 1.48 mmol) and K₂CO₃ (306 mg, 2.22 mmol) in DMF (5 mL), methyl-2-(2-chloroacetamido)-3-(1H-indol-3-yl) propionate (435 mg, 1.48 mmol) was added with cooling on ice bath. The reaction mixture was stirred at 60–70°C for 3 hr. Thereafter, the reaction mixture was cooled to room temperature before adding water. A mixture of toluene and ethyl acetate, in 1:1 ratio, was used as extraction solvent. Water and brine solution were used for washing the organic layer and anhydrous sodium sulfate for drying. Solvent was removed in vacuo after filtration and was purified by silica gel column chromatography using CHCl₃/EtOAc (4:1, v/v) as eluent (yield = 70%).

¹H-NMR (CDCl₃, 600 MHz): δ (ppm) 3.5–3.7 (m, 2H), 3.8 (s, 3H), 3.9–4.0 (m, 2H), 5.0–5.1 (m, 1H), 6.7–7.5 (m, 8H), 8.1 (br s, 1H)

¹³C-NMR (CDCl₃, 150 MHz): 24.1, 51.2, 53.1, 54.3, 110.4–148.8 (14 peaks), 155.5, 168.2, 168.8

MS (ESI) m/z: 426.3 [M–H⁺], Calculated m/z: 426.1 [M–H⁺]

HPLC: T3 column, 4.6 × 250 mm; MeCN/H₂O, 6/4–8/2 (v/v); flow rate: 0.8 mL/min; λ_{uv} = 254 nm; t_R = 7.214 min.

HRMS: m/z 428.1000 [(C₂₁H₁₈ClN₃O₅) + H]⁺.

2.4.4 | Synthesis of 2-(2-(5-bromo benzoxazolone) acetamido)-3-(1H-indol-3-yl) propanoate (MBIP-Br)

MBIP-Br was synthesized by the procedure mentioned in our previous paper (Srivastava et al., 2016).

¹H-NMR (DMSO, 400 MHz): δ (ppm) 3.1–3.2 (m, 2H), 3.6 (s, 3H), 4.4–4.6 (m, 3H), 6.9–7.5 (m, 8H)

¹³C-NMR (DMSO, 100 MHz): δ (ppm) 28.7, 44.4, 52.4, 53.9, 111.0–141.5 (14 C), 154.2, 166.3, 172.3

MS (ESI) m/z: 470.2 [M–H⁺], calculated: 470.0 [M–H⁺]

HPLC: T3 column, 4.6 × 250 mm; MeCN/H₂O, 6/4–8/2 (v/v); flow rate: 0.8 mL/min; λ_{uv} = 254 nm; t_R = 8.751 min

HRMS: m/z 474.0496 [(C₂₁H₁₈BrN₃O₅) + H]⁺.

2.5 | ^{99m}Tc radiolabeling

To evaluate the stability, specificity, and biodistribution profile of MBIP-Cl and MBIP-Br compounds, they were labeled with ^{99m}Tc using procedure from literature with slight modifications (Kakkar et al., 2012; Srivastava et al., 2013). Briefly, 100 μ L of sterile sodium pertechnetate (approximately 74–110 MBq of ^{99m}TcO₄) was reduced with 50 μ L of stannous chloride solution (1 × 10^{−2} M in 10% glacial acetic acid) and pH was adjusted to 6.5 using 0.5 M sodium bicarbonate. A solution of MBIP-Cl and MBIP-Br were added to this mixture separately and after thorough mixing, incubated for 15 min at room temperature (25°C). ITLC-SG strips as stationary phase and acetone as mobile phase were used to determine complexation of MBIP-Cl and MBIP-Br with ^{99m}Tc and purity of the labeled compound.

2.6 | In vitro human serum stability assay

In vitro human serum stability of the radiolabeled compounds was evaluated using our previous approach with some modifications (Kumar et al., 2010). Blood collected from healthy volunteers was clotted in humidified incubator for 1 hr under 5% CO₂ and 95% air and used to prepare serum. Sample was centrifuged at 400 rpm and filtered through 0.22 μ m filter into sterile plastic culture tubes.

^{99m}Tc-MBIP-Cl and ^{99m}Tc-MBIP-Br were incubated with freshly prepared serum at 37°C. Samples were analyzed at different time points using ITLC-SG strips. Acetone was used as mobile phase for measurement to find out percentage dissociation of the complex in serum with a function of time.

2.7 | Biodistribution studies

Balb/c mice were used for the initial in vivo assessment of ^{99m}Tc-MBIP-Cl and ^{99m}Tc-MBIP-Br (Srivastava et al., 2016). Radioactivity uptake was measured in specific organs of the mice at different time points, that is, 15 min, 30 min, 60 min, and 120 min postinjection of 100 μ Ci of both radioligands via a tail vein and results were expressed as percentage of injected dose per gram (%ID/g) of tissue. The experiments were performed in triplicate at each time point. Radioactivities in organs were measured with the help of a gamma counter. Radioactivity injected in each mouse was found out by subtracting the activity left in tail from the activity injected. Total blood volume was calculated as 7% of the total body weight.

3 | RESULTS AND DISCUSSION

Encouraged by the results of our recently developed TSPO ligands having TSPO affinity in nanomolar range (Tiwari, Fujinaga, et al., 2014; Tiwari, Yui, et al., 2014; Tiwari, Yui, et al., 2015), we directed our efforts towards development of analogs of ABO for ^{99m}Tc labeling to target 18 kDa TSPO. The basis of our research was the successful outcome of radioligands [^{11}C]MBMP and [^{18}F]FE/FPBMP showing promise for TSPO visualization and quantification. The new ligands conjugate acetamidobenzoxazolone to tryptophan methyl ester. Further, the ^{99m}Tc -MBIP-Cl showed fast clearance from the requisite organs as well as from circulating blood. The ^{99m}Tc -MBIP-Cl exhibited reasonable uptake in heart, lungs, kidney, and spleen, which are known to express TSPO.

ADME analysis of both the analogs, MBIP-Cl and MBIP-Br, were focused mainly on the issue of blood brain permeability and serum protein binding which were found to be in the range of 95% of well-established drugs in computational studies using QikProp module of Schrodinger. They do not violate any of the five Lipinski rules and three Jorgensen rules. Both the ligands have lower lipophilicity (2.04 for chloro and 2.31 for bromo analogs) than known TSPO ligands. Analogs of ABO, [^{11}C]MBMP and [^{18}F]FEBMP, demonstrated high specific binding with TSPO in ischemic rat brain but they have moderate brain kinetics in higher animals. These PET ligands have been modified to other ABO ligand ^{18}F -2-(5-(6-Fluoropyridin-3-yl)-2-oxobenzo[d]oxazol-3(2H)-yl)-N-methyl-N-phenylacetamide for reducing the lipophilicity for faster brain kinetics.²⁹ Thereafter, TSPO binding/affinity of MBIP-Cl was found out through docking methods with TSPO proteins (Figure 1). Score of MBIP-Cl with 4RYQ and 4UC1 were -8.99 and -9.30 , respectively. The interaction of MBIP-Cl in terms of G_{score} was found comparable with other known TSPO ligands for 4RYQ and with TSPO ligands not significantly affected by single nucleotide polymorphism such as FEBMP and PK11195 for 4UC1 (Tables 1 and 2).

The final ligand was synthesized by the procedure mentioned in Scheme 1 in three steps with modification in earlier used procedure having four steps for MBIP-Br (Srivastava et al., 2016). The synthetic procedure involved synthesis of methyl-2-(2-chloroacetamido)-3-(1H-indol-3-yl)propanoate and 5-chloro benzoxazol-2(3H)-one, as intermediates which were combined in the final step. The precursor molecule 5-chloro benzoxazolone was prepared by cyclization reaction of 4-chloro-2-amino phenol in presence of CDI. Simultaneously, chloroacetylation was performed on L-tryptophan methyl ester. Thereafter, both the above-mentioned products were combined through alkylation reaction in presence of K_2CO_3 in DMF. The synthesized MBIP-Cl had good yield (70%). Column chromatography was used for purification of the synthesized products and spectroscopic methods were used for characterization of the intermediates as well as the final products. The synthesis of final product was confirmed by $m/z = 426.3$ [$\text{M}-\text{H}^+$] peak present in mass spectroscopic data. The synthetic scheme followed for MBIP-Cl is better than reported scheme for its bromo analog in terms of yield and duration of overall synthesis (Srivastava et al., 2016).

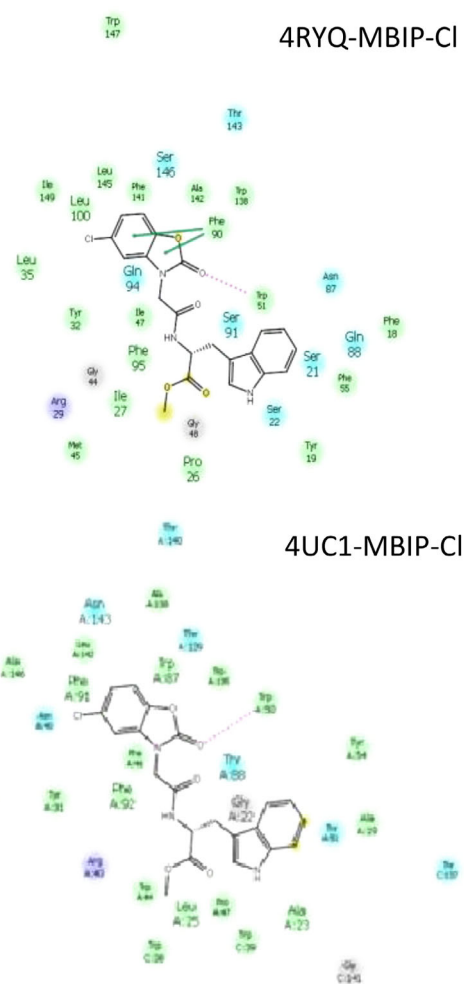


FIGURE 1 2D interaction diagram of MBIP-Cl on docking with TSPO [PDB ID: 4RYQ (a) and 4UC1 (b)] MBIP-Cl formed pi-pi interactions of aromatic rings with Phe90 and H-bond interactions with Try51 in 4RYQ interaction and Try50 is involved in H bond interaction with 4UC1

TABLE 1 G_{score}^a of TSPO ligands with PDB: 4RYQ^b

Ligand	G_{score}
MBIP-Cl	-8.99
MBIP-Br	-6.92
DAA1106	-7.06
PK11195	-7.17
PBR28	-7.14
DPA-713	-7.035

^aGlide score is an empirical scoring function that approximates the ligand binding free energy.

^b4RYQ is wild TSPO X-ray crystal structure with resolution 1.7 Å taken from RCSB protein data bank.

Subsequently, radiochemistry of MBIP-Cl was optimized with ^{99m}Tc for maximum complexation stability (Srivastava et al., 2016; Tiwari, Ji, et al., 2015). The stability of ^{99m}Tc -MBIP-Cl was found $>94\%$ in saline solution and $>91\%$ in serum at 4 hr (Figure 2) indicating

that both ^{99m}Tc -MBIP-Cl and ^{99m}Tc -MBIP-Br are suitable for SPECT application in terms of stability, the latter being relatively better (91% vs. 93% in serum at 4 hr). This technetium-99 m labeled MBIP-Cl was then used to evaluate its binding affinity to TSPO expressing A549 human lung carcinoma cells by an in vitro assay. The results of the in vitro uptake of the radiocomplex are shown in Figure 3. They demonstrate that the uptake is time dependent and increases until last time point of study, that is, 60 min for both bromo and chloro analogs. The blocking studies were also performed in the presence of PK11195 as blocking agent. The compound was incubated for 1 hr before adding radiolabeled compound. The maximum reduction was 41.1% and 43.6% for chloro and bromo analogs, respectively. Although there was an increase in the uptake of blocked cells with time implying that the cells

are not fully blocked, still it gives preliminary idea about the specificity of radiolabeled MBIP-Cl towards TSPO.

Biodistribution studies were performed to determine how ^{99m}Tc -MBIP-Cl was distributed in TSPO enriched organs as well as in excretory organs in terms of %ID/g of ^{99m}Tc -MBIP-Cl at four different time points as shown in Figure 4 and was compared with biodistribution studies of ^{99m}Tc -MBIP-Br. After 15 min, there was high uptake of radioactivity into organs known to have TSPO sites, such as kidney

TABLE 2 G score of TSPO ligands with PDB: 4UC1^a

Ligand	G _{score}
MBIP-Cl	-9.30
MBIP-Br	-9.61
FEBMP	-8.07
PK11195	-8.25

^a4UC1 is mutant TSPO X-ray crystal structure with resolution 1.8 Å taken from RCSB protein data bank.

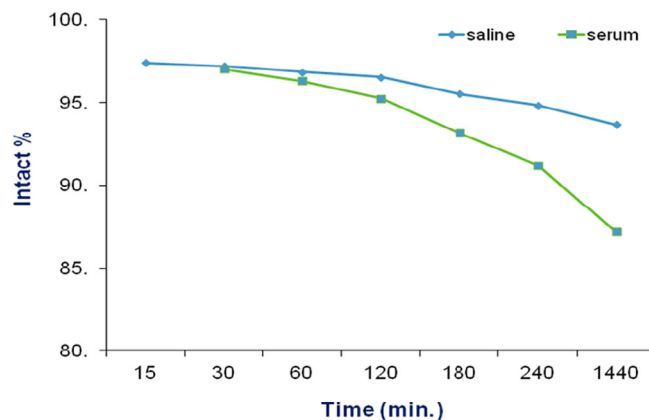
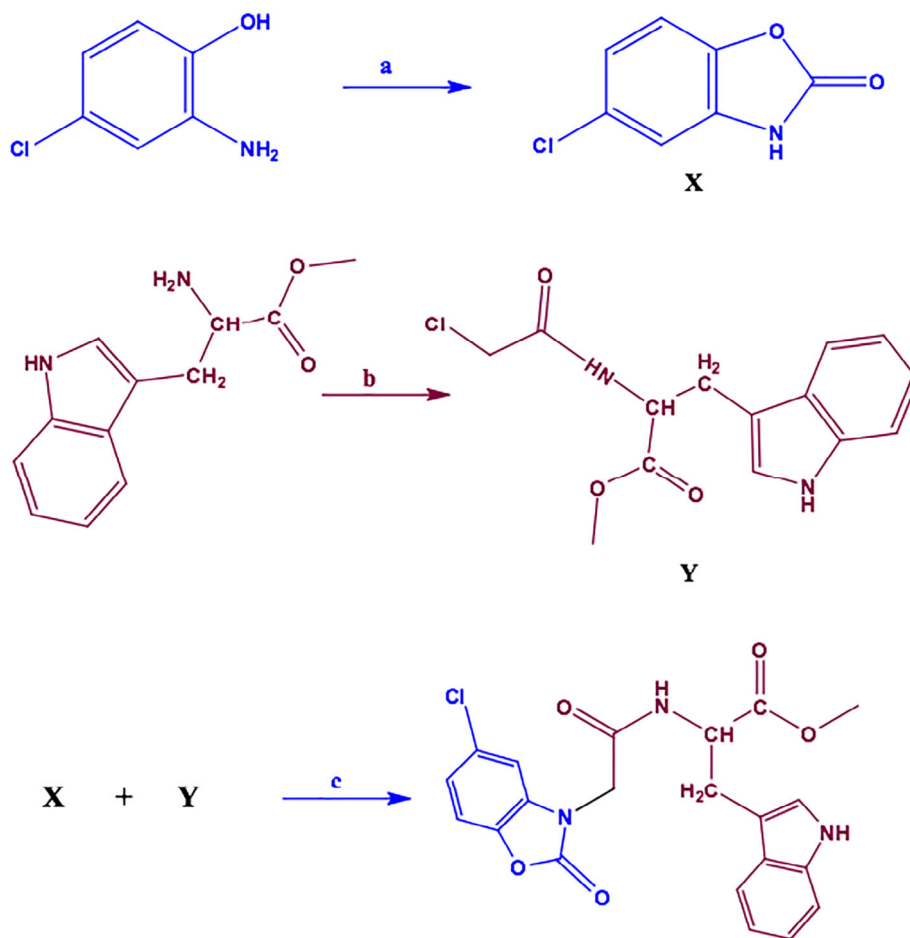


FIGURE 2 % intact ^{99m}Tc -MBIP-Cl as a function of time demonstrating stability in saline and human serum at 37°C over 24 h



(29.57%ID/g), heart (5.16%ID/g), spleen (2.87%ID/g), and lungs (12.91%ID/g). The uptake of ^{99m}Tc -MBIP-Cl in lungs and heart was approximately 2.75 and 7 folds higher to that of ^{99m}Tc -MBIP-Br uptake at 15 min showing better distribution pattern for TSPO targeting (Figure 5) which, in turn, would result in a better SPECT ligand. Uptake of ^{99m}Tc -MBIP-Cl in liver was relatively lower than that of ^{99m}Tc -MBIP-Br (19.74 vs. 23.12%ID/g).²⁴ Rate of reduction was high in heart and lungs, which was reduced to 14.7% (5.16%ID/g to 0.76%ID/g) and 8.9% (12.91%ID/g to 1.12%ID/g) between 15 and 120 min, respectively. Over the same period, uptake in kidney, liver, spleen, and blood was reduced to 54.5%, 34.0%, 33.8%, and 45.0%, respectively. The amount of radiotracer in the blood and brain decreases with time. Uptake in kidney and liver reflected that the excretion occurred through renal and hepatobiliary tract as expected for a compound with moderate lipophilicity.

Further, ^{99m}Tc -MBIP-Cl was also compared with the SPECT ligands reported in literature. As compared to ^{99m}Tc -labeled 2-quinolinecarboxamide, the uptake of ^{99m}Tc -MBIP-Cl, was found to

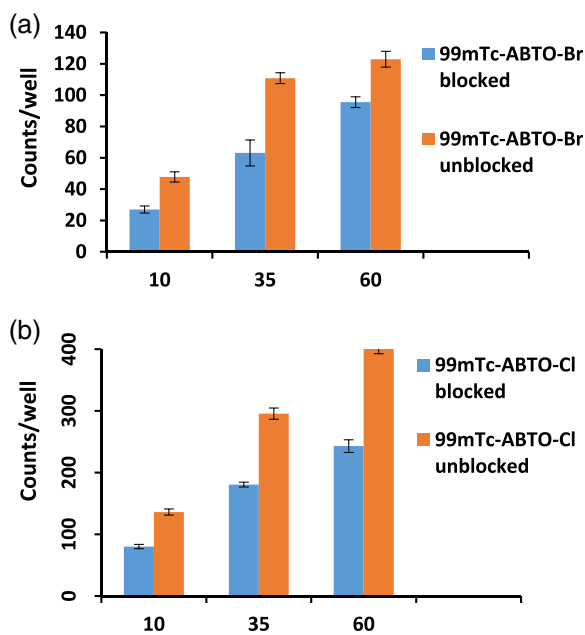


FIGURE 3 Uptake kinetics of (a) ^{99m}Tc -MBIP-Cl and (b) ^{99m}Tc -MBIP-Br in A549 cells in the presence (blue) and absence (red) of PK11195. Data are expressed as counts per well (mean with SD $n = 3$)

be higher in heart (2.96%ID/g vs. negligible uptake) and lung (6.16% ID/g vs. 1.19 %ID/g) and comparable in spleen (2.18%ID/g vs. 2.07% ID/g) at 15 min as reported in CD-1 mice.³¹ Uptake of [^{123}I]-CLINME, an iodine based SPECT ligand, in heart, lungs, and spleen of SD rat were 3.53%ID/g, 3.53%ID/g, 2.65%ID/g at 15 min. This was lower/comparable to the uptake of ^{99m}Tc -MBIP-Cl in respective organs.³² The liver uptake was lower for ^{99m}Tc -MBIP-Cl in comparison with ^{99m}Tc -labeled 2-quinolinecarboxamide and ^{99m}Tc -MBIP-Br (Cappelli et al., 2008; Cumming et al., 2018; Srivastava et al., 2016). This accounts for better image visualization (target organ to liver ratio) for ^{99m}Tc -MBIP-Cl.

Comparison of release rate among SPECT agents between 30 and 60 min for ^{99m}Tc -MBIP-Cl, [^{123}I]-CLINME (Mattner et al., 2015), ^{99m}Tc -labeled 2-quinolinecarboxamide and ^{99m}Tc -MBIP-Br reflected better release rate of ^{99m}Tc -MBIP-Cl in lung, liver, heart, and spleen (Cappelli et al., 2008; Srivastava et al., 2016). Further, it was also compared with PET and SPECT ligands of ABO category. The release kinetic rates between 15 and 60 min for ^{18}F -FEBMP (Tiwari, Ji, et al., 2015), ^{11}C -MBMP (Tiwari, Fujinaga, et al., 2014), ^{18}F -2-(5-(6-Fluoropyridin-3-yl)-2-oxobenzo[d]oxazol-3(2H)-yl)-N-methyl-N-phenylacetamide (Fujinaga et al., 2017), and ^{99m}Tc -MBIP-Cl are 0.175%ID/g/min, 0.150%ID/g/min, 0.070%ID/g/min, and 0.085%ID/g/min in heart, this ratio became more comparable as 0.382%ID/g/min, 0.375%ID/g/min, 0.155%ID/g/min and 0.231%ID/g/min in lungs. In liver and kidney, release kinetic rates were approximately 3–30 folds faster in ^{99m}Tc -MBIP-Cl which makes it interesting for further evaluation. These evaluations demonstrated release rate of ^{99m}Tc -MBIP-Cl from different organs are comparable to known TSPO ligands, therefore it can be further evaluated for TSPO targeting.

In vivo specificity of MBIP-Cl was evaluated in lung inflammation models of balb/c mice using PK11195. The preadministration of cold PK11195 in these inflammation models demonstrated significant reduction of uptake in the lung region as expected. This was clearly evident in the whole-body SPECT image taken 40 min postinjection of ^{99m}Tc -MBIP-Cl (Figure 6).

In order to have better clarity about organs uptake, in vivo imaging was performed in New Zealand rabbit. Scintigraphy study of ^{99m}Tc -MBIP-Cl was carried out by intravenous injection of 300 μCi in 200 μL of radiolabeled complex through ear vein. The acquisition was performed 4 min postinjection for 1 min. The biodistribution pattern shown in the image (figure 7) is similar to ex vivo biodistribution

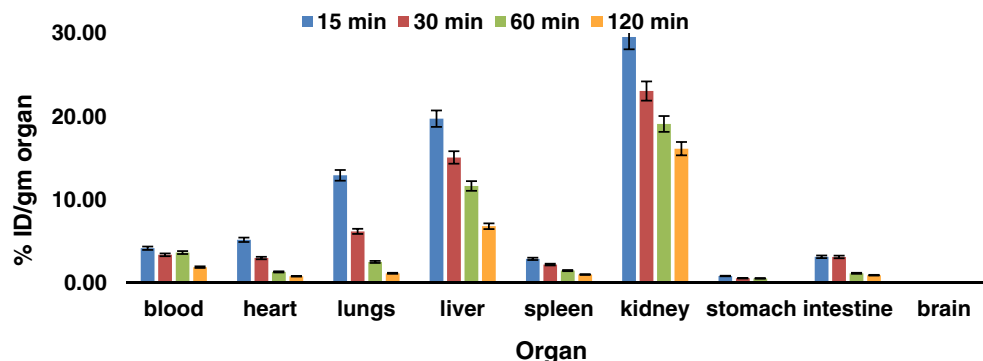


FIGURE 4 Biodistribution (% ID/g, mean \pm SD) data for ^{99m}Tc -MBIP-Cl. Data are derived from tissues taken from normal BALB/c mice ($n = 3$) at different time points after intravenous injection of 100 Ci of ^{99m}Tc -MBIP-Cl via tail vein in each mouse. Radioactivity uptake in different organs were displayed as mean of % injected dose per gram \pm SD

FIGURE 5 Time-activity curve of ^{99m}Tc -MBIP-Cl and ^{99m}Tc -MBIP-Br in organs expressed as %ID/g (y axis) versus time in min (x axis)

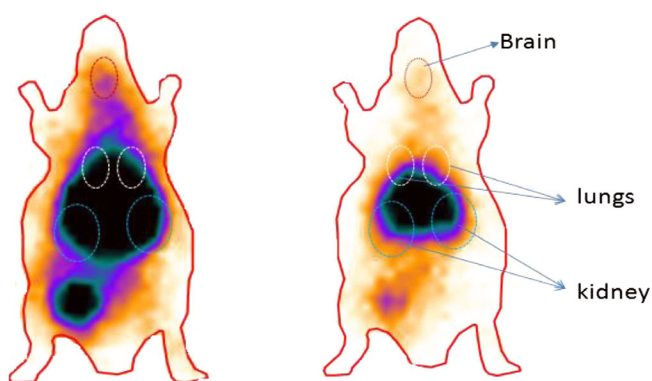
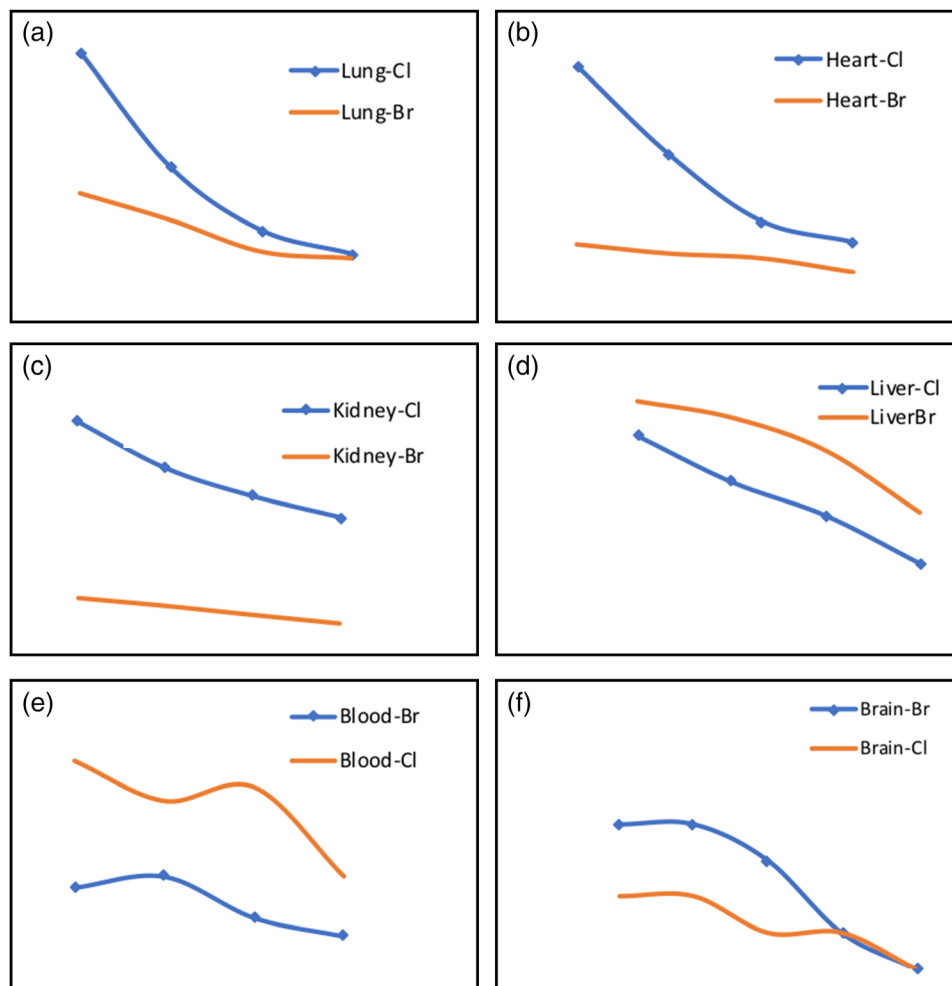


FIGURE 6 In vivo SPECT image showing activity distribution of ^{99m}Tc -MBIP-Cl in (a) normal and (b) inflamed mouse without and with blocking at 40 min postinjection. Blockage was done with PK11195 (10 mg/kg), administered 10 min before radioligand injection

observed for the radioligand. Also small uptakes in brains were observed demonstrating its blood brain barrier crossing ability.

As per these findings, ^{99m}Tc -MBIP-Cl was found to be better than ^{99m}Tc -MBIP-Br in terms of in vivo uptake of the compound in tissues expressing TSPO. This ligand therefore has the potential to specifically target TSPO. Further, the introduction of the chloro group in place of bromo

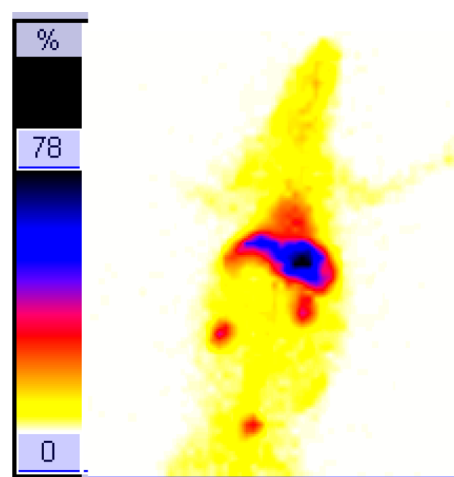


FIGURE 7 In vivo biodistribution of ^{99m}Tc -MBIP-Cl in New Zealand rabbit

in ligand shows improved pharmacokinetic properties which in turn will improve the imaging resolution in mice using the SPECT modality. These data clearly indicated that MBIP-Cl should be considered as a viable SPECT ligand for further investigation in pathological conditions expressing TSPO.

4 | CONCLUSION

The goal of this study was to optimize acetamidobenzoxazolone-tryptophan methyl ester based radiotracer for imaging inflammation in TSPO enriched organs. In this work, a new modified SPECT ligand ^{99m}Tc -MBIP-Cl has been evaluated for TSPO expression imaging. This ligand is able to form stable coordinated complex with ^{99m}Tc and remains stable (>91%) in serum up to 4 hr (in vitro). It also has favorable pharmacokinetic properties especially in terms of lipophilicity and biodistribution. The specificity of ^{99m}Tc -MBIP-Cl for TSPO was validated with the known TSPO ligand PK11195 in lung inflammation models. The current ligand for SPECT, ^{99m}Tc -MBIP-Cl, on comparison with ^{99m}Tc -MBIP-Br, has improved %ID uptake in peripheral organs, better release rate and increased synthetic yield for ligand. High uptake at early time point and fast kinetics suggests that ^{99m}Tc -MBIP-Cl may have potential as SPECT ligand for evaluation of TSPO-over expression. In vivo studies on rabbit demonstrated selectivity of ^{99m}Tc -MBIP-Cl for TSPO as only TSPO rich organs are showing significant uptake. Further studies in comparison with other known TSPO ligands are the next step to establish it as a promising TSPO ligand for TSPO.

ACKNOWLEDGMENTS

We extend special thanks to Dr Tarun Sekhri, Director INMAS and Dr A. K. Mishra, Head, Division of Cyclotron and Radiopharmaceutical Science, INMAS, Delhi, for providing us the facility to carry out experiments. I also thank Dr Sonia Gandhi, Scientist and Mr Sunil Pal, Technical Officer and Dr Ankur Kaul, Technical Officer, INMAS for their technical support. This work was supported by INMAS, Delhi under Task Project ST/15-16/INM-03.

CONFLICT OF INTEREST

There is no conflict of interest among authors of this manuscript.

ORCID

Anjani Kumar Tiwari  <https://orcid.org/0000-0001-6271-3055>

REFERENCES

- Arlicot, N., Vercouillie, J., Ribeiro, M. J., Tauber, C., Venel, Y., Baulieu, J. L., ... Guilloteau, D. (2012). Initial evaluation in healthy humans of [^{18}F]DPA-714, a potential PET biomarker for neuroinflammation. *Nuclear Medicine and Biology*, 39, 570–578.
- Best, L., Ghadery, C., Pavese, N., Tai, Y. F., & Strafella, A. P. (2019). New and old TSPO PET radioligands for imaging brain microglial activation in neurodegenerative disease. *Current Neurology and Neuroscience Reports*, 19(5), 24.
- Boutin, H., Cahuveau, F., Thominiaux, C., Gregoire, M. C., James, M. L., Trebossen, R., ... Kassiou, M. (2007). ^{11}C -DPA-713: A novel peripheral benzodiazepinereceptor PET ligand for in vivo imaging of neuroinflammation. *Journal of Nuclear Medicine*, 48, 573–781.
- Cappelli, A., Mancini, A., Sudati, F., Valenti, S., Anzini, M., Belloli, S., ... Vomero, S. (2008). Synthesis and biological characterization of novel 2-quinolinecarboxamide ligands of the peripheral benzodiazepine receptors bearing technetium-99m or rhenium. *Bioconjugate Chemistry*, 19, 1143–1153.
- Chen, M. K., & Guilarte, T. R. (2008). Translocator protein 18 kDa (TSPO) molecular sensor of brain injury and repair. *Pharmacology & Therapeutics*, 118, 1–17.
- Cumming, P., Burgher, B., Patkar, O., Breakspear, M., Vasdev, N., Thomas, P., ... Banati, R. (2018). Sifting through the surfeit of neuroinflammation tracers. *Journal of Cerebral Blood Flow and Metabolism*, 38(2), 204–224.
- Dolle, F., Luus, C., Reynolds, A., & Kassiou, M. (2009). Radiolabeled molecules for imaging the translocator protein (18 kDa) using positron emission tomography. *Current Medicinal Chemistry*, 16, 2899–2923.
- Dumoga, S., Dey, N., Kaur, A., Singh, S., Mishra, A. K., & Kakkar, D. (2016). Novel biotin-funtionalized lipidic nanocarriers for encapsulating BpT and Bp4eT iron chelators: Evaluation of potential anti tumour efficacy by in vitro, in vivo and pharmacokinetic studies in A549 mice models. *RSC Advances*, 6, 61585–61598.
- Fan, J., Lindemann, P., Feuilloley, M. G., & Papadopoulos, V. (2012). Structural and functional evolution of the translocator protein (18 kDa). *Current Molecular Medicine*, 12, 369–386.
- Fujinaga, M., Luo, R., Kumata, K., Zhang, Y., Hatori, A., Yamasaki, T., ... Zhang, M. R. (2017). Development of a ^{18}F -labeled radiotracer with improved brain kinetics for positron emission tomography imaging of translocator protein (18 kDa) in ischemic brain and glioma. *Journal of Medicinal Chemistry*, 60, 4047–4061.
- Fukaya, T., Kodo, T., Ishiyama, T., Kakuyama, H., Nishikawa, H., Baba, S., & Masumoto, S. (2012). Design, synthesis and structure–activity relationships of novel benzoxazolone derivatives as 18 kDa translocator protein (TSPO) ligands. *Bioorganic & Medicinal Chemistry*, 22, 5568–5582.
- Fukaya, T., Kodo, T., Ishiyama, T., Nishikawa, H., Baba, S., & Masumoto, S. (2013). Design, synthesis and structure–activity relationship of novel tricyclic benzimidazolone derivatives as potent 18 kDa translocator protein (TSPO) ligands. *Bioorganic & Medicinal Chemistry*, 21, 1257–1267.
- Hatori, A., Yui, J., Xie, L., Yamasaki, T., Kumata, K., Fujinaga, M., ... Zhang, M. R. (2014). Visualization of acute liver damage induced by cycloheximide in rats using PET with [^{18}F]FEDAC, a radiotracer for translocator protein (18 kDa). *PLoS One*, 9, e86625.
- Jean, R., Bribe, E., Knabe, L., Petit, A. F., Vachier, I., & Bourdin, A. (2015). TSPO is a new anti-inflammatory target in the airway of COPD. *Revue des Maladies Respiratoires*, 32, 320.
- Jones, H. A., Marino, P. S., Shakur, B. H., & Morrell, N. W. (2003). In vivo assessment of lung inflammatory cell activity in patients with COPD and asthma. *European Respiratory Journal*, 21, 567–573.
- Kakkar, D., Tiwari, A. K., Chuttani, K., Khanna, A., Datta, A., Singh, H., & Mishra, A. K. (2012). Design, synthesis, and antimycobacterial property of PEG-bis (INH) conjugates. *Chemical Biology & Drug Design*, 80, 245–253.
- Kakkar, D., Tiwari, A. K., Chuttani, K., Kumar, R., Mishra, K., Singh, H., & Mishra, A. K. (2011). Polyethylene-glycolylated isoniazid conjugate for reduced toxicity and sustained release. *Therapeutic Delivery*, 2(2), 205–212.
- Kraus, C., Kadriu, B., Lanzenberger, R., Zarate, C. A., Jr., & Kasper, S. (2019). Prognosis and improved outcomes in major depression: A review. *Translational Psychiatry*, 9(1), 127.
- Kreis, W. C., Fujita, M., Fujimura, Y., Kimura, N., Jenko, K. J., Kannan, P., ... Innis, R. B. (2010). Comparison of [(11C)-(R)-PK 11195 and [(11C)]PBR28, two radioligands for translocator protein (18 kDa) in human and monkey: Implications for positron emission tomographic imaging of this inflammation biomarker. *NeuroImage*, 49, 2924–2932.
- Kumar N. Kakkar D. Tiwari A.K., Saini N., Chand M., Mishra A.K. (2010) Design, synthesis and fluorescence lifetime study of benzothiazole derivatives for imaging of amyloids. 25: 571–575.

- Kumari, N., Chadha, N., Srivastava, P., Mishra, L. K., Bhagat, S., Mishra, A. K., & Tiwari, A. K. (2017). Modified benzoxazolone derivative as 18-kDa TSPO ligand. *Chemical Biology & Drug Design*, 90, 511–519.
- Lagarde, J., Sarazin, M., & Bottlaender, M. (2018). In vivo PET imaging of neuroinflammation in Alzheimer's disease. *Journal of Neural Transmission*, 125, 847–867.
- Mattner, F., Quinlivan, M., Greguric, I., Pham, T., Liu, X., Jackson, T., ... Katsifi, A. (2015). Radiosynthesis, in vivo biological evaluation, and imaging of brain lesions with [¹²³I]-CLINME, a new SPECT tracer for the translocator protein. *Disease Markers*; Article ID 729698, 2015, 11.
- Milenkovic, V. M., Rupprecht, R., & Wetzel, C. H. (2015). The translocator protein 18 kDa (TSPO) and its role in mitochondrial biology and psychiatric disorders. *Mini-Reviews in Medicinal Chemistry*, 15, 366–372.
- Owen, D. R., Yeo, A. J., & Gunn, R. N. (2012). An 18 kDa translocator protein (TSPO) polymorphism explains differences in binding affinity of the PET radioligand PBR28. *Journal of Cerebral Blood Flow and Metabolism*, 32, 1–5.
- Saini, N., Varshney, R., Tiwari, A. K., Kaul, A., Allard, M., Ishaq, M. P., & Mishra, A. K. (2013). Synthesis, conjugation and relaxation studies of gadolinium(III)-4-benzothiazol-2-yl-phenylamine as a potential brain specific MR contrast agent. *Dalton Transactions*, 14, 4994–5003.
- Shukla, G., Tiwari, A. K., Sinha, D., Srivastava, R., Cahndra, H., & Mishra, A. K. (2009). Synthesis and assessment of ^{99m}Tc chelate-conjugated alendronate for development of specific radiopharmaceuticals. *Cancer Biotherapy and Radiopharmaceuticals*, 24, 209–214.
- Srivastava, P., Kaul, A., Ojha, H., Kumar, P., & Tiwari, A. K. (2016). Design, synthesis and biological evaluation of methyl-2-(2-(5-bromo benzoxazolone)acetamido)-3-(1H-indol-3-yl)propanoate: TSPO ligand for SPECT. *RSC Advances*, 6, 11449–114499.
- Srivastava, P., Tiwari, A. K., Chadha, N., Chuttani, K., & Mishra, A. K. (2013). Synthesis and biological evaluation of newly designed phosphonate-based bone-seeking agent. *European Journal of Medicinal Chemistry*, 65, 12–20.
- Tiwari, A. K., Fujinaga, M., Yui, J., Yamasaki, T., Xie, L., Kumata, K., ... Zhang, M. R. (2014). Synthesis and evaluation of new (18)F-labelled acetamidobenzoxazolone-based radioligands for imaging of the translocator protein (18 kDa, TSPO) in the brain. *Organic and Biomolecular Chemistry*, 12, 9621–9630.
- Tiwari, A. K., Ji, B., Fujinaga, M., Yamasaki, T., Xie, L., Luo, R., ... Zhang, M. R. (2015). [¹⁸F]FEBMP: Positron emission tomography imaging of TSPO in a model of neuroinflammation in rats, and in vitro autoradiograms of the human brain. *Theranostics*, 5, 961–969.
- Tiwari, A. K., Yui, J., Fujinaga, M., Kumata, K., Shimoda, Y., Yamasaki, T., ... Zhang, M. R. (2014). Characterization of a novel acetamidobenzoxazolone based PET ligand for translocator protein (18 kDa) imaging of neuroinflammation in the brain. *Journal of Neurochemistry*, 129, 712–720.
- Tiwari, A. K., Yui, J., Zhang, Y., Fujinaga, M., Yamasaki, T., Xie, L., ... Zhang, M. R. (2015). [¹⁸F]FPBMP—A potential new positron emission tomography radioligand for imaging of translocator protein (18 kDa) in peripheral organs of rats. *RSC Advances*, 5(123), 101447–101454.
- Trapani, A., Palazzo, C., de Candia, M., Lasorsa, F. M., & Trapani, G. (2013). Targeting of the translocator protein 18 kDa (TSPO): A valuable approach for nuclear and optical imaging of activated microglia. *Bioconjugate Chemistry*, 24, 1415–1428.
- Veenman, L., & Gavish, M. (2006). The peripheral-type benzodiazepine receptor and the cardiovascular system. Implications for drug development. *Pharmacology & Therapeutics*, 110, 503–524.
- Veenman, L., Vainshtein, A., & Gavish, M. (2015). TSPO as a target for treatments of diseases, including neuropathological disorders. *Cell Death & Disease*, 6, e1911.
- Veenman, L., Vainshtein, A., Yasin, N., Azrad, M., & Gavish, M. (2016). Tetrapyrroles as endogenous TSPO ligands in eukaryotes and prokaryotes: Comparisons with synthetic ligands. *International Journal of Molecular Sciences*, 17, E880.
- Vicidomini, C., Panico, M., Greco, A., Gargiulo, S., Coda, A. R. D., Zannetti, A., ... Pappata, S. (2015). In vivo imaging and characterization of [¹⁸F]DPA-714, a potential new TSPO ligand, in mouse brain and peripheral tissues using small-animal PET. *Nuclear Medicine and Biology*, 42, 309–316.

SUPPORTING INFORMATION

Additional supporting information may be found online in the Supporting Information section at the end of this article.

How to cite this article: Srivastava P, Kakkar D, Kumar P, Tiwari AK. Modified benzoxazolone (ABO-AA) based single photon emission computed tomography (SPECT) probes for 18 kDa translocator protein. *Drug Dev Res.* 2019;1–9. <https://doi.org/10.1002/ddr.21547>



Cite this: *New J. Chem.*, 2019, 43, 11288

Comparative evaluation of ^{99m}Tc -MBIP-X/ ^{11}C MBMP for visualization of 18 kDa translocator protein

Pooja Srivastava,^{a,c} Neelam Kumari,^a Dipti Kakkar,^a Ankur Kaul,^a Pravir Kumar^{id}^c and Anjani K. Tiwari^{id}^{*ab}

An elevated translocator protein (18 kDa, TSPO) density is observed during inflammation in the brain and peripheral organs making it a viable target for imaging. Recently, our group has explored a pharmacophore skeleton acetamidobenzoxazolone for positron emission tomography (PET) and single photon emission computed tomography (SPECT) applications to target TSPO. 2-(2-(5-Bromo/chloro benzoxazolone)acetamide)-3-(1*H*-indol-3-yl)propionate (MBIP-Br/Cl) were synthesized by using tryptophan methyl ester and compared with 2-[5-(4-methoxyphenyl)-2-oxo-1,3-benzoxazol-3(2*H*)-yl]-*N*-methyl-*N*-phenyl acetamide (MBMP) through tracer techniques. Computational docking showed similar results for MBIP-Br/Cl in comparison to MBMP. Their *ex vivo* and *in vivo* biodistributions were assessed in TSPO-rich organs as well as their release kinetics 0–120 min post injection. The *ex vivo* biodistribution showed a 7 fold higher uptake (5.16%ID per g vs. 0.72%ID per g) in the heart and a 2.5 fold higher uptake (12.91%ID per g vs. 4.69%ID per g) in the lungs for ^{99m}Tc -MBIP-Cl compared to that of ^{99m}Tc -MBIP-Br at 15 min. These findings demonstrated that ^{99m}Tc -MBIP-Cl has improved pharmacokinetic properties compared to ^{99m}Tc -MBIP-Br for SPECT application and is comparable to [^{11}C]MBMP.

Received 6th February 2019,
Accepted 9th June 2019

DOI: 10.1039/c9nj00180h

rsc.li/njc

1. Introduction

The 18 kDa translocator protein (TSPO), also known as peripheral benzodiazepine receptor (PBR) and a highly conserved protein during evolution, has been studied for its importance in various life essential functions.^{1–4} TSPO is mainly found on the outer surface of mitochondria in the central nervous system as well as in peripheral tissues. TSPO is an intracellular protein which forms a complex with adenine nucleotide translocator (ANT, 30 kDa) and voltage dependent anion channels (VCAD, 32 kDa) in mitochondria.

The molecular imaging of TSPO in neuroinflammation was started by PET studies with isoquinoline carboxamide [^{11}C]PK11195, the prototype ligand of translocator protein-18 kDa (TSPO); besides that, RoS-4864 and FGIN-127, which are also isoquinoline carboxamides derivative, have been evaluated. These three ligands have shown compatibility with the tetrapyrrole protoporphyrin IX (PPIX) structure, a well-known endogenous TSPO ligand.^{5,6}

TSPO, a highly hydrophobic, five transmembrane domain protein expressed in the outer mitochondrial membrane, has been investigated as a biomarker for inflammatory conditions in the brain, lungs, liver and kidneys *etc.* Its role has also been studied in many neuro-disorders like depression, anxiety and in about all types of neurodegenerative disorders.^{7–12} Therefore, high affinity TSPO probes were a prime focus for non-invasive diagnosis of such conditions.^{6,13–17}

^{11}C (*R*) PK11195 is the gold standard for TSPO related studies and has been the most widely studied ligand from the first generation in the late eighties. The main limitations of this ligand were high lipophilicity and low *in vivo* specific binding, which were overcome by second generation TSPO ligands with improved imaging. Some of the TSPO ligands used in clinical human studies are [^{11}C]DAA, [^{18}F]FEDAA, [^{11}C]AC-5216, [^{11}C]PBR28, and [^{18}F]DPA714.^{6,12–16} These ligands were able to solve most of the problems from the first generation but later showed the problem of inter-subject variability due to single nucleotide polymorphism.¹⁷

Recently we have developed a new PET skeleton acetamidobenzoxazolone (ABO) which has been derived from a ligand from the first generation RoS-4864 by opening the diazepine ring and reorganizing it.^{18–20}

The first ligand which we explored in this category for diagnostic application through PET was 2-[5-(4-[^{11}C]methoxyphenyl)-2-oxo-1,3-benzoxazol-3(2*H*)-yl]-*N*-methyl-*N*-phenylacetamide (^{11}C -MBMP),

^a Division of Cyclotron and Radiopharmaceutical Sciences, Institute of Nuclear Medicine and Allied Sciences, Brig. S. K. Mazumdar Road, Delhi 110054, India. E-mail: anjanik2003@gmail.com

^b Department of Chemistry, School of Physical & Decision Sciences (SPDS), Babasaheb Bhimrao Ambedkar Central University, Lucknow 226025, UP, India

^c Molecular Neuroscience and Functional Genomics Laboratory, Department of Biotechnology, Delhi Technological University, Delhi 110042, India

which showed a promising result. Later two fluoro alkyl derivatives were also synthesized by us named 2-[5-(4-[^{18}F] fluoroethoxy/propoxyphenyl)-2-oxo-1,3-benzoxazol-3(2*H*)-yl]-*N*-methyl-*N*-phenylacetamide (^{18}F -FEBMP and ^{18}F -FPBMP). The same skeleton was also analyzed through $^{99\text{mTc}}$ -MBIP for SPECT.^{20–25} In this report we are comparing $^{99\text{mTc}}$ -MBIP-Br and $^{99\text{mTc}}$ -MBIP-Cl along with ^{11}C -MBMP in terms of the *ex vivo* and *in vivo* properties in TSPO enriched organs.

2. Materials and methods

2.1. Chemicals

All the chemicals and solvents were procured from Sigma-Aldrich and Merck. Procurement of $^{99\text{mTc}}$ was from Regional Centre for Radiopharmaceuticals, Board of Radiation and Isotope Technology (BRIT), Department of Atomic Energy, India. Thin layer chromatography (TLC), column chromatography and instant thin layer chromatography (ITLC) were carried out during the tracer study. HPLC separation and analysis were performed using JASCO and Agilent HPLC systems. Effluent radioactivity was monitored using a NaI (Tl) scintillation detector system, and radioactivity measurement was performed with a Curiometer during the radiosynthesis and animal studies.

2.2. Instrumentation

The synthesized compounds were characterized by spectroscopic techniques like ^1H and ^{13}C NMR spectroscopy (Bruker Avance III 600 MHz system) at 600 MHz and 150 MHz, respectively. An Agilent 6310 system mass spectrometer was used in ESI mode. A Siemens Symbia camera was used for imaging and a γ -scintillation counter for radioactivity counting.

2.3. Animal models

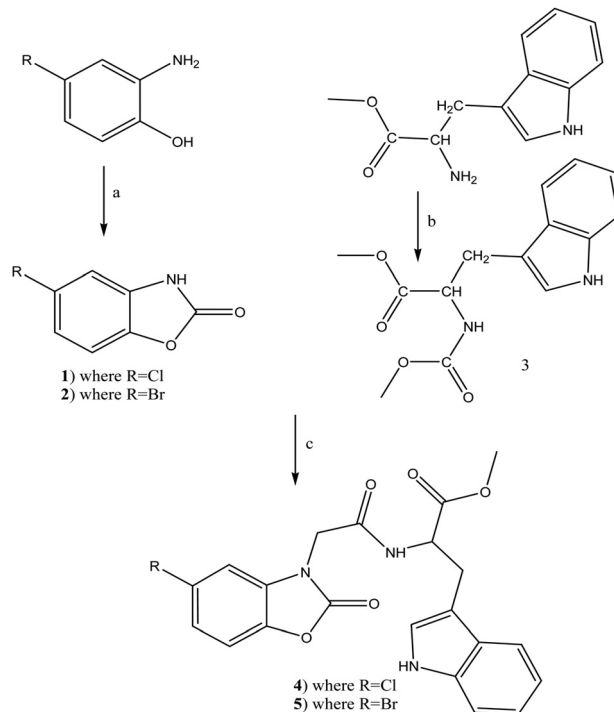
The Institutional Animal Ethics Committee (INM/DASQA/IAEC/09/015) has approved the protocols for the studies. BALB/c mice (22–28 g) were used for the biodistribution studies and imaging.

The animals were housed under a 12/12 h dark/light cycle under optimal conditions.

A lung inflammation model was prepared in balb/c mice by intratracheal delivery of lipopolysaccharide (LPS) as per our previous work.²⁴ Saturation studies were performed in these animal models by pre administering 5 mg kg^{-1} unlabelled PK11195, 10 min prior to tracer injection.

2.4. Synthesis

2.4.1 Synthesis of methyl 2-(2-chloroacetamido)-3-(1*H*-indol-3-yl)propanoate. To a solution of *L*-tryptophan methyl ester (500 mg, 2.32 mmol) and deionized water (10 mL), triethyl amine (355 μL , 2.55 mmol) was added with constant stirring under a nitrogen atmosphere in an ice bath for 5 min. To the mixture, chloroacetyl chloride (203 μL , 2.55 mmol) in dichloromethane (10 mL) was added dropwise over 1 h and the reaction was carried out for 4 h. Thereafter, the mixture was extracted with dichloromethane (3 \times). The organic layer was washed twice with deionized water and brine solution. After washing, the



Scheme 1 Synthesis of 2-(2-(5-bromo/chloro benzoxazolone)acetamido)-3-(1*H*-indol-3-yl) propanoate (MBIP-Br/Cl). Reagents and conditions: (a) CDI, THF, reflux 2 h; (b) chloroacetyl chloride, Et₃N, H₂O/DCM, 0 °C–rt; (c) K₂CO₃, DMF, 60–70 °C, 3 h.

organic layer was dried over anhydrous sodium sulphate. After filtration, the solvent was removed *in vacuo*, and purified by silica gel column chromatography using 100% CHCl₃ as the eluent (yield = 75%).

^1H -NMR (CDCl₃, 600 MHz): δ (ppm) 3.3–3.4 (d, 2H), 3.7 (s, 3H), 4.0 (s, 2H), 4.9–5.0 (m, 1H), 7.0–7.6 (m, 5H), 8.5 (br s, 1H).

^{13}C -NMR (CDCl₃, 150 MHz): δ (ppm) 27.5, 42.5, 52.6, 53.3, 109.3–136.3 (8 peaks), 166.0, 171.8.

MS (ESI) m/z : 293.1 [$\text{M} - \text{H}^+$], calculated m/z : 293.1 [$\text{M} - \text{H}^+$].

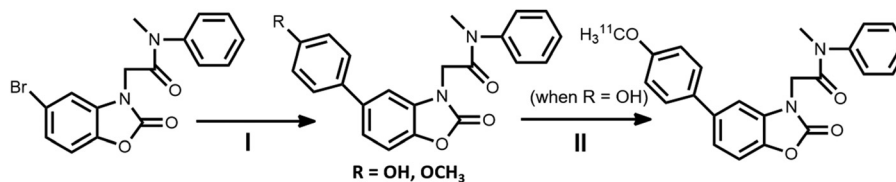
2.4.2 Synthesis of 5-chloro benzoxazol-2(3*H*)-one. To a solution of 4-chloro-2-aminophenol (5 g, 34.83 mmol) in 150 mL THF, 1,1'-carbonyldiimidazole (5.65 g, 34.83 mmol) was added. The mixture was refluxed with stirring for 2 h. The reaction mixture was quenched by adding 2 M HCl solution after cooling down to room temperature. EtOAc was used for extraction, which was washed with brine, dried over anhydrous sodium sulphate and filtered. Thereafter, the solvent was removed *in vacuo* to get the product as a white solid (yield = 91%).

^1H -NMR (DMSO, 600 MHz): δ (ppm) 7.1–7.4 (m, 3H).

^{13}C -NMR (DMSO, 150 MHz): δ (ppm) 110.3, 111.3, 122.0, 128.2, 132.2, 142.6, 154.7.

MS (ESI) m/z : 167.8 [$\text{M} - \text{H}^+$], calculated m/z : 168.0 [$\text{M} - \text{H}^+$].

2.4.3 Synthesis of 2-(2-(5-chloro benzoxazolone)acetamido)-3-(1*H*-indol-3-yl)propanoate (MBIP-Cl). To a solution of 5-chloro benzoxazol-2(3*H*)-one (250 mg, 1.48 mmol) and K₂CO₃ (306 mg, 2.22 mmol) in DMF (5 mL), methyl-2-(2-chloroacetamido)-3-(1*H*-indol-3-yl)propionate (435 mg, 1.48 mmol) was added with cooling in an ice bath. The reaction mixture was stirred at 60–70 °C



Scheme 2 Synthesis of [5-(4-hydroxyphenyl)-2-oxo-1,3-benzoxazol-3(2H)-yl]-N-methyl-N-phenylacetamide and radiosynthesis of [¹¹C]MBMP. Reagents and conditions: (I) Pd(PPh₃)₄, K₂CO₃, 4-(4,4,5,5-tetramethyl-1,3,2-dioxaborolan-2-yl)phenol (when R = OH)/4-methoxyphenylboronic acid (when R = OCH₃), 1,4-dioxane : water (v/v-3/1) reflux at 100 °C under a nitrogen atmosphere for 4–4.5 h (II) [¹¹C]CH₃I, NaOH at 70 °C for 5 min in DMF.

for 3 h. Thereafter, the reaction mixture was cooled to room temperature before adding water. A mixture of toluene and ethyl acetate, in a 1 : 1 ratio, was used as the extraction solvent. Water and brine solution were used for washing the organic layer and anhydrous sodium sulphate for drying. The solvent was removed *in vacuo* after filtration and was purified by silica gel column chromatography using CHCl₃/EtOAc (4 : 1, v/v) as the eluent (yield = 70%).

¹H-NMR (CDCl₃, 600 MHz): δ (ppm) 3.5–3.7 (m, 2H), 3.8 (s, 3H), 3.9–4.0 (m, 2H), 5.0–5.1 (m, 1H), 6.7–7.5 (m, 8H), 8.1 (br s, 1H).

¹³C-NMR (CDCl₃, 150 MHz): 24.1, 51.2, 53.1, 54.3, 110.4–148.8 (14 peaks), 155.5, 168.2, 168.8.

MS (ESI) *m/z*: 426.3 [M – H⁺], calculated *m/z*: 426.1 [M – H⁺].

2.4.4 Synthesis of 2-(2-(5-bromo benzoxazolone)acetamido)-3-(1H-indol-3-yl)propanoate (MBIP-Br). MBIP-Br was synthesized by the procedure mentioned in Scheme 1 as per our previous paper.²⁴

¹H-NMR (DMSO, 400 MHz): δ (ppm) 3.1–3.2 (m, 2H), 3.6 (s, 3H), 4.4–4.6 (m, 3H), 6.9–7.5 (m, 8H).

¹³C-NMR (DMSO, 100 MHz): δ (ppm) 28.7, 44.4, 52.4, 53.9, 111.0 141.5 (14 C), 154.2, 166.3, 172.3.

MS (ESI) *m/z*: 470.2 [M – H⁺], calculated: 470.0 [M – H⁺].

2.4.5 Synthesis of 2-[5-(4-methoxyphenyl)-2-oxo-1,3-benzoxazol-3(2H)-yl]-N-methyl-N-phenylacetamide (MBMP). It was synthesised as per Scheme 2. Briefly, a mixture of 2-(5-bromo-2-oxo-1,3-benzoxazol-3(2H)-yl)-N-methyl-N-phenylacetamide (0.72 g, 2.0 mmol) and 4-methoxyphenylboronic acid (365 mg, 2.4 mmol), K₂CO₃ (415 mg, 3.0 mmol) and tetrakis(triphenylphosphine)palladium(0) Pd(PPh₃)₄ (230 mg, 0.2 mmol) in 1,4-dioxane/water (3/1, 4.0 mL) was heated at 100 °C under a nitrogen atmosphere. The reaction mixture was stirred for 4 h and cooled to room temperature. Subsequently, the mixture was extracted with EtOAc. The organic layer was washed with brine and dried over anhydrous sodium sulphate. After filtration, the solvent was removed *in vacuo*, and the residue was purified by silica gel column chromatography using hexane/EtOAc (2/1, v/v) as the eluent to give MBMP (1.23 g, 79.9% yield).

¹H NMR (CDCl₃, δ) 3.32 (3H, s), 3.86 (3H, s), 4.35 (2H, s), 6.96–7.00 (3H, m), 7.19–7.23 (2H, m), 7.34 (2H, d, *J* = 7.7 Hz), 7.41–7.54 (5H, m).

HRMS (FAB) calcd for C₂₃H₂₁O₄N₂, 389.4320; found, 389.1511.

2.7 Radiopharmaceutical efficacy of ^{99m}Tc-MBIP-Br/Cl

The compounds were labeled with ^{99m}Tc using a procedure from the literature with slight modifications.^{26–29} Briefly, 100 μL of sterile sodium pertechnetate (approximately 75–110 MBq of ^{99m}TcO₄)

was reduced with 50 μL of stannous chloride solution (1 × 10^{−2} M in 10% glacial acetic acid) and the pH was adjusted to 6.5 using 0.5 M sodium bicarbonate. Solutions of MBIP-Cl and MBIP-Br were added to this mixture separately and after thorough mixing, incubated for 15 min at room temperature (25 °C). ITLC-SG strips as the stationary phase and acetone as the mobile phase were used to determine the complexation of MBIP-Cl and MBIP-Br with ^{99m}Tc and the purity of the labelled compound.

The *in vitro* human serum stability of the radiolabeled compounds was evaluated using our previous approach with some modifications.²⁸ Blood collected from healthy volunteers was clotted in a humidified incubator for 1 h under 5% CO₂ and 95% air and used to prepare serum. The sample was centrifuged at 400 rpm and filtered through a 0.22 μm filter into sterile plastic culture tubes. ^{99m}Tc-MBIP-Cl and ^{99m}Tc-MBIP-Br were incubated with freshly prepared serum at 37 °C. The samples were analyzed at different time points using ITLC-SG strips. Acetone was used as the mobile phase for the measurement to find out the percentage dissociation of the complex in serum as a function of time.

Balb/c mice were used for the initial *in vivo* assessment of ^{99m}Tc-MBIP-Cl and ^{99m}Tc-MBIP-Br.²⁴ The radioactivity uptake was measured in specific organs of the mice at different time points *i.e.* 15 min, 30 min, 60 min and 120 min post injection of 100 μCi of both radioligands *via* a tail vein and the results were expressed as the percentage of the injected dose per gram (%ID per g) of tissue (*n* = 3). The total blood volume was calculated as 7% of the total body weight.

2.8 Radiolabeling of 2-[5-(4-[¹¹C]methoxyphenyl)-2-oxo-1,3-benzoxazol-3(2H)-yl]-N-methyl-N-phenylacetamide ([¹¹C]MBMP)

Cyclotron-produced [¹¹C]CO₂ was bubbled into 0.4 M LiAlH₄ in anhydrous tetrahydrofuran (THF, 0.3 mL). After the evaporation of THF, the remaining complex was treated with 56% hydroiodic acid (0.3 mL) to give [¹¹C]CH₃I, which was distilled with heating and transferred under N₂ gas flow to a solution of desmethyl MBMP (1 mg) and NaOH (5 μL, 0.5 M) in DMF (0.3 mL) at −15 °C. After trapping was completed, this reaction mixture was heated at 80 °C for 3 min. HPLC separation was performed on a Capcell Pack UG80 C₁₈ column (10 mm i.d. × 250 mm) using MeCN/H₂O/Et₃N (6/4/0.01, v/v/v) at 5.0 mL min^{−1}.

3. Results and discussion

Encouraged by the outcome of our recently developed TSPO ligands [¹¹C]MBMP and [¹⁸F]FEBMP, [¹⁸F]FPBMP and ^{99m}Tc-MBIP-Br

having k_i in the nanomolar range,^{20–22} we directed our efforts towards improvement of the acetamidobenzoxazolone (ABO) skeleton for ^{99m}Tc labeling to target 18 kDa TSPO. The new ligand contains ABO conjugated to tryptophan methyl ester. ^{99m}Tc -MBIP-Cl showed fast clearance from the TSPO enriched organs as well as from circulating blood. ^{99m}Tc -MBIP-Cl exhibited reasonable uptake in the heart, lungs, kidneys and spleen, which are known to express TSPO.

The two SPECT ligands MBIP-Cl/Br were synthesized by the procedure mentioned in Scheme 1 and MBMP and its carbon-11 derivative were synthesized as per our previous work.^{22,24}

The synthesis of MBIP-Cl/Br was performed by synthesizing two important intermediates, namely methyl-2-(2-chloroacetamido)-3-(1*H*-indol-3-yl)propanoate and 5-chloro benzoxazol-2(3*H*)-one, which were combined in the final step. The synthesized MBIP-Cl had a good yield (70%). The synthetic scheme followed for MBIP-Cl is better than the reported scheme for its bromo analog in terms of the yield and duration of the overall synthesis.²⁴

Subsequently MBIP-Br/Cl analogs were radiolabeled with ^{99m}Tc and studied for their stability in saline as well as in serum ($n = 5$). The purified compounds MBIP-Br and MBIP-Cl were radiolabeled with >96% radiochemical yields. Both the radiolabeled compounds showed around 94% stability in saline after 24 h indicating the stable nature of the radiocomplexes. The *in vitro* serum stability clearly indicates the stable nature of the radio complexes without any transchelation to serum proteins like albumin, which were observed to have >91% and >89% intactness, for ^{99m}Tc -MBIP-Br and ^{99m}Tc -MBIP-Cl, respectively, after 24 h (Fig. 1). The stability studies showed the requisite stability of the complex to act as a SPECT agent.

The blood clearance was studied on normal rabbits of weight in the range of 2–2.5 kg. 300 μL of the complex having 4.3 MBq activity was administered intravenously through the dorsal vein of the ear. Both the tryptophan methyl ester analogs demonstrated a rapid radioactivity clearance from blood circulation. The ^{99m}Tc -MBIP-Br and ^{99m}Tc -MBIP-Cl activity clearance were >62% and >66% in 1 h; and >92% and >84% in 3 h. This reflects fast release kinetics, which is desirable for diagnostic imaging.

The time activity curve (TAC, $n = 3$) has been drawn for ^{99m}Tc -MBIP-Br (Fig. 2), ^{99m}Tc -MBIP-Cl (Fig. 3) and [^{11}C] MBMP (Fig. 4).

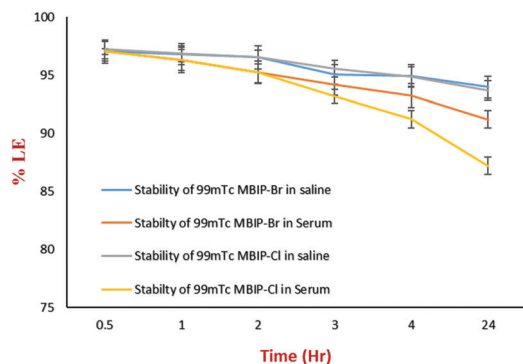


Fig. 1 Stability profile of ^{99m}Tc MBIP-Cl/Br.

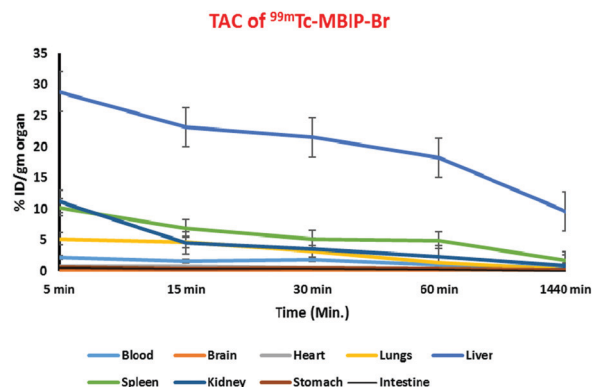


Fig. 2 Time activity curve (TAC) of ^{99m}Tc -MBIP-Br.

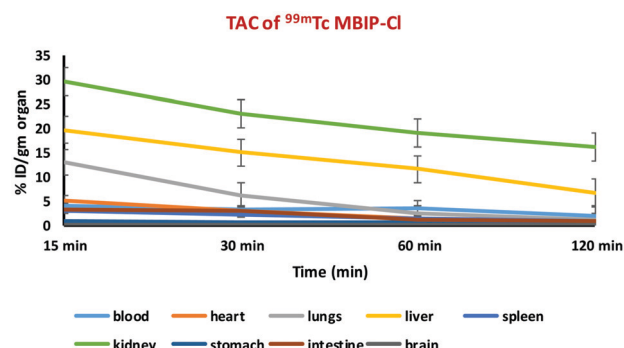


Fig. 3 Time activity curve (TAC) of ^{99m}Tc -MBIP-Cl.

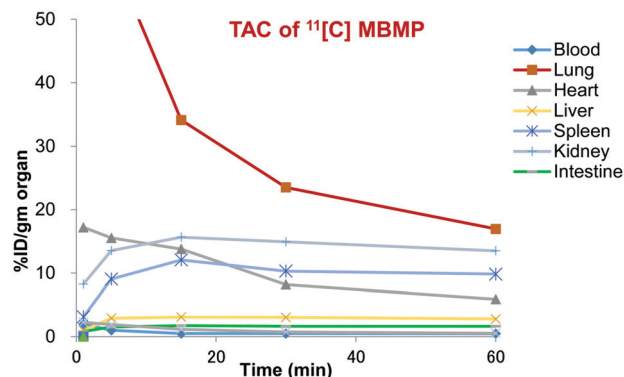


Fig. 4 Time activity curve (TAC) of [^{11}C] MBMP.

All three showed uptake in TSPO enriched organs, which was maximum in the liver for ^{99m}Tc -MBIP-Br, kidneys for ^{99m}Tc -MBIP-Cl and lungs for [^{11}C] MBMP.

All three showed rapid clearance in the lungs where the initial uptake was high. The blood clearance was fast in ^{99m}Tc -MBIP-Cl and [^{11}C] MBMP. The main difference in the SPECT and PET ligands was the uptake in the liver, which was 28.86%ID per g and 19.74%ID per g in ^{99m}Tc -MBIP-Br and ^{99m}Tc -MBIP-Cl while in [^{11}C]MBMP it was just 0.56%ID per g. The maximum quantity of radioactivity in the liver showed that the clearance of the SPECT radioligand is through a hepatobiliary route.

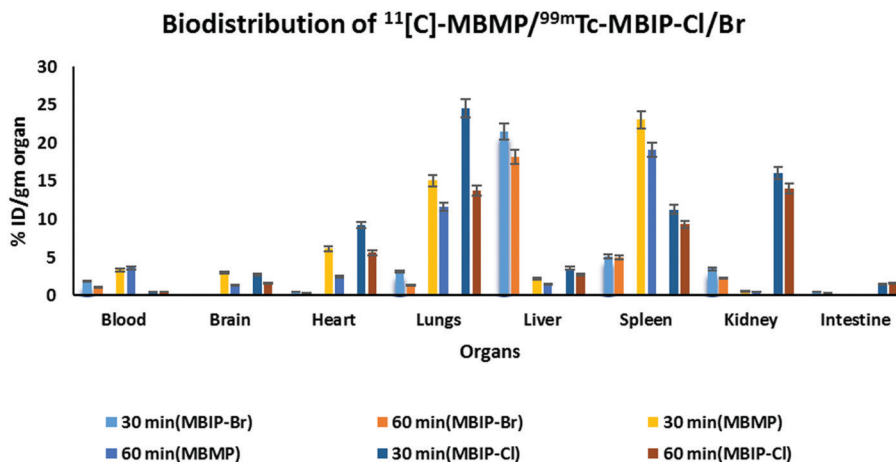


Fig. 5 Comparative *ex vivo* biodistributions of $^{99\text{m}}\text{Tc}$ -MBIP-Br, $^{99\text{m}}\text{Tc}$ -MBIP-Cl and ^{11}C MBMP. Data are derived from tissues taken from animal tissue ($n = 3$) at different time points after intravenous injection via the tail vein in each mouse. The radioactivity uptake in different organs is displayed as the mean of % injected dose per gram \pm SD.

In the brain, a small uptake was observed which decreased with the time point of observation. The small %ID in the brain could be attributed to the moderate expression of TSPO in a healthy brain.

The comparative *ex vivo* biodistributions of $^{99\text{m}}\text{Tc}$ -MBIP-Br, $^{99\text{m}}\text{Tc}$ -MBIP-Cl and ^{11}C MBMP are shown in Fig. 5, which demonstrate that at 30 and 60 min the maximum radioactivity is reached in the lungs, spleen and heart, which are supposed to be TSPO organs. Only one unexpected outcome was found for $^{99\text{m}}\text{Tc}$ -MBIP-Cl in terms of the kidneys, which was relatively very high, and further investigation in this direction may help to find the possible reason for it.

Further, $^{99\text{m}}\text{Tc}$ -MBIP-Cl/Br were compared with the ligands reported in the literature. As compared to $^{99\text{m}}\text{Tc}$ -labeled 2-quinolinecarboxamide, the uptake of $^{99\text{m}}\text{Tc}$ -MBIP-Cl was found to be higher in the heart (2.96%ID per g vs. negligible uptake) and the lungs

(6.16%ID per g vs. 1.19%ID per g) and comparable in the spleen (2.18%ID per g vs. 2.07%ID per g) at 30 min as reported in CD-1 mice.³¹ Comparison with ^{123}I -CLINME demonstrated higher uptake of $^{99\text{m}}\text{Tc}$ -MBIP-Cl in heart (5.15%ID per g vs. 3.53%ID per g) and lungs (12.91%ID per g vs. 3.53%ID per g) and comparable for spleen (2.87%ID per g vs. 2.65%ID per g).³⁰ This was lower/comparable to the uptake of $^{99\text{m}}\text{Tc}$ -MBIP-Cl/Br in the respective organs.³⁰ The liver uptake was lowest for $^{99\text{m}}\text{Tc}$ -MBIP-Cl in comparison with $^{99\text{m}}\text{Tc}$ -labeled 2-quinolinecarboxamide and $^{99\text{m}}\text{Tc}$ -MBIP-Br.^{24,31} This accounts for better visualization of target images for $^{99\text{m}}\text{Tc}$ -MBIP-Cl.

In addition, the release kinetic rates between 15 and 60 min for ^{18}F -FEBMP,²⁰ ^{11}C -MBMP,²² ^{18}F -2-(5-(6-fluoropyridin-3-yl)-2-oxobenzo[*d*]oxazol-3(2*H*)-yl)-*N*-methyl-*N*-phenylacetamide³² and $^{99\text{m}}\text{Tc}$ -MBIP-Cl are 0.175%ID per g per min, 0.150%ID per g per min, 0.070%ID per g per min and 0.085%ID per g per min in the heart; 0.382%ID per g per min, 0.375%ID per g per min,

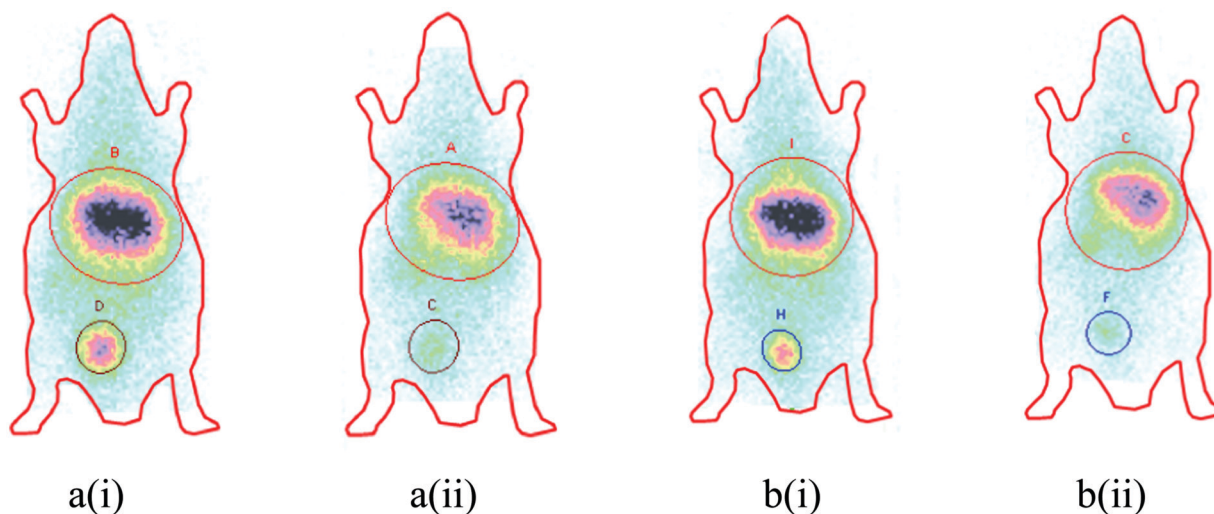
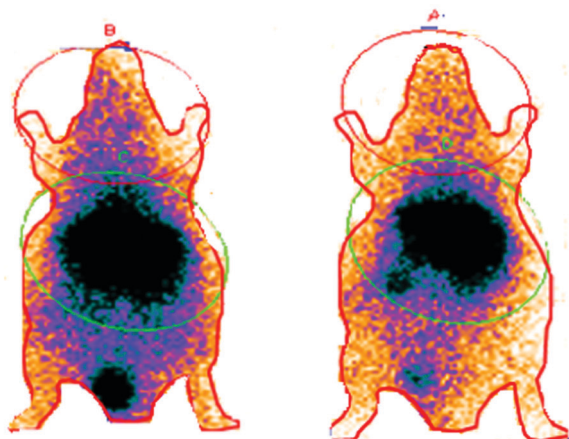
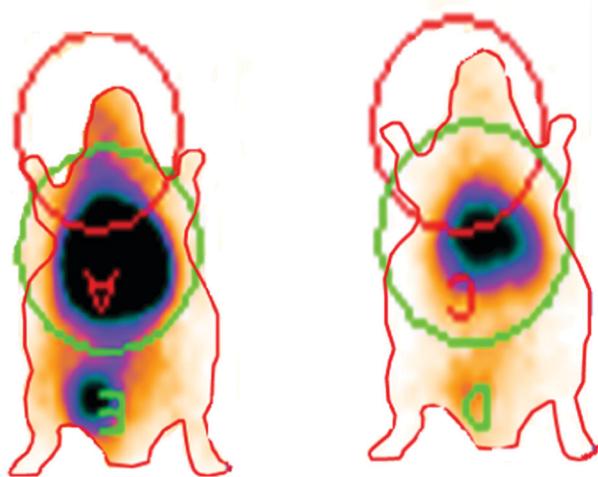


Fig. 6 *In vivo* SPECT imaging of $^{99\text{m}}\text{Tc}$ -MBIP-Cl a(i) without and a(ii) with PK11195 preadministration and $^{99\text{m}}\text{Tc}$ -MBIP-Cl b(i) without and b(ii) with PK11195 preadministration at 40 min post injection of the radioligand (A to H are the points of higher uptake of radioactivity taken randomly by the operator).



(a)



(b)

Fig. 7 *In vivo* SPECT image showing the activity distribution of ^{99m}Tc -MBIP-Cl in (a) normal and (b) inflamed mice without and with blocking at 40 min post injection.

0.155%ID per g per min and 0.231%ID per g per min in the lungs. The faster release kinetic rates in liver and kidney than other TSPO ligands taken for comparison makes it suitable for evaluation as SPECT agent. The *in vivo* specificity of MBIP-Cl was analyzed by saturation study with PK11195 in inflammation models. SPECT images 40 min post injection in normal and inflamed mice confirm uptake in TSPO enriched organs (Fig. 6 and 7).

As per the comparative evaluation, all the three ligands ^{99m}Tc -MBIP-Br, ^{99m}Tc -MBIP-Cl and [^{11}C] MBMP were found suitable for TSPO targeting. In the SPECT ligands ^{99m}Tc -MBIP-Cl was found to be better than ^{99m}Tc -MBIP-Br in terms of the *in vivo* uptake of the compound in tissues expressing TSPO but has a limiting factor of sustained activity in the kidneys. Further investigation in other specific models may warrant human clinical studies.

4. Conclusion

The cost of production of these synthetic TSPO ligands and easy chemistry make them potential candidates for further exploration as imaging agents. Though few models have been used for validation, other TSPO expressing pathological conditions can also be used for validation and quantification. These skeletons can also be modified for other metal-based PET and SPECT agents.

Conflicts of interest

There is no conflict of interest among the authors of this manuscript.

Acknowledgements

We extend special thanks to the Director, INMAS and Dr A. K. Mishra, Head, Division of Cyclotron and Radiopharmaceutical Science, INMAS, Delhi, for providing us the facility to carry out experiments. Besides that we also thank Dr Sonia Gandhi, and Mr Sunil Pal, INMAS for their technical support. This work was supported by INMAS, Delhi under Task Project ST/15-16/INM-03.

References

- 1 J. Fan, P. Lindemann, M. G. Feuilleley and V. Papadopoulos, Structural and functional evolution of the translocator protein (18 kDa), *Curr. Mol. Med.*, 2012, **12**, 369–386.
- 2 V. M. Milenkovic, R. Rupprecht and C. H. Wetzl, The Translocator Protein 18 kDa (TSPO) and Its Role in Mitochondrial Biology and Psychiatric Disorders, *Mini-Rev. Med. Chem.*, 2015, **15**, 366–372.
- 3 L. Veenman, A. Vainshtein and M. Gavish, TSPO as a target for treatments of diseases, including neuropathological disorders, *Cell Death Dis.*, 2015, **6**, e1911.
- 4 M. K. Chen and T. R. Guilarte, Translocator protein 18 kDa (TSPO) molecular sensor of brain injury and repair, *Pharmacol. Ther.*, 2008, **118**, 1–17.
- 5 A. Batarseh and V. Papadopoulos, Regulation of translocator protein 18 kDa (TSPO) expression in health and disease states, *Mol. Cell. Endocrinol.*, 2010, **327**, 1–12.
- 6 L. Veenman, A. Vainshtein, N. Yasin, M. Azrad and M. Gavish, Tetrapyrroles as Endogenous TSPO Ligands in Eukaryotes and Prokaryotes: Comparisons with Synthetic Ligands, *Int. J. Mol. Sci.*, 2016, **17**, E880.
- 7 C. Vicidomini, M. Panico, A. Greco, S. Gargiulo, A. R. D. Coda, A. Zannetti, M. Gramanzini, G. N. Roviello, M. Quarantelli, B. Alfano, B. Tavitian, F. Dolle, M. Salvatore, A. Brunetti and S. Pappata, *In vivo* imaging and characterization of [^{18}F]DPA-714, a potential new TSPO ligand, in mouse brain and peripheral tissues using small-animal PET, *Nucl. Med. Biol.*, 2015, **42**, 309–316.
- 8 R. Jean, E. Bribe, L. Knabe, A. F. Petit, I. Vachier and A. Bourdin, TSPO is a new anti-inflammatory target in the airway of COPD, *Rev. Mal. Respir.*, 2015, **32**, 320.

- 9 H. A. Jones, P. S. Marino, B. H. Shakur and N. W. Morrell, *In vivo* assessment of lung inflammatory cell activity in patients with COPD and asthma, *Eur. Respir. J.*, 2003, **21**, 567–573.
- 10 L. Veenman and M. Gavish, The peripheral-type benzodiazepine receptor and the cardiovascular system. Implications for drug development, *Pharmacol. Ther.*, 2006, **110**, 503–524.
- 11 A. Hatori, J. Yui, L. Xie, T. Yamasaki, K. Kumata, M. Fujinaga, H. Wakizaka, M. Ogawa, N. Nengaki, K. Kawamura and M. R. Zhang, Visualization of Acute Liver Damage Induced by Cycloheximide in Rats Using PET with [¹⁸F]FEDAC, a Radiotracer for Translocator Protein (18 kDa), *PLoS One*, 2014, **9**, e86625.
- 12 N. Arlicot, J. Vercouillie, M. J. Ribeiro, C. Tauber, Y. Venel, J.-L. Baulieu, S. Maia, P. Corcia, M. G. Stabin, A. Reynolds, M. Kassiou and D. Guilloteau, Initial evaluation in healthy humans of [¹⁸F]DPA-714, a potential PET biomarker for neuroinflammation, *Nucl. Med. Biol.*, 2012, **39**, 570–578.
- 13 F. Dolle, C. Luus, A. Reynolds and M. Kassiou, Radiolabeled molecules for imaging the translocator protein (18 kDa) using positron emission tomography, *Curr. Med. Chem.*, 2009, **16**, 2899–2923.
- 14 W. C. Kreisl, M. Fujita, Y. Fujimura, N. Kimura, K. J. Jenko, P. Kannan, J. Hong, C. L. Morse, S. S. Zoghbi, R. L. Gladding, S. Jacobson, U. Oh, V. W. Pike and R. B. Innis, Comparison of [(11C)-(R)-PK 11195 and [(11C)PBR28, two radioligands for translocator protein (18 kDa) in human and monkey: implications for positron emission tomographic imaging of this inflammation biomarker, *Neuroimage*, 2010, **49**, 2924–2932.
- 15 A. Trapani, C. Palazzo, M. de Candia, F. M. Lasorsa and G. Trapani, Targeting of the translocator protein 18 kDa (TSPO): a valuable approach for nuclear and optical imaging of activated microglia, *Bioconjugate Chem.*, 2013, **24**, 1415–1428.
- 16 H. Boutin, F. Cahuveau, C. Thominiaux, M. C. Gregoire, M. L. James, R. Trebossen, P. Hantraye, F. Dolle, B. Tavitian and M. Kassiou, ¹¹C-DPA-713: a novel peripheral benzodiazepinereceptor PET ligand for *in vivo* imaging of neuroinflammation, *J. Nucl. Med.*, 2007, **48**, 573–781.
- 17 D. R. Owen, A. J. Yeo and R. N. Gunn, An 18 kDa translocator protein (TSPO) polymorphism explains differences in binding affinity of the PET radioligand PBR28, *J. Cereb. Blood Flow Metab.*, 2012, **32**, 1–5.
- 18 T. Fukaya, T. Kodo, T. Ishiyama, H. Nishikawa, S. Baba and S. Masumoto, Design, synthesis and structure–activity relationship of novel tricyclic benzimidazolone derivatives as potent 18 kDa translocator protein (TSPO) ligands, *Bioorg. Med. Chem.*, 2013, **21**, 1257–1267.
- 19 T. Fukaya, T. Kodo, T. Ishiyama, H. Kakuyama, H. Nishikawa, S. Baba and S. Masumoto, Design, synthesis and structure–activity relationships of novel benzoxazolone derivatives as 18 kDa translocator protein (TSPO) ligands, *Bioorg. Med. Chem.*, 2012, **22**, 5568–5582.
- 20 A. K. Tiwari, B. Ji, M. Fujinaga, T. Yamasaki, L. Xie, R. Luo, Y. Shimoda, K. Kumata, Y. Zhang, A. Hatori, J. Maeda, M. Higuchi, F. Wang and M. R. Zhang, [¹⁸F]FEBMP: Positron Emission Tomography Imaging of TSPO in a Model of Neuroinflammation in Rats, and *in vitro* Autoradiograms of the Human Brain, *Theranostics*, 2015, **5**, 961–969.
- 21 A. K. Tiwari, M. Fujinaga, J. Yui, T. Yamasaki, L. Xie, K. Kumata, A. K. Mishra, Y. Shimoda, A. Hatori, B. Ji, M. Ogawa, K. Kawamura, F. Wang and M. R. Zhang, Synthesis and evaluation of new (18F)-labelled acetamidobenzoxazolone-based radioligands for imaging of the translocator protein (18 kDa, TSPO) in the brain, *Org. Biomol. Chem.*, 2014, **12**, 9621–9630.
- 22 A. K. Tiwari, J. Yui, M. Fujinaga, K. Kumata, Y. Shimoda, T. Yamasaki, L. Xie, A. Hatori, J. Maeda, N. Nengaki and M. R. Zhang, Characterization of a novel acetamidobenzoxazolone-based PET ligand for translocator protein (18 kDa) imaging of neuroinflammation in the brain, *J. Neurochem.*, 2014, **129**, 712–720.
- 23 A. K. Tiwari, J. Yui, Y. Zhang, M. Fujinaga, T. Yamasaki, L. Xie, Y. Shimoda, K. Kumata, A. Hatori and M. R. Zhang, [¹⁸F]FPBMP- a potential new positron emission tomography radioligand for imaging of translocator protein (18 kDa) in peripheral organs of rats, *RSC Adv.*, 2015, **123**, 101447.
- 24 P. Srivastava, A. Kaul, H. Ojha, P. Kumar and A. K. Tiwari, Design, synthesis and biological evaluation of methyl-2-(2-(5-bromo benzoxazolone)acetamido)-3-(1H-indol-3-yl)propanoate: TSPO ligand for SPECT, *RSC Adv.*, 2016, **6**, 11449.
- 25 N. Kumari, N. Chadha, P. Srivastava, L. K. Mishra, S. Bhagat, A. K. Mishra and A. K. Tiwari, Modified benzoxazolone derivative as 18-kDa TSPO ligand, *Chem. Biol. Drug Des.*, 2017, **90**, 511–519.
- 26 P. Srivastava, A. K. Tiwari, N. Chadha, K. Chuttani and A. K. Mishra, Synthesis and biological evaluation of newly designed phosphonate based bone-seeking agent, *Eur. J. Med. Chem.*, 2013, **65**, 12–20.
- 27 G. Shukla, A. K. Tiwari, D. Sinha, R. Srivastava, H. Cahndra and A. K. Mishra, Synthesis and assessment of ^{99m}Tc chelate-conjugated alendronate for development of specific radiopharmaceuticals, *Cancer Biother. Radiopharm.*, 2009, **24**(2), 209–214.
- 28 N. Kumar, D. Kakkar, A. K. Tiwari, N. Saini, M. Chand and A. K. Mishra, Design, synthesis and fluorescence lifetime study of benzothiazole derivatives for imaging of amyloids, *Cancer Biother. Radiopharm.*, 2010, **25**, 571–575.
- 29 D. Kakkar, A. K. Tiwari, K. Chuttani, R. Kumar, K. Mishra, H. Singh and A. K. Mishra, Polyethylene-glycolylated isoniazid conjugate for reduced toxicity and sustained release, *Ther. Delivery*, 2011, **2**(2), 205–212.
- 30 F. Mattner, M. Quinlivan, I. Greguric, T. Pham, X. Liu, T. Jackson, P. Berghofer, C. J. R. Fookes, B. Dikic, M. C. Gregoire, F. Dolle and A. Katsifi, Radiosynthesis, *in vivo* biological evaluation, and imaging of brain lesions with [¹²³I]-CLINME, a new SPECT tracer for the Translocator Protein, *Dis. Markers*, 2015, 729698.
- 31 A. Cappelli, A. Mancini, F. Sudati, S. Valenti, M. Anzini, S. Belloli, R. M. Moresco, M. Matarrese, M. Vaghi, A. Fabro, F. Fazio and S. Vomero, Synthesis and biological characterization

- of novel 2-quinolinecarboxamide ligands of the peripheral benzodiazepine receptors bearing technetium-99m or rhenium, *Bioconjugate Chem.*, 2008, **19**, 1143–1153.
- 32 M. Fujinaga, R. Luo, K. Kumata, Y. Zhang, A. Hatori, T. Yamasaki, L. Xie, W. Mroi, Y. Kurihara, M. Ogawa, N. Nengaki, F. Wang and M.-R. Zhang, Development of a ^{18}F -labeled radiotracer with improved brain kinetics for positron emission tomography imaging of translocator protein (18 kDa) in ischemic brain and glioma, *J. Med. Chem.*, 2017, **60**, 4047–4061.

Curriculum Vitae

Name: **Pooja Srivastava**

Position: Scientist D, INMAS, DRDO

Email id: pushree14@gmail.com

Mobile: +91-9899537382

Pooja Srivastava is currently working as Scientist D with INMAS, DRDO. She joined DRDO as Scientist B in the year 2003 through all India competitive examination. She is an alumna of IIT Kanpur, IIT Kharagpur and Krannert School of Management, Purdue University, USA.

Educational background

Education	Year	University/Institute	Discipline	Marks/Recognition
Ph.D.		DTU	Biotechnology	Pursuing
MBA	2010	Purdue University, USA	General Management	Distinction
M. Tech.	2002	IIT Kanpur	Material Science	8.32/10
Integrated M.Sc. (5 years)	2000	IIT Kharagpur	Chemistry	7.77/10

Professional details

Post	From	To	Establishment /Lab
Scientist D	01 Jul 2015	Till date	INMAS, Delhi
Scientist C	01 Jul 2008	30 Jun 2015	INMAS, Delhi
Scientist B	10 Sep 2007	30 Jun 2008	INMAS, Delhi
Scientist B	1 Aug 2003	9 Sep 2007	TBRL, Chandigarh
Scientist B	6 Mar 2003	31 Jul 2003	DIAT, Pune

Awards and honours

1. Director's commendation for contribution in the area of Project Management (Group award) (2019) (Lab level)
2. Third prize in poster presentation, Recent approaches and innovations in Chemical Sciences (RAICS), Nov 2018
3. Second prize in Hindi workshop (2012) (Lab level)

4. Laboratory Technology group award for significant contribution towards implementation of quality management system ISO 9001-2008 (2011) (Lab level)
5. Membership in Beta Gamma Sigma, the International honor society for collegiate schools of business, Purdue University Chapter, 2010, in recognition of high scholastic achievement
6. Dean's list, in recognition of excellent work and academic achievement during MBA, 2010
7. GATE qualified 2000
8. NET qualified 1999
9. Awards from Governor of UP & Education Minister for 9th position among girls and 19th in general in UP state in class X
10. National Talent Search Examination (NTSE) scholar

Publications

1. **Srivastava, P.**, Kumari, N., Kakkar, D., Kaul, A., Kumar, P., & Tiwari, A. K. (2019). Comparative evaluation of ^{99m}Tc-MBIP-X/11 [C] MBMP for visualization of 18 kDa translocator protein. *New Journal of Chemistry*, 43,11288-11295. (IF: 3.069)
2. **Srivastava, P.**, Kakkar, D., Kumar, P., & Tiwari, A. K. (2019). Modified benzoxazolone (ABO-AA) based single photon emission computed tomography (SPECT) probes for 18 kDa translocator protein. *Drug Development Research*, 2019, 1-9. (IF: 1.742)
3. **Srivastava, P.**, Kumar, P., & Tiwari A. K. (2019). Design, synthesis and in silico evaluation of methyl 2-(2-(5-bromo/chloro-2-oxobenzooxazol-3(2*H*)-yl) acetamido)-3-phenylpropanoate for TSPO targeting, *Radiochemistry*, Accepted
4. Kumari, N., Chadha, N., **Srivastava, P.**, Mishra, L. C., Bhagat, S., Mishra, A. K., & Tiwari, A. K. (2017). Modified benzoxazolone derivative as 18-kDa TSPO ligand. *Chemical Biology & Drug Design*, 90(4), 511-519. (IF: 2.256)
5. **Srivastava, P.**, Kaul, A., Ojha, H., Kumar, P., & Tiwari, A. K. (2016). Design, synthesis and biological evaluation of methyl-2-(2-(5-bromo benzoxazolone) acetamido)-3-(1*H*-indol-3-yl) propanoate: TSPO ligand for SPECT. *RSC Advances*, 6(115), 114491-114499. (IF: 3.049)

6. **Srivastava, P.**, Tiwari, A. K., Thukral, D. K., Kumar, V., & Mishra, A. K. (2014). Bis (histidine) with N₂ Vehicle: An Important Skeleton for MR/Chelation Therapy. *Chemical Biology & Drug Design*, 83(6), 682-687. (IF: 2.256)
7. **Srivastava, P.**, Tiwari, A. K., Chadha, N., Chuttani, K., & Mishra, A. K. (2013). Synthesis and biological evaluation of newly designed phosphonate based bone-seeking agent. *European Journal of Medicinal Chemistry*, 65, 12-20. (IF: 4.833)
8. **Srivastava, P.**, Kumar, V., Tiwari, A. K., & Mishra, A. K. (2013). Quantitative structure activity relationship of tetraaza macrocyclic vehicle DO3A with lanthanide relaxivity and hydrophobicity. *Medicinal Chemistry Research*, 22(12), 5861-5867. (IF: 1.720)
9. Aggarwal, S., Tiwari, A. K., **Srivastava, P.**, Chadha, N., Kumar, V., Singh, G., & Mishra, A. K. (2013). Investigation for the Interaction of Tyramine-Based Anthraquinone Analogue with Human Serum Albumin by Optical Spectroscopic Technique. *Chemical Biology & Drug Design*, 81(3), 343-348. (IF: 2.256)
10. Tiwari, A. K., Ojha, H., Kaul, A., Dutta, A., **Srivastava, P.**, Shukla, G., & Mishra, A. K. (2009). Quantitative Structure–Property Relationship (Correlation Analysis) of Phosphonic Acid-Based Chelates in Design of MRI Contrast Agent. *Chemical Biology & Drug Design*, 74(1), 87-91. (IF: 2.256)

Conferences Abstract (Oral and poster presentation)

1. Evaluation of acetamidobenzoxazolone derivatized biomarkers for assessing translocator protein in brain and peripheral organs, 50th Annual Conference of the Society of Nuclear Medicine, India (SNMICON2018), 22-25 Nov, 2018, Chandigarh
2. Modified third generation translocator protein-selective positron emission tomography radiotracer to access microglial activation in ischemic rat brain, 50th Annual Conference of the Society of Nuclear Medicine, India (SNMICON2018), 22-25 Nov, 2017, Chandigarh
3. Synthesis of biocompatible hydrogel based on CMCNa salt-system crosslinked with EDTA and enhances the absorbing property by PEG, Recent approaches and innovations in Chemical Sciences (RAICS), Nov 2018, Lucknow (Third Prize)

4. Acetamidobenzoxazolone (ABO) based derivative for assessment of Translocator Protein (18 kDa) for brain injury/inflammation, 49th Annual Conference of the Society of Nuclear Medicine, India (SNMICON2017), 14-17 Dec, 2017, New Delhi
5. N₄ vehicle based acetamidobenzoxazolone derivative for imaging of Translocator Protein (18 kDa) during inflammatory condition, Indian J Nucl Med. 2015 Dec; 30(Suppl 1): S29–S72, Lucknow
6. Evaluation of DO3MPEA as bifunctional bone imaging agent for PET application, 2nd World Congress on Gallium-68, 23 Feb-3 Mar 2013, Chandigarh
7. Hands on Gallium-68 generators, Post congress workshop on germanium-68/gallium-68 generator, 4-5 Mar 2013, Delhi
8. Design, synthesis and evaluation of ^{99m}Tc-DO3MPEA as bifunctional bone imaging agent, Annual Congress of the European association, 26-30 Oct, 2012, Milan, Italy
9. Design and synthesis of a novel gadolinium based MR contrast Gd(DOBAPATA) and its derivative for MR imaging, International conference on radiation biology, 2010, Chennai
10. Synthesis and characterization of novel SPECT/PET radiopharmaceutical based on methionine with macrocyclic chelating agent, 9th Asia Oceania Congress of nuclear medicine and biology, 2008, Delhi
11. A Novel Bifunctional pH Sensitive Contrast Agent for Targeted MR, Special symposium on Advanced MR Applications and 14th National Magnetic Resonance Society Meeting, 16th – 19th January, 2008, Delhi

Continuation of Education Programme

1. Combating neurological Disorders: Approaches and Methods, 17-19 Sep 2019
2. Nanomaterial and life, 19-23 Aug 2019
3. Alternatives to animal research, 13-15 Mar 2019
4. Non-invasive imaging of small animals: An insight to minimal use of small animals, 4-8 Sep 2017
5. Neuroimaging in cognitive research, 2016
6. Application of metabolomics in Biomedical Research, 23-25 Nov 2016

7. Process Safety Audit, 28-30 Jul 2015
8. Computational Chemistry and Bioinformatics, 26-28 Aug 2015
9. Quality management and laboratory management for NABL accreditation, Delhi, 30-31 Mar 2012
10. Internal quality auditor course, Training from STQC, Delhi 14-16 Mar 2011

Techno-managerial assignments

1. Member Secretary, Specialist panel “Soldier Health & Drug Development (SHDD)”, Life Science Research Board (LSRB), DRDO
2. Programme coordinator of workshops to create awareness on “funding research proposals under LSRB of DRDO”
 - i. Jadavpur University on 06 Mar 2018
 - ii. Banaras Hindu University on 17 Jan 2019
3. Organizing member of course “Quality control and quality assurance requirements for medical testing laboratory, 11-12 Oct, 2012, Delhi
4. Organizing member, Quality management system and laboratory management for NABL accreditation, 30-31 Mar, 2012, Delhi
5. INMAS representative, India International Trade Fair, Nov 2012, Delhi
6. Organizing member, Brig S. K. Mazumdar Memorial Lecture, 14 Aug 2012, Delhi
7. Internal ISO Auditor for INMAS

Membership of professional society

1. Member, Society of Nuclear Medicine, India
2. Member, Indian Science Congress
3. Member, Indian Society of Nanomedicine